



# University of HUDDERSFIELD

## University of Huddersfield Repository

Elarrami, Ablasem M.

Experimental and Numerical Based Analysis of Performance Characterisation of Roots Blower

### Original Citation

Elarrami, Ablasem M. (2018) Experimental and Numerical Based Analysis of Performance Characterisation of Roots Blower. Doctoral thesis, University of Huddersfield.

This version is available at <http://eprints.hud.ac.uk/id/eprint/35040/>

The University Repository is a digital collection of the research output of the University, available on Open Access. Copyright and Moral Rights for the items on this site are retained by the individual author and/or other copyright owners. Users may access full items free of charge; copies of full text items generally can be reproduced, displayed or performed and given to third parties in any format or medium for personal research or study, educational or not-for-profit purposes without prior permission or charge, provided:

- The authors, title and full bibliographic details is credited in any copy;
- A hyperlink and/or URL is included for the original metadata page; and
- The content is not changed in any way.

For more information, including our policy and submission procedure, please contact the Repository Team at: [E.mailbox@hud.ac.uk](mailto:E.mailbox@hud.ac.uk).

<http://eprints.hud.ac.uk/>

Experimental and numerical based analysis of performance characterisation of Roots blower  
Ablgasem Elarrami-PhD Thesis 2018



**EXPERIMENTAL AND NUMERICAL BASED ANALYSIS OF  
PERFORMANCE CHARACTERISATION OF ROOTS BLOWER**

By

**ABLGASEM M. ELARRAMI**

A thesis submitted to the University of Huddersfield in partial fulfilment of the requirements  
for the degree of Doctor of Philosophy

Director of Research: Prof. Rakesh Mishra

School of Computing and Engineering  
University of Huddersfield UK,  
December 2018

Experimental and numerical based analysis of performance characterisation of Roots blower  
Ablgasem Elarrami-PhD Thesis 2018

## Copyright Statement

- The author of this thesis (including any appendices and/or schedules to this thesis) owns any copyright in it (the “Copyright”) and s/he has given The University of Huddersfield the right to use such copyright for any administrative, promotional, educational and/or teaching purposes.
- Copies of this thesis, either in full or in extracts, may be made only in accordance with the regulations of the University Library. Details of these regulations may be obtained from the Librarian. This page must form part of any such copies made.
- The ownership of any patents, designs, trademarks and any and all other intellectual property rights except for the Copyright (the “Intellectual Property Rights”) and any reproductions of copyright works, for example graphs and tables (“Reproductions”), which may be described in this thesis, may not be owned by the author and may be owned by third parties. Such Intellectual Property Rights and Reproductions cannot and must not be made available for use without the prior written permission of the owner(s) of the relevant Intellectual Property Rights and/or Reproductions.

## **Abstract**

Roots blower is a positive displacement machine widely used as pressure or vacuum device in several industrial processes due to its simple construction, large volumetric efficiency and it has been most effective in low or moderate compression ratios. There are several geometric and flow relevant variables that affect its operation and performance. Internal leakage is an essential issue of the Root blower's design. The leakage (slip) in the Roots blower effect the process efficiency by affecting the mass flow rate and therefore the volumetric efficiency, so the proper sizes of clearances must be provided inside the blower. The flow field conditions, inside clearances, and at the inlet and the exit of the blower are unsteady. The temperatures, pressures, and velocities vary significantly and are a function of operating condition and geometry of the Roots blower.

Based on available literature, extensive studies are being carried out to improve the efficiency of current models of Roots blowers, as well as to develop new blower models. But, the detailed knowledge of the flow behaviour in such machines is still a subject of active research. This is because most of the studies conducted lack details analysis of flow characteristics and limited studies on the local flow behaviour within these blowers have been reported. Therefore, the main aim of this study is the in-depth characterisation of internal flow with varying clearance sizes of Roots blower in order to improve their performance. Experimental approach and numerical method using Computational Fluid Dynamics (CFD) have been used in this research study.

Qualitative and quantitative analyses were carried out to establish the effect of operating conditions and clearance sizes on the flow and performance characteristics of the Roots blower. Based on these in-depth analysis, the performance characterisation of the influence of rotational speed and pressure difference on the Roots blower performance under the transient condition has been conducted and it is a new add to available knowledge in this field. Also, the effect of pressure difference, rotational speed and gap size on the variation and the distribution of other performance parameters such as pressure, temperature and velocity within the blower was established. Moreover, a new non-dimensional analysis of performance parameters and develop novel empirical and semi-empirical correlations for performance factors of Roots blower are main contributions to the knowledge have been achieved in this research study.

Furthermore, a new clearance model of Roots blower has been developed which considered as a main novelty in this study. Numerical characterisation of pressure fluctuations in both time and frequency domain with clearance variation inside the blower has been achieved. A new methodology for detection of the change of clearance size inside Roots blower has been developed.

## **Acknowledgements**

All praises are for the Almighty Allah alone, the Merciful and peace be upon his prophet who is forever a torch of guidance and knowledge for humanity as a whole. Thus, an unlimited pleasure and Great thanks to Allah for giving me this opportunity and patience to carry out this work.

I would like to acknowledge and give special and grateful thanks to my parents (especially my mother) and, my wife for their never-ending interest, support, understanding and encouragement during my life, in particular in this study and their comfort, through a very difficult time, that I faced.

I would like to express my greatest gratitude and deep appreciation to my supervisor, Prof. Rakesh Mishra for being so generous with his time and constructive criticism, his invaluable aid, and useful suggestion throughout the study. I sincerely appreciate all the help and encouragement. My thanks extended to my second supervisor, Dr Taimoor Asim, whose expertise, encouragement and direction were vital in completing my research project and writing this thesis.

Great thanks are also extended to my colleagues, research fellows and staff members for their help during my study. I would like to thank my close family, brothers, sister, sons and daughters for their continued support and encouragement during this study.

Lastly, I would like to thank my teachers, my friends, and all science students and researchers who helped me through my academic life.

## Table of Contents

Copyright Statement .....	iii
Abstract .....	iv
Acknowledgements .....	vi
Table of Contents .....	vii
Table of Figures .....	xiii
Table of Tables .....	xxv
Abbreviations .....	xxix
Symbols .....	xxx
Subscripts .....	xxx
Chapter 1 .....	1
Introduction .....	1
1.1 The history of Roots blower .....	2
1.2 Roots blower Applications and Advantages .....	3
1.3 Roots blower design and operation .....	3
1.4 Performance parameters and their limitations .....	6
1.4.1 Temperature variation considerations .....	7
1.4.2 Pressure variation considerations .....	7
1.4.3 Rotational speed considerations .....	8
1.4.4 Flow through leakage paths (slip) considerations .....	8
1.4.5 Considerations of compressibility: .....	9
1.4.6 Working pressure considerations .....	9
1.5 Roots blower Performance factors .....	9
1.5.1 Pumping Speed (Q): .....	9
1.5.2 Volumetric Efficiency .....	9

1.5.3 Power of Roots blower system .....	10
1.5.4 Geometry: .....	10
1.5.5 Clearance: .....	10
1.5.6 Inlet-outlet cross-section:.....	10
1.6 The Motivation.....	11
1.7 The organisation of the Thesis .....	12
Chapter 2.....	15
Literature review .....	15
2.1 Quantitative evaluation of Performance characteristics of a Roots blower.....	16
Baseline.....	16
2.1.1 Summary of the literature review regarding Quantitative evaluation of .....	26
Performance characteristics of a Roots blower baseline model.....	26
2.2 Quantitative evaluation of Roots blower performance undergoing .....	27
Geometrical changes .....	27
2.2.1 Summary of the literature review regarding Quantitative evaluation of .....	32
Roots blower performance undergoing geometrical changes .....	32
2.3 Quantitative evaluation of Unsteady flow characteristics and.....	32
comparative analysis with clearance variation inside the Roots blower.....	32
2.3.1 Summary of the literature review regarding the Quantitative evaluation of unsteady flow characteristics and comparative analysis with clearance variation inside the Roots blower .....	36
2.4 Scope of Research.....	37
2.5. Aims of the research .....	38
2.6. Specific Research Objectives.....	39
Chapter 3.....	41
Experimental and Numerical investigations of a Roots blower.....	41
3.1. Experimental method based investigations of a Roots blower .....	42

3.1.1 Roots blower Test Rig .....	42
3.1.2 Experimental method and facilities .....	54
3.1.3. The measurement procedures .....	55
3.1.4. Mass flow rate measurements by Orifice plates and related calculations .....	56
3.1.5. Uncertainty.....	60
3.1.6. Experimental results and Roots blower performance calculations .....	62
3.1.7. Analytical method calculations of Roots blower performance.....	66
3.2 Numerical method based investigation of performance parameters of Roots blower ...	69
3.2.1 Introduction.....	69
3.2.2. The development of CFD blower dynamic model using ANSYS FLUENT.....	70
3.2.3 Roots blower Flow Domain Identification and Pre-processing .....	70
3.2.4 Solver Settings .....	74
3.2.5. The Numerical Investigations framework .....	78
Chapter 4.....	82
Quantitative evaluation of Performance characteristics of baseline Roots blower model.....	82
4.1 The performance characterisation based on the experimental results .....	83
4.1.1 Establish the relations between different non-dimensional parameters.....	83
4.1.2. Determine the blower performance baseline factors (mass flow rate, efficiencies, power consumption and head pressure or pressure ratio).....	88
4.1.3. Deriving empirical equations depending on non-dimensional relation between different performance parameters .....	93
4.2 The performance characterisation of numerical results .....	100
4.2.1 Introduction to Computational Fluid Dynamics (CFD).....	100
4.2.2. The mesh independence test .....	101
4.2.3. The time independence test.....	103
4.2.4. Validation of CFD model.....	104
4.2.5. Roots blower internal flow characteristics.....	109

4.2.6 Effect of pressure difference on Roots blower performance characteristics .....	111
4.2.7. Effect of the rotational speed on the Roots blower performance characteristics.	133
4.2.8 Conclusion summary .....	154
Chapter 5.....	157
Quantitative evaluation of Roots blower performance undergoing geometrical changes .....	157
5.1 Roots blower geometrical models.....	158
5.2 Effect of Geometrical Parameters .....	158
5.3 Effect of the clearance size on the performance of Roots blower .....	160
5.4 Establish the effect of the gap between the rotor and the casing (Tip clearance) on the Roots blower performance.....	160
5.4.1 Effect of Gap between Rotor and Casing on pressure distributions .....	161
5.4.2 The Effect of clearance between rotor and casing on the mass flow rate.....	168
5.4.3 Effect of clearance between rotor and casing on temperature distributions .....	170
5.4.4. Effect of the gap between rotor and casing on velocity distributions.....	175
5.5 Effect of clearance between two rotors (centre clearance) on Roots blower performance .....	179
5.5.1. Effect of the gap between two rotors on pressure characteristics .....	179
5.5.2 The Effect of the gap between two rotors on the mass flow rate.....	187
5.5.3. Effect of the gap between two rotors on temperature characteristics in Roots blower .....	189
5.5.4. Effect of Gap between two rotors on velocity distributions .....	195
5.6. Establish the non-dimensional relations between different geometrical and flow related parameters of Root blower.....	199
5.6.1. Mass flow rate analysis.....	200
5.6.2 Volumetric efficiency .....	204
5.6.3 Adiabatic Efficiency .....	205
5.6.4 Power consumption.....	207

5.7. Deriving semi-empirical equations depending on non-dimensional relations between different geometrical and flow related performance parameters .....	208
5.7.1 Development an equation to predict mass flow rate within Roots blower .....	208
5.7.2 Develop semi-empirical correlation to predict the volumetric efficiency of Roots blower .....	209
5.7.3 Develop semi-empirical correlation to predict the efficiency of Roots blower....	210
5.7.4 Develop an equation to predict the power consumption of Roots blower .....	211
5.8 Conclusion summary .....	212
CHAPTER 6 .....	214
Quantitative evaluation of unsteady flow characteristics and comparative analysis with clearance variation inside the Roots blower .....	214
6.1 Establish the effect of the clearance sizes in order to develop a new clearance model of the Roots blower .....	215
The mesh independence test of 3D model .....	216
6.1.1. Comparison analysis of the influence of different clearance models on pressure distributions.....	219
6.1.2. Comparison analysis of the influence of different clearance models on the mass flow rate .....	229
6.1.3. Comparison analysis of the influence of different clearance models on temperature distributions.....	233
6.1.4. Comparison analysis of the influence of different clearance models on velocity distributions.....	242
6.1.5 Summary .....	247
6.2 Pressure fluctuation and flow pattern of Roots blower with different clearance models .....	248
6.2.1 Analysis of the Pressure Fluctuations of the baseline blower model (M2) in Frequency Domain.....	249

6.2.2 Analysis of the Pressure Fluctuations of the blower model 1 (M1) in Frequency Domain.....	251
6.2.3 Analysis of the Pressure Fluctuations of the blower model 3 (M3) in Frequency Domain.....	255
6.2.4 Conclusion summary .....	257
6.3 Develop a methodology for detection of clearance size change inside Roots blower.	259
6.3.1 Determine of pressure fluctuation characteristics with clearance size change in Roots blower using frequency domain.....	259
6.3.2 Summary .....	264
Chapter 7.....	265
Conclusions.....	265
7.1. Research Problem Synopsis .....	265
7.2. Research Objectives and Most important Achievements .....	266
7.3 Thesis Contributions .....	270
7.4. Recommendations for future work and limitations of the presented work.....	272
References.....	273
APPENDEICES .....	278
APPENDEX A1 .....	278
APPENDEX A2.....	286
APPENDEX A3.....	288
APPENDIX A4.....	291

## Table of Figures

Figure 1.1: Cross-sectional View of a Roots Blower with Twin Bi-lobe Rotors (Choi, 2013).	4
Figure 1.2: Roots Blower consists of two rotors with 2-lobes or more for each rotor (Thai & Trung, 2015).....	4
Figure 1.3: Blower Operating Principle .....	5
Figure 1.4: The Geometries of a Bi-Lobe Rotor and a Stator (casing) (Choi, 2013).....	6
Figure 3.1: The similar Roots blower package used for experimental tests .....	43
<b>Figure 3.2: Experimental test rig diagram with piping and instrumentation of HRVB 613 type Roots blower system</b> .....	44
Figure 3.3: The actual Roots blower used for experimental tests (model HRBV613).....	45
Figure 3.4: Manual Pressure regulator valve (left), Relief valve (right) .....	46
Figure 3.5: Pressure gauges; Blower inlet (left), Blower outlet (right) .....	47
Figure 3.6: Orifice plate type .....	48
Figure 3.7: Differential pressure transducer and orifice plate with mechanical fittings.....	49
Figure 3.8: Pressure transducers for barometer, system inlet, blower Inlet (left), and for blower outlet and system outlet (right) .....	50
Figure 3.9: the Temperature sensor (PT100) .....	51
Figure 3.10: A Dynamic data acquisition system .....	53
Figure 3.11: Devices and graphics display of the acquisition system .....	53
Figure 3.12: The pressure and the temperature sensors installed on the suction side (left) and discharge side (right).....	54
Figure 3.13: The pressure sensors and the pressure gauge installed on the discharge side.....	55
Figure 3.14: Standard orifice plate (Baker, 2005). .....	57
Figure 3.15: Pressure tapping locations for orifice plates with corner pressure taps and D and D/2 pressure taps arrangements (Baker, 2005). .....	57
Figure 3.16: Maximum adiabatic efficiency of lobe blower.....	68
Figure 3.17: HRVB613 Roots blower numerical model and their rotors .....	71
Figure 3.18: The 3D and 2D geometry of the fluid domain .....	72
Figure 3.19: 2D/3D fluid mesh domains.....	73
Figure 3.20: The meshing elements and the inflation layers inside the gap between the rotors and the casing (right) and inside the gap between the two rotors (left).....	74

Figure 4.1: The relation between the mass flow rate of the blower and a pressure ratio at a different blower speed.....	88
Figure 4.2: The relation between mass flow rate coefficient of the blower and pressure coefficient at a different blower speed.....	90
Figure 4.3: The variation of volumetric efficiency of the blower with a pressure ratio .....	91
Figure 4.4: The variation of volumetric efficiency of the blower with a pressure coefficient	91
Figure 4.5: Variation of the adiabatic efficiency of the blower with a pressure ratio .....	92
Figure 4.6: Variation of power consumption of the blower with a pressure ratio.....	92
Figure 4.7: Temperature ratios and Pressure ratios relation in Roots blower at different speeds .....	94
Figure 4.8: Comparison between Measurement data and Regression data for different pressure and temperature ratios .....	94
Figure 4.9: Comparison between Measurement data and Regression data for different pressure ratios .....	95
Figure 4.10: Comparison between Measurement data and Regression data for different pressure and temperature ratios .....	96
Figure 4.11: depicts the comparison between experimental data and predicted data.....	97
Figure 4.12: the comparison between experimental data and predicted data .....	99
Figure 4.13: Mass flow rate spatial discretization results.....	101
Figure 4.14: Outlet temperature spatial discretisation results.....	102
Figure 4.15: Mass flow rate temporal discretization results .....	103
Figure 4.16: Outlet temperature temporal discretization results.....	104
Figure 4.17: The behaviour of outlet temperature for five periods of rotation at rotational speed of 1800 rpm and for different pressure loads.....	105
Figure 4.18: Roots blower model dimensions .....	106
Figure 4.19: Validation of mass flow rates as f (pressure ratio across the blower).....	107
Figure 4.20: Validation of out temperature as f (pressure ratio across the blower).....	108
Figure 4.21: Pressure contour at speed 1800 rev/min at 15 <sup>0</sup> and 45 <sup>0</sup> .....	110
Figure 4.22: Velocity and vector contours at speed 1800 rev/min at different time steps ....	110
Figure 4.23: Number of points has been chosen inside the blower for more depth analysis.	111
Figure 4.24: The variations of static pressure contour at a speed of 1800 rev/min and for different pressures of (a)- 300 millibar, (b)- 500 millibars, (c)- 700 millibar .....	113

Figure 4.25: Pressure fluctuations at blower inlet at 1800 rev/min and for different pressures .....	114
Figure 4.26: Pressure fluctuations at blower outlet at 1800 rev/min and for different pressures .....	114
Figure 4.27: The behaviour of pressure fluctuations from the inlet to the outlet of the blower for one rotation.....	115
Figure 4.28: The variation of maximum-pressures at 1800 rev/min and under different discharge pressures .....	116
Figure 4.29: The variation of maximum negative-pressures at 1800 rev/min and under different discharge pressures.....	116
Figure 4.30: The distribution of maximum-pressures at 1800 rev/min and under different discharge pressures .....	118
Figure 4.31: The distribution of maximum negative pressures at 1800 rev/min and under different discharge pressures.....	118
Figure 4.32: Root Mean Square (RMS) of effective pressure zones at 1800 rev/min and for different pressure difference. ....	119
Figure 4.33: The peak-peak amplitudes at speed 1800 rev/min and for different discharge pressures.....	120
Figure 4.34: The average mass flow rate at the speed 1800 rev/min and for different discharge pressures.....	121
Figure 4.35: The fluctuations of the inlet mass flow rate at 1800 rev/min and for different pressure loads.....	121
Figure 4.36: The fluctuations of the outlet mass flow rate at 1800 rev/min and for different pressure loads.....	122
Figure 4.37: Mass flow rate fluctuation coefficient (Mf) at 1800 rev/min and for different pressure loads at the inlet (left) and an outlet (right).....	123
Figure 4.38: The temperature contours and distribution for the last revolution and at 45 <sup>0</sup> rotation degrees, 1800 rev/min and for pressures loads of (a) - 300 millibars, (b) - 500 millibars, and (c) - 700 millibars.....	123
Figure 4.39: Outlet temperature at 1800 rev/min and for different pressure loads for full five rotations in the Roots blower .....	124

Figure 4.40: The maximum outlet temperature at a speed 1800 rev/min and for different pressure loads for the last rotation in the Roots blower .....	125
Figure 4.41: The distribution and the variation of maximum temperature at 1800 rev/min and for different pressure loads .....	126
Figure 4.42: The variation of minimum temperature at rotational speed 1800 rev/min and for different pressure loads .....	128
Figure 4.43: The distribution and the variation of minimum temperature at 1800 rev/min and for different pressure loads .....	128
Figure 4.44: The velocity vector and streamline contours at a rotational speed 1800 rev/min, meshing angle at $45^{\circ}$ and for pressure differences of (300, 500, and 700) millibar from up to down respectively. ....	129
Figure 4.45: The variation of average velocity at 1800 rev/min and different pressure loads .....	131
Figure 4.46: The distribution and the variation of Maximum velocity at 1800 rev/min and different pressure loads .....	132
Figure 4.47: The distribution and the variations of static pressure at 700 millibar and for rotational speed of (a) - 1200 rev/min, (b) - 1800 rev/min, (c) - 2400 rev/min.....	134
Figure 4.48: Pressure fluctuations at blower inlet at 1800 rev/min and for different pressures .....	135
Figure 4.49: Pressure fluctuations at blower inlet at 1800 rev/min and for different pressures .....	135
Figure 4.50: The distribution of max-pressures at 700 millibars and under different rotational speeds.....	137
Figure 4.51: The distribution of min-pressure at 700 millibars and under different rotational speeds.....	138
Figure 4.52: Root Mean Square (RMS) of effective pressure zones at 700 millibars and different rotational speed. ....	139
Figure 4.53: The peak-peak amplitudes at different speeds and 700-millibars discharge pressure. ....	140
Figure 4.54: The average mass flow rate at different speeds and 700 millibars pressure difference .....	141

Figure 4.55: The fluctuations of the inlet mass flow rate at 1800 rev/min and different pressure loads..... 142

Figure 4.56: The amplitude of fluctuations of the mass flow rate at 700 millibars pressure difference and different rotational speeds..... 143

(c) Figure 4.57: The temperature contours for the last revolution and at 45<sup>0</sup> rotation degrees, 700 mbar and for rotational speeds of (a) 1200 rev/min, (b) 1800 rev/min, and (c) 2400 rev/min. .... 144

Figure 4.58: Outlet temperature at a pressure difference 700 millibars and for different rotational speeds..... 145

Figure 4.59: The distribution and the variation of minimum temperature at same discharge pressure 700 millibars and under different rotational speeds. .... 147

Figure 4.60: The distribution and the variation of minimum temperature at a discharge pressure of 700 millibars and under different rotational speeds ..... 148

Figure 4.61: The velocity vectors and streamline contours at a pressure difference of 700 millibars, meshing angle of 45<sup>0</sup> and for rotational speeds of (1200, 1800, and 2400) rev/min from up to down respectively. .... 149

Figure 4.62: The variation of average velocity at 700 millibars pressure difference and different rotational speeds..... 151

Figure 4.63: The distribution and the variety of maximum velocity at 700 millibars pressure difference and different rotational speeds..... 153

Figure 4.64: The relationship between the velocity field, temperature field and pressure field ..... 156

Figure 5.1: The 3D/2D geometry of Roots blower model..... 159

Figure 5.2: The static pressure contours at a speed of 2400 rev/min, a pressure difference of 700 millibars, and for tip clearances of (a) 0.22 mm, (b) 0.24 mm, and (c) 0.26 mm..... 161

Figure 5.3: Pressure fluctuations at blower inlet at 2400 rev/min, 700 millibars, and for different tip clearances. .... 162

Figure 5.4: Pressure fluctuations at blower outlet at a speed 2400 rev/min, a pressure difference 700 millibars, and for different tip clearances. .... 162

Figure 5.5: The distribution of average-pressures at a speed 2400 rev/min, a pressure difference 700 millibars and for different tip clearances. .... 163

Figure 5.6: The distribution of maximum-pressures at 2400 rev/min, a pressure difference 700 millibars and for different tip clearances. .... 164

Figure 5.7: The distribution of maximum negative pressures at a speed 2400 rev/min, a pressure difference 700 millibars and for different tip clearances..... 165

Figure 5.8: Root Mean Square (RMS) of effective pressure zones at 1800 rev/min and different pressure difference. .... 165

Figure 5.9: The peak-peak amplitudes at a speed 2400 rev/min, a pressure difference 700 millibars and for different tip gaps..... 166

Figure 5.10: the relation between the impeller diameter and tip clearance with the pressure variation in the blower ..... 167

Figure 5.11: The average mass flow rate at speed 2400 rev/min, pressure differences 700 millibars, and different tip clearances. .... 168

Figure 5.12: Mass flow rate fluctuation at 2400 rev/min, 700 mbars and different tip gaps at the inlet..... 169

Figure 5.13: Mass flow rate fluctuation at 2400 rev/min, 700 millibars and for different tip gaps at inlet and outlet. .... 169

Figure 5.14: Mass flow rate fluctuation coefficient ( $M_F$ ) at 2400 rev/min, 700 millibars and for different tip clearances at the inlet (left) and the outlet (right) of the blower. .... 169

Figure 5.15: The temperature contours and distribution for the last revolution and at 45<sup>0</sup> rotation degrees, 2400 rev/min, a difference pressure 700 millibars, and for tip gaps of (a) 0.22 mm, (b) 0.24 mm, and (c) 0.26 mm. .... 170

Figure 5.16: Outlet total temperature at 2400 rev/min, different pressure 700 millibars and different tip clearances. .... 171

Figure 5.17: The distribution and the variation of average temperature at 2400 rev/min, 700 millibars pressure load and different tip clearances..... 172

Figure 5.18: The distribution and the variation of maximum temperature at 2400 rev/min, 700 millibars pressure load and for different tip clearances. .... 173

Figure 5.19: The distribution and the variation of maximum negative temperature at 2400 rev/min, a pressure load 700 millibars and for different tip clearances. .... 174

Figure 5.20: The relation between the tip clearance and the maximum and minimum-recorded points of temperature in the blower ..... 174

Figure 5.21: The velocity vectors and streamline contours at a rotational speed 2400 rev/min, meshing angle at  $45^{\circ}$  degrees, a pressure difference 700 millibars and for tip clearances of (0.22 mm, 0.24 mm, and 0.26 mm from up to down respectively)..... 175

Figure 5.22: The average velocity distribution at rotational speed 2400 rev/min, pressure differences 700 millibars and for clearances of (0.22 mm, 0.24 mm, and 0.26 mm. .... 177

Figure 5.23: The Maximum velocity distribution at rotational speed 2400 rev/min, pressure differences 700 millibars and for clearances of (0.22 mm, 0.24 mm, and 0.26 mm). .... 178

Figure 5.24: The static pressure contours at a speed 2400 rev/min, a pressure difference 700 millibars, and for centre clearances of (a) 0.3 mm, (b) 0.34 mm, (c) 0.38 mm. .... 179

Figure 5.25: Pressure fluctuations at blower inlet at 2400 rev/min, 700 millibars, and different centre clearances (CC). .... 180

Figure 5.26: Pressure fluctuations at blower outlet at 2400 rev/min, 700 millibars, and for different centre clearances (CC). .... 181

Figure 5.27: The distribution of average-pressures at 2400 rev/min, 700 millibars and under different centre clearances. .... 182

Figure 5.28: The distribution of maximum-pressures at 2400 rev/min, 700 millibars and under different centre clearances. .... 183

Figure 5.29: The distribution of maximum negative pressures at 2400 rev/min, 700 millibars and under different centre clearances. .... 184

Figure 5.30: The relation between effective pressure zones and RMS..... 185

Figure 5.31: The peak-peak pressure amplitudes at speed 2400 rev/min, 700 millibars and different centre gaps..... 185

Figure 5.32: The relation between the centre clearances with the pressure in the blower .... 186

Figure 5.33: The average mass flow rate at speed 2400 rev/min, pressure difference 700 millibars, and different centre clearances ..... 187

Figure 5.34: Mass flow rate fluctuation at 2400 rev/min, 700 millibars and different centre gaps at inlet and outlet of the blower ..... 188

Figure 5.35: Mass flow rate fluctuation coefficient (Mf) at 2400 rev/min, 700 millibars and different centre clearances at the inlet (left) and outlet (right). .... 189

Figure 5.36: The contours of the temperature for the last revolution and at angle  $45^{\circ}$  degrees of rotation, 2400 rev/min, a difference pressure 700 millibars and for centre clearances of (a ) 0.3 mm, (b) 0.34 mm, and (c) 0.38 mm. .... 190

Figure 5.37: Outlet total temperature at 2400 rev/min, different pressure 700 millibars and different Centre clearances. .... 191

Figure 5.38: The distribution and the variation of average temperature at 2400 rev/min, 700 millibars pressure load and for different centre clearances ..... 192

Figure 5.39: The distribution and the variation of maximum temperature at a speed 2400 rev/min, a pressure difference 700 millibars pressure load and for different centre clearances ..... 194

Figure 5.40: The distribution and the variation of the minimum temperature at a speed 2400 rev/min, a pressure load 700 millibars and for different centre clearances ..... 194

Figure 5.41: The relation between the impeller diameter and centre clearance with the temperature in the blower ..... 195

Figure 5.42: The velocity vectors and the streamline contours at a rotational speed 2400 rev/min, meshing angle 45<sup>0</sup> degrees, a pressure difference 700 millibars and for centre clearances of (0.3 mm, 0.34 mm, and 0.38 mm from up to down respectively)..... 196

Figure 5.43: The average velocity distribution at a rotational speed 2400 rev/min, a pressure differences 700 millibars and for different clearances..... 198

Figure 5.44: The Maximum velocity distribution at a rotational speed 2400 rev/min, a pressure differences 700 millibars and for different centre clearances..... 198

Figure 5.45: Deviation of the mass flow rate coefficient of the blower with a pressure coefficient at different speeds and for different tip clearances ..... 200

Figure 5.46: Deviation of the mass flow rate coefficient of the blower with a pressure ratio at different speeds and for different tip clearances ..... 201

Figure 5.47: Deviation of the mass flow rate coefficient of the blower at a rotating speed 2400 rev/min, with different pressure coefficients and for different tip clearances ..... 201

Figure 5.48: Deviation of the mass flow rate coefficient of the blower at a rotating speed 1800 rev/min, with different pressure coefficients and for different tip clearances ..... 202

Figure 5.49: Deviation of the mass flow rate coefficient of the blower at a rotating speed 1200 rev/min, with different pressure coefficients and for different tip clearances ..... 202

Figure 5.50: The relation between the leakage flow rate of the blower with different pressure ratios at different speeds and for different tip clearances (TC). .... 203

Figure 5.51: Deviation of the mass flow rate coefficient of the blower with different pressure coefficients at different speeds and for different centre clearances (CC). .... 203

Figure 5.52: The relation between the leakage flow rate of the blower with different pressure ratios at different speeds and for different centre clearances (CC).....	204
Figure 5.53: The variation of the blower volumetric efficiency with a pressure coefficient at different speeds and different tip clearances.....	204
Figure 5.54: The variation of the blower volumetric efficiency with a pressure coefficient at different speeds and different centre clearances (CC) .....	205
Figure 5.55: Variation of the adiabatic efficiency of the blower with a pressure coefficient at different speeds and different tip clearances.....	206
Figure 5.56: Variation of the adiabatic efficiency of the blower with a pressure coefficient at different speeds and different centre clearances .....	206
Figure 5.57: Variation of power coefficient of the blower with a pressure coefficient at different speeds and different tip clearances.....	207
Figure 5.58: Variation of power coefficient of the blower with a pressure coefficient at different speeds and different centre clearances. ....	207
Figure 5.59: The comparison between CFD data and predicted equation of mass flow rate	209
Figure 5.60: Comparison between CFD data and the predicted equation of volumetric efficiency.....	210
Figure 5.61: Comparison between CFD data and predicted equation data of efficiency .....	211
Figure 5.62: The comparison between CFD data and predicted equation data of power consumption.....	212
Figure 6.1: 3D model-Mass flow rate spatial discretization results.....	217
Figure 6.2: 3D model-Outlet temperature spatial discretisation results .....	217
Figure 6.3: Number of points has been chosen inside the middle plane of 3D blower model for more depth analysis.....	218
Figure 6.4: The static pressure contours at a speed 1800 rpm and a pressure difference 500 millibars for different blower models .....	219
Figure 6.5: Pressure fluctuations at blower inlet and outlet at 1800 rpm, 500 millibars for different models clearances.....	220
Figure 6.6: The distribution of average-pressures at 1800 rpm, 500 millibars and for different model clearances.....	221
Figure 6.7: The distribution of average-pressures at 1800 rpm, 500 millibars in 2D/3D blower baseline models.....	222

Figure 6.8: The distribution of maximum-pressures at 1800 rpm, 500 millibars and for different model clearances. ....224

Figure 6.9: The distribution of maximum negative pressures at 1800 rpm, 500 millibars and for different model clearances. ....224

Figure 6.10: The distribution of maximum-pressures at 1800 rpm, 500 millibars in 2D/3D blower baseline models.....226

Figure 6.11: The distribution of minimum-pressures at 1800 rpm, 500 millibars in 2D/3D blower baseline models.....226

Figure 6.12: The peak-peak amplitudes at speed 1800 rpm, 500 millibars and for different models .....228

Figure 6.13: The comparison of the maximum pressure and the maximum negative pressure for different clearance models .....229

Figure 6.14: the comparison of maximum pressure amplitudes for different clearance models .....229

Figure 6.15: The average mass flow rate at speed 1800 rpm, pressure differences 500 millibars, for different clearance models. ....230

Figure 6.16: The fluctuations of the inlet mass flow rate at 1800 rpm and 500 millibars for different gap models .....230

Figure 6.17: The fluctuations of outlet mass flow rate at 1800 rpm, 500 millibars for different gap models .....231

Figure 6.18: Mass flow rate fluctuation coefficient ( $M_F$ ) at a speed 2400 rpm, a pressure difference 700 millibars and for different model clearances at the inlet (left) and outlet (right). ....231

Figure 6.19: The average mass flow rate at speed 1800 rpm, pressure differences 500 millibars, for different clearance models. ....232

Figure 6.20: The fluctuations of the inlet mass flow rate at 1800 rpm and 500 millibars for 3D/2D models .....233

Figure 6.21: The fluctuations of outlet mass flow rate at 1800 rpm and 500 millibars for 3D/2D models .....233

Figure 6.22: The temperature contours for the last revolution at angle  $45^0$  rotation degrees, a speed 1800 rpm and a difference pressure 500 millibars for different clearance models.....234

Figure 6.23: Outlet total temperature at 1800 rpm, different pressure 500 millibars and different model clearances. ....235

Figure 6.24: The distribution and the variation of average temperature at 1800 rpm and 500 millibars pressure load for different clearance models. ....236

Figure 6.25: The average temperatures at 1800 rpm and 500 millibars for 2D/3D blower baseline models.....237

Figure 6.26: The distribution and the variation of maximum temperature at 1800 rpm and 500 millibars pressure load for different clearance models. ....238

Figure 6.27: The distribution and the variation of minimum temperature at 2400 rev/min, pressure load 700 millibars and different model clearances. ....239

Figure 6.28: The maximum temperatures at 1800 rpm and 500 millibars for 2D/3D blower baseline models.....240

Figure 6.29: The minimum temperatures at 1800 rpm and 500 millibars for 2D/3D blower baseline models.....240

Figure 6.30: The comparisons of the average, the maximum and the minimum temperatures for different clearance models of the Roots blower.....241

Figure 6.31: The velocity vector and streamline contours at a rotational speed 1800 rpm, a meshing angle  $45^{\circ}$  of rotation degrees and a pressure differences 500 millibars within mode 1, model 2, and model 3 from up to down respectively.....242

Figure 6.32: The average velocity distribution at rotational speed 1800 rpm and pressure difference 500 millibars for different clearance models. ....244

Figure 6.33: The Maximum velocity distribution at rotational speed 1800 rpm and pressure difference 500 millibars for different clearance models. ....244

Figure 6.34: The average velocities at 1800 rpm and 500 millibars for 2D/3D blower baseline models.....246

Figure 6.35: The maximum velocities at 1800 rpm and 500 millibars for 2D/3D blower baseline models.....246

Figure 6.36: The Pressure Fluctuations of the baseline blower model (M2) in Frequency Domain at a speed 1800 rpm and a pressure difference 500 millibars .....250

Figure 6.37: The Pressure Fluctuations of the blower model (M1) in Frequency Domain at a speed 1800 rpm and a pressure difference 500 millibars.....253

Figure 6.38: The Pressure Fluctuations of the blower model (M 3) in Frequency Domain at a speed 1800 rpm and a pressure difference 500 millibars.....	256
Figure 6.399: The maximum pressure fluctuation amplitudes in the Roots blower for 3 models at frequency 120.13 Hz .....	261
Figure 6.400: The maximum pressure fluctuation amplitudes in the Roots blower for 3 models at frequency 60.07 Hz .....	261
Figure 6.411: The maximum pressure fluctuation amplitudes in the Roots blower for 3 model at frequency 180.2 Hz .....	263

## Table of Tables

Table 3.1: The main components of (Model HRBV613) blower system .....	43
Table 3.2: The main specifications of Roots blower type .....	46
Table 3.3: The main specifications of orifice plate.....	48
Table 3.4: The specifications of Differential Pressure transducer .....	49
Table 3.5: The main specifications of pressure transducers .....	50
Table 3.6: The main specifications of Temperature Sensors.....	51
Table 3.7: Rotational speeds and pressure loads have been used in experimental measurements.....	56
Table 3.8: The uncertainty of some measurements .....	62
Table 3.9: Orifice plate constants .....	63
Table 3.10: The experimental results of the mass flow rate at different speed and for different pressure load condition .....	64
Table 3.11: The experimental calculation results of volumetric efficiency and adiabatic efficiency at a different speed and for different pressure load condition. ....	66
Table 3.12: The boundary conditions used for the Roots blower simulation models.....	77
Table 3.13: The running conditions used for the Roots blower model according to the mesh sensitivity analysis which are provided later in the chapter 4 .....	77
Table 3.14: The boundary conditions of the simulations required in chapter 4 to carry out the verification and the validation. ....	78
Table 3.15: The boundary conditions to carry out the simulations required in chapter 4 .....	79
Table 3.16: the boundary conditions and geometry configurations to carry out the simulations and obtain the numerical results required in chapter 5. ....	79
Table 3.17: the boundary conditions and geometry configurations to carry out the simulations and obtain the numerical results required in chapter 6 .....	81
Table 4.1: The relation between the mass flow rate of the blower and a pressure ratio at different blower speeds .....	89
Table 4.2: Non-dimension relations have been used to develop the mass flow prediction correlation .....	97
Table 4.3: the non-dimension relations have been used to prediction correlation develop the power consumption.....	98

Table 4.4: Mass flow rate spatial discretisation results .....	101
Table 4.5: Outlet temperature spatial discretization results .....	102
Table 4.6: Mass flow rate temporal discretization results .....	103
Table 4.7: Outlet temperature temporal discretization results .....	104
Table 4.8: Roots blower model specifications .....	106
Table 4.9: The maximum and minimum pressures at 1800 rev/min and under different discharge pressures in Pascal. ....	117
Table 4.10: The distribution and the variation of the temperature at speed 1800 rev/min and for different discharge pressures .....	126
Table 4.11: The distribution and the variation of the velocity at a speed 1800 rev/min and under different discharge pressure conditions inside the blower from the inlet to the outlet. ....	130
Table 4.12: The max-pressures and the min-pressures at 700 millibars and under different rotational speeds.....	136
Figure 4.13: The average and the fluctuation coefficient of the mass flow rate at different speeds and 700 millibars pressure difference .....	141
Table 4.14: The distribution and the variation of the temperature inside the blower from the inlet to the outlet at a discharge pressure of 700 millibars and under different rotational speeds.....	146
Table 4.15: The distribution and the variation of the average velocity inside the blower from the inlet to the outlet at a pressure difference of 700 millibars and under different rotational speed. ....	151
Table 4.16: The distribution and the variation of the maximum velocity inside the blower from the inlet to the outlet at a pressure difference of 700 millibars and under different rotational speed. ....	152
Table 5.1: Roots blower models specifications. ....	158
Table 5.2: The average pressure at a speed 2400 rev/min, a pressure difference 700 millibars, and for different tip clearances. ....	163
Table 5.3: The maximum and the minimum pressure at 2400 rev/min, 700 millibars, and for different tip clearances in Pascal.....	164
Table 5.4: The distribution, and the variation of the average temperature at a speed 2400 rev/min, a discharge pressure 700 millibars, and for different tip clearances. ....	172

Table 5.5: The distribution, and the variation of the maximum and the minimum temperatures at a speed 2400 rev/min, a discharge pressure 700 millibars, and for different tip clearances. .....	173
Table 5.6: The distribution and the variation of the velocity at a rotational speed 2400 rev/min, a pressure difference 700 millibars and for different clearances.....	177
Table 5.7: The average pressure, at 2400 rev/min, 700 millibars, and under different centre clearances in Pascal.....	181
Table 5.8: The maximum positive and negative pressures, at 2400 rev/min, 700 millibars, and under different centre clearances in Pascal.....	182
Table 5.9: The Root Mean Square (RMS) and the peak to peak amplitudes of the pressure at a speed 2400 rev/min, a pressure difference 700 millibars and for different centre clearances. .....	184
Table 5.10: The average temperature, at 2400 rev/min, 700 millibars, and under different centre clearances .....	192
Table 5.11: The variation, and the distribution of the maximum and the minimum temperatures at a rotational speed 2400 rev/min, a discharge pressure 700 millibars, and for different centre clearances. ....	193
Table 5.12: The distribution and the variation of the velocity at a speed 2400 rev/min, a pressure differences 700 millibars and for different centre clearances.....	197
Table 6.1: Roots blower models specifications .....	216
Table 6.2: 3D model-Mass flow rate spatial discretisation results .....	216
Table 6.3: Outlet temperature spatial discretization results.....	217
Table 6.4: The average pressure at 1800 rpm, 500 millibars for different model clearances. .....	221
Table 6.5: The average pressure in 2D/3D baseline models at 1800 rpm and 500 millibars.	222
Table 6.6: The maximum and the minimum pressures at 1800 rpm, 500 millibars for different model clearances in Pascal.....	223
Table 6.7: The maximum and the minimum pressures at 1800 rpm and 500 millibars for 2D/3D blower baseline models.....	225
Table 6.8: The peak to peak amplitudes at 1800 rpm, 500 millibars for different model clearances.....	227

Table 6.9: The distribution, and the variation of the average temperature at a speed 1800 rpm, and a discharge pressure 500 millibars for different clearance models. ....	235
Table 6.10: The average pressure in 2D/3D baseline models at 1800 rpm and 500 millibars .....	236
Table 6.11: The distribution, and the variation of the maximum and the minimum temperatures at a speed 1800 rpm and a discharge pressure 500 millibars for different clearance models. ....	238
Table 6.12: The maximum and the minimum temperatures at 1800 rpm and 500 millibars for 2D/3D blower baseline models. ....	239
Table 6.13: The distribution and the variation of the velocity at a rotational speed 1800 rpm, and a pressure difference 500 millibars and for different model clearances .....	243
Table 6.14: The average and the maximum velocities at 1800 rpm and 500 millibars for 2D/3D blower baseline models in m/s. ....	245
Table 6.15: The maximum pressure fluctuation amplitudes at various frequencies and different points within the Roots blower baseline model (M2) in Pascal .....	251
Table 6.16: The maximum pressure fluctuation amplitudes in the Roots blower model (M1) in Pascal .....	252
Table 6.17: The comparison of maximum pressure amplitudes between M2 and M1 in Pascal .....	254
Table 6.18: The maximum pressure fluctuation amplitudes at in the Roots blower model (M3) in Pascal. ....	255
Table 6.19: The comparison of maximum pressure amplitudes between M2 and M3 in Pascal. ....	257
Table 6.20: The maximum pressure fluctuation amplitudes in the Roots blower for 3 models at frequency 120.13 Hz in Pascal.....	260
Table 6.21: The maximum pressure fluctuation amplitudes in the Roots blower for 3 models (M 1, M 2, and M3) at frequency 60.13 Hz in Pascal. ....	262
Table 6.22: The maximum pressure fluctuation amplitudes in the Roots blower for 3 models (M 1, M 2, and M3) at frequency 180.13 Hz in Pascal.....	263

## Abbreviations

$T_{in}$	Total temperature at the inlet of the blower (K <sup>0</sup> )
$T_{out}$	Total temperature at the outlet of the blower (K <sup>0</sup> )
$p_{out}$	Total pressure at the inlet of the blower (Pa)
$p_{in}$	Total pressure at the outlet of the blower (Pa)
$\dot{V}$	Volume flow rate, m <sup>3</sup> /s
$\dot{m}$	Mass flow rate, kg/s
a	Sonic velocity, m/sec
A <sub>0</sub>	Total leakage area under cold conditions
A <sub>E</sub>	Leakage Area (m <sup>2</sup> )
C	Swept volume (m <sup>3</sup> /rev)
D	Diameter of the rotor (m)
d	Clearance gap (mm)
K	Constant
M	Mach number
N	Non-dimensional rotational speed
P	Power
p	Static pressure (Pa)
p <sub>d</sub>	Differential pressure, (Pa)
p <sub>t</sub>	Total pressure (Pa)
Q	Flow Rate (m <sup>3</sup> /sec)
Q <sub>d</sub>	Displacement or geometric flow delivered, in (m <sup>3</sup> /sec)
Q <sub>s</sub>	Slip through the clearance, (m <sup>3</sup> /sec)
R	Gas constant (J/kg. K)
Re	Reynolds Number

T	Static temperature (k)
T <sub>t</sub>	Total temperature (k)
V	Flow Velocity (m/sec)
$\Delta h_0$	stagnation enthalpy rise
$\Delta T_0$	stagnation temperature rise
w	Width of clearance, in (m)
W	Work (J)
$\Delta P$	Pressure Drop (Pa)
l	Length of clearance, in (m)
k	Specific heat ratio
K	Differential expansion coefficient

## Symbols

$\rho$	Density (Kg/m <sup>3</sup> )
$\mu$	Dynamic Viscosity (Pa-sec)
$\gamma$	Specific heat capacity
$\eta$	Efficiency of the blower
$\theta$	Angular Position (°)
$\theta = \frac{p_{out}}{p_{in}}$	Pressure ratio
$\phi = \left(\frac{T_{out}}{T_{in}}\right)$	Temperature ratio
$\eta_v$	Volumetric efficiency
$\nu$	Absolute viscosity, N-sec/m <sup>2</sup>
$\psi$	a constant for the particular rotor geometry

## Subscripts

ave	Average
-----	---------

Max	Maximum
Min	Minimum
r	Reference condition
e	experimental
t	theoretical
in	Inlet
out	Outlet
01	Stagnation state at the inlet of the blower
02	Stagnation state at the outlet of the blower

## **Chapter 1**

### **Introduction**

Roots blowers are positive displacement machines used to move or deliver the fluids from low pressure to high pressure as pressure devices or vice versa as vacuum devices. The operations of these devices are achieved by rotating action using mechanical or electrical energy sources. These type of machines are an essential part of many industries. It is vital initially to understand the structure and the characteristics of the internal flow before efficiently analysing the underlying complex flow phenomena occurring in Roots blower. Therefore, this chapter provides a preliminary discussion regarding flow field in Roots blower. Furthermore, the present chapter describes in details of the Roots blower components and the performance parameters that need consideration.

## 1.1 The history of Roots blower

The Roots-type blower was invented 1848 by G. Jones in Birmingham, England and the name of this machine is related to the American inventors; brothers Francis and Philander Marion Roots, who patented the basic design in 1860 as an air blower for use in blast furnaces and other industrial applications (Carbutt, 1877). In 1900 a Roots-style blower was included by Gottlieb Daimler in the design of the engine. The rotary blower progressed from a design of the water wheel invented by the Roots brothers for their woollen mill. The machine is composed of two counter-rotating wooden blades (or rotors) within a cylinder. The course of water flow is directed through the machine and forces the rotors to revolve, rotating the shaft and powering the machine until the point that the wood swelled and the blades jammed. After it had been reconstructed and arranged for new activity, the action of the rotors forced an amount of air within the device. The siblings concluded that they have a superior blower than a water wheel, which stimulated the advent of the globally recognised rotary positive-displacement blower (occasionally indicated to as the "Roots blower") (Reuleaux, 2013). Today there are various remarkable blower producers around the world. Its main significant utility is in foundry vault heaters. The initial foremost use was in foundry cupola furnaces, and the first two trial machines were tested in foundries. Several blowers were later made for different services and applications. In 1872, the Engineering Journal recorded a large blower for the West Cumberland Hematite Iron Works in England. Another main application was in mine ventilation, a generally new field. Rotational blowers comprised the most prominent establishments of the nineteenth century. By 1870, some were at that point being used for ventilating mines of the Comstock Lode. Two of the biggest blowers ever fabricated were introduced in England in 1877. The rotor had a radius of 12.5 feet, 13 feet wide, and blower flow rate of 200,000 ft<sup>3</sup>/min. A London engineering journal inferred that the positive displacement blower was the greatest production of its kind ever seen (Air & Rollins, 1961). Roots machines became widely adopted in different industrial applications due to simplicity and capability to move large volumes of fluids. Further improvement have been achieved with the development of higher speed versions and pressure differences, to include other new applications such as automotive, maritime and, aerospace (Masuda et al., 1988; Ritchie, 1966; RYDE, 1942; Tryhorn, 1956; Ware & Wilson, 1929). The other uses are in pneumatic conveying, air circulation and agitation of fluid, supercharging and scavenging of large diesel motors, and for different vacuum systems (Patterson & Ritchie, 1969; Priede, 1966).

## **1.2 Roots blower Applications and Advantages**

Roots Blower is widely used in applications where a large volume of gas is required to move across a relatively small or moderate pressure differential. The applications include several industrial processes such as mine ventilation, pneumatic conveying, aeration and agitation of liquid. Also, it includes supercharging and scavenging of large diesel engines, cryogenics, and water treatment plant, electrical and electronic industries and for various vacuum applications. Moreover, Single-stage machines are used for low-pressure applications, and multistage designs are used for the blowers working with average and higher-pressure ratios. Furthermore, other advantages of this blower are simple construction, good volumetric efficiency and are most effective in moderate compression ratios from (1.1 to 2). Since, the rotors rotating within the blower with finer gaps, the lubrication of internal parts is not required. Thus, the fluid is delivered free from the oil. The flow rate in this type of blower is reliant, mainly on the operational speed and the blower delivers, nearly, a constant rate of flow independent of the outlet pressure conditions.

Because of the above-mentioned design features of this blower, the following main characteristics are concluded (Salaskar & Inamadar, 2012; Umraht, 1998):

- The flow rate mainly depends on operational speed.
- The operating power of the blower is mainly reliant on the total pressure across it.
- The inlet and outlet pressures are determined by the conditions of the system.
- The rise of the outlet and the blower temperatures mainly depend on the differential pressure across it.

## **1.3 Roots blower design and operation**

Significant developments have been made in the manufacture and the design of the main parts of this type of blower in recent years, for example, the bearings and the impellers. As a result, both the reliability and the performance of this blower are improved considerably and resulting in wide use of it in both pressure and vacuum applications. Also, there are several geometric and flow relevant variables that affect its operation and therefore their performance. If the internal gaps between the two impellers themselves and between the impellers and the casing are small, the volumetric and the adiabatic efficiencies can maintain high over a wide range of operation conditions. The advanced manufacturing machines and their tools nowadays allow

the most complex profiles of the Roots blower impellers to be manufactured with high tolerances at a reasonable cost. Together with the developed rolling bearings, has led to considerable enhancements in the performance and the reliability of the Roots blower.

Roots blower mainly consists of five main parts, namely the rotors, chamber, inlet, outlet and casing as shown in figure 1.1. It consists of two rotors with 2-lobes or more for each rotor as shown in figure 1.2; one is a driving rotor, which is driven by the external driving source connected directly to the shaft while the rotation of synchronous gears drives the second rotor. Hence in the process, both rotors rotate at equal speed and in the opposite direction, one in clockwise while the other in a counter-clockwise direction as shown 1.1. Also, there are finite clearances between rotors, and between the rotors and the housing.

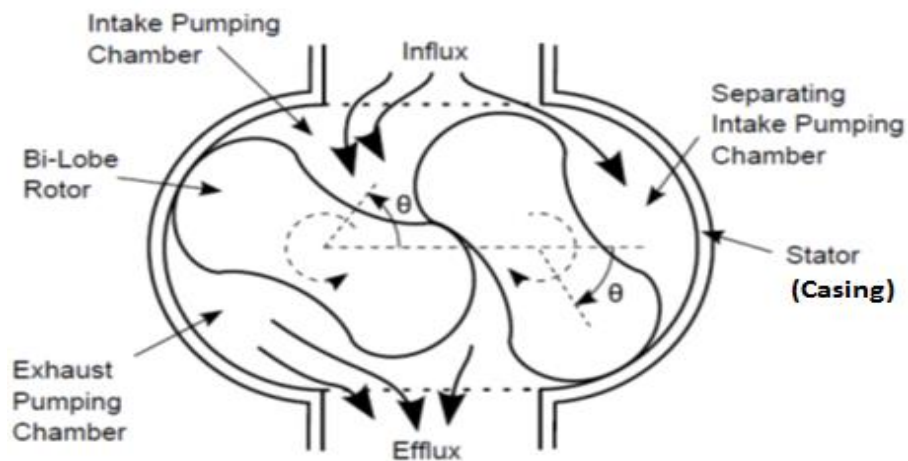


Figure 1.1: Cross-sectional View of a Roots Blower with Twin Bi-lobe Rotors (Choi, 2013)

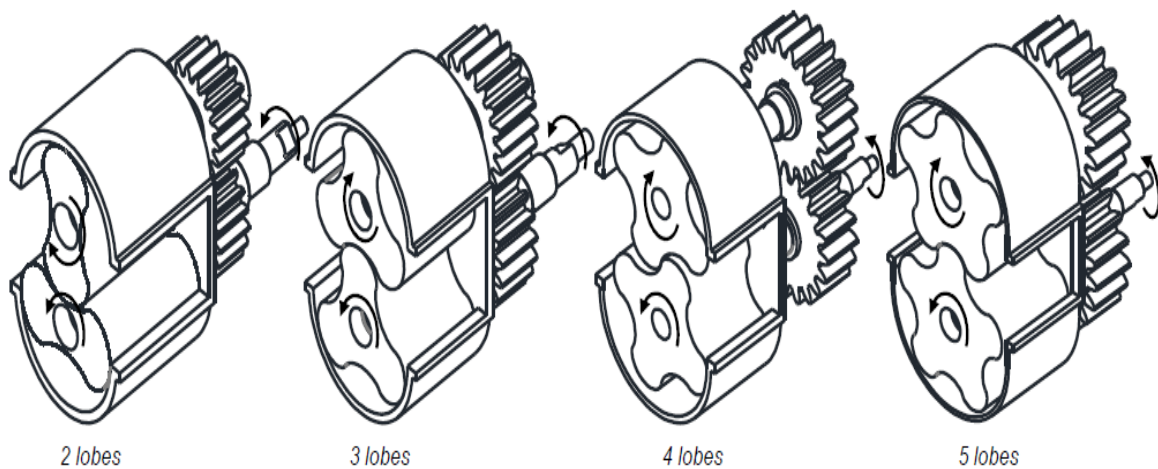


Figure 1.2: Roots Blower consists of two rotors with 2-lobes or more for each rotor (Thai & Trung, 2015)

There is no change in the volume of the air in the blower, as the rotor turns, fluid is drawn inside at the inlet of the blower and forced to the discharge side against system pressure as illustrated in figure 1.3 (Choi, 2013; McDougald, Imrie, & Cole, 1974). The impellers rotating and meshing with positive tolerance by timing gears. Lubrication of inside parts is unnecessary, therefore the delivered fluid is free of oil. Compression takes place by backflow each time the impeller tip uncovers the outlet port of the blower. Since the impellers can be driven at high rotational speeds by synchronous gears or connected directly to electric motors, high flow rates of fluid can be delivered. The generated pressure is generally less than 100 kPa in a single stage. (Barber, 1997).

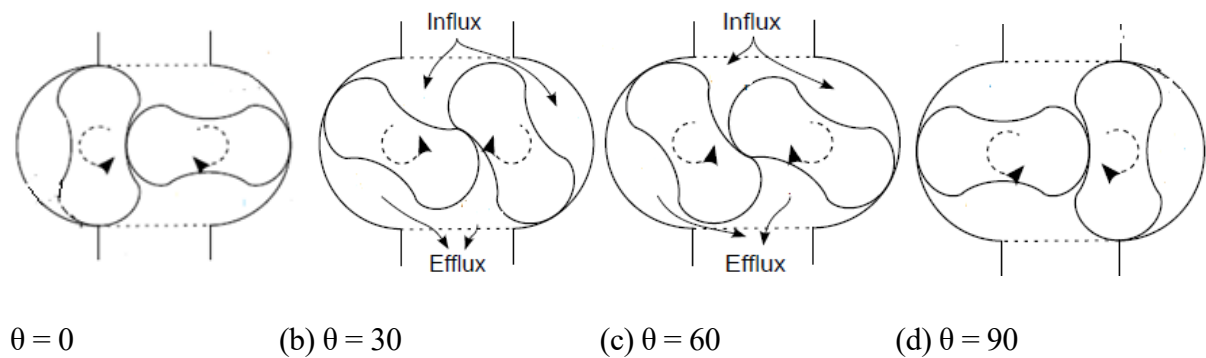


Figure 1.3: Blower Operating Principle

The important dimensions representing a Roots blower include dimensions of a bi-lobe rotor having convex ends and concave mid-sections profiles, a stator (casing), and inlet and outlet ports as shown in figure 1.4. The intermeshing of the twin rotors is permitted by the conforming convex and concave sections (Choi, 2013). There are many types of rotor profile such as Involute, Circular, Hypocycloidal, and Epicyclical and elliptical or combination of them.



### **1.4.1 Temperature variation considerations**

The increase in temperature results from the variation of inlet temperature and discharge temperature due to the heat being generated from the compression. Rotors are influenced interchangeably by the inlet and subsequently through the discharge temperature (Karassik et al., 1986). The casing is affected by the ambient temperature present on the outer surfaces. As a result, the casing would have a lower temperature when compared to the rotors. Also, rotors would tend to expand more than the casing; this would result in a different expansion that causes the reduction of the end clearance among the rotors and the casing. Temperature would continue to increase because of the newly increased compression ratio because of expansion. Extreme increase in temperature creates the end clearances to reduce, and thus, rotor-casing contact would occur, which ultimately results in a rub that causes failure of the blower (Umrath, 1998; Yoshimura, 2007).

Numerous issues arise if the outlet temperature rises to a degree higher than the suggested level. Initially, the heat transmission will cause the lubricant to deteriorate when the temperature is higher than the limit (Karassik et al., 1986). Excessive temperature rise causes the lubricant to decrease in quality and formation of carbon, which creates additional issues for the oil flow and rubbing surfaces. Increased temperature may cause a reduced lifespan of bearings and gears. Ultimately, seal breakdown may take place as the components within the seal is exposed to greater thermal stress (Umrath, 1998; Yoshimura, 2007). Furthermore, this could cause damage to components and thermal distortion, which may result in misalignment and maybe complete breakdown.

### **1.4.2 Pressure variation considerations**

There are particular issues relevant to surpassing the design ratings of pressure variation. Greater pressure variations result in greater shaft stress that decreases the life of the bearings and gears. Therefore, restrictions are required to circumvent excessive deflections and potential shaft fractures. In addition, the torque on the shaft of the rotary blower will directly vary with the pressure variations (Karassik et al., 1986). The deviations resulting from increased pressure variations cause the clearances on the inlet region located between the rotors and casing to start to decrease. Pressure would be higher on the side of the discharge, and this would force the rotors to deflect upon the inlet. If deflection results in the available clearances to be decreased, contact can be occur and that may result in friction and subsequently, failure (Umrath, 1998).

Undoubtedly, a positive pressure pulse exists throughout the rotation at a frequency of four or six times, which is dependent on the number of lobes in each rotor. Furthermore, this pulse corresponds to the pressure variations and results in noise and vibration. A rise in pressure variations results in a corresponding increase in noise and vibration, which must be maintained within appropriate limits. Excessive amounts of noise and vibration can cause destruction (P. X. Huang, Yonkers, & Hokey, 2014).

### **1.4.3 Rotational speed considerations**

All blowers have restrictions for the acceleration of the rotation of the shafts. Displacement and torques corresponding to the rates of revolutions have an impact on the life of bearings and gears. Furthermore, the noise and vibration can rise to a possibly harmful degree, when the shaft speed rate is permitted to exceed a reasonable level. Additionally, the increase of angular speed causes the rise in stress levels within the rotating components approximately to the square of the speed. Higher operating speeds can cause the components to deteriorate (Umrath, 1998; Yoshimura, 2007)

### **1.4.4 Flow through leakage paths (slip) considerations**

Slip (leakage), in regards to blowers, can be defined as the amount of flow that is returned from the high pressure zone at the outlet to the low pressure zone at the inlet of the blower. The leakages in Roots blower play an important role because they influence the process efficiency by affecting the mass flow rate and therefore the volumetric efficiency (Stosic et al., 2005).

The Root blowers' clearances must be kept based on the design and manufacturing capabilities. The leakage paths or clearances can be found between the two rotors themselves, between rotors and the cylinder and head-plates. These clearances or leakage paths, together with pressure variations, permits a specific quantity of air to pass back from the outlet to inlet (Burmistrov, Salikeev, Bronshtein, Fomina, & Rayko, 2015). Furthermore, particular implementations have demonstrated that roughly two-thirds ( $2/3$ ) of the slip exists between the rotors and rotors/casing while roughly one-third ( $1/3$ ) occurs at the ends of the rotors. Internal leakage that has an important effect on performance and maintaining efficiency is an inherent issue of the Root blower's design (Türk & Verhülsonk, 2006).

**1.4.5 Considerations of compressibility:**

When the fluid flow is compressible, the fluid density varies with its pressure. Compressible flows are generally at high-speed flows with Mach numbers greater than about 0.3

The total temperature,  $T_t$ , is a key parameter for running compressible analyses (Dixon & Hall, 2013):

$$T_t = T \left( \frac{P_t}{P} \right)^{\frac{\gamma-1}{\gamma}} \dots\dots\dots (1.1)$$

The total pressure,  $P_t$ , is another useful quantity for running compressible analyses.

$$\frac{P_t}{P} = \left( \frac{T_t}{T} \right)^{\frac{\gamma}{\gamma-1}} \dots\dots\dots (1.2)$$

$$P_t = P \left( \frac{\rho_t}{\rho} \right)^{\frac{1}{\gamma}} \dots\dots\dots (1.3)$$

**1.4.6 Working pressure considerations**

Generally, the maximum working pressure is twenty-five psi-g (25 PSI-gauge) for a standard PD blower, which is essentially based on the outcome of the casing design. Therefore, surpassing this design limit can cause damaging distortions, interior rub, and maybe a casing fracture (Umrath, 1998).

**1.5 Roots blower Performance factors**

Performance factors of the blower can be explained using the following parameters.

**1.5.1 Pumping Speed (Q):**

The volumetric flow rate at the inlet of the blower is one of the main performance factors for Roots blower. It is often measured in m<sup>3</sup>/sec, m<sup>3</sup>/h, and L/sec and L/min. Blower speed of a particular pump varies as the type of fluid varies (Verma, 2014).

**1.5.2 Volumetric Efficiency**

Volumetric efficiency  $\eta_{vol}$  is the ratio of the actual volume flow rate to theoretical output flow. It is an indication that blower has the ability to handle more flow rate under a given differential pressure (Karassik et al., 1986).

### **1.5.3 Power of Roots blower system**

The theoretical power or the required power independent of mechanical friction power losses, and fluid frictional power. The useful output power  $HP_{out}$  is less than  $HP_{hyd}$  by an amount  $HP_s$  loss due to leakage  $Q_s$  through the clearances (Karassik et al., 1986).

### **1.5.4 Geometry:**

The volumetric flow capacity of the blower greatly depends on the empty space in the Roots blower. It is because of that the volumetric flow through the blower is solely dependent on the volume of the casing of the blower and the volume of the rotor profile. If the volume of the rotors is large, the flow volume will be low and vice versa (as the volume of impellers increases the volumetric flow decrease) (Verma, 2014).

### **1.5.5 Clearance:**

It is crucial to maintaining clearance between the case and the rotor and between rotors themselves so that the losses due to a frictional force can be minimized. If there is no clearance, mechanical parts will make contact, and as a result, rotational speed will become less than the intended speed. Also, the amount of heat will be dissipated, which then leads to heating of the equipment and surrounding of the blower system. Tear-wear can also occur, and its consequences can be severe to the foundation of the blower due to the massive amount of vibration (Türk & Verhülsdonk, 2006).

### **1.5.6 Inlet-outlet cross-section:**

Inlet-outlet cross-section is another parameter that plays a vital role in the flow analysis of the Roots blower. For the inlet to be equal to the distance between the two rotor axes, the volumetric flow would be maximum, but at the same time, backflow is also increased. More so, if the inlet cross-section is reduced a little from both sides, then volumetric flow is reduced by a small amount, but backflow through to the blower is minimised by considerable amount (Verma, 2014).

Furthermore, the main feature of Roots blower is the provision of reasonably constant inlet volumetric flow as well as high volumetric efficiency with different differential pressure conditions. The pressure is not formed within the blower but is established through the systems' demand. The discharge pressure will vary by differing of the pressure load condition of the

system and its flow rate (Yoshimura, 2007). Relief valves are there to alleviate pressures during flow restriction so that the pressure could increase over the blower's design limits. The volume is approximately equivalent to the pressure except for a minor rise within the slip during the increase in pressure.

The horsepower would approximately be proportional to the pressure variation and shaft speed (rev/min). Within any pressure value, the HP would be proportional to the rev/min (Umrath, 1998). HP is proportional to pressure variation when rev/min is constant, resulting in the value of torque to be varied according to the pressure variation. Such a unit is being termed "constant torque" machine, where its functions are to decide the required drivers' attributes particularly variable speed motors. The roots blower attributes are ideal for low-pressure applications and vacuum service. It supplies air that is free of oil and drivers can be accurately sized according to the necessary vacuum or pressure (Yoshimura, 2007).

## **1.6 The Motivation**

The flow field conditions inside the Roots blower and at the inlet and the exit are non-uniform. The temperature, pressure, and velocity are vary significantly during the blower operation. These non-uniformities are a function of the Roots blower flow arrangement and geometry. Hence, it is an important but challenging issue to map the fluid flow inside the blower during wide operating conditions. In recent years, Roots blower development has been focused on improving volumetric efficiency, reducing power consumption and developing quieter blowers, which are the basic needs of current and future blower technology. Roots blower has complex flow behaviour. Understanding this behaviour is very important for the analysis and design of such a high-performance product [3].

Development approaches for design and analysis of Roots blower have been depended on the extensive use of an experience database, empirical and semi-analytical correlations along with extensive testing programs. Such approaches historically have been reasonably successful in developing the blowers based on proven analysis and design concepts, but, the development time and cost involved in these traditional ways are nowadays considerable. For this investigation and characterisation, experimental approach is expensive regarding both cost and time. Advances in computational fluid dynamics (CFD) are one of the reasonable alternative research approaches.

The motivation for this research is to conduct detailed investigations on some essential parameters and aspects of flow inside Roots blower under the transient conditions of operation. Because, the characterisation and understand of flow field inside the Roots blower is quite essential in order to improve existing or develop new design of Roots blower performance. Also, the analysis of the effect of pressure differences, rotational speeds and gap change on the variation and the distribution of other performance parameters such as pressure, temperature and velocity within the blower are required. Moreover, to conduct the in-depth analysis of the variation and the distribution of the internal flow and related parameters within the blower, and Non-dimensional analysis of performance parameters and develop sim-empirical correlations for performance factors of Roots blower. Furthermore, to develop of new clearance model of Roots blower. To establish the effect of the clearance size on pressure fluctuations in both time and frequency domain with clearance variation inside the blower. To develop a new methodology for detection of the change of clearance size inside Roots blower.

## **1.7 The organisation of the Thesis**

According to the discussions that have been carried out for the present research in the earlier sections, this thesis has been arranged into seven chapters.

**Chapter 1:** Deals with the introduction to the Roots blower in more detail which provides an overview of the mechanism and the flow field characteristics in the Roots blowers. Based on this overview, the description of motivation to carry out this research is done, which enumerates the aims of the present investigation and recognises essential areas to be reviewed in Chapter 2.

**Chapter 2:** Consists of an in-depth review of the studies that are carried out in the field of Roots blower applications. It includes the review of available literature concerning the Performance characterisation of Roots blower. Also, a review of the published literature for the key improvements of the Roots blower performance using geometrical variations. It additionally comprises of the literature review carried out on the unsteady flow characteristics with clearance variation inside the Roots blower. Furthermore, details of the scope of research are provided in the form of specific research objectives.

**Chapter 3:** Contains the details of the experimental facility that has been used to investigate the effect of rotational speeds and pressure loads on the flow field and Roots blower performance parameters. The procedures and the equations that have been used for the calculations of analytical and the experimental results. Also, the principles of Computational Fluid Dynamics which include the CFD modelling of the Roots blower, as well as the geometry and meshing techniques that are used for the flow domain of the Roots blower have been discussed and determined. Moreover, it includes the settings of the solver and the boundary conditions that have been defined to resolve the flow domain. Furthermore, the detailed simulations that have been conducted in this study.

**Chapter 4:** Comprises the performance characterisation and the flow structure using results obtained from experiments and numerical simulations have been conducted on the Roots blower baseline model. The effect of rotational speed and the differential pressure have been analysed in detail to establish the effect of the parameters mentioned above on the variation and distribution of the pressure, the temperature and the velocity fields in Roots blower. Furthermore, to formulate the influence of these parameters on Roots blower performance, the flow within the blower has been analysed under various flow conditions. Moreover, a non-dimensional analysis to identify fluid dynamic parameters that influence the Roots blower performance has also been included. Also, the empirical models and correlations that can be used to characterise the flow in Roots blower and for the prediction of blower performance factors such as mass flow and power consumption have been developed.

**Chapter 5:** This chapter includes the quantitative evaluation of the flow characteristics and the key improvements of the Roots blower performance using geometrical variations. The effect of rotor diameter (tip clearance) and the effect of centre clearance have been analysed in detail to establish the influences of the parameters mentioned above on the pressure distribution, on the temperature field and the velocity field in Roots blower. Also, to formulate the influence of these parameters on Roots blower performance, the flow of various geometric variables has been analysed under different flow conditions. Furthermore, it includes a non-dimensional analysis to recognise the geometric and fluid dynamic parameters that influence the Roots blower performance using CFD simulations. Also, semi-empirical models and correlations that can be used to characterise the flow field within Roots blower and for the prediction of blower

performance factors such as mass flow and power consumption have been developed using numerical results to reduce development time and cost.

**Chapter 6:** It includes the unsteady flow characteristics and the clearance variation effects inside the Roots blower. The effects of rotor size and the clearances inside the blower have been analyzed in detail to formulate the influence of these parameters on Roots blower performance during the transient state, the flow of various rotor geometry and clearance variations has been analysed under different flow conditions. The analysis has been performed using FFT techniques. Furthermore, the diagnostics of flow fields within the blower using pressure and temperature fluctuations have been highlighted.

**Chapter 7:** Summarises the work undertaken in this thesis and the conclusions of the outcomes of this research, obviously stating the goals achieved and accomplishments to enhance the current knowledge about Roots blower regarding both the characteristics and the key improvements of the Roots blower performance. Also, suggestions for future work are provided. The description of research project has been done, while the extensive literature reviews have been carried out to formulate the objectives for this research study which will be discussed in the next chapter.

## **Chapter 2**

### **Literature review**

The in-depth review of existing literature has been conducted in this chapter, which will highlight the knowledge gaps in the available literature after getting detailed information related to the parameters that affect the Performance of Roots blower in the previous chapter. It includes the published works regarding the performance characterisation and the flow structure of the Roots blower, determination of the characteristics and the key improvements of the Roots blower performance using geometrical variations and unsteady flow characteristics with clearance variation inside the Roots. Based on the knowledge gaps found in the literature review, the scope of research has been defined, and research objectives of this study have been formulated.

## 2.1 Quantitative evaluation of Performance characteristics of a Roots blower

### Baseline

In the design of Roots blower machines, the thermodynamic process inside a blower mostly depends on the flow field characteristics. The blower characterisation not only determines the pressure, temperature and velocity distributions within the blower but also the influences of different operational condition on the blower performance. Severe operational conditions can lead to blower failure. Therefore, thermodynamic blower limitation must be considered in the design process to ensure that the machine performance meets the required application.

In this section, a survey of the literature of the flow characteristics analysis of Roots blower is presented. It can be categorised into analytical, experimental, and numerical methods. Hence, an understanding of the flow distribution in Roots blower machines and flow characteristics is essential to improve blower performance. The problems of fluid mechanics are normally studied using dimensional analysis. However, the review of existing literature also reveals that the literature describing how the rotational speed and pressure difference affect the variation and the distribution of the flow parameters such as pressure, temperature, and velocity in the blower is quite limited. Also, The dimensional analysis and translates the experimental investigation into a form of systematic empirical approach, which allows the investigation of one prototype to be applied to other models having geometric and dynamic similarities is very limited. More research needs to be carried out on this topic and is the first aim of the present study.

Cole et al. (Brynych, Macek, Vitek, & Cervenka, 2013) carried out theoretical and experimental studies on the flow fields of a two-lobe Roots blower to analyse the flow characteristics at different operating conditions and a wide range of rotational speed. Also, the authors have developed some thermo-dynamic expressions for the non-dimensional performance of the Roots bower model system under certain assumptions which they consider the effect of leakage flows across the whole blower. The expressions include the temperature ratio ( $\phi$ ), pressure ratio ( $\theta$ ), volumetric efficiency ( $\eta_v$ ), isentropic efficiency ( $\eta_{is}$ ) and work input ( $w$ ) as illustrated below;

$$\phi = \frac{T_{out}}{T_{in}} = 1 + \frac{1}{\eta_v} \cdot \frac{k-1}{k} \cdot (\theta - 1), \quad \eta_{is} = \frac{\frac{k}{k-1} \eta_v \cdot \left( \theta^{\frac{k-1}{k}} - 1 \right)}{\theta - 1}, \quad \frac{W}{RT_{in}} = \frac{1}{\eta_v} \cdot (\theta - 1)$$

Moreover, they presented the leakage area expression ( $A_E$ ), to permit for the possibility of appreciable differential expansion between impellers and their casing, the expression is:

$$A_E = \psi A_0 (1 + K(\phi - 1))$$

Furthermore, they develop a non-dimensional relationship between blower speeds, pressure ratios, and volumetric efficiency. The relationship conveniently expressed regarding a non-dimensional speed,  $N$ , where:

$$N^2 = \left( \frac{nC}{a_0 A_E} \right)^2$$

However, the effect of pressure differences, rotational speeds and gap change on the variation and the distribution of other performance parameters such as pressure, temperature and velocity within the blower are not included. Moreover, the in-depth analysis of the variation and the distribution of the internal flow and related parameters within the blower is very limited, and Non-dimensional analysis of performance parameters and develop correlations with geometric variation for performance factors of Roots blower are not included. Furthermore, no new clearance model of Roots blower has been developed. The study lack of a methodology for detection of the change of clearance size inside Roots blower. The effect of the clearance size on pressure fluctuations in both time and frequency domain with clearance variation inside the blower is not investigated.

Hsieh & Zhou et al. (Hsieh & Zhou, 2015) developed three-dimensional fluid analysis numerical model for a two-lobe rotor of cylindrical and screw type Roots pumps by using (CFD) solver Pump-Linx to analyse the differences of flow characteristics, like pressure and flow rate. The flow is considered to be unsteady, isothermal, and compressible. The inlet pressure is assumed to be one atmospheric pressure (101.325 kPa), the outlet operation pressure is 150 kPa, and the rotational speed of the rotor is 3000 rev/min. The clearance between the rotors is set at 0.3 mm, and the clearance between the rotor and chamber at 0.1 mm. A number of measurement points are set inside the pump. The interval of each inner measurement point is based on each  $18^\circ$  of rotation. Hence, from 0 to 180, there are 11 points in a row to analyse the fluctuation and the distribution of the pressure. The findings demonstrate that the Roots-

type blower with cylinder-shape can achieve higher flow rate capacity than the screw type Roots pumps, but the pressure in screw type pump is characterised by less fluctuation and then less pressure pulsation and noise.

However, the performance characterisation of the influence of rotational speed and pressure difference on the Roots blower performance under the transient condition is not included. Also, the effect of pressure differences, rotational speeds and gap change on the variation and the distribution of other performance parameters such as pressure, temperature and velocity within the blower are not included. Moreover, the in-depth analysis of the variation and the distribution of the internal flow and related parameters within the blower is very limited, and Non-dimensional analysis of performance parameters and develop semi-empirical correlations for performance factors of Roots blower are not included. Furthermore, no new clearance model of Roots blower has been developed. The study lack of a methodology for detection of the change of clearance size inside Roots blower. The effect of the clearance size on pressure fluctuations in both time and frequency domain with clearance variation inside the blower is not investigated.

Liu et al. (Z. Huang & Liu, 2009), carried out a numerical study to analyse and evaluate the characteristics of internal flow within a three-lobe positive discharge blower through the CFD approach. Comparative analysis between the semi-empirical techniques and numerical simulation have been conducted. Two cases have been studied, and the pressure and the temperature boundary conditions were applied at the inlet and of the outlet of the blower. At the suction, the total pressure is set as 0 Pa, and the total inlet temperature is 24 °C for both cases. At the discharge of the blower, the static pressure is assigned a value of 39100Pa, and the temperature is kept at 60°C for case 1. Also, the static pressure and the temperature are set to 99300Pa, and 90°C respectively for case 2. For the study, the rotational speed of the blower rotors is kept at 1493 rev/min. Contrasts were identified between the two exhaust rate curves attained through the semi-empirical techniques and simulation with the variations being examined by identifying pressure contours and speed vectors at varying points within a single working period. These outcomes recognized that the exhaust rate possesses two V-type fluctuations while the semi-empirical technique identifies the exhaust rate as possessing only a single V-type variation. The differing results are caused by differences in compression and the occurrence of a vortex within the mixing zone.

However, the performance characterisation of the influence of rotational speed and pressure difference on the Roots blower performance under the transient condition is not included. Also, the effect of pressure differences, rotational speeds and gap change on the variation and the distribution of other performance parameters such as pressure, temperature and velocity within the blower are not included. Moreover, the in-depth analysis of the variation and the distribution of the internal flow and related parameters within the blower is very limited, and Non-dimensional analysis of performance parameters and develop sim-empirical correlations for performance factors of Roots blower are not included. Furthermore, no new clearance model of Roots blower has been developed. The study lack of a methodology for detection of the change of clearance size inside Roots blower. The effect of the clearance size on pressure fluctuations in both time and frequency domain with clearance variation inside the blower is not investigated.

Huang et al. (S. Huang, Guo, & Yang, 2013) conducted the numerical simulation regarding of unsteady flow using 3D model and Dynamic mesh methods for three types of conventional revolving pumps, Roots blower, rotor-jet pump, and centrifugal pump. The process of fluid flow was assumed to be ideal compressible and isothermal. The unsteady solutions of flow field and pressure distribution were obtained. The analysis of the variation and characteristics of flow field on the middle section of the blower domain subsequent to the startup stage are presented. Also, after a start-up stage, the flow parameters show time-periodic behaviour corresponding to blade passing frequency of the impeller.

However, the performance characterisation of the influence of rotational speed and pressure difference on the Roots blower performance under the transient condition is not included. Also, the effect of pressure differences, rotational speeds and gap change on the variation and the distribution of other performance parameters such as pressure, temperature and velocity within the blower are not included. Moreover, the in-depth analysis of the variation and the distribution of the internal flow and related parameters within the blower is very limited, and Non-dimensional analysis of performance parameters and develop sim-empirical correlations for performance factors of Roots blower are not included. Furthermore, no new clearance model of Roots blower has been developed. The study lack of a methodology for detection of the change of clearance size inside Roots blower. The effect of the clearance size on pressure

fluctuations in both time and frequency domain with clearance variation inside the blower is not investigated.

Jun et al. (X. Liu & Lu, 2014) investigated the unsteady flow characteristics numerically in three-lobe positive blowers using the CFD and comparing the numerical results to the experimental measurements on the variation of flow rate with the outlet pressure. The pressure and the temperature boundary conditions were applied at the inlet and the outlet of the blower. At the suction, the total pressure is set as 0 Pa, and the total inlet temperature is 24 °C. At the discharge of the blower, the static pressure is assigned a value of 58 800Pa, and the total temperature is kept at 80°C according to the designed operating condition. For the present study, the rotational speed of the blower rotors is kept at 1250 rev/min. The results show that in the intake region, the direction of the velocity vectors influence the fluctuations of the inlet flow significantly. For the outlet zone, the temperature changes significantly, which leads to the increase of the airflow pulsation. Moreover, three-dimensional unsteady flow characteristics in the positive displacement blower are revealed during the analysis of the pressure, the temperature, and the velocity fields. Furthermore, by comparing with the experimental measurements, the maximum error of the flow rate is less than 2.15% even at the maximum discharge pressure condition.

However, the performance characterisation of the influence of rotational speed and pressure difference on the Roots blower performance under the transient condition is not included. Also, the effect of pressure differences, rotational speeds and gap change on the variation and the distribution of other performance parameters such as pressure, temperature and velocity within the blower are not included. Moreover, the in-depth analysis of the variation and the distribution of the internal flow and related parameters within the blower is very limited, and Non-dimensional analysis of performance parameters and develop sim-empirical correlations for performance factors of Roots blower are not included. Furthermore, no new clearance model of Roots blower has been developed. The study lack of a methodology for detection of the change of clearance size inside Roots blower. The effect of the clearance size on pressure fluctuations in both time and frequency domain with clearance variation inside the blower is not investigated.

Bhuyan et al. (Bhuyan, Ghosh, & Sarangi, 2016) carried out numerical analysis to study the lobe profile, the unsteady internal flow phenomena and heat transfer mechanism in a two-lobe

Roots blower. The variation of outlet parameters (Discharge velocity, outlet mass flow rate, exhaust temperature) with time have been investigated. Also, the velocity vectors and streamlines are plotted at different time-instances. Also, the effect of rotating speed on outlet mass flux, outlet velocity and outlet temperature has been studied. The results show that the outlet velocity and mass flow rate rise as speed increases. Moreover, the increase in outlet temperature, the backflow, and the leakage are prominent at low blower speed. Furthermore, a significant recirculation and vorticities are observed in the flow field.

However, the performance characterisation of the influence of rotational speed and pressure difference on the Roots blower performance under the transient condition is not included. Also, the effect of pressure differences, rotational speeds and gap change on the variation and the distribution of other performance parameters such as pressure, temperature and velocity within the blower are not included. Moreover, the in-depth analysis of the variation and the distribution of the internal flow and related parameters within the blower is very limited, and Non-dimensional analysis of performance parameters and develop semi-empirical correlations for performance factors of Roots blower are not included. Furthermore, no new clearance model of Roots blower has been developed. The study lacks a methodology for detection of the change of clearance size inside Roots blower. The effect of the clearance size on pressure fluctuations in both time and frequency domain with clearance variation inside the blower is not investigated.

Shu-Kai Sun et al. (S.-K. Sun, Zhao, Jia, & Peng, 2017) carried out experimental and numerical studies on the flow field of two same 3-lobe Roots blower cases but in two different pipe diameters to analyse the flow characteristics in Roots blowers by using a 3D computational fluid dynamic model and dynamic mesh method. Physical measurements of mass flow rate and the distribution of the pressure are conducted in order to validate the CFD models. The pressure value of 0 kPa at the inlet and a pressure value of 30 kPa is applied at the outlet boundary, and the rotor speed was kept at 2400 rev/min. Some discussion on the pressure and velocity distributions has been included. The velocity contours show that there are vortices at both the inlet and the outlet zones during the rotation of the impellers. The vortices at the suction zone were near to the impeller wall, but those at the discharge zone were around the casing wall. Furthermore, the two-dimensional model has been developed to determine whether or not this

model can predict blower performance accurately. The results showed that the 2-D model can predict mass flow and pressure distribution in good accuracy.

However, the performance characterisation of the influence of rotational speed and pressure difference on the Roots blower performance under the transient condition is not included. Also, the effect of pressure differences, rotational speeds and gap change on the variation and the distribution of other performance parameters such as pressure, temperature and velocity within the blower are not included. Moreover, the in-depth analysis of the variation and the distribution of the internal flow and related parameters within the blower is very limited, and Non-dimensional analysis of performance parameters and develop sim-empirical correlations for performance factors of Roots blower are not included. Furthermore, no new clearance model of Roots blower has been developed. The study lack of a methodology for detection of the change of clearance size inside Roots blower. The effect of the clearance size on pressure fluctuations in both time and frequency domain with clearance variation inside the blower is not investigated.

Shu-Kai Sun et al. (S. Sun, Zhou, Wen, & Peng, 2017) extended their work by taking into account the flow analysis in the Roots blower with and without backflow pipes arrangement design. Physical measurements of the variation and distribution of the pressure in the Roots blower with backflow design are conducted in order to validate the CFD models. The outcomes illustrate that the CFD models were suitable in predict of the flow characteristics. Also, the results show that the use of backflow pipes could decrease the pressure pulsation amplitude in the discharge of the Roots blower by more than 50%, but the volumetric efficiency is reduced by 3.5%. However, the effect of pressure ratio and rotational speed on flow parameters is not included. Also, the study lacks in-depth analysis of the variation and the distribution of the flow and related parameters within the Roots blower.

However, the performance characterisation of the influence of rotational speed and pressure difference on the Roots blower performance under the transient condition is not included. Also, the effect of pressure differences, rotational speeds and gap change on the variation and the distribution of other performance parameters such as pressure, temperature and velocity within the blower are not included. Moreover, the in-depth analysis of the variation and the distribution of the internal flow and related parameters within the blower is very limited, and Non-dimensional analysis of performance parameters and develop sim-empirical correlations

for performance factors of Roots blower are not included. Furthermore, no new clearance model of Roots blower has been developed. The study lack of a methodology for detection of the change of clearance size inside Roots blower. The effect of the clearance size on pressure fluctuations in both time and frequency domain with clearance variation inside the blower is not investigated.

Ying et al. (Ying-jie, Li-gang, & Bei-jiang, 2016) carried out numerical simulations by using 2D CFD models to study characteristics of the internal flow in Roots blower consists of the new rotor profile. An atmospheric pressure 101325 Pa is applied at the inlet and a gauge pressure 70000 Pa is set at the outlet of the blower. Also, the rotor speed is kept at 1460 rev/min. The results show that the air volume of the Roots blower with the new rotor profile increases by 15.3%, meanwhile the pulsation and noise are reduced noticeably. Also, the temperature in the blower with the new rotor profile has declined in different degrees. Moreover, the distribution of flow velocity is more uniform, only the air outlet temperature increased slightly. In comparison with the original rotor profile, the new rotor profile has recorded better performance.

However, the performance characterisation of the influence of rotational speed and pressure difference on the Roots blower performance under the transient condition is not included. Also, the effect of pressure differences, rotational speeds and gap change on the variation and the distribution of other performance parameters such as pressure, temperature and velocity within the blower are not included. Moreover, the in-depth analysis of the variation and the distribution of the internal flow and related parameters within the blower is very limited, and Non-dimensional analysis of performance parameters and develop sim-empirical correlations for performance factors of Roots blower are not included. Furthermore, no new clearance model of Roots blower has been developed. The study lack of a methodology for detection of the change of clearance size inside Roots blower. The effect of the clearance size on pressure fluctuations in both time and frequency domain with clearance variation inside the blower is not investigated.

LIU et al. (X. Liu, Lu, Gao, & Xi, 2013) conducted a numerical study to investigate the effect of spiral shape design at the suction and the discharge of the blower on the characteristics of 3D unsteady flow in a three-lobe Roots blower. Two models with and without the spiral inlet and outlet at a spiral angle 85° degrees have been performed using commercial CFD software,

SC/Tetra. The pressure and the temperature boundary conditions were applied at the inlet and the outlet of the blower. At the inlet, the total pressure is set as 0 Pa, and the total inlet temperature is set at 24 °C. At the discharge of the blower, the pressure is set as 58800Pa, and the total temperature is set at 80°C. For the current study, the rotational speed of the blower rotors is kept at 1250 rev/min.

The validity of the computational model and numerical computational method is verified by comparing the numerical results with the experimental result. The outcomes illustrate that the mass flow rate with the variation of pressure is marginally affected, but the flow condition inside the blower is significantly affected. In the discharge zone, the oscillations of pressure, velocity, and temperature are considerably reduced. It proves that the spiral outlet can efficiently suppress the fluctuations of pressure, accordingly dropping energy dissipation. In the suction region, the average value of velocity, pressure, and temperature are slightly reduced, but the instabilities in them declined, representing that the spiral inlet can make the flow steadier. The optimisation of the spiral inlet and outlet shape and angle is not addressed in this study.

However, the performance characterisation of the influence of rotational speed and pressure difference on the Roots blower performance under the transient condition is not included. Also, the effect of pressure differences, rotational speeds and gap change on the variation and the distribution of other performance parameters such as pressure, temperature and velocity within the blower are not included. Moreover, the in-depth analysis of the variation and the distribution of the internal flow and related parameters within the blower is very limited, and Non-dimensional analysis of performance parameters and develop sim-empirical correlations for performance factors of Roots blower are not included. Furthermore, no new clearance model of Roots blower has been developed. The study lack of a methodology for detection of the change of clearance size inside Roots blower. The effect of the clearance size on pressure fluctuations in both time and frequency domain with clearance variation inside the blower is not investigated.

Yaw-Hong Kang et al. (Kang & Vu, 2014) developed and studied numerically a rotor profile of two-lobe pump known as the ECE (epicyclic-circular-epicyclic) profile. The numerical investigations are conducted to evaluate, analyse and compare the performance of this profile with three other profiles known as CEC (circular-epicyclic-circular), circular and

epicycloidal via volume flow rate calculations, and to carry out flow field analysis. Different operating conditions and a range of rotational speed from 1000rev/min to 5000rev/min have been used in these studies. The static pressure and velocity fields of the simulated models were analysed. The study was conducted using a 2D model and CFD approach, with a fluid that is incompressible and isothermal. The outcomes revealed that configurations of rotor surface significantly impact the blower's performance, and an epicycloidal profile supplies substantial advantages compared to a circular profile. Also, the newly developed rotor profile (ECE) has achieved a performance that more by (55%) per cent compared to conventional profiles. Furthermore, these results confirm that three or four lobe designs do not enhance the pump's performance but can provide a more steady output with greater capacity compared to blowers with two lobes.

However, the performance characterisation of the influence of pressure difference on the Roots blower performance under the transient condition is not included. Also, the effect of pressure differences, rotational speeds and gap change on the variation and the distribution of other performance parameters such as pressure, temperature and velocity within the blower are not included. Moreover, the in-depth analysis of the variation and the distribution of the internal flow and related parameters within the blower is very limited, and Non-dimensional analysis of performance parameters and develop semi-empirical correlations for performance factors of Roots blower are not included. Furthermore, no new clearance model of Roots blower has been developed. The study lack of a methodology for detection of the change of clearance size inside Roots blower. The effect of the clearance size on pressure fluctuations in both time and frequency domain with clearance variation inside the blower is not investigated.

Sang et al. (Li, Sang, Meng, Shen, & Jia, 2013) developed two lobe and three-lobe blowers by using three types of profiles, the circular arc, involute, and cycloid respectively. Also, they analysed the influence of the number of lobes, by simulating the variation of internal flow field inside a lobe pump under transient condition. CFD software FLUENT as simulation tool with dynamic mesh techniques are used. The results show that dynamic mesh technology can capture dynamics variations and the distribution of its velocity and pressure corresponding to the internal flow field easily. Both of the double-lobe and tri-lobe are consisting of vortex which changes size, shape and position during a rotating. The pressure pulsation and velocity corresponding to two lobes are higher than that of tri-lobe.

However, the performance characterisation of the influence of rotational speed and pressure difference on the Roots blower performance under the transient condition is not included. Also, the effect of pressure differences, rotational speeds and gap change on the variation and the distribution of other performance parameters such as pressure, temperature and velocity within the blower are not included. Moreover, the in-depth analysis of the variation and the distribution of the internal flow and related parameters within the blower is very limited, and Non-dimensional analysis of performance parameters and develop sim-empirical correlations for performance factors of Roots blower are not included. Furthermore, no new clearance model of Roots blower has been developed. The study lack of a methodology for detection of the change of clearance size inside Roots blower. The effect of the clearance size on pressure fluctuations in both time and frequency domain with clearance variation inside the blower is not investigated.

### **2.1.1 Summary of the literature review regarding Quantitative evaluation of**

#### **Performance characteristics of a Roots blower baseline model**

Based on the discussion and evaluation of the literature review concerning the characterisation of the Roots blower performance some gaps in knowledge have been identified. It can be summarised that there is a severely limited range of investigation parameters in the published literature. Furthermore, the earlier studies are limited in certain of aspects, such as; the performance characterisation of the influence of rotational speed and pressure difference on the Roots blower performance under the transient condition. Also, the effect of pressure differences, rotational speeds and gap change on the variation and the distribution of other performance parameters such as pressure, temperature and velocity within the blower. Moreover, the in-depth analysis of the variation and the distribution of the internal flow and related parameters within the blower, and Non-dimensional analysis of performance parameters and develop sim-empirical correlations for performance factors of Roots blower Furthermore, new clearance model of Roots blower. The effect of the clearance size on pressure fluctuations in both time and frequency domain with clearance variation inside the blower. The studies lack of a methodology for detection of the change of clearance size inside Roots blower.

Based on the results summarised here, there is a necessity for an enhanced understanding of the flow structure within Roots blower. Also, a more range of studies is required in order to develop database for accurate analysis of the performance characteristics of Roots blower.

## **2.2 Quantitative evaluation of Roots blower performance undergoing**

### **Geometrical changes**

A Root blower's essential components is a rotor. Therefore, the rotor's design directly affects the performance of Root blowers. When the rotor space is small, then the rotor only covers a limited area with the least volume causing the flow rate to be as large as possible. Also, a slight sealing between the two rotors, and the casing and the two rotors will cause leakage flow to be as small as possible. Therefore, a decrease in the leakage in the clearances causes the volumetric efficiency to rise. Numerous endeavours have taken place to create unique or enhance and evaluate current profiles, and many techniques have been utilised to examine and evaluate clearances for reducing leakage between the two rotors and the rotors/casing. This section reviews the published literature highlighting the effects of fluid and geometrical parameters on the flow field and Roots blower performance, which is an effect that needs to be considered in Roots blower modelling. However, the review of existing literature also reveals that the literature describing how the clearance size effects flow characteristics and therefore the blower performance is very limited. Furthermore, the non-dimensional analysis of numerical results and develop semi-empirical correlations, which allows the prediction model to be applied to other models having geometric similarity is quite limited. More research needs to be carried out on this topic and is the second aim of the present study.

Cai et al. (ZHANG & WANG, 2011) carried out numerical simulation on Roots blower with gradually expanding gap using the CFD/FLUENT software in order to investigate the inside flow field under the compressible and unsteady flow conditions. The results showed that the dynamic mesh techniques used to simulate the flow field in Roots blower could reflect truly the distribution of internal turbulent flow and the characteristic of air flow fluctuation, and the method could provide a scientific basis for the analysis of the characteristic of the internal airflow of the Roots blower. The numerical results show that the optimisation of the casing

structure could decrease or even avoid the backflow effectively at the discharge outlet and reduce power consumption and noise.

However, the performance characterisation of the influence of rotational speed and pressure difference on the Roots blower performance under the transient condition is not included. Also, the effect of pressure differences, rotational speeds and gap change on the variation and the distribution of other performance parameters such as pressure, temperature and velocity within the blower are not included. Moreover, the in-depth analysis of the variation and the distribution of the internal flow and related parameters within the blower is very limited, and Non-dimensional analysis of performance parameters and develop sim-empirical correlations for performance factors of Roots blower are not included. Furthermore, no new clearance model of Roots blower has been developed. The study lack of a methodology for detection of the change of clearance size inside Roots blower. The effect of the clearance size on pressure fluctuations in both time and frequency domain with clearance variation inside the blower is not investigated.

Hsieh et al. (Hsieh, 2015) proposed a mathematical model and evaluated a new rotor profile; an elliptical roulette applies to two-lobed Roots pump using numerical CFD techniques. The flow is unsteady and compressible. The boundary conditions have been applied are 101.325 kPa at the inlet and 150 kPa at the outlet, also the rotational speed is kept at 3000 rev/min. New six rotor profiles have been tested and analysed under the same volume, the same clearance conditions and compared with traditional one based on the elliptical axial ratio parameter  $\lambda$ . This study analyses the flow characteristics of a two-lobe pump. The results prove that an elliptical axial ratio of less than 0.6 produces better flow characteristics and can achieve higher efficiency. Among all the cases, the  $\lambda=0.4$  design gives the highest positive flow rate and the lowest negative flow rate. This observation confirms that the rotor geometry significantly influences pumping performance.

However, the performance characterisation of the influence of rotational speed and pressure difference on the Roots blower performance under the transient condition is not included. Also, the effect of pressure differences, rotational speeds and gap change on the variation and the distribution of other performance parameters such as pressure, temperature and velocity within the blower are not included. Moreover, the in-depth analysis of the variation and the distribution of the internal flow and related parameters within the blower is very limited, and

Non-dimensional analysis of performance parameters and develop semi-empirical correlations for performance factors of Roots blower are not included. Furthermore, no new clearance model of Roots blower has been developed. The study lacks a methodology for detection of the change of clearance size inside Roots blower. The effect of the clearance size on pressure fluctuations in both time and frequency domain with clearance variation inside the blower is not investigated.

Joshi et al. (Joshi, Blekhman, Felske, Lordi, & Mollendorf, 2006) carried out numerical and experimental analyses on a prototype of a multi-recompression heating system that utilises two-lobe Roots-type mechanisms to increase the temperature of the gas to excessive levels through pressurising the gas. The analysis is accomplished by employing Star-CD (Commercial CFD codes) to mimic the leakage flows within a machine, initiating analysis of clearance. The CFD simulation was conducted through one angle of rotation. The investigations are performed for the following impeller-impeller and impeller-casing gap combinations (II = 0.014 inch & IC = 0.006 inch, II = 0.014 inch & IC = 0.011 inch, and II = 0.013 inch & IC = 0.014 inch). Impeller-casing gaps differ in practice due to the tip strip manufacturing tolerances of  $\pm 0.005$  and along with the expansion and the wear during operation.

The CFD calculations are performed for four pressure ratios (1.24, 2.09, 3.11, and 4.18). The visualisation and the analysis of the flow field, the Mach number, the static pressure, and the temperature are presented. The results show that the gap between the two rotors remains at a stable rate of 96% per cent of rotation degrees. Additionally, the 3D analysis showed that the flow field is identical alongside the impeller length, not including the leakage via the end plates. Moreover, in general, it is realised that the flow velocities in the chamber areas are considerably less than in the clearances zones. The static pressure commonly declines through the machine. Furthermore, the static temperature field is uniform at the influx boundary but decreases in the rotor-rotor and rotor-casing clearances.

However, the performance characterisation of the influence of rotational speed on the Roots blower performance under the transient condition is not included. Also, the effect of pressure differences, rotational speeds and gap change on the variation and the distribution of other performance parameters such as pressure, temperature and velocity within the blower are not included. Moreover, the in-depth analysis of the variation and the distribution of the internal flow and related parameters within the blower is very limited, and Non-dimensional analysis

of performance parameters and develop empirical and sim-empirical correlations for performance factors of Roots blower are not included. Furthermore, no new clearance model of Roots blower has been developed. The study lack of a methodology for detection of the change of clearance size inside Roots blower. The effect of the clearance size on pressure fluctuations in both time and frequency domain with clearance variation inside the blower is not investigated.

Y.-H. Kang et al. (Y.-H. Kang, H.-H. Vu, & C.-H. Hsu, 2012) carried out a numerical investigation to evaluate the fluid dynamics of lobe pumps and main factors that might affect the pump's performance like the profile of the rotor, lobe numbers, and size of the gap between rotor and casing, and the clearance between the two rotors. The study was conducted to analyse and compare the performance of two different models, one with a circular rotor profile type and the other with epicycloid rotor profile type. The study was conducted with different operating conditions and a range of rotational speed from 1000rev/min to 5000rev/min. The air flow process was assumed to be isothermal, incompressible and unsteady. The static pressure and velocity fields of the simulated models were analysed.

The analysis has demonstrated that the multi-lobes, three and four lobes, do not enhance the pump's performance. However, multi-lobes do supply more stable output with higher capacity than pumps with two lobes. Therefore, the outcomes verify the substantial effect of gap size between rotor and casing wall to the pump's efficiency. Reducing this gap size from 1.25 millimetres to 0.5 millimetres causes the pressure head to rise by 425% per cent. Furthermore, the clearance between the two rotors has been demonstrated to differ from 0.12 millimetres to 0.15 millimetres without impacting the pump's performance.

However, the performance characterisation of the influence of pressure difference on the Roots blower performance under the transient condition is not included. Also, the effect of pressure differences, rotational speeds and gap change on the variation and the distribution of other performance parameters such as pressure, temperature and velocity within the blower are not included. Moreover, the in-depth analysis of the variation and the distribution of the internal flow and related parameters within the blower is very limited, and Non-dimensional analysis of performance parameters and develop sim-empirical correlations for performance factors of Roots blower are not included. Furthermore, no new clearance model of Roots blower has been developed. The study lack of a methodology for detection of the change of clearance size inside

Roots blower. The effect of the clearance size on pressure fluctuations in both time and frequency domain with clearance variation inside the blower is not investigated.

Yingyuan Liu et al. (Y. Liu, Wang, & Zhu, 2015) carried out numerical and experimental analysis to study the characteristics of the flow of four-lobe pump including cavitation. The studies conducted by simplifying and developed a two-dimensional numerical model. The flow process was assumed to be isothermal, incompressible and unsteady. The studies conducted within the range of rotational speed from 0 to 730 rev/min and pressure difference from 0 to 0.4MPa. The effect of pressure differences, rotational speeds, inlet pressures and clearance sizes on the pump performance with and without cavitation are discussed. The results show that mass flow rates without cavitation are slightly smaller than that with cavitation, but amplitudes of mass flow rates without cavitation are much smaller than that with cavitation. Meanwhile, the volume fraction of the water vapour rises with the decreasing of the pressure differences and the increasing rotational speeds.

Compared with the effect of the pressure differences on the vapour contents, the influence of rotational speeds is relatively more significant. Concerning the gap size, the smaller the gap size is, the stronger the cavitation will be. Furthermore, the effect of gap size between two rotors on the cavitation is higher than that between the rotor and pump case. Regarding the inlet pressure, it presents a significant influence on the model with cavitation, but it has a little consequence on the mass flow rates without cavitation.

However, the range of performance characterisation of the influence of rotational speed and pressure difference on the Roots blower performance under the transient condition is quite limited. Also, the effect of pressure differences, rotational speeds and gap change on the variation and the distribution of other performance parameters such as pressure, temperature and velocity within the blower are not included. Moreover, the in-depth analysis of the variation and the distribution of the internal flow and related parameters within the blower is very limited, and Non-dimensional analysis of performance parameters and develop empirical and sim-empirical correlations for performance factors of Roots blower are not included. Furthermore, no new clearance model of Roots blower has been developed. The study lack of a methodology for detection of the change of clearance size inside Roots blower. The effect of the clearance size on pressure fluctuations in both time and frequency domain with clearance variation inside the blower is not investigated.

### **2.2.1 Summary of the literature review regarding Quantitative evaluation of**

#### **Roots blower performance undergoing geometrical changes**

Based on the evaluation and discussion of a literature review regarding the determination of the characteristics of the Roots blower performance using geometrical variations, the gaps in the knowledge are highlighted. It can be summarised that the range of investigation parameters in the available literature is limited. Furthermore, the earlier studies lack or restrict in certain of aspects, including the performance characterisation of the influence of rotational speed and pressure difference on the Roots blower performance under the transient condition. Also, the effect of pressure differences, rotational speeds and gap change on the variation and the distribution of other performance parameters such as pressure, temperature and velocity within the blower.

Moreover, the in-depth analysis of the variation and the distribution of the internal flow and related parameters within the blower, and Non-dimensional analysis of performance parameters and develop sim-empirical correlations for performance factors of Roots blower. Furthermore, new clearance model of Roots blower. The effect of the clearance size on pressure fluctuations in both time and frequency domain with clearance variation inside the blower. The studies lack of a methodology for detection of the change of clearance size inside Roots blower. Hence, there is a need for in-depth analysis and understanding of the flow characteristics with the effect of geometrical parameters on blower performance such as clearance size within Roots blower. Furthermore, more investigation is necessary in order to carry out appropriate database with more accurate analysis of geometrical parameters that effect Roots blower performance.

### **2.3 Quantitative evaluation of Unsteady flow characteristics and**

#### **comparative analysis with clearance variation inside the Roots blower**

This section reviews the published literature highlighting the effects of unsteady fluid behaviour and geometrical parameters (gap sizes) on the flow field and Roots blower performance, which is an effect that needs to be considered in Roots blower modelling and design. However, the review of existing literature also reveals that the literature describing how the clearance size effects flow characteristics and therefore the blower performance is very

limited. Furthermore, the in-depth analysis of pressure fluctuation with the effect of clearance size is quite limited. More investigation needs to be carried out on this topic and is the third aim of the current study.

Hsieh & Zhou et al. (Hsieh & Zhou, 2015) developed three-dimensional fluid analysis numerical model for a two-lobe rotor of cylindrical and screw type Roots pumps by using (CFD) solver Pump-Linx to analyse the differences in characteristics of the flow field, such as mass flow rate and pressure between cylindrical and screw type pumps. The flow is unsteady, isothermal, and compressible. The suction pressure is 100 kPa, the discharge operation pressure is 150 kPa, and the rotational speed of the rotor is 3000 rev/min. The gap between the two impellers is set at 0.3 mm, and the gaps between the impellers and the casing are set at 0.1 mm. In order to analyse the fluctuation and the distribution of the pressure, 45 measurement points are chosen within the pump. The measurement points are set every 18<sup>0</sup> degrees of rotation. Hence, from 0 degrees to 180 degrees of rotation, there are 11 points in a row. The findings demonstrate that the Roots-type blower with cylinder-shaped can achieve higher flow rate capacity than the screw type Roots pumps, but the pressure in screw type pump is characterised by less fluctuation and then less pressure pulsation and noise.

However, the performance characterisation of the influence of rotational speed and pressure difference on the Roots blower performance under the transient condition is not included. Also, the effect of pressure differences, rotational speeds and gap change on the variation and the distribution of other performance parameters such as pressure, temperature and velocity within the blower are not included. Moreover, the in-depth analysis of the variation and the distribution of the internal flow and related parameters within the blower is very limited, and Non-dimensional analysis of performance parameters and develop sim-empirical correlations for performance factors of Roots blower are not included. Furthermore, no new clearance model of Roots blower has been developed. The study lack of a methodology for detection of the change of clearance size inside Roots blower. The effect of the clearance size on pressure fluctuations in both time and frequency domain with clearance variation inside the blower is not investigated.

Shu-Kai Sun et al. (S.-K. Sun et al., 2017) carried out experimental and numerical studies on the flow field of two same 3lobe Roots blower cases but in two different pipe diameters to

analyse the flow characteristics in Roots blowers by using a 3D computational fluid dynamic models and dynamic mesh method. Physical measurements of mass flow rate and the pressure distribution are conducted in order to validate the CFD models. The pressure 0 kPa inlet and pressure 30 kPa outlet boundary conditions were applied, and the rotor was rotating at 2400 rev/min. The pressure contours and velocity fields of the simulated models were analysed to determine the most accurate simulated case. Some discussion on the pressure and velocity distributions has been included. The velocity contours show that there are vortices at both the inlet and the outlet zones during the rotation of the impellers. The vortices at the suction zone were near to the impeller wall, but those at the discharge zone were around the casing wall. Furthermore, the two-dimensional model has been developed to determine whether or not this model can predict blower performance accurately. The results showed that the 2-D model can predict mass flow and pressure distribution in good accuracy.

However, the performance characterisation of the influence of rotational speed and pressure difference on the Roots blower performance under the transient condition is not included. Also, the effect of pressure differences, rotational speeds and gap change on the variation and the distribution of other performance parameters such as pressure, temperature and velocity within the blower are not included. Moreover, the in-depth analysis of the variation and the distribution of the internal flow and related parameters within the blower is very limited, and Non-dimensional analysis of performance parameters and develop empirical and sim-empirical correlations for performance factors of Roots blower are not included. Furthermore, no new clearance model of Roots blower has been developed. The effect of the clearance size on pressure fluctuation and flow pattern of Roots blower is not investigated. The study lack of a methodology for detection of the change of clearance size inside Roots blower.

Shu-Kai Sun et al. (S. Sun et al., 2017) extended their work by taking into account the flow analysis in the Roots blower with and without backflow design. Physical measurements of the variation and distribution of the pressure in the Roots blower with backflow design are conducted in order to validate the CFD models. The outcomes illustrate that the CFD models were suitable in predict of the flow characteristics. Also, the results show that the use of backflow pipes could decrease the pressure pulsation amplitude in the discharge of the Roots blower by more than 50%, but the volumetric efficiency is reduced by 3.5%.

However, the performance characterisation of the influence of rotational speed and pressure difference on the Roots blower performance under the transient condition is not included. Also, the effect of pressure differences, rotational speeds and gap change on the variation and the distribution of other performance parameters such as pressure, temperature and velocity within the blower are not included. Moreover, the in-depth analysis of the variation and the distribution of the internal flow and related parameters within the blower is very limited, and no empirical and sim-empirical prediction correlations including rotor and clearance geometry have been developed. Furthermore, no new clearance model of Roots blower has been developed. The effect of the clearance size on pressure fluctuation and flow pattern of Roots blower is not included. The study lack of a methodology for detection of the change of clearance size inside Roots blower.

Joshi et al. (Joshi et al., 2006) carried out numerical and experimental analyses on a prototype of a multi-recompression heating system that utilises two-lobe Roots-type mechanisms to increase the temperature of the gas to excessive levels through pressurising the gas. The analysis is accomplished by employing Star-CD (Commercial CFD codes) to mimic the leakage flows within a machine, initiating analysis of clearance, The CFD simulation was conducted through one angle of rotation. The investigations are performed for the following impeller-impeller and impeller-casing gap combinations (II = 0.014 inch & IC= 0.006 inch, II= 0.014 inch & IC= 0.011 inch, and II= 0.013 inch & IC= 0.014 inch). Impeller-case gaps differ in practice due to the tip strip manufacturing tolerances of  $\pm 0.005$  and along with the expansion and the wear during operation.

The CFD calculations are performed for four pressure ratios (1.24, 2.09, 3.11, and 4.18). The visualisation and the analysis of the flow field, the Mach number, the static pressure, and the temperature are presented. The results show that the gap between the two rotors remains at a stable rate of 96% per cent of rotation degrees. Additionally, the 3D analysis showed that the flow field is identical alongside the impeller length, not including the leakage via the end plates. Moreover, in general, it is realised that the flow velocities in the chamber areas are considerably less than in the clearances zones. The static pressure commonly declines through the machine. Furthermore, the static temperature field is uniform at the influx boundary but decreases in the rotor-rotor and rotor-casing clearances.

However, the studies were conducted through one angle of rotation. Therefore performance characterisation of the influence of rotational speed on the Roots blower performance under the transient condition is not included. Also, the effect of pressure differences, rotational speeds and gap change on the variation and the distribution of other performance parameters such as pressure, temperature and velocity within the blower are not included. Moreover, the in-depth analysis of the variation and the distribution of the internal flow and related parameters within the blower is very limited, and no empirical and sim-empirical prediction correlations including rotor and clearance geometry have been developed. Furthermore, no new clearance model of Roots blower has been developed. The effect of the clearance size on pressure fluctuation and flow pattern of Roots blower is not studied. The study lack of a methodology for detection of the change of clearance size inside Roots blower.

### **2.3.1 Summary of the literature review regarding the Quantitative evaluation of unsteady flow characteristics and comparative analysis with clearance variation inside the Roots blower**

Based on the evaluation and discussion of a literature review regarding the aim3, roughly gaps in the knowledge are underlined. It can be concluded that the range of investigation parameters in the available literature is limited. Furthermore, the earlier studies lack or restrict in certain of aspects, including the performance characterisation of the influence of rotational speed and pressure difference on the Roots blower performance under the transient condition. Also, the effect of pressure differences, rotational speeds and gap change on the variation and the distribution of other performance parameters such as pressure, temperature and velocity within the blower. Moreover, the in-depth analysis of the variation and the distribution of the internal flow and related parameters within the blower, and Non-dimensional analysis of performance parameters and develop sim-empirical correlations for performance factors of Roots blower. Furthermore, new clearance model of Roots blower. The effect of the clearance size on pressure fluctuations in both time and frequency domain with clearance variation inside the blower. The studies lack of a methodology for detection of the change of clearance size inside Roots blower.

According to the finding discussed above, there is a necessity for a well understanding of the flow characteristics with the geometrical effect such as clearances within Roots blower. Furthermore, a wider range of investigations is necessary in order to construct-up sufficient

database for more accurate analysis of geometrical parameters that effect Roots blower performance.

## **2.4 Scope of Research**

Based on the literature overview that has been made, it can be concluded that the current base of knowledge regarding the performance characterisation of the influence of rotational speed and pressure difference on the Roots blower performance under the transient condition. Also, the effect of pressure differences, rotational speeds and gap change on the variation and the distribution of other performance parameters such as pressure, temperature and velocity within the blower. Moreover, the in-depth analysis of the variation and the distribution of the internal flow and related parameters within the blower, and Non-dimensional analysis of performance parameters and develop sim-empirical correlations for performance factors. Furthermore, new clearance model of Roots blower. The effect of the clearance size on pressure fluctuations in both time and frequency domain with clearance variation inside the blower. The studies lack of a methodology for detection of the change of clearance size inside the blower are quite limited. Therefore, understanding the flow field characteristics under transient behaviour is quite essential in order to improve existing or develop new design of this blower. Furthermore, the practical use of the Roots blower involves a broad range of operating conditions in which the pressure loading input and the thermal loading conditions continuously vary. In the present research, further experimental and numerical investigations have been conducted in order to in-depth understand the natural physicals of fluid inside Roots blower and the main factors effect on Roots blower performance. Based on the studies that have been reviewed in this chapter, the main gaps and the key areas of research have been established. Therefore, the scope of the research regarding a Roots blower has been decided.

The first area of research that has been presented is the investigation and analysis of performance characteristics of the Roots blower baseline model under different rotational speeds and pressure loads; to achieve that, both of the experimental and the numerical investigations have been carried out on the this blower model. This research aims to investigate and analyse the effect of rotational speeds and pressure differences on other related flow parameters and therefore on the blower performance. Furthermore, different empirical

correlations to predict some of the performance parameters with acceptable accuracy have been developed.

The second research area in this study is to recognise the influence of geometrical parameters on the performance of the Roots blower under different rotational speeds and a variety of pressure loading conditions. The practical use of this blower includes a wide range of operating conditions with varying pressure loads. In the current research, numerical investigations in detail are proposed to be carried out on the pressure, temperature and velocity variations and distributions within the blower. Moreover, the comparison between the baseline model and different geometrical models has been carried out. Furthermore, the development of different semi-empirical correlations to predict some of the performance factors with acceptable accuracy has been carried out. It is proposed to improve or develop modified model of the blower with better performance characteristics.

The third research area of this study is the quantitative evaluation of unsteady flow characteristics and comparative analysis with clearance variation inside the Roots blower. The relation between various parameters has been established by analysing the numerical result of these models. These parameters (rotational speed, pressure difference, rotor diameter, tip gap size, centre gap size) have a significant impact on the performance characteristics. Also, to develop new clearance model and new methodology for detection of clearance change inside the blower. This methodology will use the pressure fluctuation characteristics with frequency domain analysis to detect any change in the clearance within the blower. Also, to help designers to develop a more efficient product model. Moreover, to study the effect of the clearance size on pressure fluctuations in both time and frequency domain with clearance variation inside the blower

## **2.5. Aims of the research**

An experimental test rig was designed and built to investigate the effect of some operational conditions on flow related parameters and therefore on the performance of Roots blower. The size and the internal flow inside the clearances between the rotating parts and stationary parts have a significant influence on the Roots blower performance. However, it is difficult in measuring, time consuming, and costly to investigate experimentally the effect of gap size and the flow behaviour within these gaps in the blower. Also, because of an increase in the processing speed

and power of computers over recent years, it has helped the engineers to model, predict and analyse flow fields in Roots blower machine in an acceptable level of accuracy with reduced time and cost.

The project will focus on the development of an inclusive approach that facilitates the analysis and prediction of Roots blower performance with better accuracy. This approach is Computational fluid dynamics (CFD) in ANSYS FLUENT and dynamic mesh techniques as prediction tools to reduce development time and cost. Also, this numerical methodology can generate quantitative and qualitative data to capture and help in understanding the physics and internal flow characteristics of a blower system.

The description of research aims for this research project has been done, while the extensive literature reviews have been carried out to formulate the objectives for this research study. According to the motivation of this research study, the research aims can be summarised as below:

1. Quantitative evaluation of Performance characteristics of a Roots blower baseline model
2. Quantitative evaluation of Roots blower performance undergoing geometrical changes
3. Quantitative evaluation of unsteady flow characteristics with clearance variation inside the Roots blower

The aims of this research will cover most of the applied problems faced in the Roots blower machines and therefore can be considered acceptable for this research study. The detailed review of the literature have been presented in the next chapter, which emphasises on the above aims to find knowledge gaps in the existing literature.

## **2.6. Specific Research Objectives**

In this study, an effort will be made to achieve a better understanding of the flow structure within a Roots blower by analysing some geometrical and flow related parameters and its impact on the characteristics performance of Roots blower. After a careful review of the literature mentioned above, the following objectives are defined to achieve the aims of this project:

1. Performance characterisation of the influence of pressure difference and rotational speed on the Roots blower performance under the transient condition.
2. Non-dimensional analysis of performance parameters and develop empirical correlations for performance factors of Roots blower.
3. Numerical characterisation of the influence of the clearance size on blower performance characteristics under a transient condition.
4. Deriving semi-empirical prediction equations depending on non-dimensional relations between different flow and geometric performance parameters.
5. Establish the effect of the clearance sizes in order to develop a new clearance model of Roots blower.
6. Establish the effect of the clearance size on pressure fluctuation and flow pattern of Roots blower.
7. Develop a methodology for detection of the change of clearance size inside Roots blower.

Targeted to complete of the research successfully and to achieve all the aims and the objectives mentioned earlier, both experimental and numerical investigations have been carried out on the Roots blower machine. The next chapter aiming to provide a detailed description of both the experimental apparatus and the numerical method that has been adopted in the present research study.

## **Chapter 3**

### **Experimental and Numerical investigations of a Roots blower**

According to the objectives of this research that have been acknowledged in the chapter 2, experimental and Computational Fluid Dynamics (CFD) approaches have been used in this investigation. An experimental test rig has been built and suitable equipment, instruments, and another measurement auxiliaries have been chosen to measure the necessary flow parameters for this investigation. Moreover, CFD approach with dynamic mesh techniques have been presented to simulate and solve the transient internal flow in Roots blower model. The boundary conditions and the setting of the solver used in this investigation have been described and justified in detail. Furthermore, the numerical simulations of Roots blower model conducted for this research study have been identified. The measurement results are used to verify and validate the numerical findings.

### **3.1. Experimental method based investigations of a Roots blower**

This section defines and demonstrates the main features of the experimental setup and includes a complete description and explanation of test system components. Also, the equipment, the instrumentation, calibration procedure, test procedure, and measurement of mass flow rate, pressure and temperature have been explained in detail. Also, volumetric and adiabatic efficiencies are investigated and analysed. Furthermore, uncertainties of experiment results have been inspected.

#### **3.1.1 Roots blower Test Rig**

The motivation for the test rig system is to study and examine Roots blower performance under varying operating conditions. The test bench has been installed in a laboratory of HR Blowers Company at Huddersfield. The main purposes of the measurements are; validation of CFD Roots blower numerical model predictions by comparing the results obtained from the CFD results with experimental tests. Also, to analyse and evaluate the influence of different parameters on the blower performance. The characteristics of the Roots blower baseline model will be analysed and evaluated in the next chapter.

##### **3.1.1.1. The components of Roots blower test rig**

The test rig of the Roots blower system consists of many components and instruments. The instrumentation system contains apparatus to measure mass flow rate, temperature, and pressure at different conditions. An orifice plate device has been used for mass flow rate measurement in the blower. Pressure gauges and pressure transducers have been used to measure pressure along the blower test rig at different conditions. Prop temperature Sensors have been used to measure the temperature of gas streams along of blower system. The next sections include the main specifications of components and instruments, the explanation and visualisation of the apparatuses used during this experimental measurement. The nomenclatures of all main parts of the blower test rig are listed in Table 3.1.

Table 3.1: The main components of (Model HRBV613) blower system

1	RHBV613 type blower	7	Pressure transducers	13	Expansion joint
2	Pressure relief valve	8	Temperature sensors	14	Silencers
3	Manual pressure regulator	9	Data Acquisition	15	Drive motor
4	Pressure gauges (manometers)	10	Computer station	16	Power station
5	Orifice plate	11	Pipes	17	Electrical cables
6	Differential pressure	12	Air filter	18	Metal stands

Photographs of blower system is given in Figures 3.1 and the full Photograph of test rig is shown in figure A1.1 in appendix A1. The schematic diagram of the experimental test rig using the model of the blower is shown in Figure 3.2.



Figure 3.1: The similar Roots blower package used for experimental tests

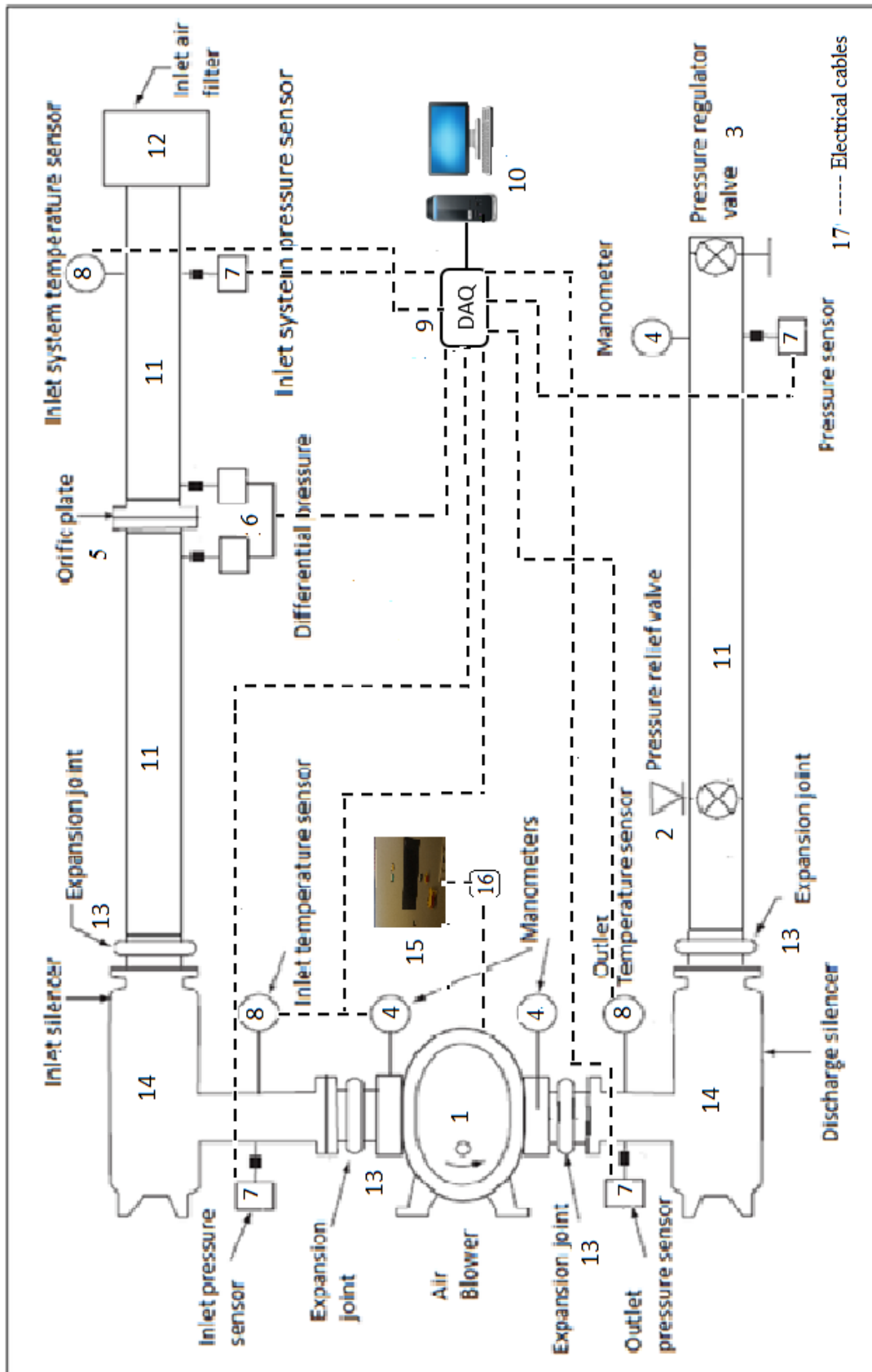


Figure 3.2: Experimental test rig diagram with piping and instrumentation of HRVB 613 type Roots blower system

## 1- Roots blower type

In this study, a two lobe blower (model HRBV613) is used and investigated for the experimental purpose on a test-rig.

Figure 3.1 shows the type of Roots blower that has been used in experimental setup and table 3.2 contains some specifications of this type of blower. The Roots blower model used is HRBV613 from HR Company in Huddersfield. This type of blower mainly involves two rotors, casing, suction cavity, and discharge cavity. Each of both rotors consist 2-lobes; one of the rotors is a driving rotor, which is driven by the external driving source connected directly to the shaft while the rotation of synchronous gears drives the second rotor. Hence in the process, both rotors rotate at equal speed and in the opposite direction, one in clockwise while the other in a counter-clockwise direction. Also, there are finite clearances between rotors, and between the rotors and the housing. The working medium in the blower is air. The nominal swept volume was  $0.01816 \text{ m}^3/\text{rev}$ .

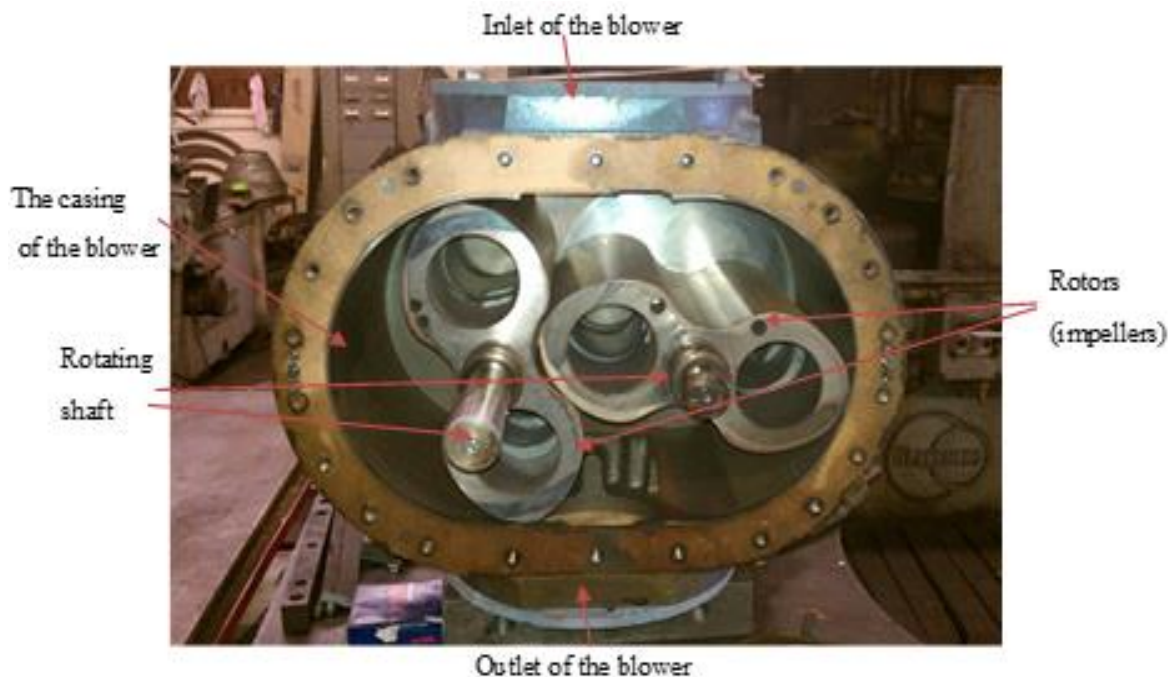


Figure 3.3: The actual Roots blower used for experimental tests (model HRBV613).

Table 3.2: The main specifications of Roots blower type

Make	HR Blower (Britain)
Model	HRBV613
Rotor profile	involute
Volume flow rate	2300 m <sup>3</sup> /hr
Inlet pressure	Atmospheric
Extreme Pressure	1 bar gauge
Motor	Motor: 45 kW, 50 Hz, 415V±10%, 1475 rev/min
Cooling method	Air (free convection)

This type of Roots blower is widely used in several industrial applications because it simple and can achieve high flow rate and volumetric efficiency at low and moderate pressure. The reason behind the selection of this type of blower that are not expensive, the limited research has been done on this type of blower, HR blower company needs to study and understand the flow characteristics in order to improve the performance of this blower, and it adequate to conduct the measurements required to achieve the aims and the objectives of this research

## 2- Pressure relief valve

This is type of pressure valves used in blower system for safety purposes when the pressure exceeds the acceptable level as shown in figure 3.4 right.



Figure 3.4: Manual Pressure regulator valve (left), Relief valve (right)

### 3- Pressure regulator valve

The regulator valve generally used to control and regulate the pressure according to blower system requirement. In this test rig an upstream pressure regulating valve is provided at the discharge end of a pipe connecting to the blower in order to control discharge pressure from (1.0 bar to 2 bars) as shown in figure 3.4 left.

### 4- Pressure Gauges

Figure 3.5 show the types of pressure gauges have been mounted in Roots blower test rig. These type of gauges are used to measure the pressure at the inlet and the outlet of the blower to compare it with the pressure that measured by pressure transducers. Also, other gauge pressure has been instilled in the outlet of blower system to regulate the pressure load.



Figure 3.5: Pressure gauges; Blower inlet (left), Blower outlet (right)

### 5- Orifice plate

The main specifications of orifice plate are illustrated in table 3.3. Also, figure 3.6 depicts the orifice plates have been chosen according to UK industrial standards (ISO 5167) to measure mass flow rate in roots blower system, because they are easy to connect with the blower piping system, low cost as compared to other flow measurement devices. Also, the measurement accuracy of this device is adequate for this study.

Table 3.3: The main specifications of orifice plate

Make.	Rosemount Inc.
Type	Plate type, round edged, corner tapping,
Diameter size [mm]	152
Orifice hole size [mm]	80.68
Plate Thickness [mm]	7.6
Orifice Thickness [mm]	3.04
Discharge coefficient	0.6058
Flow rate	The lowest accurate flow: 0.01 m <sup>3</sup> /sec, the highest is: 0.12 m <sup>3</sup> /sec



Figure 3.6: Orifice plate type

## 6- Differential pressure transducer

The main specifications of differential pressure transducer is illustrated in table 3.4 and figure 3.7 depicts the pressure transducers have been used in test rig of Roots blower system. This type of pressure transducer is used to measure the pressure difference between the upstream flow and the downstream flow through orifice plate by using two pressure taps, one at the upstream zone and another at the downstream zone according to UK industrial standards (ISO 5167).

Table 3.4: The specifications of Differential Pressure transducer

Make.	Impress
Model	DMD 331
Type	Differential pressure transmitter
Pressure range:	Range: 0.4 bars to 2.5 bar
Differential pressure range	0.4 bar
Output	0-10 V/3-wire
Temperature range	-25-85 °C
Accuracy	±0.5% bar

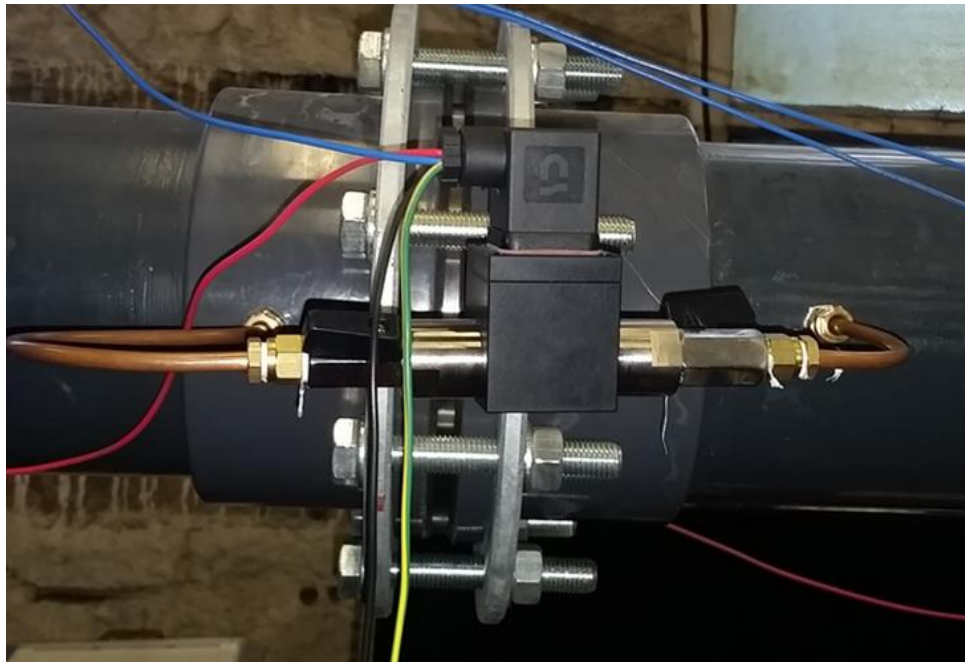


Figure 3.7: Differential pressure transducer and orifice plate with mechanical fittings.

### 7- Pressure transducers (Barometer, System, Inlet, and outlet) of the blower

The main specifications of pressure transducers are illustrated in table 3.5 and figure 3.8 depicts the pressure transducers have been chosen according to UK industrial standards. These types of pressure transducers are used to measure atmospheric pressure and the pressure at different positions; at inlet blower system, at suction and discharge of the blower. These types

of pressure transducers have been chosen, because their capability and accuracy is sufficient for the measurement required in this study.

Table 3.5: The main specifications of pressure transducers

Make.	OMEGA
Model	PXM319-002AI
Type	Pressure transducer
Range:	0.0 bars to 2 bar for blower inlet, system inlet, and atmospheric pressure
Range:	0.0 bars to 3.5 bar for blower outlet and system outlet
Accuracy	$\pm 0.5\%$ bar
Temperature range	-20 to +85 °C
Output range	4-20 mA
Calibration	Calibrated



Figure 3.8: Pressure transducers for barometer, system inlet, blower Inlet (left), and for blower outlet and system outlet (right)

## 8- Temperature sensors

The main specifications of temperature sensors are illustrated in table 3.6 and figure 3.8 depicts the temperature sensors have been chosen according to UK industrial standards. These temperature sensors are used to measure atmospheric temperature and the temperature at different positions; at the inlet blower system, at suction and discharge of the blower. The reason behind select this type of temperature sensor that there are not expensive and adequate for the measurement required in this research.

Table 3.6: The main specifications of Temperature Sensors

Make.	Omega
Model	PT100
Type	Prop
Accuracy	$\pm 0.3^{\circ}\text{C}$
Temperature range	0-100 $^{\circ}\text{C}$
Output range	4-20 mA



Figure 3.9: the Temperature sensor (PT100)

## 9- Data acquisition system (USB-201)

The device offers the following features:

- Eight single-ended 12-bit analogue inputs
- 100 ks/s max sample rate
- Eight separately configurable digital I/O channels
- 32-bit counter input
- Digital trigger input
- Exterior pacer clock input
- Interior/exterior pacer clock output
- User voltage output
- Two screw terminal banks for field wiring connections

This device powered by the +5 V USB source from the computer; no external power is required

## 10- Computer station and Tracer-DAQ Pro software

Computer station with Pro software installed inside it to monitor and record the data from Data acquisition system have been used. Pro software is a more powerful than normal Tracer-DAQ – with extra active resources and controls. It acquires, analysis, displays data, and produces signals within minutes, offers easy export to Excel and it also acquires and plots data from up to 48 channels. Moreover, also acquires up to 1 million samples per channel.

The pressure and temperature signals were input to the device using ten synchronous channels. After undertaking amplification and conditioning, both the pressure and temperature signals were composed by the high-speed acquisition card and showed on a computer screen. The construction of the data acquisition system is shown in figure. 3.10.

Figure. 3.11 illustrate the devices and a graphic display of acquisition system programmed by Tracer-DAQ Pro. This type of Data acquisition system has been chosen according to UK industrial specification, because they are easy to use and the measurement accuracy of this device is satisfactory.

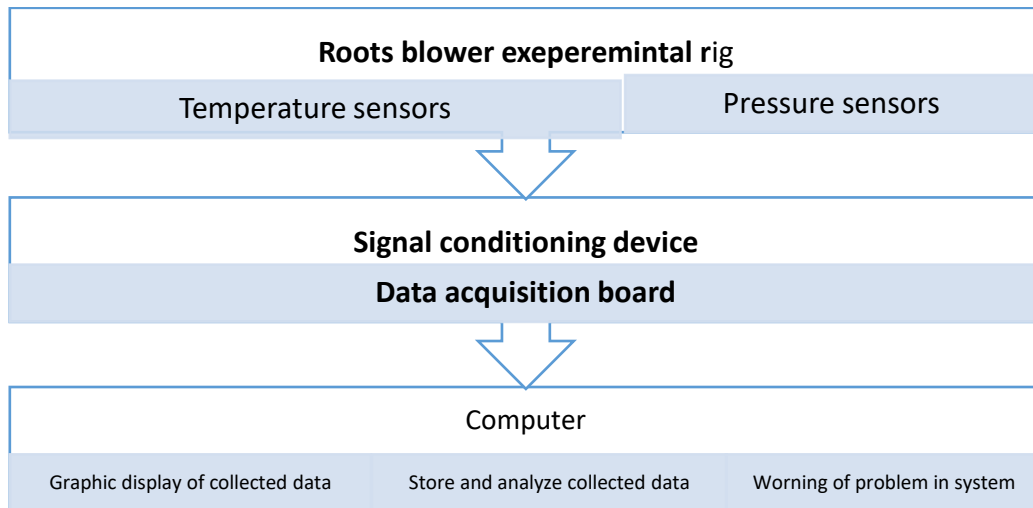


Figure 3.10: A Dynamic data acquisition system

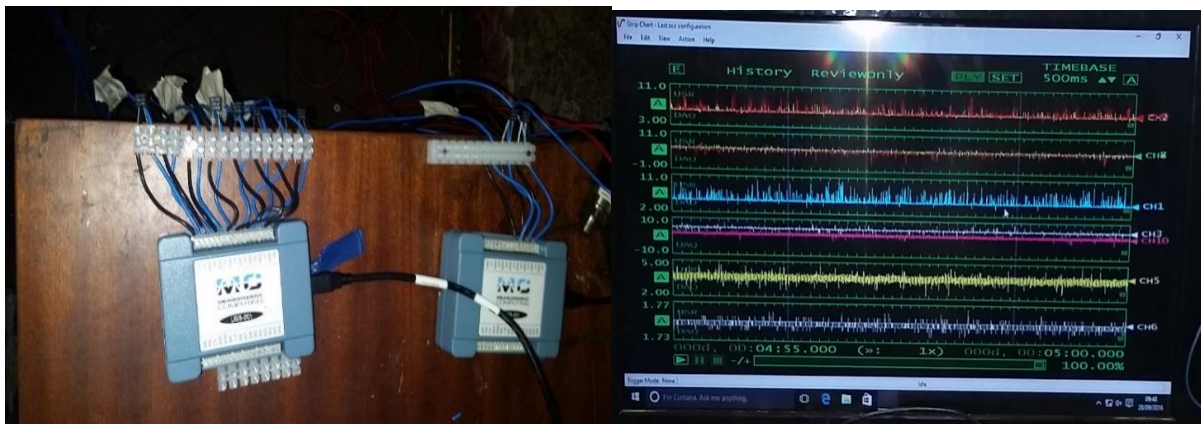


Figure 3.11: Devices and graphics display of the acquisition system

## 11- Pipes

Different lengths and measurements of tubes, ducts, and fittings have been bought and used in the test rig. The main pipes are made from steel, but the extended pipes were plastic type. There are some reasons behind that, the plastic pipes are easier to carry and install, and they are low cost as compared to the stainless steel pipes. The diameter of both inlet pipe and the outlet pipe are 152 mm.

### 3.1.1.2. Calibration of instruments

In this experimental work, all the pressure transducers and temperature sensors have been calibrated by the seller Company, and all the certificates and converter procedures are found in table A1.1 in appendix A1.

### 3.1.2 Experimental method and facilities

The standard test method and facilities have been used by follow the ISO 5167 standards in these measurements. Investigation study to record the pressure (P) and the temperature (T) values were conducted in order to measure the transient pressure and transient temperature with the rotational speed. The signal was collected and analysed by the acquisition and analysing system. The maximum operational pressure was 0.1MPa with an output voltage current of 100 mv, and the variety of operational temperature was between  $-40^{\circ}\text{C}$  and  $85^{\circ}\text{C}$  for every one temperature degree.

Temperature sensors with an accuracy of  $\pm 0.3^{\circ}\text{C}$  and pressure sensors were arranged and installed through the Roots blower test rig, including two sensors that were installed to measure the gas temperature ( $T_{\text{in}}$ ) and the gas pressure ( $P_{\text{in}}$ ) at the suction side of the blower. Other two sensors were installed to measure the gas temperature ( $T_{\text{out}}$ ) and the gas pressure ( $P_{\text{out}}$ ) at the discharge side of the blower as shown in Figure. 3.12. Two sensors were also installed to measure the pressure ( $P_{\text{sys.in}}$ ) and temperature ( $T_{\text{sys.in}}$ ) at the system inlet, and two sensors were also installed to measure the pressure ( $P_{\text{amp}}$ ) and temperature ( $T_{\text{amp}}$ ) of the ambient.

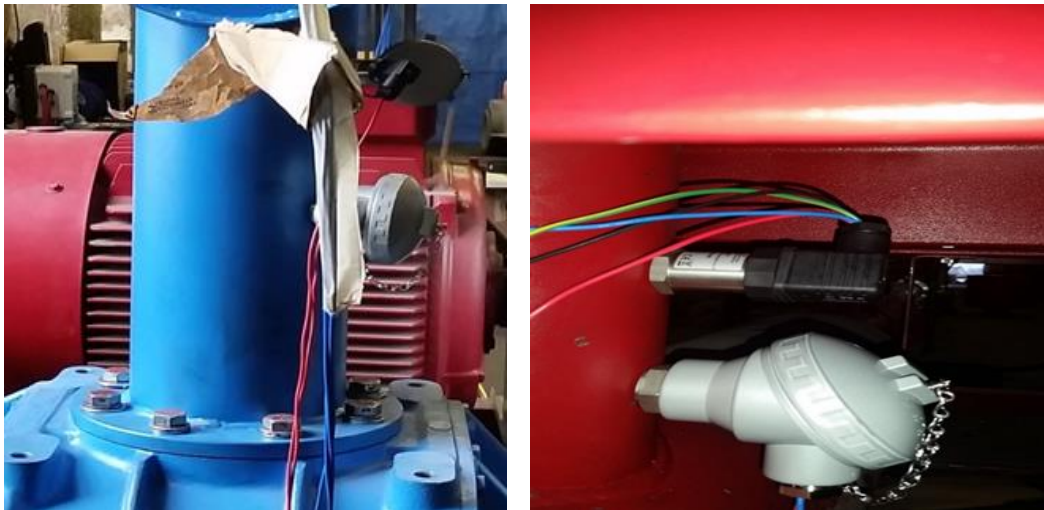


Figure 3.12: The pressure and the temperature sensors installed on the suction side (left) and discharge side (right)

Two pressure gauges were installed on the blower system to monitor the pressure of the suction chamber and the pressure in the discharge side. Also, other pressure gauge were installed at the end discharge system to regulate the pressure load according to the measurement required in this investigation as shown in Figure 3.13.

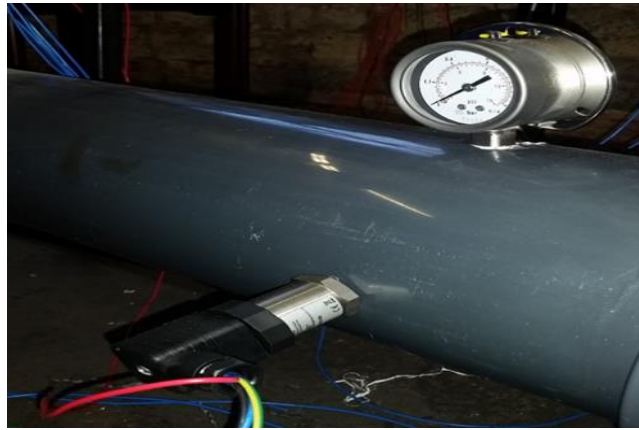


Figure 3.13: The pressure sensors and the pressure gauge installed on the discharge side

All the pressure sensors displayed the absolute pressure with an accuracy of  $\pm 0.5\%$ . Flow meter system including a differential pressure transducer with accuracy  $\pm 0.5\%$  bar and orifice plate with mechanical fittings were installed between the suction of the system and the suction blower. The lowest accurate flow was  $0.01 \text{ m}^3/\text{sec}$  while the highest is  $0.12 \text{ m}^3/\text{sec}$ . In addition to the various gauges listed above, the blower system includes a main pressure regulator valve that controls the air pressure in the system. This valve regulates the pressure of the system from 0 bars to 1 bar. Pressure Regulator is located at the end of the outlet system

### 3.1.3. The measurement procedures

The blower characteristics and the pressure and temperature pulsations at different operation points are measured. During one measurement series, the blower speed  $N$  was kept at a constant level while the discharge was regulated using a manually actuated control valve. The mass flow rate characteristics were measured within a speed range of  $N=1200 \text{ rev}/\text{min}$  to  $2400 \text{ rev}/\text{min}$  with an increment of  $200 \text{ rev}/\text{min}$ , while the differential pressure  $\Delta p$  was changed with an increment of  $100 \text{ mbar}$  for every speed between 0 bar and 1bar. Additionally, the speed-dependent efficiency curves were calculated and plotted. The data has been recorded for every speed and pressure load and every five minutes. The detailed procedures of measurement are found in appendix A1.3

The measurements have been performed according to rotational speeds and pressure loads listed in the table 3.7.

Table 3.7: Rotational speeds and pressure loads have been used in experimental measurements

Rotational speed (rev/min)	Pressure loads (kPa) have been applied in Roots blower test rig					
1200	0	10	20	30	40	50
1400	0	10	20	30	40	50
1600	0	10	20	30	40	50
1800	0	10	20	30	40	High Tem.
2000	0	10	20	30	40	High Tem.
2200	0	10	20	30	40	High Tem.
2400	0	10	20	30	40	High Tem.

The data did not recorded for high speeds 1800 and above for 50 kPa pressure load because the temperature was increased quickly and may be effect the blower system.

### 3.1.4. Mass flow rate measurements by Orifice plates and related calculations

An orifice plate is a thin circular plate with a hole inside it, which is typically located in the pipe. It is a tool used for quantifying flow rate, for dropping pressure or for limiting flow. Also, the mass volumetric flow rate can be determined depending on the computation linked with the orifice plate (Linford, 1961). Bernoulli's principle is used to demonstrate the relationship between the fluid pressure and the fluid velocity: As the fluid is enforced to pass through the hole, the velocity rises and the pressure of fluid declines and vice versa. By determining the difference in pressure of the fluid between upstream pressure tap and downstream pressure tap, the flow rate can be found from Bernoulli's equation using discharge coefficients that have been obtained from extensive research on flow rate calculations (Baker, 2005; Crane, 1977; Miller, 1983).

The cross-section of a typical orifice plate is shown in Figures 3.14. The symbols given in subsequent text denotes to the consistent references. The portion of the plate inside the pipe would be round and concentric with the centerline of the pipe. The surfaces of the plate would continuously be flat and parallel (Baker, 2005).

**Key**

1 = upstream face,

2 = downstream face,

a = Direction of flow

D = Diameter of the pipe

E = Thickness of the plate

e = Thickness of the orifice

Figure 3.14: Standard orifice plate (Baker, 2005).

The arrangements and the positions of pressure taps for orifice plates measurement with corner pressure taps and D and D/2 pressure taps is shown in Figure 3.15. The symbols given in subsequent text denotes to the consistent references

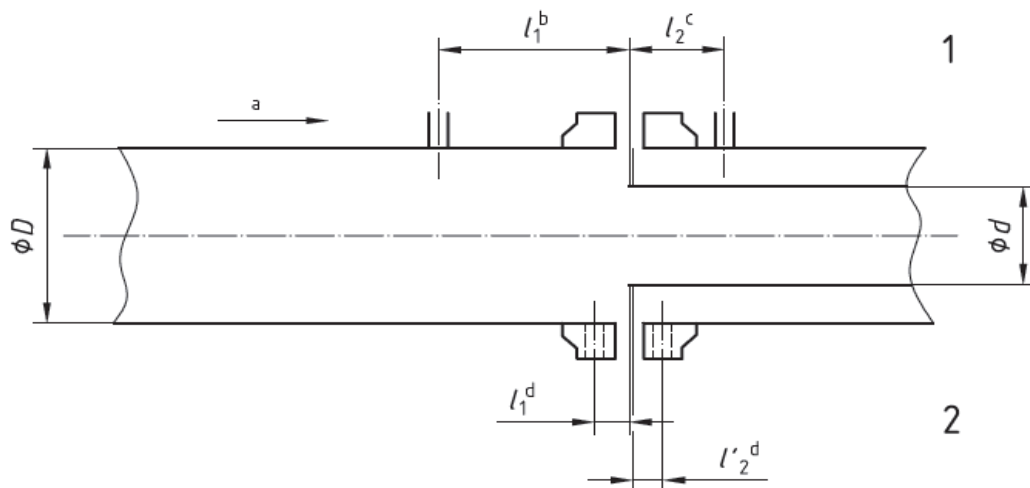


Figure 3.15: Pressure tapping locations for orifice plates with corner pressure taps and D and D/2 pressure taps arrangements (Baker, 2005).

**Key**

- 1 = upstream face, b.  $l_1 = D \pm 0.1D$
- 2 = downstream face, c.  $l_2 = 0.5D \pm 0.02D$  for  $\beta \leq 0.6$ ,
- a = Direction of flow. =  $0.5D \pm 0.01D$  for  $\beta > 0.6$

The measurement techniques are dependent on the installation of an orifice plate inside a duct in which a fluid is running through. The existence of the orifice plate produces a static pressure variance between the upstream and downstream borders of the plate. The volumetric flow rate  $\dot{V}$  can be obtained using Equation below (Bean, 1971).

“The discharge coefficient for sharp-edged orifice plates is calculated by using *Reader-Harris/Gallagher (1998)* equation, which has been used in European and American industry standards. The equations below basically follow the international standard ISO 5167 and use SI units” (Reader-Harris, 2007; Standard & ISO, 1991).

$$\dot{V} = \frac{\dot{m}}{\rho_1} \dots\dots\dots (3.1)$$

$$\dot{m} = \frac{C}{\sqrt{1-\beta^4}} \varepsilon \frac{\pi}{4} d^2 \sqrt{2\rho_1 \Delta p} \dots\dots\dots (3.2)$$

Where:

C = discharge coefficient, dimensionless

d = inside orifice diameter, m

$\dot{m}$  = mass flow rate, kg/s

$\dot{V}$  = volume flow rate, m<sup>3</sup>/s

$\beta = \frac{d}{D}$  = diameter ratio of orifice diameter to pipe diameter, dimensionless

$\Delta p$  = differential pressure, Pa

$\varepsilon$  = expansibility factor (expansion factor), dimensionless

$\rho_1$  = density of the fluid in the level of upstream tapping, kg/m<sup>3</sup>

According to ISO 5167, the coefficient of discharge, C, is reliant on the Reynolds number, Re, which is itself dependent on  $\dot{m}$  and has to be obtained by initial estimates and iterations.

It is essential to distinguish the fluid density and the fluid viscosity at the operational conditions.

In the situation of a compressible fluid, it is also compulsory to identify the isentropic exponent of the fluid at operational conditions.

The discharge coefficient, C, is specified by the Reader-Harris/Gallagher (1998) equation (Bean, 1971):

$$C = 0.5961 + 0.0261\beta^2 - 0.216\beta^8 + 0.000521 \left(\frac{10^6\beta}{ReD}\right)^{0.7} + (0.0188 + 0.0063A)\beta^{3.5} \left(\frac{10^6}{ReD}\right)^{0.3} + (0.043 + 0.080e^{-10L_1} - 0.123e^{-7L_1})(1 - 0.11A) \frac{\beta^4}{1-\beta^4} - 0.031(M'_2 - 0.8M'_2)^{1.1} \beta^{1.3} \dots (3.3)$$

When  $D < 71.12$  mm (2.8 in), the next additional term shall be in Equation (3.3) (ISO; Reader-Harris, 2007):

$$+0.011(0.75 - \beta) \left(2.8 - \frac{D}{0.0254}\right) \dots (3.4)$$

In the equation for C,

$$A = \left(\frac{19000\beta}{ReD}\right)^{0.8} \dots (3.5)$$

$$M'_2 = \frac{2L_2}{1-\beta} \dots (3.6)$$

$$ReD = \frac{4\dot{m}}{\pi\mu D} \dots (3.7)$$

Where,

$ReD$  = Reynolds number in the, dimensionless

$\mu$  = dynamic viscosity of the fluid, Pa.s

$L_1$  ( $= l_1/D$ ) is the distance of the upstream tapping from the *upstream* face of the plate and the pipe diameter

$L_2 = l'_2/D$  is the distance of the downstream tapping from the *downstream* face of the plate and the pipe diameter

$L'_2$  = the position of the downstream spacing from the *downstream* surface,

$L_2$  = the location of the downstream spacing from the *upstream* surface;

The values of  $L_1$  and  $L_2$  for D and D/2 tapping locations are (ISO):

$$L_1 = 1, \quad L_2 = 0.47$$

For compressible flows, an *expansibility factor* or *expansion factor* is similarly considered. The empirical formula (Reader-Harris, 2007; Standard & ISO, 1991) for calculating the expansion factor,  $\varepsilon$ , is as

$$\varepsilon = 1 - (0.351 + 0.256\beta^4 + 0.93\beta^8) \left( 1 - \left( \frac{p_2}{p_1} \right)^{\frac{1}{k}} \right) \dots\dots\dots (3.8)$$

The above equation is valid only if  $p_2/p_1 \geq 0.75$  (Lau, 2008; Reader-Harris, 2007).

### 3.1.5. Uncertainty

The uncertainties of experimental measurements can be defined as the deviations or the percentage of inaccuracies in the experimental measurements commonly due to various errors. In the measurements accomplished for this investigation, such human errors can be reflected and reproduced in the measurement of the pressure, the temperature and the mass flow of operating fluid in the system. The errors in measurement are occurred by various measuring tools and apparatuses that do not necessarily operate under perfect measurement conditions.

The procedures of uncertainty estimation are as follows:

1. Calculate the mean of the samples,  $\bar{X}$  by using the equation (3.9) (Bell, 2001).

$$\bar{X} = \frac{1}{n} \sum_{i=0}^n X_i \dots\dots\dots (3.9)$$

Where,

$\bar{X}$  = Mean value of samples

$X_i$  = Sample value

n = Number of samples

2. Compute the standard deviation of the sample,  $S_X$  using equation 3.10 (Castrup & Castrup, 2010):

$$S_X = \sqrt{\frac{1}{n-1} \sum_{i=0}^n (X_i - \bar{X})^2} \dots\dots\dots (3.10)$$

The (n-1) value is the degree of freedom of assessment, which refers to the number of independent parts of the information that is included in the estimation calculation. In the lack of any systematic effects during collection of the sample, the standard deviation of the sample will be close to its population as the size of the sample or the degrees of freedom rise. The degrees of freedom for uncertainty estimation are beneficial in determining confidence limits and other values of uncertainty variables in the experimental measurement.

3. Compute the standard uncertainty of the sample,  $Eu$  using equation 3.11 (Castrup & Castrup, 2010):

$$Eu = \frac{S_X}{\sqrt{n}} \dots\dots\dots (3.11)$$

As example, the uncertainty calculations in the measurement for 2000 rev/min and no load test is shown below. The mean value of the outlet temperature samples can be calculated by:

Mean value:

$$\overline{T}_{out} = \frac{1}{6.6 * 10^5} \sum_{i=0}^{6.6*10^5} T_i = \frac{1}{6.6 * 10^5} (32.657 * 10^6) = 49.48 C^0$$

Sample standard deviation:

$$S_X = \sqrt{\frac{1}{6.6 * 10^5 - 1} \sum_{i=0}^{6.6*10^5} (T_i - \overline{T}_{out})^2}$$

$$= \sqrt{\frac{1}{6.6 * 10^5 - 1} \sum_{i=0}^{6.6*10^5} (32 * 10^6)^2} = 6.96 C^0$$

Estimated standard uncertainty:

$$Eu = \frac{S_X}{\sqrt{n}} = \frac{6.963}{\sqrt{6.6 * 10^5}} = 8.57E - 03 C^0$$

According to the same procedures described above, the uncertainty of the other measurements can be calculated. Some samples of uncertainty calculation are shown in Table 3.8. Furthermore, the full standard uncertainty results in this study are depicted in APPENDIX A2.

The mean estimated standard uncertainty,

$$E_{u\ mean} = \frac{1}{n_t} \sum_{i=1}^n E_u \dots\dots\dots (3.12)$$

Where  $n_t$  it is number of tests

Table 3.8: The uncertainty of some measurements

Rotor speed [rev/min]	Imposed Load [bar]	Mean standard uncertainty			
		Inlet temperature	Outlet temperature	Inlet pressure (Pa)	Outlet pressure (Pa)
2400	320	3.40E-03	8.90E-03	10.738	23.010
	200	3.40E-03	1.07E-02	9.9465	25.16
	100	5.50E-03	9.10E-03	16.086	18.367
	0	4.10E-03	1.24E-02	12.343	23.254
2200	400	2.60E-03	5.80E-03	8.586	15.165
	300	1.50E-03	3.80E-03	4.950	8.838
	200	1.60E-03	4.20E-03	5.065	9.066
	100	1.60E-03	4.80E-03	5.154	9.006
	0	1.60E-03	4.80E-03	5.154	9.004
2000	400	1.60E-03	4.00E-03	5.422	9.497
	300	1.60E-03	4.30E-03	5.373	9.466
	200	1.70E-03	4.50E-03	5.422	9.336
	100	3.10E-03	8.30E-03	9.587	16.439
	0	2.70E-03	8.50E-03	9.195	15.919

### 3.1.6. Experimental results and Roots blower performance calculations

#### 3.1.6.1 Calculation of mass flow rate

The calculation takes into account orifice plate constants as shown in table 3.9, the measured differential pressure, upstream and downstream pressure and temperature. It also takes into account the discharge coefficient of the orifice plate. These calculations of performance factors

have been obtained by using the equations 3.1 to 3.16 and the ideal gas equations at different fluid conditions and at different speeds of Roots blower. Some of the final results of mass flow rate are summarised in table 3.10. The full final results of mass flow rate are found in APPENDIX A3.

Table 3.9: Orifice plate constants

Pipe diameter D [m]	0.152	Upstream Tapping Distance l1 [mm]	152
Orifice plate inner diameter d [m]	0.0806	Downstream Tapping Distance (l'2) [m]	1
Beta ( $\beta$ )	0.53078	L1	0.45
Plate Thickness (E) [m]	7.6	L'2	0.68
Orifice Thickness (e) [m]	3.04	M_2	1.918

The values of density ( $\rho_{in}$ ) of air as working fluid have been obtained in different pressure and temperature fluid conditions at blower inlet by using the ideal gas equation:

$$P_{in} = \rho_{in}RT_{in} \dots\dots\dots (3.13)$$

The values of Reynolds number ( $R_{eD}$ ) have been obtained in different pressure and temperature fluid conditions at blower inlet by using equation (3.7):

Where,

$R_{eD}$  = pipe Reynolds number

$\mu$  = dynamic viscosity of the fluid, Pa. s

D = internal pipe diameter under operating conditions, m

$\dot{m}$  = mass flow rate, kg/s

For the dynamic viscosity  $\mu$  of air as working fluid, Sutherland's law formula has been used, which defines the relationship of an ideal gas absolute temperature T with the dynamic viscosity  $\mu$ . This formulation is still generally used frequently and provides properly correct results with a fewer percentage of error over a varied range of temperatures. Sutherland's law formula is (Sutherland, 1893):

$$\mu = \mu_{ref} \left( \frac{T}{T_{ref}} \right)^{3/2} \frac{T_{ref} + S}{T + S} \dots\dots\dots (3.14)$$

Where,

$T_{ref}$  = a reference temperature = 273.15 [K]

$\mu_{ref}$  = the viscosity at the  $T_{ref}$  reference temperature of the air =  $(1.716 \cdot 10^{-5})$ , [kg/ms]

S = the Sutherland temperature for the air = 110.4 [K]

The real mass flow rate of the blower is measured with an orifice plate at condition ( $P_{in}$ ,  $T_{in}$ ) and is corrected at reference condition ( $P_r$ ,  $T_r$ ). The corrected mass flow rate is obtained by using the equation below [65]

$$\dot{m}_{e,corr} = \dot{m}_e \sqrt{\frac{p_{in} * T_r}{p_r * T_{in}}} \dots\dots\dots (3.15)$$

The formula of an ideal gas is used to calculate the theoretical mass flow rate at conditions ( $P_{in}$ ,  $T_{in}$ ) and is as below [66]:

$$\dot{m}_t = \frac{p_{in} V_{rev}}{RT_{in}} * N / 60 \dots\dots\dots (3.16)$$

Table 3.10: The experimental results of the mass flow rate at different speed and for different pressure load condition

Rotor 3.speed of blower [rev/min]	Imposed Load [mbar]	The theoretical mass flow rate $\dot{m}_t$ (kg/s)	Mass flow rate $\dot{m}_e$ (kg/s)	Corrected Mass flow rate $\dot{m}_{e,corr}$ (kg/s)
2400	320	0.849	0.650	0.643
	200	0.854	0.674	0.668
	100	0.858	0.692	0.684
	0	0.859	0.716	0.707
2200	400	0.781	0.597	0.593
	300	0.784	0.613	0.608
	200	0.786	0.627	0.620
	100	0.788	0.641	0.633
	0	0.786	0.663	0.649

### 3.1.6.2 Calculation of volumetric Efficiency

The definition of the blower's volumetric efficiency is the real volume flow rate at the reference condition divided by the theoretical volumetric flow rate at the same condition. The equation has been used to calculate the volumetric efficiency at the inlet condition ( $P_{in}$ ,  $T_{in}$ ) is as below:

$$\eta_{vol} = \frac{\dot{V}_e}{\dot{V}_t} = \frac{\dot{m}_e}{\dot{m}_t} \dots\dots\dots (3.17)$$

Where,

$\dot{m}_e$  is the measured mass flow rate and  $\dot{m}_t$  is the real mass flow rate well-matched with the speed and the geometry of the blower. Some of the final results of volumetric efficiency are summarised in table 3.11.

### 3.1.6.3 Calculation of adiabatic efficiency

The adiabatic efficiency is defined at condition ( $P_{in}$ ,  $T_{in}$ ) as:

$$\eta_{ad,e} = \frac{\dot{W}_{ad}}{\dot{W}_{sys,e}} \dots\dots\dots (3.18)$$

Where,

$\dot{W}_{sys,e}$  = the power used by the blower system

$\dot{W}_{ad}$  = the adiabatic work is calculated by using the standard equation [66]:

$$\dot{W}_{ad} = \dot{m}_{e,corr} C_p T_{in} \left( \theta^{\frac{K-1}{K}} - 1 \right) \dots\dots\dots (3.19)$$

$\dot{m}_e$  is the measured mass flow rate and  $\dot{m}_t$  is the real mass flow rate well-matched with the speed and the geometry of the blower. Some of the final results of efficiencies are summarised in table 3.11. The full final results of efficiencies are found in APPENDIX A3.

Table 3.11: The experimental calculation results of volumetric efficiency and adiabatic efficiency at a different speed and for different pressure load condition.

Rotor speed [rev/min]	Imposed Load [mbar]	Volumetric Efficiency	Efficiency
2400	320	0.757	0.681
	200	0.782	0.728
	100	0.797	0.767
	0	0.823	0.819
2200	400	0.759	0.668
	300	0.775	0.702
	200	0.789	0.736
	100	0.803	0.773
	0	0.825	0.822
2000	400	0.750	0.661
	300	0.772	0.699
	200	0.787	0.734
	100	0.797	0.768
	0	0.831	0.828

### 3.1.7. Analytical method calculations of Roots blower performance

#### 3.1.7.1 Mass flow rate calculations

The design volume flow rate of the blower is constant for every revolution and equal 0.01816 m<sup>3</sup>/rev, and isentropic exponent (k) = 1.4 for air. Flow rate per revolution can be converted to flow rate per second for different rotor speeds by using the following formula:

$$\dot{V} \left( \frac{m^3}{sec} \right) = \dot{V}_d \left( \frac{m^3}{rev} \right) * N/60 \dots\dots\dots (3.20)$$

$$\dot{m}_d = \dot{V} * \rho_1 \dots\dots\dots (3.21)$$

Where,

$\dot{V}$  = volume delivery ( $\frac{m^3}{sec}$ )

$m_d$  = actual mass delivery (kg/s)

$V_d$  = Displaced volume ( $\frac{m^3}{rev}$ )

$N$  = rotor speed (rev/min)

### 3.1.7.2 Adiabatic efficiency calculations as f (Θ)

The ideal compression process from  $P_{in}$  to  $P_{out}$  are reversible adiabatic (i.e. isentropic) process.

The isentropic work required is:

$$W_i = p_{in} \dot{V} \left[ \frac{k}{k-1} \left( \theta^{\frac{k-1}{k}} - 1 \right) \right] = C_p T_{in} \left( \theta^{\frac{K-1}{K}} - 1 \right) \dots\dots\dots (3.22)$$

In general, the actual theoretical work done can be written as

$$W_a = p \dot{V} \left[ \frac{\theta}{v_i} + \frac{k}{k-1} \left( \frac{1}{k} * v_i^{k-1} - 1 \right) \right] \dots\dots\dots (3.23)$$

With:

$v_i$  = built-in volume ratio ( $v_i = 1$  for a lobe blower)

$C_p$  = constant pressure specific heat for air ~1.004 kJ/kg.k

For a lobe blower, the actual theoretical work done is:

$$W_a = \dot{V} (p_{out} - p_{in}) \dots\dots\dots (3.24)$$

$$\eta_{ad} = \frac{\text{work done isentropically}}{\text{Actual work done}} \dots\dots\dots (3.25)$$

The theoretical maximum achievable adiabatic efficiency

$$\eta_{ad,max} = \frac{W_i}{W_a} = \frac{p_{in} \dot{V} \frac{k}{k-1} \left( \theta^{\frac{k-1}{k}} - 1 \right)}{\dot{V} (p_{out} - p_{in})} \dots\dots\dots (3.26)$$

For a lobe, the theoretical maximum achievable adiabatic efficiency

$$\eta_{ad,max} = \frac{\frac{k}{k-1} \left( \theta^{\frac{k-1}{k}} - 1 \right)}{\theta - 1} \dots\dots\dots (3.27)$$

If the results of the above formula are plotted in a graphical format and at different values of  $\theta$  are used, the resulting represent is shown below in Figure 3.17.

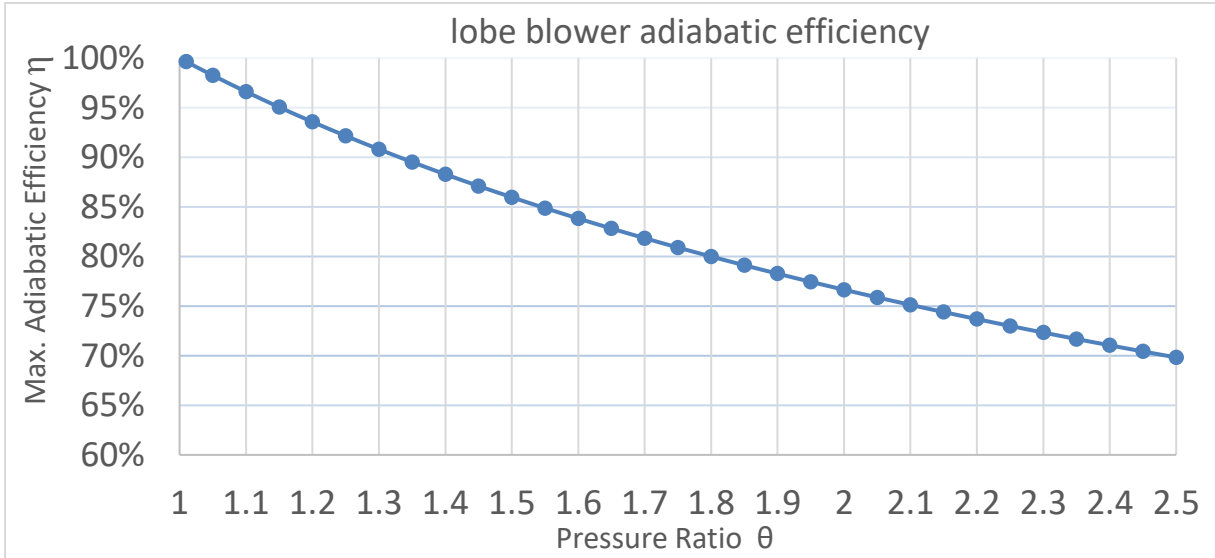


Figure 3.16: Maximum adiabatic efficiency of lobe blower

From figure 3.17 can be seen that the highest theoretical efficiency for lobe type blowers is 76.5% at a pressure ratio of 2. High efficiency can be achieved by decrease pressure ratio. As a result, from dynamic, friction, and leakages losses at suction and discharge sides, the actual compression work is higher, and consequently, the adiabatic efficiency is decreased. Across the whole blower, the effect of leakage flows is to introduce volumetric and adiabatic efficiencies into these expressions:

$$\phi = \frac{T_{out}}{T_{in}} = 1 + \frac{1}{\eta_v} \cdot \frac{k-1}{k} \cdot (\theta - 1) \dots\dots\dots (3.28)$$

$$\frac{W}{RT_{in}} = \frac{1}{\eta_v} \cdot (\theta - 1) \dots\dots\dots (3.29)$$

$$\eta_{is} = \frac{\frac{k}{k-1} \cdot \eta_v \cdot \left( \theta^{\frac{k-1}{k}} - 1 \right)}{\theta - 1} \dots\dots\dots (3.30)$$

By using equations above, volume and mass delivery, volumetric  $\eta_{vol}$ , and isentropic efficiency  $\eta_{is}$  can be calculated at a different speed, pressure, and temperature that have been obtained from the Roots blower test rig in different fluid conditions.

## **3.2 Numerical method based investigation of performance parameters of**

### **Roots blower**

Based on a literature review and research objectives have been acknowledged, most of the available Roots blower models lack in-depth investigation and analysis of flow characteristics. Currently, there is a limited understanding of the aero-thermo-dynamics behaviour of Roots blower under transient conditions which need to be evaluated both numerically and experimentally. The following research progress in this chapter covers the development of 2D/3D-dimensional models using the commercial software ANSYS/FLUENT CFD package and dynamic mesh technique. The incorporation of such computational simulation to simulate the flow behaviour inside Roots blower under transient behaviour offers the potential benefit of a methodology that is predictive, confer increased understanding of complex coupled behaviour, and promise a reduced reliance on expensive experimental tests. In this proposal, a 2D/3D-dimensional model of the HRBV613 Roots-type blower has been developed to simulate the internal flow inside it. The effect of operational conditions and other parameters on flow field behaviour in the Roots blower will be examined to deliver a reliable calculation of fluid properties at different rotational speeds and pressure ratios. This chapter illustrates the Roots blower numerical modelling. Also, the explanation and the justification of the solver and the boundary conditions have been presented.

#### **3.2.1 Introduction**

Several approaches to study and analyse the Roots blower are considered to choose the methodology that better predicts the internal flow behavior and the pressure, the temperature, and the velocity fields in the blower to find the optimal characteristics of flow process. There is a trend of continuous development of different methods to solve the problems connected to complex fluid flow in this type of blower. Several authors around a century ago have developed CFD-codes. Commercial CFD software packages nowadays offer several approaches to investigate Roots blower such as ANSYS FLUENT using the “Moving Dynamic Mesh” and ANSYS CFX using the “Moving-Mesh-Method” Options for the 2D or 3D numerical simulation.

ANSYS FLUENT using the dynamic mesh technique has been used in this project to study and investigate the aero-thermodynamic behaviour and performance characteristics and to get a better

prediction of the internal flow of a typical Roots blower under transient conditions. It is the competent software package among the other existing packages regarding analytical capability and time consumption, especially for optimisation model purposes. Furthermore, this package consists of different well-validated physical models. Accordingly, in a comprehensive range of CFD application, Fluent can afford a precise outcome in a reasonable time.

### **3.2.2. The development of CFD blower dynamic model using ANSYS FLUENT.**

Using the computational fluid dynamics CFD to predict a transient flow in Roots blower requires a solution of fluid dynamics equations (continuity and energy conservation), and suitable thermodynamics equations of state of real fluid behaviour, heat transfer and friction effects. ANSYS FLUENT 17.0 CFD package can provide comprehensive modelling capabilities for a wide range of incompressible and compressible, laminar and turbulent, ideal or real gas, steady-state or transient fluid flow in complex geometries (ANSYS, 2010). The methodology of using CFD in modeling fluid flow has dependent on some principles (H. K. Versteeg & W. Malalasekera, 2007), which should be followed: (1) define the modeling goals (domain identification) and Pre-processing, which is used to define the geometry, generate the grids (mesh), input the flow parameters and the boundary conditions to the code. (3) Solver setting, which is used to resolve the governing equations of the flow process at given conditions. Four different methods in CFD simulations are used as a flow solver: (I) finite element method; (II) finite difference method, (III) finite volume method, and (IV) spectral method. However, ANSYS FLUENT 17.0 solver is based on a finite volume method. (4) Post-processing, which is used to deliver the data and show modelling results in graphical and easy to read format.

### **3.2.3 Roots blower Flow Domain Identification and Pre-processing**

In CFD simulations, identifying the flow domain that will be modelled is an essential step because it gives an idea about the boundaries of the geometry and where the domain starts and finishes. The first model in this research will be developed for simulating air dynamics process.

#### **3.2.3.1 Roots blower Geometry Establishment**

The CFD software can model the geometry, dimensions; rotors shape or preferably with faster and flexible software such as a Solid-Work and then, the data can be transferred through an

interface to the simulation software. The flow domain has been done by considering three-dimensional geometry see figure 3.18. Using this feature will simplify the governing flow equation. The geometry has been established using the Solid-Work software, and data then transferred to the simulation software through an interface. However, in the case of fluid flow modelling and before setting up the mesh, it is necessary to convert the surface body of the geometry from a solid surface to a fluid zone. This step allows FLUENT to read the domain as fluid flow (C. ANSYS, 2014).

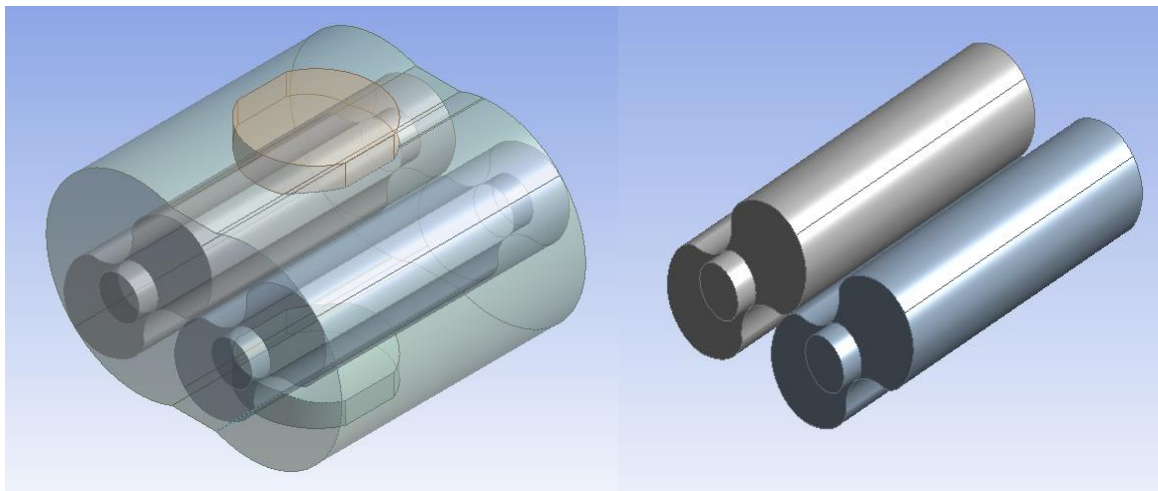


Figure 3.17: HRVB613 Roots blower numerical model and their rotors

The Roots blower model has been simplified to a two-dimensional (2D) model in several studies according to available literature in order to investigate the flow characteristics within it (see Figure 3.19). The Roots blower domain of computation is normally divided into three regions: the suction pipe region, the discharge pipe region and the impellers meshing region. There are two essential distinctions between a three-dimensional model (3D) and a two-dimensional model (2D) of Roots blower: the first difference is that the suction/the discharge pipe for the three-dimensional model is a cylindrical shape, whereas it is four-sided for the two-dimensional model; the second difference is that the leakage between the two plates and the two rotors (axial leakage) is not considered in the a two-dimensional model. Although there are some variances between both models, the two-dimensional model has been proven to be accurate enough to understand the effect of the main operation and geometric parameters on flow characteristics of Roots blowers (Y. Liu et al., 2015; S.-K. Sun et al., 2017; S. Sun et al., 2017).

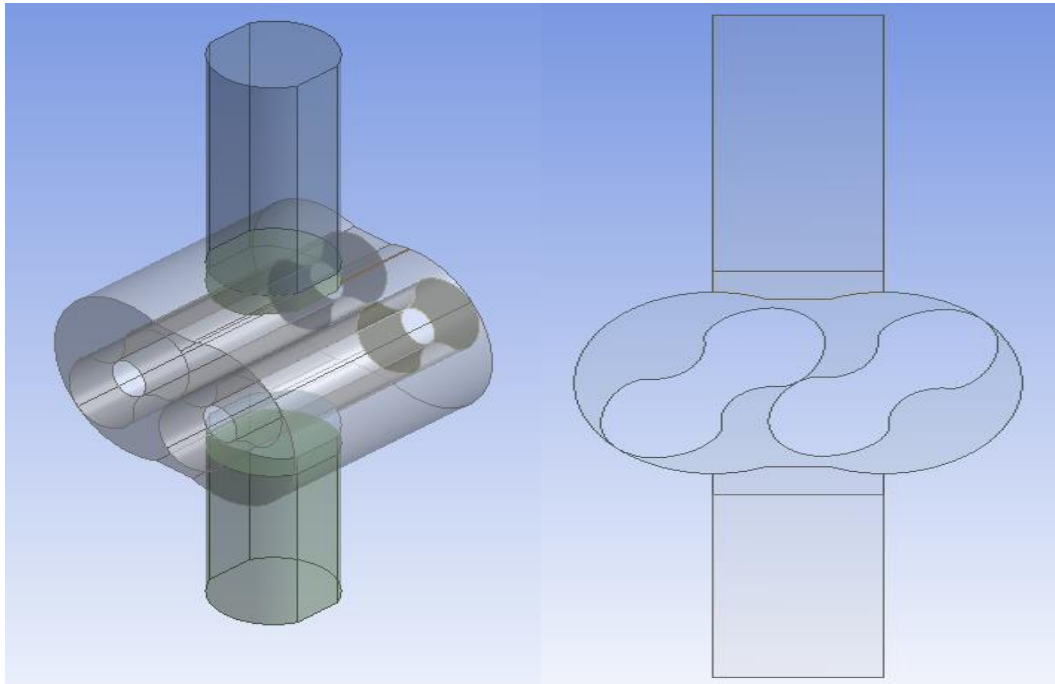


Figure 3.18: The 3D and 2D geometry of the fluid domain

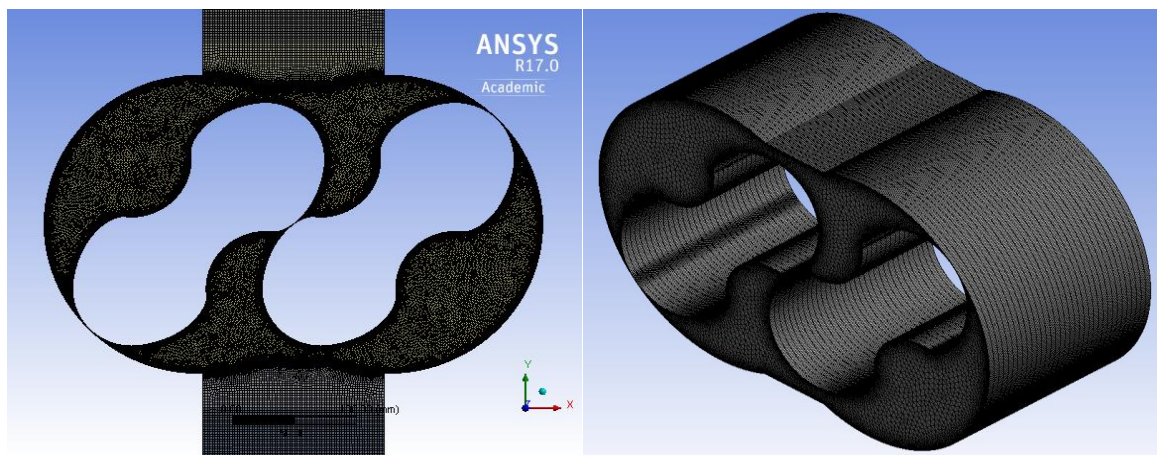
### 3.2.3.2 Mesh or Grid generation of Roots blower model

Define the boundary zones for the flow domain of the geometry is crucial to generate the grid system (mesh) of the Roots blower geometry. Boundary zone type determines the physical and operational characteristics of the model. For modelling two-dimensional Roots blower, three boundary zones have been defined including an inlet; outlet and rotary domains as seen in Figures 3.19 and 3.20. This step must follow the standard naming conventions for naming named selections as FLUENT just can read those boundary names. The mesh generation is conducted by dividing the geometry into some elements. These elements connected by nodes generate a grid on the entire flow domain. For most of CFD simulation, number, size and location of these elements are significant for solution converging particularly when the turbulent models are used (H. Ansys, 2014).

The quadrilateral elements were altered in the inlet and outlet areas, and the unstructured triangular element was employed in the rotary region to reach high quality with low quantity mesh. Considering the periodical variation of the chamber, local re-meshing, and spring-based smoothing methods were used in the rotating region to produce moving mesh to match the constraint of practical flow. The rotor should be rigid, and its location is determined by a control parameter in the process of mesh generation using a user-defined function (UDF) technique.

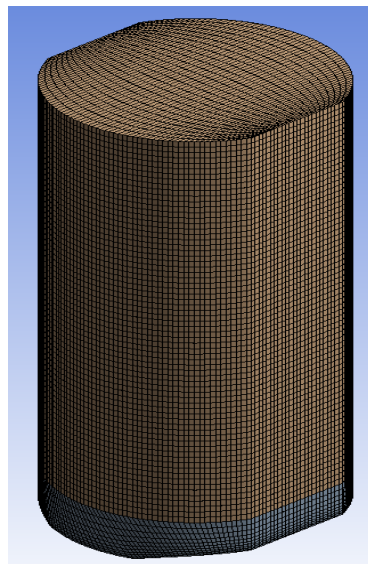
The mesh quality has a significant influence on CFD-results. Therefore a grid sensitivity test was applied, where the critical variables are the mass flow rate and the outlet temperature. Three levels of total grid number in the fluid regions were obtained for 2D model, 72800, 122000, and 234000. Also, three levels of total grid number in the fluid regions were obtained for 3D model, 1.20E+06, 1.84E+06, and 2.42E+06.

The total number of elements 122000 and 1.84E+06 are used for 2D and 3D model simulations respectively. As a result of mesh quality and to decrease the time of calculations, more details of the mesh sensitivity analysis are provided later in the next chapters.

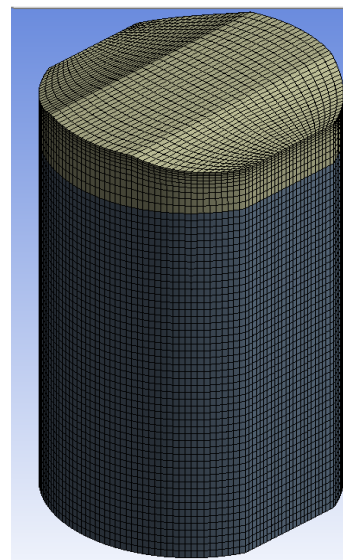


2D mesh

3D mesh (re-meshing zone)



3D inlet zone mesh



3D outlet zone mesh

Figure 3.19: 2D/3D fluid mesh domains

Also, more than four elements are specified inside the tip clearance (the gap between the rotors and the casing) and centre clearance (the gap between the two rotors). Furthermore, three inflation layers have been implemented around the wall of rotors and the two others around the casing wall to predict the flow field and the effect of leakage losses as shown in figure 3.21. However, the numbers of inflation layers are applied using trial and error because there are restrictions related to the dynamic mesh technique.

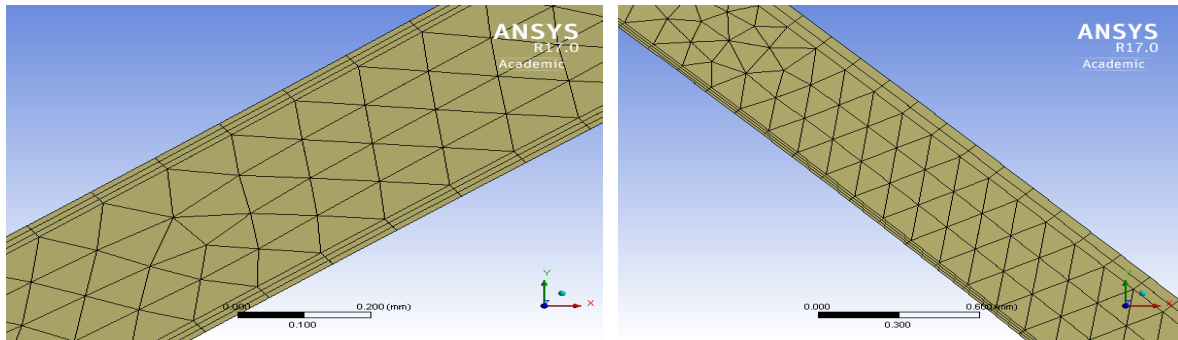


Figure 3.20: The meshing elements and the inflation layers inside the gap between the rotors and the casing (right) and inside the gap between the two rotors (left).

### 3.2.4 Solver Settings

In ANSYS FLUENT, there is an instrumental group of models, which can be used for analysis of fluid domain, solid domain, porous media (C. ANSYS, 2014). ANSYS FLUENT CFD package aims to solve numerically, the equations of motion (continuity and motion) for a fluid, for a given flow domain plus transport equations for any additional models such as turbulent and heat transfer models. In the solver, there are four distinct streams of numerical solution techniques which are; Finite element, Finite difference, finite volume method and Spectra methods. However, most of the established CFD codes such as CFX, Fluent, and Phoenix uses the finite volume method, which is a special finite difference formulation. In general, there are some steps should be follow to estimate the solution of the governing equations of fluid dynamics. The first step is a formal integration of governing equation over all the control volume, and the second step is the conversion of integrated forms of equations to algebraic equations, and then calculations of algebraic equations by an iterative method should give approximate solution for the governor equation (Ashgriz & Mostaghimi, 2002).

In this case, there are pressure variations in the system; the gas density variations with pressure have a significant impact on the pressure, temperature, and the flow velocity. Therefore, the

flow is considered to be a transient compressible flow. There are two formulations of solution that exist: implicit and explicit. In ANSYS FLUENT the implicit algorithm is considered to be the default solution formulation. The reason is that broader stability characteristic of the implicit formulation can obtain a converged steady-state solution much faster than the explicit formulation. However, the explicit formulation needs less memory than the implicit formulation (Henk Kaarle Versteeg & Weeratunge Malalasekera, 2007).

### 3.2.4.1 Turbulent Models

In ANSYS FLUENT, there are several turbulent models available, some for exceptional cases; others can be applied to a broader range of flow applications with a reasonable degree of confidence. These models including RANS Eddy-viscosity Models (Zero Equation model, Standard  $k$ - $\epsilon$  model,  $k$ - $\omega$  model, and SST model), RANS Reynolds-Stress Models (SSG model, LRR model and BSL EARSM model), Eddy Simulation Models (Scales Resolving Models SRS) (Detached Eddy Simulation (DES), Scale Adaptive Simulation SST (SAS) and Large Eddy Simulation (LES)). Historically, two-equations  $k$ - $\epsilon$  models are the most widely used turbulence models in industrial CFD (C. ANSYS, 2014). Some methods such as DES, LES and E-LES are very time-consuming, required high computational effort and mostly are not used in an industrial context, but have been used in researches. The insensitivity to adverse pressure gradients and separation of boundary layer are the main disadvantages of all  $k$ - $\epsilon$  models. They usually predict a reduced and delayed separation relative to observations. This can lead to evaluating the flow separation from smooth surfaces (aerodynamic bodies, diffusers, etc.) in excessively optimistic design. The  $k$ - $\epsilon$  models are therefore rarely used in external aerodynamics. However, for internal flow, the  $k$ - $\omega$  models can provide quite reasonable prediction results compared to other turbulent models (C. ANSYS, 2014). The computational cost in a CFD computation is due to the model of turbulence, the mesh and the time step used. The turbulence model, the mesh, and the time step are interconnected. Usually, for a more demanding turbulence model, finer mesh and short time step are required, preferably two-equation, linear turbulence models because the cost of computation is low (C. ANSYS, 2014). The two-equation turbulence model SST typically is one of the most often used model in ANSYS FLUENT. It consists of the  $k$ - $\epsilon$  and  $k$ - $\omega$  models combination. The  $k$ - $\epsilon$  model can be used in the free stream zone and the  $k$ - $\omega$  model can be used near the wall. Thus the best of

both models can be provided. Also, the eddy viscosity is limited by the SST model (Škerlavaj, Škerget, Ravnik, & Lipej, 2011).

In this research, a transient compressible flow has been simulated by implementing SST  $k-\omega$  turbulent modelling. This model can predict the solution with reasonable accuracy.

#### **3.2.4.2 Solution Steps**

For validating the current CFD model, the Roots blower performance data obtained from test rig measurements have been used. Air as ideal gas will be modelled with different initial conditions of pressures and temperature. The linearization of mass, x-, y-, z- momentum and energy partial differential equations will produce unknown variables ( $\rho$ , P, T, u, v, w) that need to be calculated to complete the solution. Therefore, to simplify the calculation, the ideal gas equations will be used to predict the thermodynamic properties of air. These equations have the capability of modeling one phase flow. Furthermore, it is well known that boundary conditions need to be provided before they can solve the differential equations. The fluid or heat flow problems can be defined by boundary conditions. It conveys the necessary information about the quantity of the fluid entering the domain, what is its inlet temperature and where it can leave. In this case, the boundary conditions are summarized in table (3.12).

The next steps were followed to run the simulation:

- 1- For solution convergence, the maximum convergence criteria,  $1e-06$  is used.
- 2- Before running the calculation, it is important to initialise the solution to the initial conditions. This step means that the entire flow domain is at the initial state.

For running the calculation, the rotational speed, the total time, the number of time steps and time step for different cases are illustrated in Table (3.13)

#### **3.2.4.3 Boundary conditions**

The pressure and the temperature boundary conditions were applied at the inlet and the outlet of the blower. At the suction, the total pressure is set as 0 Pa, and the total inlet temperature is 15 °C for all cases. At the discharge of the blower, the gauge pressure is assigned with values ranged from 0 to 70 KPa, and the temperature is kept at 0°C for all cases. Also, the rotational speed of the blower is ranged from 1200 to 2400 rev/min. Furthermore, the time step is a critical factor in the transient simulation, particularly for the dynamic mesh method. For this research study, every 0.2 degree of rotor rotation is set as a one time step.

### 3.2.4.4. Post-processing

The post processing here was focused on collecting data that will lead to obtaining the best understanding of internal flow process, and then later will be used for necessary gas calculation. The first step in post processing was to use the graphics and animations task page provided in FLUENT to visualize the results of CFD simulation. This feature allows setting up plots of contours, vectors, path-lines, particle tracks, scene descriptions and animations of the flow domain parameters (e.g. pressure, density, temperature, velocity).

Table 3.12: The boundary conditions used for the Roots blower simulation models

Boundary zone	Boundary type	Boundary condition
Inlet	Pressure inlet	0 gauge
	Temperature inlet	288.15 K <sup>0</sup>
	Operating pressure or (Reference pressure)	1 atm
Outlet	Pressure outlet	Variable from 0 to 700 millibar gauge
Rotors	Rotating	Variable from 1200 rev/min to 2400 rev/min
Cylinder or the casing	Stationary	No slip

Table 3.13: The running conditions used for the Roots blower model according to the mesh sensitivity analysis which are provided later in the chapter 4

Rotational speed (rev/min)	Time step (sec)	Number of time steps	Time for one rotation (sec)	Total time for five rotations ( sec)
1200	$2.77 \times 10^{-5}$	9000	0.05	0.25
1800	$1.85 \times 10^{-5}$	9000	0.0333	0.166
2400	$1.38 \times 10^{-5}$	9000	0.025	0.125

### 3.2.5. The Numerical Investigations framework

The flow within the Roots blower is associated with some flow and related geometrical variables. The following tables are listed the numerical simulations for each chapter. Table 3.14 contains the boundary conditions of the simulations required in chapter 4 to carry out the verification and the validation between the experimental results and the numerical outcomes. Table 3.15 contains the boundary conditions to carry out the simulations and obtain the numerical findings required in chapter 4 to characterise the Roots blower baseline model. Table 3.16 includes the boundary conditions and geometry configurations to carry out the simulations and obtain the numerical results required in chapter 5. Table 3.17 comprises the boundary conditions and geometry configurations to carry out the simulations and obtain the numerical results needed in chapter 6.

Table 3.14: The boundary conditions of the simulations required in chapter 4 to carry out the verification and the validation.

Rotational speed (rev/min)	Inlet pressure (kPa/abs)	Inlet temperature (K <sup>0</sup> )	Outlet pressure (kPa/ abs)	Pressure ratio (P <sub>out</sub> /P <sub>in</sub> )	Atmospheric Pressure (kPa/abs)
1200	94.61416	293.76	163.86	1.73	100.82
	93.96727	293.34	152.87	1.62	100.82
	93.35482	293.00	141.85	1.51	100.82
	92.81786	292.86	131.84	1.42	100.82
	92.24720	293.51	121.37	1.31	100.80
	90.54387	295.24	102.77	1.13	100.84
1800	84.17185	296.53	152.73	1.81	100.10
	83.37958	295.15	143.81	1.72	100.10
	82.40152	294.25	131.12	1.59	100.18
	81.3632	293.25	116.50	1.43	100.24
	80.54565	292.21	103.52	1.28	100.22
2400	86.11961	295.22	147.38	1.71	100.37
	85.25945	293.35	132.98	1.55	100.41
	84.78824	292.08	122.25	1.44	100.42
	83.55400	291.38	106.24	1.27	100.40

Table 3.15: The boundary conditions to carry out the simulations required in chapter 4

Rotational speed (rev/min)	Outlet pressure (kPa/ abs)	Pressure difference (kPa/abs)	Pressure ratio ( $P_{out}/P_{in}$ )	Tip clearance (TC) (mm)	Centre clearance (CC) (mm)
1200	131.325	30	1.296	0.24	0.34
	151.325	50	1.493		
	171.325	70	1.690		
1800	131.325	30	1.296		
	151.325	50	1.493		
	171.325	70	1.690		
2400	131.325	30	1.296		
	151.325	50	1.493		
	171.325	70	1.690		

Table 3.16: the boundary conditions and geometry configurations to carry out the simulations and obtain the numerical results required in chapter 5.

Rotational speed (rev/min)	Pressure difference (kPa/abs)	Pressure ratio ( $P_{out}/P_{in}$ ) abs	Tip clearance (TC) (mm)	Centre clearance (CC) (mm)
1200	30	1.296	0.22	0.34
			0.24	
			0.26	
			0.24	
			0.3	
			0.38	
	50	1.493	0.22	0.34
			0.24	
			0.26	
			0.24	
			0.3	
			0.38	

	70	1.690	0.22 0.24 0.26	0.34	
			0.24	0.3 0.34 0.38	
1800	30	1.296	0.22 0.24 0.26	0.34	
			0.24	0.3 0.34 0.38	
	50	1.493	0.22 0.24 0.26	0.34	
			0.24	0.3 0.34 0.38	
	70	1.690	0.22 0.24 0.26	0.34	
			0.24	0.3 0.34 0.38	
	2400	30	1.296	0.22 0.24 0.26	0.34
				0.24	0.3 0.34 0.38
			0.22 0.24	0.34	

	50	1.493	0.26	
			0.24	0.3
				0.34
	70	1.690	0.22	0.34
			0.24	
			0.26	
			0.24	0.3
				0.34
				0.38

Table 3.17: the boundary conditions and geometry configurations to carry out the simulations and obtain the numerical results required in chapter 6

Rotational speed (rev/min)	Outlet pressure (kPa/ abs)	Pressure difference (kPa/abs)	Pressure ratio ( $P_{out}/P_{in}$ )	Tip clearance (TC) (mm)	Centre clearance (CC) (mm)
1800	151.325	50	1.493	0.18	0.297
				0.24	0.342
				0.3	0.385

In the current investigation, mass flow rate and static temperature at the inlet and outlet of the Roots blower model has been monitored throughout the iterative process. The solution has been considered converged once the mass flow rate and static temperature fluctuations have become cyclic having the same amplitude in each cycle.

Many results have been collected using the monitoring method and post-processing from the experimental tests and the numerical simulations listed above at different flow conditions and geometrical configurations of the Roots blower. Moreover, the discussion in detail on these outcomes are presented in the next chapters, where the following chapter deals with the performance characterisation of flow within the baseline Roots blower model.

## **Chapter 4**

### **Quantitative evaluation of Performance characteristics of baseline Roots blower model**

The outcome from both the qualitative and quantitative analysis obtained from the experiments and the numerical simulations for different cases, concerning the Roots blower have been presented in this chapter. The analysis carried out had the objectives of understanding the complex flow field and their structure within Roots blower. Also, the influence of different flow-related parameters on Roots blower performance has been investigated. Furthermore, the correlations for estimating and predicting the blower performance, have been developed. This chapter has been divided into two sections, the first section dealing with the performance characterisation based on the experimental results, while the second part, concerning the performance characterisation based on the CFD numerical data. Both sections related to baseline Roots blower model.

## **4.1 The performance characterisation based on the experimental results**

This section presents the experimental result that include mass flow rate, pressure and temperature that have been obtained from test rig measurements. The Process for analysing the real measurements and the result of related calculation has been presented. The operational parameters included in this analysis are; Inlet and outlet temperature, inlet and outlet pressure, or pressure and temperature ratios.

### **4.1.1 Establish the relations between different non-dimensional parameters**

The characterisation of the performance of fluid machines using a dimensionless analysis is extremely useful. Thus, the current study presents a dimensionless analysis of the characteristics of Roots blower through results obtained in the course of experimental and numerical investigations. The main aim of this analysis is the in-depth understand of the characteristics and the behaviour of internal flow in the blower. Also to determine the main parameters that effect the performance of Roots blower. The dimensionless analysis carried out had the objective of developing the correlations for estimating and predicting the blower performance, so that these results may be applied to any blower with the same rotor shape (Hall & Dixon, 2013).

The inclusive understanding of the overall behaviour of all machineries generally is obtained from the dimensional analysis. This is the formal strategy in which the set of variables that represent some physical conditions decreases to a less number of non-dimensional sets. Once the number of independent variables is not large, dimensional analysis allows experimental relations between variables to be found with the greatest economy of effort. The applied of non-dimensional analysis to Roots blower-machines include additional essential practices which are: (1) to predict the blower model performance from experiments directed on a scale model; (2) to determine of the most appropriate sort of machine, based on greatest efficiency, for a predefined scope of flow rate, pressure head, and speed. Numerous approaches for developing non-dimensionless sets have been defined and depicted by several authors (Massey & Ward-Smith, 1998; Sawhney, 2011; Schetz & Fuhs, 1999; Shepherd, 1956). The subject of dimensional analysis was made straightforward and substantially by Edward Taylor (Taylor, 1974).

The performance of the machine will be affected if the fluid flow properties such as density  $\rho$ , and viscosity  $\mu$  are changed. For machines handling compressible fluids, other fluid properties are important.

The performance of a Roots blower machine can now be expressed in terms of the control variables, geometric variables, and fluid properties. By the procedure of dimensional analysis using the three primary dimensions, mass, length, and time, or alternatively, using three of the independent variables we can form the dimensionless groups.

The use of dimensional analysis to compressible flow has been increased considerably because the operational relationships obtained for compressible fluids is more complex in comparison with those already found for incompressible fluids. In addition to the fluid properties density  $\rho$ , and viscosity  $\mu$ , two additional variables are required for compressible flow; these are  $a_{01}$ , the stagnation speed of sound at the inlet of the machine, and  $\gamma$ , the specific heat ratio. In this analysis, the fluid regarded as an ideal gas

Another variables have been used in dimensional analysis of compressible flow are the mass flow rate  $\dot{m}$  and the isentropic stagnation enthalpy change  $\Delta h_{0s}$ .

The performance parameters  $\Delta h_{0s}$ ,  $\eta$ , and  $P$ , for machines dealing with a compressible flow, can be expressed functionally as

$$\Delta h_{0s}, \eta, P = f\{\mu, N, D, \dot{m}, \rho_{01}, a_{01}, \gamma\} \dots\dots\dots (4.1)$$

Because  $\rho_{01}$  and  $a_{01}$  are varying within the blower, their values are chosen at the inlet of the machine. Equation (4.1) show three relationships that are expressed functionally, each of it comprises of eight factors. Once more, choosing  $\rho_{01}$ ,  $N$ , and  $D$  as normal variables, each of it might be diminished to five dimensionless sets.

$$\frac{\Delta h_{0s}}{N^2 D^2}, \eta, \frac{P}{\rho_{01} N^3 D^5} = f\left\{\frac{\dot{m}}{\rho_{01} N D^3}, \frac{\rho_{01} N D^2}{\mu}, \frac{N D}{a_{01}}, \gamma\right\} \dots\dots\dots (4.2)$$

The group  $\frac{N D}{a_{01}}$  can be regarded as impeller Mach number because  $N D$  is proportional to impeller speed. Since this appears as an independent variable on the right-hand side of the

equation, it can be used to re-write the preceding relationships in terms of the inlet stagnation speed of sound  $a_{01}$ :

$$\frac{\Delta h_{0s}}{a_{01}^2}, \eta, \frac{P}{\rho_{01} a_{01}^3 D^2} = f \left\{ \frac{\dot{m}}{\rho_{01} a_{01} D^2}, \frac{\rho_{01} a_{01} D}{\mu}, \frac{ND}{a_{01}}, \gamma \right\} \dots \dots \dots (4.3)$$

By considering the fluid is ideal gas, useful groups of functional relationships can be obtained. The isentropic relationships for the rise of stagnation enthalpy as function of temperature and pressure can be expressed as:

$$\Delta h_{0s} = C_p (T_{02} - T_{01}). \dots \dots \dots (4.4)$$

Since  $\frac{T_{02}}{T_{01}} = \left( \frac{p_{02}}{p_{01}} \right)^{\frac{(\gamma-1)}{\gamma}}$

Then

$$\Delta h_{0s} = C_p T_{01} \left[ \left( \frac{p_{02}}{p_{01}} \right)^{\frac{(\gamma-1)}{\gamma}} - 1 \right] \dots \dots \dots (4.5)$$

Since  $C_p = \gamma R / (\gamma - 1)$  and  $a_{01}^2 = \gamma R T_{01}$ , then  $a_{01}^2 = (\gamma - 1) C_p T_{01}$   
 $a_{01}^2 = (\gamma - 1) C_p T_{01}$  and thus,

$$\frac{\Delta h_{0s}}{a_{01}^2} = \frac{\Delta h_{0s}}{(\gamma-1) C_p T_{01}} = \frac{1}{(\gamma-1)} \left[ \left( \frac{p_{02}}{p_{01}} \right)^{\frac{(\gamma-1)}{\gamma}} - 1 \right] = f \left( \frac{p_{02}}{p_{01}}, \gamma \right) \dots \dots \dots (4.6)$$

Using the equation of state,  $p/\rho = RT$ , the non-dimensional mass flow can be more conveniently expressed as

$$\hat{m} = \frac{\dot{m}}{\rho_{01} a_{01} D^2} = \frac{\dot{m} R T_{01}}{p_{01} \sqrt{\gamma R T_{01}} D^2} = \frac{\dot{m} \sqrt{\gamma R T_{01}}}{D^2 p_{01} \gamma} \dots \dots \dots (4.7)$$

The power coefficient can also be re-written as

$$\frac{P}{\rho_{01} a_{01}^3 D^2} = \frac{\dot{m} c_p \Delta T_0}{(\rho_{01} a_{01} D^2) a_{01}^2} = \hat{m} \frac{c_p \Delta T_0}{a_{01}^2} = \frac{\hat{m} \Delta T_0}{(\gamma - 1) T_{01}} \dots\dots\dots (4.8)$$

By assembling these new formed non-dimensional groups and inserting them in the equation (4.3), the simpler and more useful functional relationship are:

$$\frac{p_{02}}{p_{01}}, \eta, \frac{\Delta T_0}{T_{01}} = f \left\{ \frac{\dot{m} \sqrt{\gamma R T_{01}}}{D^2 p_{01} \gamma}, \frac{ND}{\sqrt{\gamma R T_{01}}}, Re, \gamma \right\} \dots\dots\dots (4.9)$$

A key advantage of the equation. (4.9) over equation. (4.3) is that the non-dimensional groups are in terms of inlet and outlet stagnation temperatures and pressures, which are parameters that are readily measured for Roots blower machine.

The performance parameters,  $p_{02}/p_{01}$ ,  $\eta$ , and  $\Delta T_0/T_{01}$  are not entirely independent and it is straightforward to write an equation relating the three. For a compressor, the isentropic efficiency is defined as

$$\eta_c = \frac{\Delta h_{0s}}{\Delta h_0} = \left[ \frac{\left( \frac{p_{02}}{p_{01}} \right)^{\frac{\gamma-1}{\gamma}} - 1}{\frac{\Delta T_0}{T_{01}}} \right] \dots\dots\dots (4.10)$$

A study was carried out on the dimensionless characteristics of the operating conditions of Roots blower, were collected measurement are analysed with the aid of the following dimensionless groups;

$$\text{Pressure ratio} = p_r = \frac{p_{02}}{p_{01}} \dots\dots\dots (4.11)$$

$$\text{Temperature ratio} = T_r = \frac{\Delta T_0}{T_{01}} \dots\dots\dots (4.12)$$

$$\text{Renolds number} = R_e = \frac{\rho_{01}ND^2}{\mu} = \frac{\rho_{01}a_{01}D}{\mu} \dots\dots\dots (4.13)$$

$$\text{Impeller mach number} = M_i = \frac{ND}{a_{01}} \dots\dots\dots (4.14)$$

$$\text{flow coefficient} = \hat{m} = \frac{\dot{m}}{\rho_{01}ND^3} = \frac{\dot{m}}{\rho_{01}a_{01}D^2} = \frac{\dot{m}\sqrt{\gamma RT_{01}}}{D^2 p_{01} \gamma} = \frac{\dot{m}\sqrt{(\gamma-1)C_p T_{01}}}{D^2 p_{01} \gamma} \dots\dots\dots (4.15)$$

$$\text{Pressure coefficient} = \hat{p} = \frac{\Delta p_0}{\rho_{01}N^2 D^2} = \frac{\Delta p_0}{\rho_{01}a_{01}^2} \dots\dots\dots (4.16)$$

$$\text{Enthalpy coefficient} = \hat{h} = \frac{\Delta h_{0s}}{N^2 D^2} = \frac{\Delta h_{0s}}{a_{01}^2} = \frac{1}{(\gamma-1)} \left[ \left( \frac{p_{02}}{p_{01}} \right)^{\frac{(\gamma-1)}{\gamma}} - 1 \right] \dots\dots\dots (4.17)$$

$$\text{Power coefficient} = \hat{P} = \frac{P}{\rho_{01}N^3 D^5} = \frac{P}{\rho_{01}a_{01}^3 D^2} = \frac{\hat{m}\Delta T_0}{(\gamma-1)T_{01}} \dots\dots\dots (4.18)$$

$$\text{Isentropic efficiency} = \eta = \left[ \frac{\left( \frac{p_{02}}{p_{01}} \right)^{\frac{(\gamma-1)}{\gamma}} - 1}{\frac{\Delta T_0}{T_{01}}} \right] \dots\dots\dots (4.19)$$

$$\text{Isentropic efficiency} = \eta = \frac{\gamma}{(\gamma-1)} \left[ \frac{\left( \frac{p_{02}}{p_{01}} \right)^{\frac{(\gamma-1)}{\gamma}} - 1}{\left( \frac{p_{02}}{p_{01}} - 1 \right)} \right] \dots\dots\dots (4.20)$$

$$\text{efficiency} = \eta = \frac{\dot{m} C_p T_{01} \left[ \left( \frac{p_{02}}{p_{01}} \right)^{\frac{(\gamma-1)}{\gamma}} - 1 \right]}{Q_{th} \Delta p_0} = \frac{\dot{m} C_p \rho_{01} T_{01} \left[ \left( \frac{p_{02}}{p_{01}} \right)^{\frac{(\gamma-1)}{\gamma}} - 1 \right]}{\dot{m}_{th} \Delta p_0} \dots\dots\dots (4.21)$$

$$\text{Volumatric efficiency} = \eta_v = \frac{\dot{m}}{\dot{m}_{th}} \dots\dots\dots (4.22)$$

$$\text{efficiency} = \eta = \frac{\eta_v C_p \rho_{01} T_{01} \left[ \left( \frac{p_{02}}{p_{01}} \right)^{\frac{(\gamma-1)}{\gamma}} - 1 \right]}{\Delta p_0} = \frac{\eta_v \gamma}{(\gamma-1)} \left[ \frac{\left( \frac{p_{02}}{p_{01}} \right)^{\frac{(\gamma-1)}{\gamma}} - 1}{\left( \frac{p_{02}}{p_{01}} - 1 \right)} \right] \dots\dots\dots (4.23)$$

#### 4.1.2. Determine the blower performance baseline factors (mass flow rate, efficiencies, power consumption and head pressure or pressure ratio)

In the practical applications, the design of the fluid machine depending mainly on utilise of empirical data that obtained from a large number of experiments. The presentation of the data in the understandable form is usually hard to achieve. Indeed, even from diagrams and charts, it might be hard to understand. The dimensional analysis of experiments data offers an approach for selecting related data and how it can be presented.

The non-dimensional based analysis is a valuable strategy for all experimental results and engineering design. In the event that it is conceivable to recognize the variables engaged with physical conditions, dimensionless analysis can provide useful relationships. It can be used to obtain any unknown factors from experimental analysis.

##### 4.1.2.1. Mass flow rate analysis

The relation between some operational parameters and the mass flow rate of the blower has been illustrated in Figure 4.1 and table 4.1. Experimentations have been carried out at different inlet pressures and temperatures. It is concluded that the rotational speed is the dominant factor affecting the mass flow rate which increases as the blower speed increases and declines with an increase of pressure ratio or pressure difference, this is due to that leakage rate is increasing at high levels of pressure differences (Ucer & Celik, 1980).

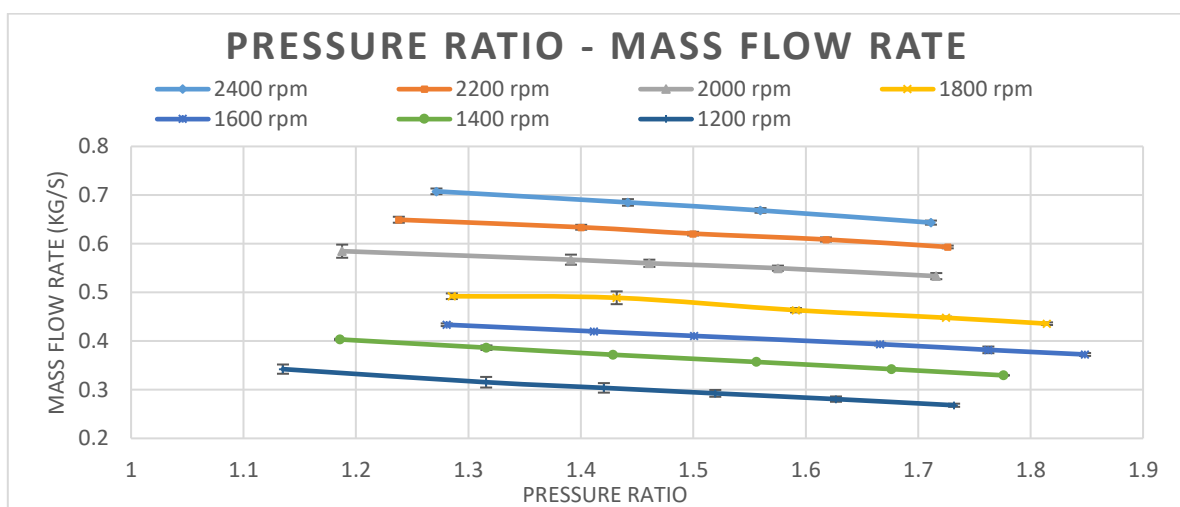


Figure 4.1: The relation between the mass flow rate of the blower and a pressure ratio at a different blower speed

Table 4.1 shows that the difference of mass flow rate at different blower speed is obvious which mass flow increases as blower speed increases. The maximum mass flow rate is 0.707 at speed 2400 rev/min, 0.649 at 2200 rev/min, 0.584 at 2000 rev/min, 0.492 at 1800 rev/min, 0.433 at 1600 rev/min, 0.403 at 1400 rev/min, and 0.342 at 1200 rev/min. Also, it can be concluded that the effect of pressure ratio on mass flow rate is not significant, for example as we can see in table 4.1 that the difference of mass flow rate between low-pressure ratio and high-pressure ratio for almost blower speed is about 0.05 kg/s. On the other hand, the difference in mass flow rate between low speed and high speed is about 0.36 kg/s

Table 4.1: The relation between the mass flow rate of the blower and a pressure ratio at different blower speeds

Blower speed Rev/min	Pressure ratio $\theta = \frac{p_2}{p_1}$	Mass flow rate $\dot{m}$ kg/s	Blower speed Rev/min	Pressure ratio $\theta = \frac{p_2}{p_1}$	Mass flow rate $\dot{m}$ kg/s
2400	1.711	0.643	1600	1.848	0.372
	1.559	0.668		1.762	0.381
	1.441	0.684		1.666	0.393
	1.271	0.707		1.500	0.410
2200	1.726	0.593	1400	1.411	0.419
	1.617	0.608		1.280	0.433
	1.499	0.620		1.775	0.329
	1.400	0.633		1.676	0.342
2000	1.238	0.649	1200	1.556	0.357
	1.716	0.533		1.428	0.371
	1.575	0.549		1.3160	0.386
	1.460	0.559		1.185	0.403
	1.391	0.567		1.731	0.268
1800	1.187	0.584		1.626	0.281
	1.814	0.435		1.519	0.293
	1.724	0.447		1.420	0.303
	1.591	0.463		1.315	0.315
	1.431	0.488		1.135	0.342
	1.285	0.492			

Moreover, the relation between mass flow coefficient and the pressure coefficient is shown in figure 4.2. It can absorb the same trend of the previous relationship between mass flow rate coefficient and pressure ratio which the difference of flow coefficient at different blower speed is apparent. Also, it can be concluded that the effect of pressure coefficient on flow coefficient is less significant

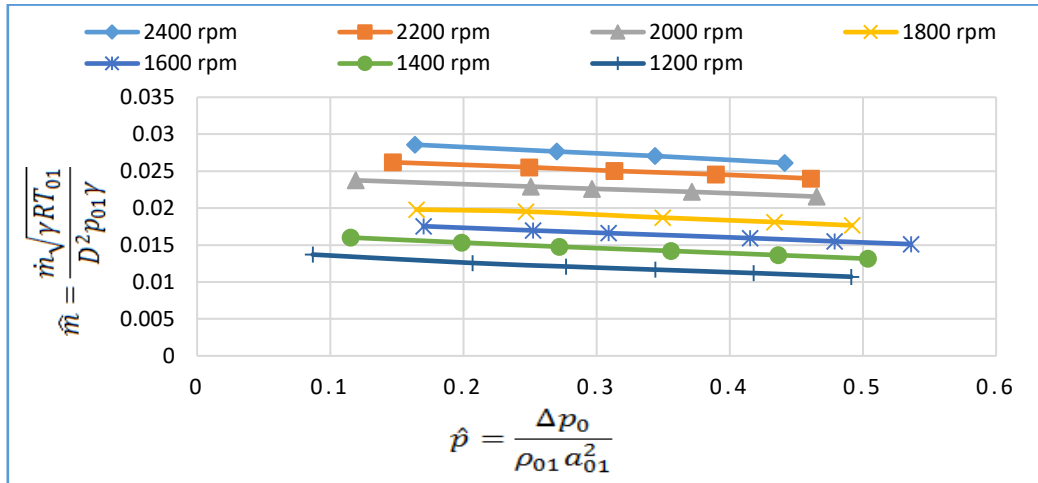


Figure 4.2: The relation between mass flow rate coefficient of the blower and pressure coefficient at a different blower speed

#### 4.1.2.2 Volumetric efficiency

The blower's volumetric efficiency in different working conditions is shown in Figure 4.3. It is concluded that the blower's volumetric efficiency rises when blower speed increases and pressure difference declines and vice versa. This is due to the influence of pressure losses inside the internal clearances which the leakage flow with increase of pressure losses causes the machine's volumetric efficiency to decline. Also, it is because the real inlet mass flow rate remains nearly constant during the measurements with inlet temperature and the theoretical inlet mass flow rate reducing when the temperature increases. This deviation is owed to that increases in pressure ratio enhance the leakage and consequently, reduces the efficiency. Improvement of volumetric efficiency can be achieved by raising the speed or lowering pressure differences or combination between them.

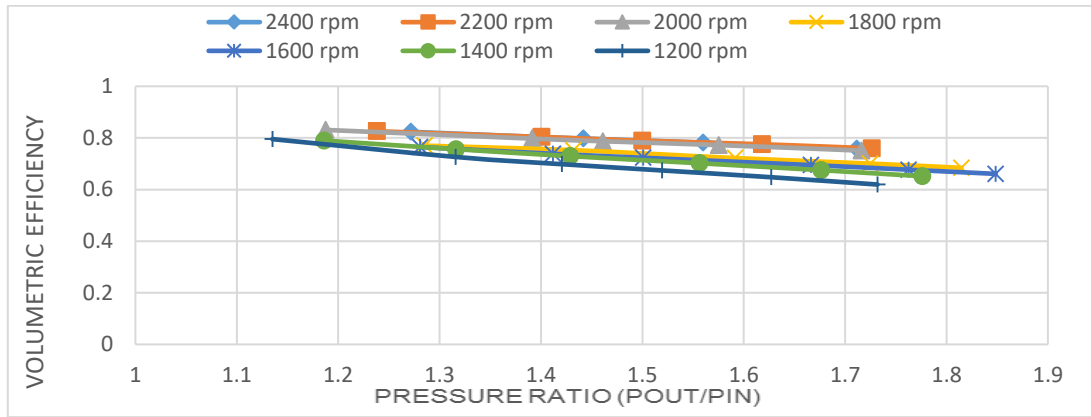


Figure 4.3: The variation of volumetric efficiency of the blower with a pressure ratio

Moreover, the relation between volumetric efficiency and the pressure coefficient is shown in table 4.4. It can absorb the same trend of the previous relationship between volumetric efficiency and pressure ratio which the difference of volumetric efficiency at different blower speed is apparent. Also, it can be concluded that the effect of pressure coefficient on flow coefficient is less significant

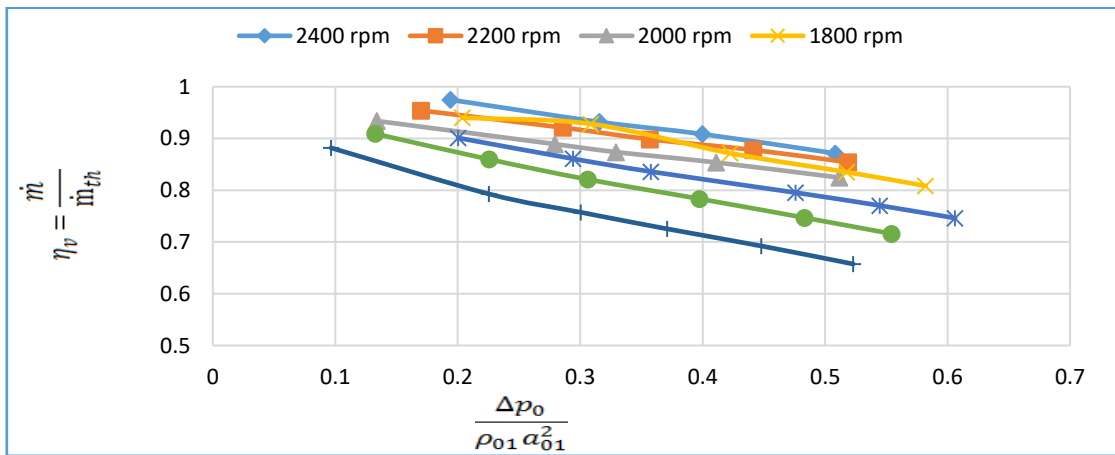


Figure 4.4: The variation of volumetric efficiency of the blower with a pressure coefficient

#### 4.1.2.3 Adiabatic Efficiency

The calculations for adiabatic efficiency has been done at different conditions. The effect of pressure on adiabatic efficiency with different operational gas conditions at a different speed is shown in Figure 4.5. The increase in adiabatic efficiency is owed to the rise in volumetric efficiency which reduces the real work consumed per unit mass of gas. It has been observed too from the curves that adiabatic efficiency illustrates the highest values at low-pressure ratios.

The reason is that adiabatic efficiency increases with the rise of speed and decrease in pressure ratio and also, the other reason is that mass flow rate of the blower increases with speed and declines at higher pressure ratios, which causes a reduction in volumetric efficiency and therefore decreases the adiabatic efficiency.

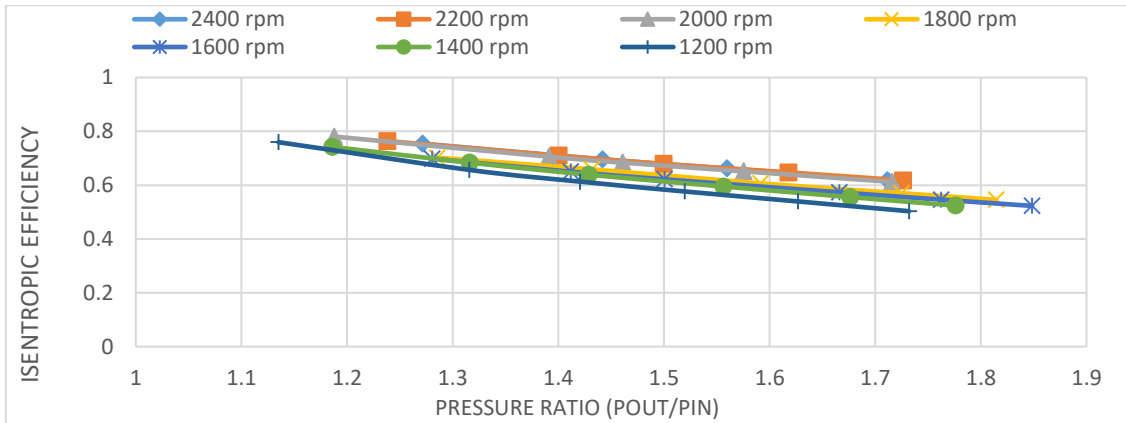


Figure 4.5: Variation of the adiabatic efficiency of the blower with a pressure ratio

#### 4.1.2.4 Power consumption

The power consumption is one of the performance factors that affect the efficiency of the blower which any increase of the power consumption of the blower will decline the efficiency of the blower.

The power consumption of the blower against pressure ratio are shown in Figure 4.6. It may be observed that it is higher with increasing pressure ratio. Also, it may be concluded that power consumption increases with the rise of speed.

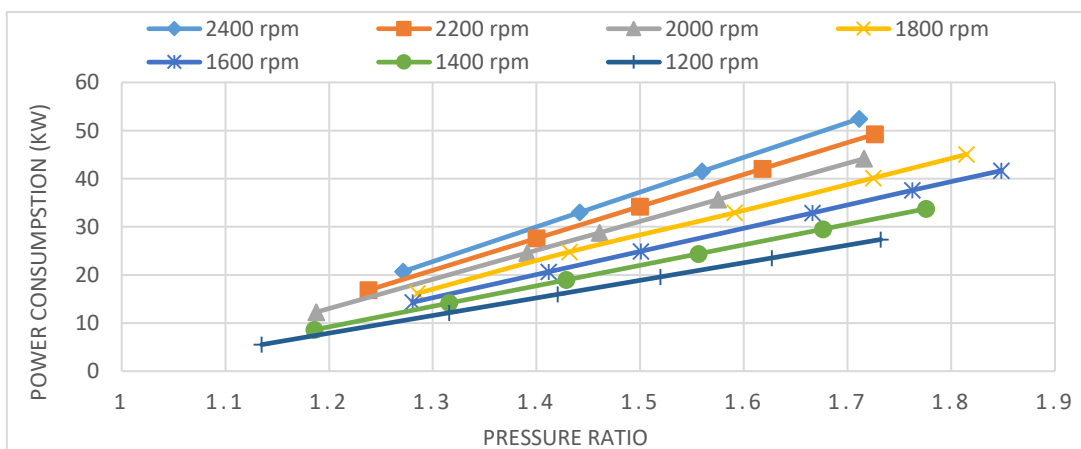


Figure 4.6: Variation of power consumption of the blower with a pressure ratio

#### 4.1.2.5 Blower performance

The main criteria of blower overall performance are the volumetric and the isentropic efficiencies. These are commonly assessed by variable pressure ratios and constant speed. Also, they introduced in the curve form as shown in figures 4.4 and 4.5. The volumetric efficiency generally declines with the increase of pressure ratios, but this decline becomes less significant when the speed of rotors reaches high levels. The curves display the maximum values of isentropic efficiency at low-pressure ratios and the essential limitation of the efficiency is at high-pressure differences or pressure ratios which are described by equation (4.23). The performance of Roots blower can be generally presented in the form of a chart in the most of applied studies. One of the main limitations of blower performance is that pressure ratio mainly depends on the highest discharge temperature which may be permitted without risk of overheating and deformation of blower components. This limit is reached early when the speed of impeller is low and therefore the volumetric efficiency is low.

#### 4.1.3. Deriving empirical equations depending on non-dimensional relation between different performance parameters

This part regarding developing empirical functions for Roots blower under study which are able to reproduce the experimental outputs from a reduced number of predefined inputs and may be applied to any Roots blower with the same rotor shape.

##### 4.1.3.1 Develop empirical correlation between Temperature ratio, Pressure ratio and volumetric efficiency in Roots blower

The relationship between the temperature ratio, pressure ratio and volumetric efficiency at different working gas conditions (at different inlet temperatures, inlet pressures, and speeds) that have been measured at Roots blower test rig are shown in Figure 4.7. It may be observed from the figures that temperature ratio increases as the pressure ratio increases and therefore volumetric efficiency decreases. As a result from multi regression analysis of the above relationship, empirical formula has been developed to predict the discharge temperature at the outlet of blower. The formula is given below:

$$\phi = C1\theta^{C2} * N^{C3} * \eta_v^{C4} = \frac{T_{out}}{T_{in}} = C1 \left( \frac{p_{out}}{p_{in}} \right)^{C2} * N^{C3} * \eta_v^{C4} \dots\dots\dots (4.24)$$

Where,

$N$  = non-dimensional speed

$C_1$ ,  $C_2$ ,  $C_3$  and  $C_4$  are constants and are dependent on the case study which for this case is equal to 1.035, 0.511, -0.048, and 0.0491 respectively.

The formula above has been tested for different air gas conditions which gave a good match with experimental results with error differences less than 3% as shown in figure 4.8. The main benefit from this formula is to help in the prediction of volumetric efficiency and discharge temperature of the Roots blower. Also, to reduce the time and the cost of blower development.

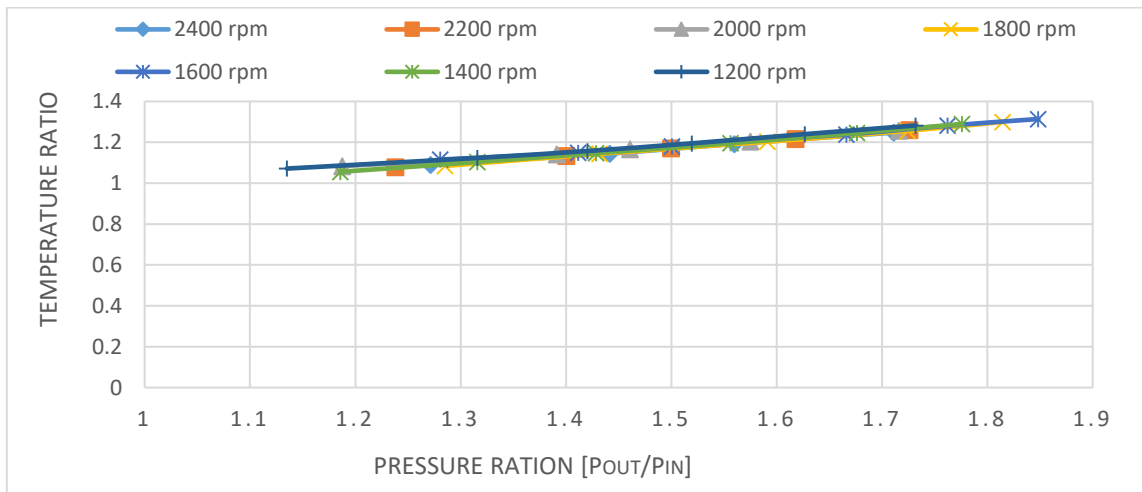


Figure 4.7: Temperature ratios and Pressure ratios relation in Roots blower at different speeds

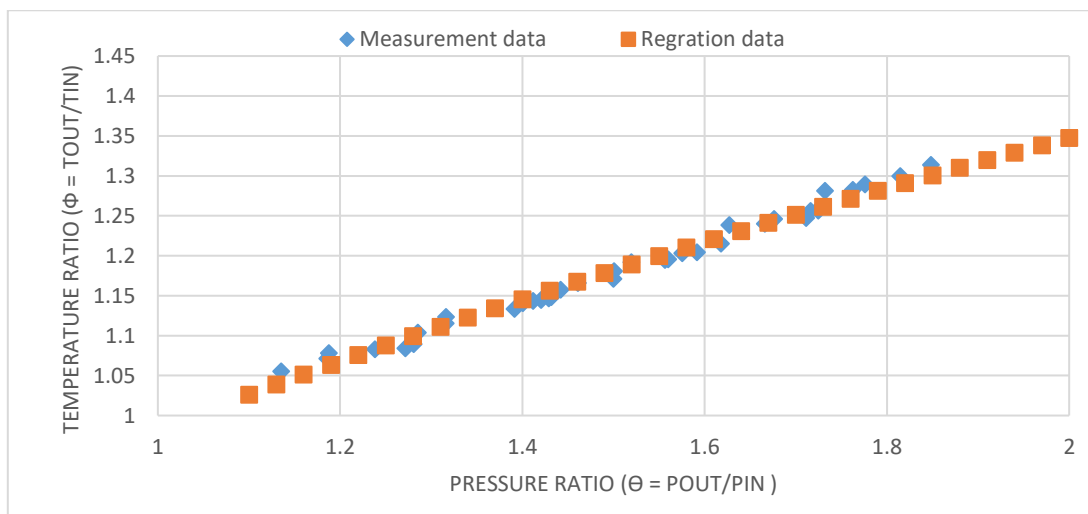


Figure 4.8: Comparison between Measurement data and Regression data for different pressure and temperature ratios

#### 4.1.3.2 Develop empirical correlation between, Pressure ratio, volumetric efficiency and speed in Roots blower

The relationship between the pressure ratio, volumetric efficiency and speed at different operating fluid conditions are shown in Figure 4.9. It may be observed from the figures that volumetric efficiency increases as speed increases and decreases as pressure ratio increases this is because mass flow rate increases with rise of speed and declines when pressure ratio increases and conversely. Multi regression analysis of this relationship have been conducted, to develop empirical formula in order to predict the volumetric efficiency of the blower. The formula is given below:

$$\eta_v = 0.5099\theta^{-0.407} * N^{0.224} \dots\dots\dots (4.25)$$

The formula above has been tested for different air gas conditions which gave a good match with experimental results with error differences less than 4% as shown in figure 4.10. The mean benefit from this formula is to help in the prediction of volumetric efficiency of Roots blower and to reduce development time and cost.

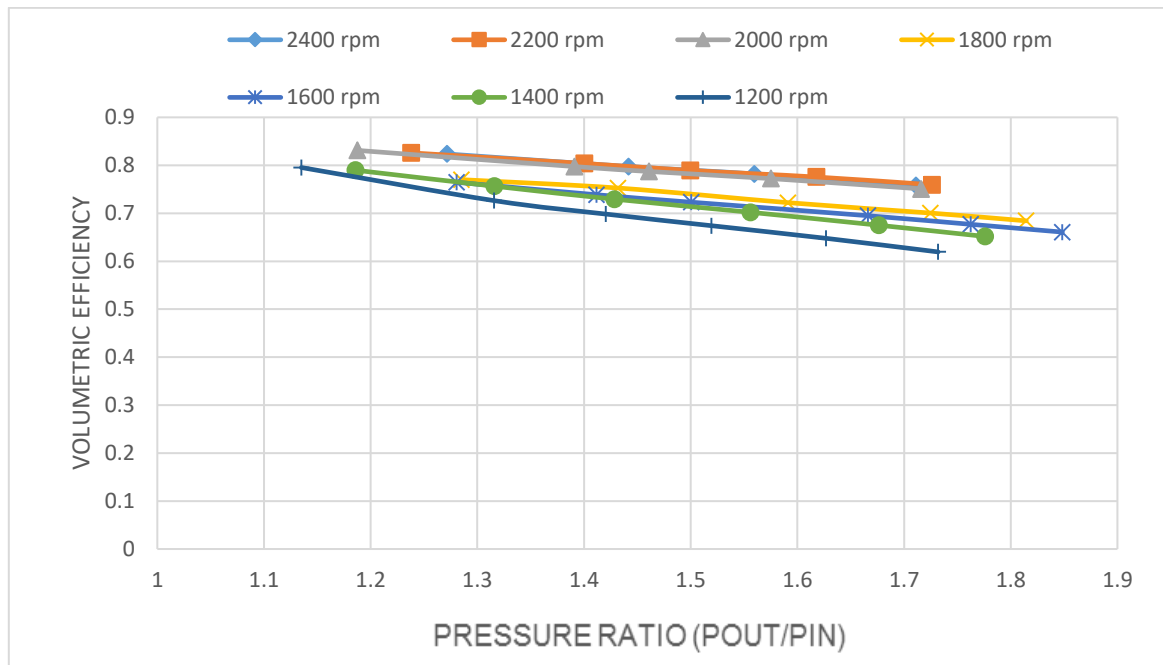


Figure 4.9: Comparison between Measurement data and Regression data for different pressure ratios

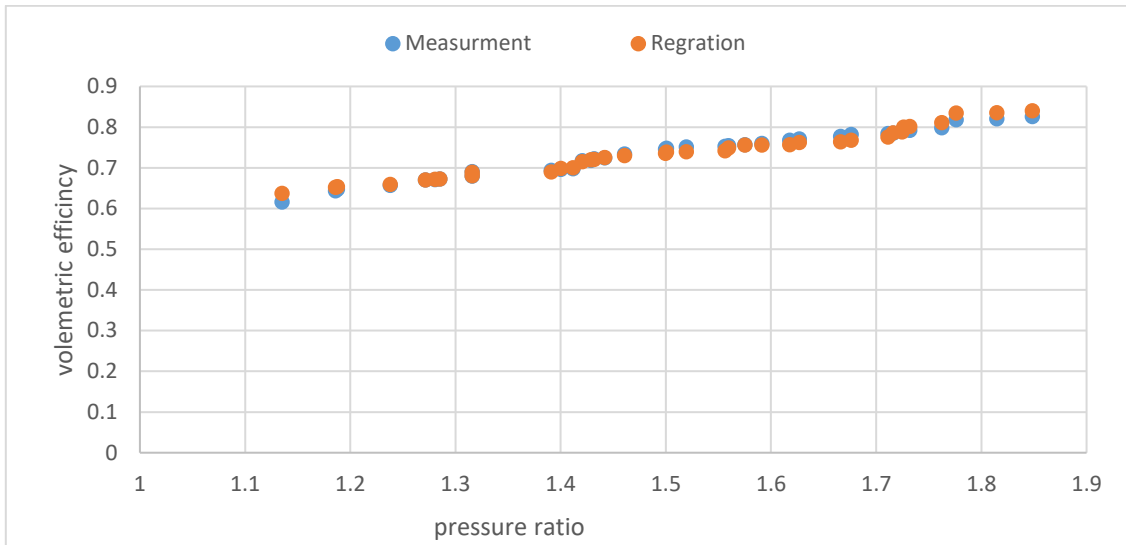


Figure 4.10: Comparison between Measurement data and Regression data for different pressure and temperature ratios

#### 4.1.3.3 Development an equation to predict mass flow rate within Roots blower

Based on the data presented in Table 4.2, and using multiple variable regression analysis, a semi-empirical equation to predict the mass flow rate of working fluid through the Roots blower, has been developed. This correlation is a function of the impeller Mach number, impeller speed, pressure ratio and the specific heat of working fluid.

$$\hat{m} = 10^{-0.716} * \hat{h}^{-0.131} * M_i^{1.230}$$

$$\frac{\dot{m}\sqrt{\gamma RT_{01}}}{D^2 p_{01} \gamma} = 10^{-0.716} * \left( \frac{1}{(\gamma - 1)} \left[ \left( \frac{p_{02}}{p_{01}} \right)^{\frac{(\gamma-1)}{\gamma}} - 1 \right] \right)^{-0.131} * \left( \frac{ND}{a_{01}} \right)^{1.230}$$

$$\dot{m} = 10^{-0.716} * \left( \frac{D^2 p_{01} \gamma}{\sqrt{\gamma RT_{01}}} \right) * \left( \frac{1}{(\gamma-1)} \left[ \left( \frac{p_{02}}{p_{01}} \right)^{\frac{(\gamma-1)}{\gamma}} - 1 \right] \right)^{-0.131} * \left( \frac{ND}{a_{01}} \right)^{1.230} \dots\dots\dots (4.26)$$

Figure 4.11 depicts the comparison between the prediction result of mass flow rate that has been obtained by using the developed equation (4.26) and the measuring result of mass flow rate.

It can be concluded that the outcome from both experimental and prediction equation is consistent and have the same trend. Hence, the correlation that has been developed can predict the mass flow rate of operating fluid in the Roots blower with good accuracy.

Table 4.2: Non-dimension relations have been used to develop the mass flow prediction correlation

$\hat{m} = \frac{\dot{m}\sqrt{\gamma RT_{01}}}{D^2 p_{01} \gamma}$	$\hat{h} = \frac{1}{(\gamma - 1)} \left[ \left( \frac{p_{02}}{p_{01}} \right)^{\frac{(\gamma-1)}{\gamma}} - 1 \right]$	$M_i = \frac{ND}{a_{01}}$
2.61E-02	4.15E-01	1.83E-01
2.70E-02	3.39E-01	1.81E-01
2.76E-02	2.76E-01	1.81E-01
2.85E-02	1.78E-01	1.81E-01
2.40E-02	4.22E-01	1.65E-01
2.45E-02	3.68E-01	1.66E-01
2.50E-02	3.07E-01	1.66E-01
2.55E-02	2.52E-01	1.66E-01
2.61E-02	1.57E-01	1.66E-01
2.15E-02	4.17E-01	1.50E-01
2.21E-02	3.47E-01	1.50E-01
2.26E-02	2.86E-01	1.50E-01
2.29E-02	2.47E-01	1.50E-01
2.37E-02	1.26E-01	1.50E-01
1.76E-02	4.64E-01	1.35E-01
1.81E-02	4.21E-01	1.35E-01
1.87E-02	3.55E-01	1.35E-01
1.95E-02	2.70E-01	1.36E-01

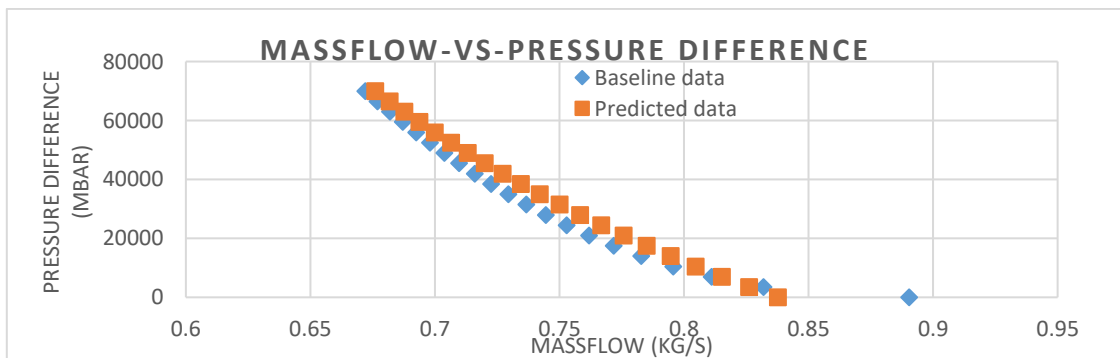


Figure 4.11: depicts the comparison between experimental data and predicted data

#### 4.1.3.4 Develop an equation to predict the power consumption of Roots blower

Based on the data presented in Table 4.3, and using multiple variable regression analysis, a semi-empirical equation to predict the power consumption of the Roots blower, has been developed. This correlation is a function of the impeller Mach number, impeller speed, pressure difference, inlet sound speed and density of working fluid.

Table 4.3: the non-dimension relations have been used to prediction correlation develop the power consumption

$\hat{P} = \frac{P}{\rho_{01} a_{01}^3 D^2}$	$\hat{p} = \frac{\Delta p_0}{\rho_{01} a_{01}^2}$	$M_i = \frac{ND}{a_{01}}$
1.56E-02	4.41E-01	1.83E-01
1.22E-02	3.44E-01	1.81E-01
9.70E-03	2.70E-01	1.81E-01
6.00E-03	1.64E-01	1.81E-01
1.49E-02	4.61E-01	1.65E-01
1.27E-02	3.90E-01	1.66E-01
1.03E-02	3.13E-01	1.66E-01
8.20E-03	2.49E-01	1.66E-01
5.00E-03	1.47E-01	1.66E-01
1.36E-02	4.65E-01	1.50E-01
1.10E-02	3.71E-01	1.50E-01
8.80E-03	2.96E-01	1.50E-01
7.50E-03	2.51E-01	1.50E-01
3.70E-03	1.19E-01	1.50E-01
1.29E-02	4.92E-01	1.35E-01
1.15E-02	4.34E-01	1.35E-01
9.30E-03	3.50E-01	1.35E-01
6.60E-03	2.47E-01	1.36E-01

$$\hat{P} = 10^{-0.732} * \hat{p}^{0.950} * M_i^{0.992}$$

$$= 10^{-0.732} * \left( \frac{\Delta p_0}{\rho_{01} a_{01}^2} \right)^{0.950} * \left( \frac{ND}{a_{01}} \right)^{0.992}$$

$$P = 10^{-0.732} * \rho_{01} a_{01}^3 D^2 * \left( \frac{\Delta p_0}{\rho_{01} a_{01}^2} \right)^{0.95} * \left( \frac{ND}{a_{01}} \right)^{0.992} \dots\dots\dots (4.27)$$

Figure 4.12 presents the comparison between the prediction result of power consumption that has been obtained by using the developed equation (4.27) and the measuring result of power consumption (baseline model). It can be determined that the outcome from both experimental and prediction equation is consistent and have the same trend. Hence, the correlation that has been developed can predict the power consumption of the Roots blower with reasonable accuracy

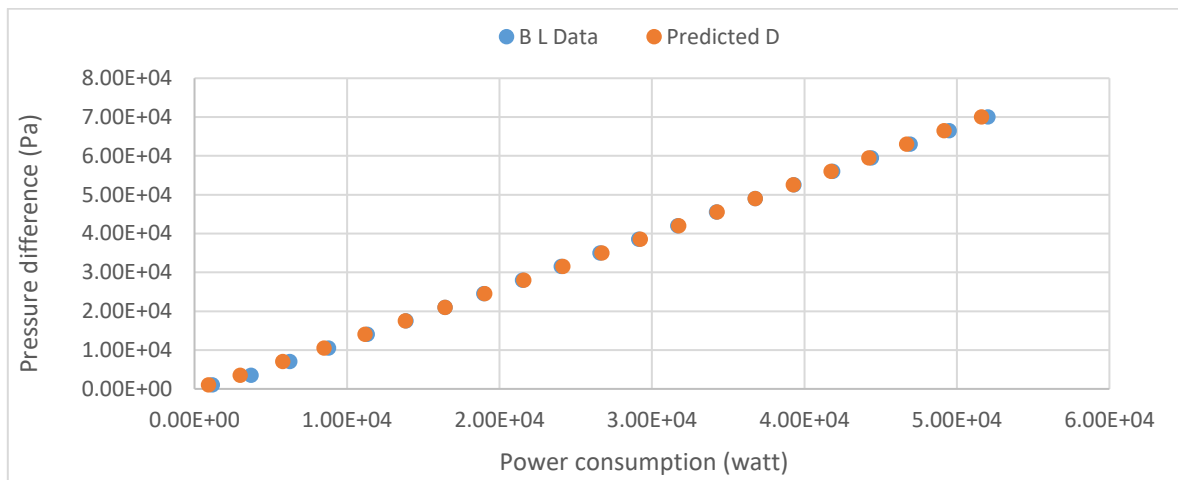


Figure 4.12: the comparison between experimental data and predicted data

In the present research study, the non-dimensional analysis has been introduced to predict of performance factors of Roots blower. The new non-dimensional expressions are obtained from the utilization of compressible flow relationships by characterising some condition factors that have a direct connection with the factors obtained from the measurement.

The non-dimensional correlations that have been developed can introduce the characteristics that make it simple to apply to numerous equivalent machines. Also, the other main feature of the non-dimensional equations is that it tends to be solved expressly with no iterative procedure. These relationships can be utilised to the changes in the design and performance between two blowers with a similar structure. The affinity laws are clearly valuable to predict the changes in the characteristics of the performance of the current blower or to evaluate the performance of modified blower structure before the development of the model.

The investigation and the characterisation of the performance of the Roots blower using the experimental approach is expensive regarding both time and cost. Advances in computational fluid dynamics (CFD) are one of the reasonable alternative research approaches. This approach can generate quantitative and qualitative data in order to better capture and understanding the natural physics of such type of blowers. Also, can provide a piece of detailed information related to the internal flow dynamics and the characteristics of the Roots blower. So performance characterisation of internal flow in detail of this blower has been performed in the next section by using CFD techniques.

## **4.2 The performance characterisation of numerical results**

This second part of this chapter present, the results that obtained from CFD simulations for different blower models that have been explained and summarised in chapter 3. Also, the process to analyse the CFD numerical result and related calculation are presented here. Moreover, in order to understand the behaviour and the complex structure of internal flow in Roots blower, a detailed qualitative and quantitative analysis is conducted. Furthermore, the effect of rotational speed, pressure, temperature, and velocity under different pressure loading conditions on the Roots blower performance are investigated and analysed.

### **4.2.1 Introduction to Computational Fluid Dynamics (CFD)**

The usage of Computational Fluid Dynamics (CFD) plays a significant role in fluid mechanics. Improvements that have been made to the capabilities of computers over the years have allowed for numerical approaches through the use of CFD software to advance the improvements in predicting the performance of the Roots blower quite easily. Moreover, internal flow inside the passages between the rotating parts and stationary parts have a significant influence on the Roots blower performance. Therefore, it is challenging experimentally to investigate the flow within the blower. Consequently, computational fluid dynamics CFD code has been used to examine and analyse the behaviour and the distribution of the flow inside the blower in good accuracy. In this current chapter, the transient numerical calculations using CFD codes and dynamic mesh technique (DMT) are carried out under different operating conditions for the flow field within a Roots blower. This chapter consists of, the mesh and time independence (sensitivity analysis). Also, the validation of the results obtained from CFD simulations against that obtained from the experimental results. Moreover, the main aim of this chapter is the

numerical investigation and characterisation of internal flow through the Roots blower. For this aim, the blower has been run at different rotational speeds under different pressure load conditions for five revolutions. Furthermore, detailed qualitative and quantitative analyses have been performed on local flow parameters (e.g. pressure, flow velocity, temperature and pressure fluctuations).

#### 4.2.2. The mesh independence test

The accuracy of the numerical results depends on the discretisation of the domain, which is known as the meshing process. The mesh independence is a critical stage because meshing can affect the accuracy of the CFD numerical results depending on the elements number. Table 4.4 and figure 4.13 summarise the numerical results of the mass flow rate for various mesh configurations.

Table 4.4: Mass flow rate spatial discretisation results

case	No. of elements	Mass flow rate (kg/s)	Percentage Difference (%)
1200 rev/min 100 mbar	2.34E+05	0.2838	7.42E-04
	1.22E+05	0.2837	
	7.28E+04	0.2856	
1200 rev/min 500 mbar	2.34E+05	0.2941	0.192
	1.22E+05	0.2935	
	7.28E+04	0.2980	

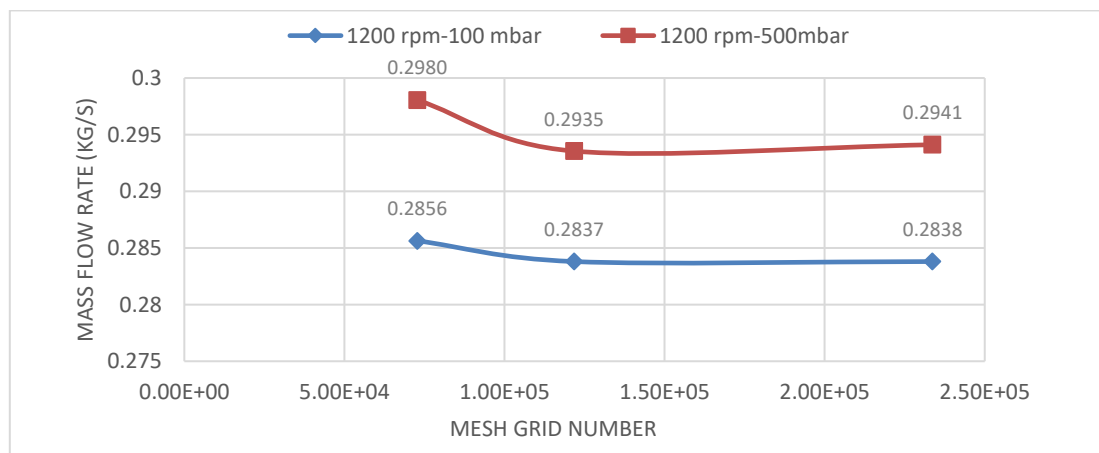


Figure 4.13: Mass flow rate spatial discretization results

Table 4.5 and figure 4.14 summarise the numerical results of air temperature at outlet blower with multiple mesh configurations. This analysis has been conducted to ensure the numerical results are independent of the mesh quality. According to the results shown in Table 4.4, for case 1 the percentage difference between the results for  $2.34E+05$  and  $1.22E+05$  number of mesh elements is minimal and negligible (0.00074 %). Also, for case 2 as shown in Table 4.5, the percentage difference between the results for  $2.34E+05$  and  $1.22E+05$  number of mesh elements is small and negligible (0.192 %).

Table 4.5: Outlet temperature spatial discretization results

case	No. of elements	Outlet temperature (K <sup>0</sup> )	Percentage Difference (%)
1200 rev/min 100 mbar	$2.34E+05$	327.88	4.26E-2
	$1.22E+05$	327.74	
	$7.28E+04$	327.40	
1200 rev/min 500 mbar	$2.34E+05$	341.69	0.2151
	$1.22E+05$	342.43	
	$7.28E+04$	347.94	

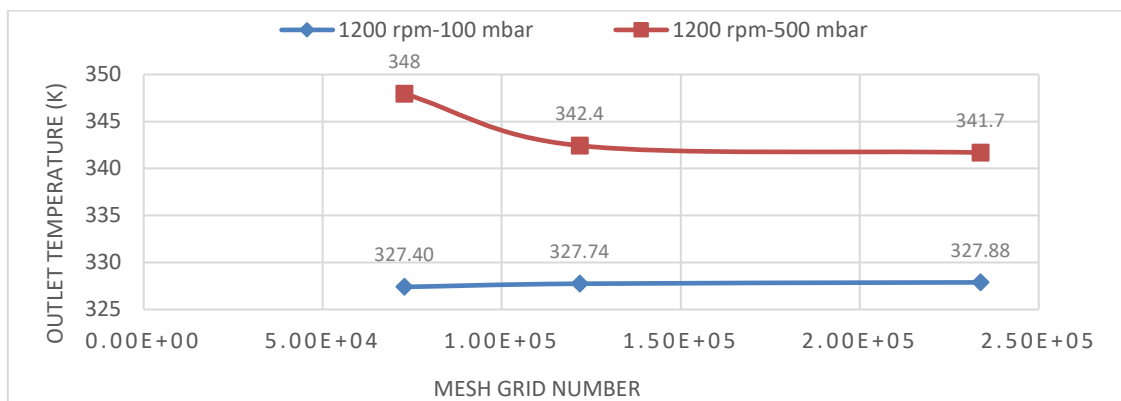


Figure 4.14: Outlet temperature spatial discretisation results

Henceforward, the mesh with  $1.22E+05$  elements has been considered in this investigation because it can capture the flow behaviour inside the Roots blower with good accuracy and to reduce the computation of the time and the cost as a compared with the mesh with  $2.34E+05$  elements. Therefore, the mesh with lower elements has been used for further investigation. Moreover, the meshes for other Roots blower models have been determined by using same procedures.

### 4.2.3. The time independence test

Since all the cases under investigations are transient states, for this reason, the time independence test should be performed. Otherwise, it can lead to inaccurate results of CFD. Therefore, the temporal discretisation test has been conducted with three different time steps. For more certainty and clarity to use this time-step independence test with different rotational speeds, this test has been performed for various time steps (1.38E-05, 2.77E-05 and 3.47E-05) or different rotational degrees, (0.1, 0.2, and 0.3) on Roots blower case study as mentioned in Tables 4.6 and 4.7 under the 1200 rev/min and 100 millibar operating conditions.

Table 4.6: Mass flow rate temporal discretization results

case	Time steps (s)	Mass flow rate (kg/s)	Percentage Difference (%)
1200 rev/min 100 mbar	1.38E-05	0.2834	0.1365
	2.77E-05	0.2837	
	3.47E-05	0.2842	

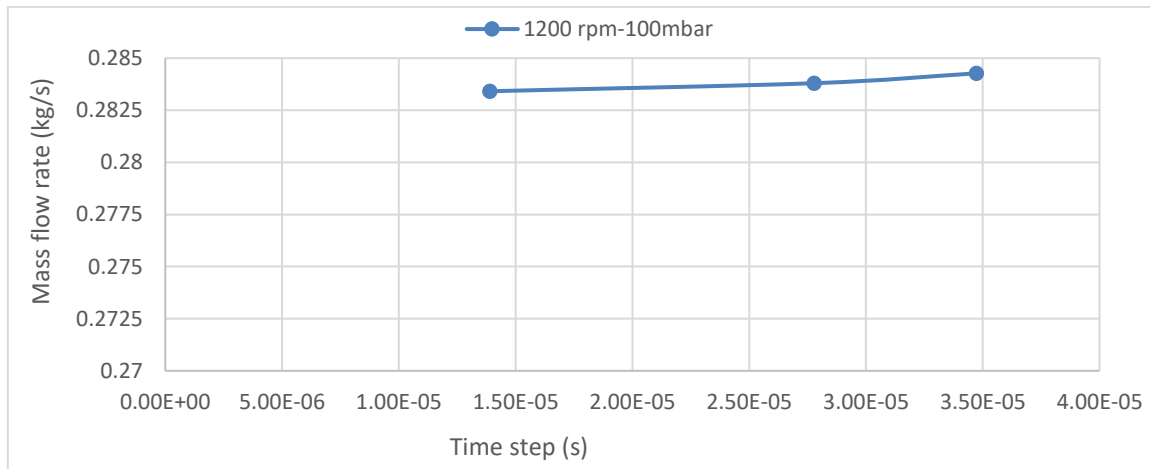


Figure 4.15: Mass flow rate temporal discretization results

Table 4.6 and Figure 4.15 summarise the result of time step independence test of mass flow rate, which shows that the difference is less than 0.14 % for mass flow rate between the three-time steps under consideration. Table 4.7 and Figure 4.16 summarise the result of time steps independence test of outlet temperature, which shows that the difference in outlet temperature of the blower is less than 0.04 % between the three-time steps under consideration. Hence, it can be concluded that the time step with 0.2 degrees is capable of predicting the flow features

accurately; therefore, time step for 0.2 degrees has been chosen for further analysis of Roots blower. When increase the time step more than  $3.5E-05$ , the dynamic mesh fail to work.

Table 4.7: Outlet temperature temporal discretization results

case	Time steps (s)	Outlet temperature (K <sup>0</sup> )	Percentage Difference (%)
1200	1.38E-05	327.71	8.8E-3
rev/min	2.77E-05	327.74	
100 mbar	3.47E-05	327.87	

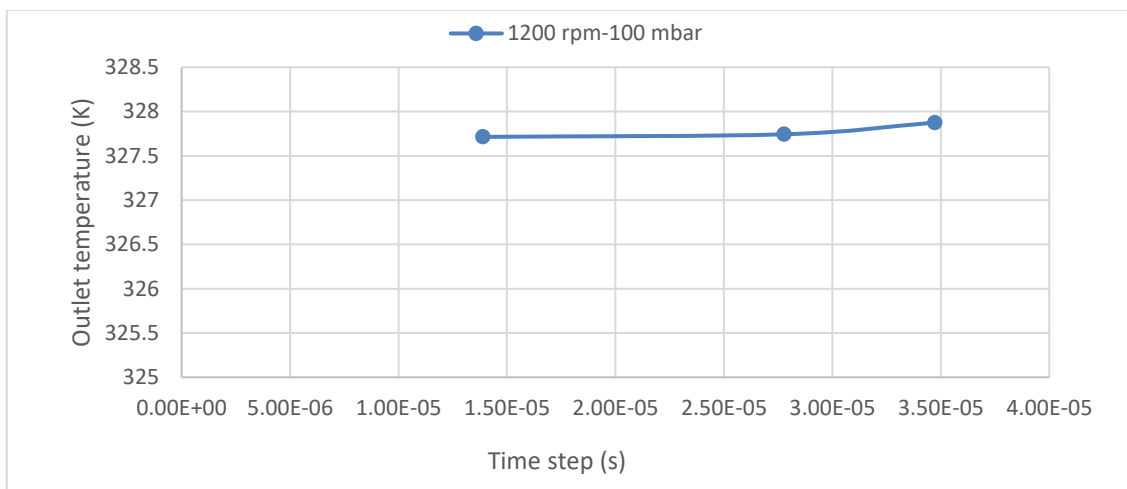


Figure 4.16: Outlet temperature temporal discretization results

#### 4.2.4. Validation of CFD model

This part presents the validation of the numerical model by analysing and comparing the results that have been obtained, experimentally against the results that have been obtained by using ANSYS Fluent (CFD) and dynamic mesh techniques. Procedures of CFD model processing and data have been presented.

The transient numerical simulations have been performed in this investigation for validation and verification of numerical results with measurements, and also to more clarify the effect of different parameters on roots blower performance. The simulation could be considered steady when the variance in the average mass flow between the suction and discharge of the blower during the rotation period could be ignored. Generally, the output of simulations has become cyclic and steady in the third cycle of rotation of the impellers in the blower while the calculations were run to the fifth period for more accuracy and to validate the outlet temperature

as shown in figure 4.17. It can be concluded from this figure that temperature starts to stabilize after the third rotation which is equal to 5400-time steps (every 5-time step is equal to one rotation degree) because the calculation in the simulation has been performed every 0.2 degrees.

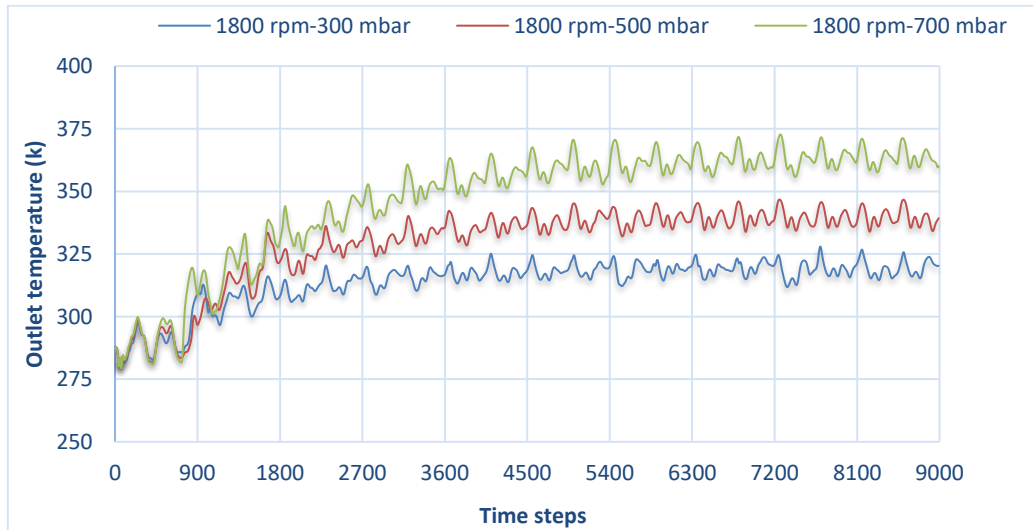


Figure 4.17: The behaviour of outlet temperature for five periods of rotation at rotational speed of 1800 rpm and for different pressure loads.

#### 4.2.4.1 The Roots blower model (HRBV613 Roots-type blower)

The blower model has been used for this study is HRBV613 Roots-type blower with an axial suction and an axial discharge ports. The rotor has two lobes with ‘involute’ profile. The nominal inter-lobe (centre gap), radial (tip gap), gearing axial and bearing axial leakage gaps are 0.34 mm, 0.24 mm, 0.3176 mm and 0.1524 mm respectively. The main rotor diameter is 247.32 mm. The operating speed of the machine is between 1200 rev/min and 2400 rev/min; discharge pressure can vary between 0 bar and 1.0 bar. Measurements at few operating points were carried out at the blower test rig at HR Blower Company at Huddersfield, and the results have been used in this study for comparison with CFD model predictions. A 45kW motor drives the compressor with a variable frequency drive for speed control. A valve controls the discharge pressure and gas flow is measured using an orifice plate in the suction line. Roots blower model specifications are summarised in table 4.8 and shown in figure 4.18.

Table 4.8: Roots blower model specifications

Casing radius	200.0065 mm	Bearing plate gap	0.1524 mm
Rotor radius	123.66 mm	Casing-Rotor gap	0.24 mm
Casing length	330.2 mm	Rotor-Rotor gap	0.34 mm
Rotor length	329.73 mm	Suction Diameter	146.23 mm
Length between centres	76.162 mm	Discharge Diameter	146.23 mm
Gearing plate gap	0.3176 mm	Rotors profile type	Involute

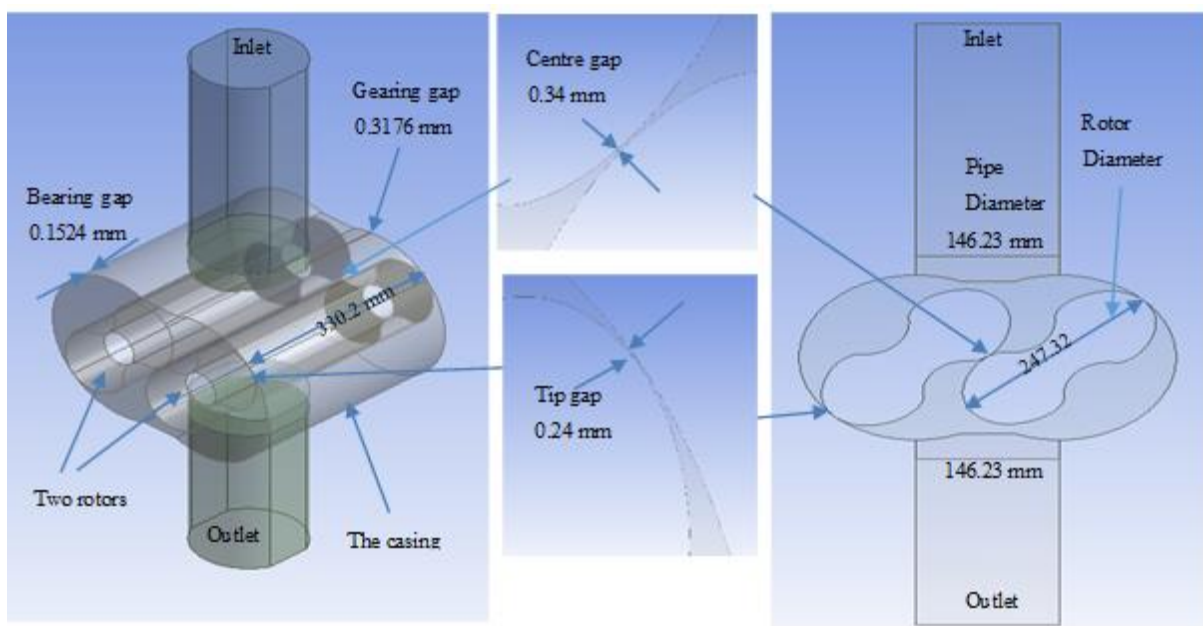


Figure 4.18: Roots blower model dimensions

Verification of the measurement outcomes has been done with the 2D CFD numerical model results in this investigation by comparing the mass flow rate and the outlet temperature of working fluid within the Roots blower system under constant pressure load.

#### 4.2.4.2 The Validation of CFD data using mass flow rate results

The Root blower model is simplified in 2D model, therefore, in order to compare the result of mass flow rate from the numerical simulations with measurement results, the numerical results must be multiplied by the length of the blower rotor (0.32973m). The flow rates present a periodic flow pulsation, and their average values are used for the comparison.

Figure 4.19 presents both the mass flow rates of the numerical simulations and the experiments at different operational speed and pressure loading. It shows that the numerical simulation results were higher than the measurements. It is because of the existence of different types of connectors such as fittings, elbows, filters and silencers that have been used in the experimental test rig. These connectors lead to an increase in the resistance of flow and hence decrease in the mass flow rate of operating fluid in the blower. Also, in the CFD model, the clearances between the front and back plates of the blower and the rotors have been ignored and converted to equivalent gap distance in casing-rotor clearance because of difficulty in meshing with dynamic mesh technique.

Figure 4.19 also shows that the mass flow rates of the Roots blower increased as speed rises and decreases when pressure differences rise. It is because of the higher pressure between the working chamber and the inlet leading to more leakage, which reduces the mass flow rate on the outlet. Moreover, the accordance of the numerical results indicates that the effect of pressure difference on the average mass flow rates of rotor blowers under operating conditions is relatively small. Furthermore, it is observed that the results of the mass flow rate have been obtained from the CFD model are quite consistent with the measured experimental data and, the maximum difference in results is about 3%. It displays the accuracy of the numerical model.

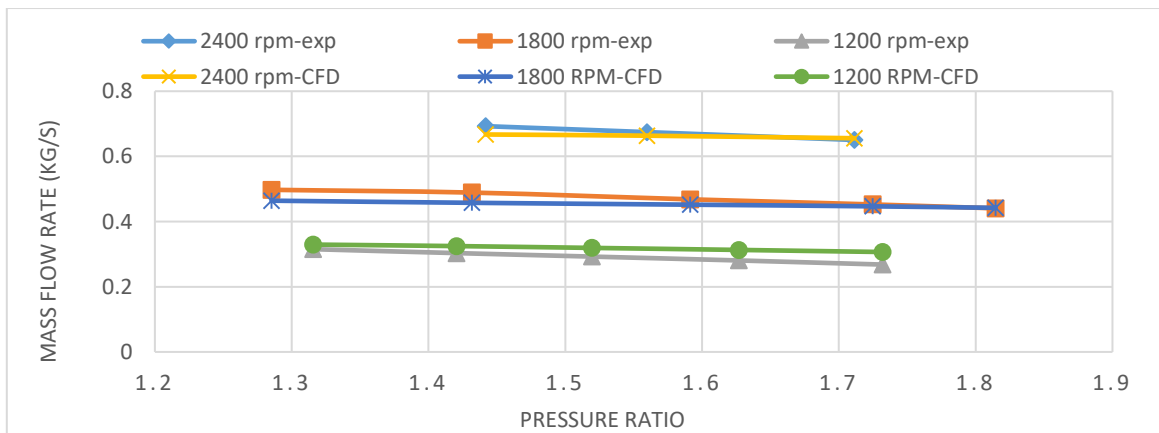


Figure 4.19: Validation of mass flow rates as f (pressure ratio across the blower)

#### 4.2.4.3 The Validation of CFD data using Outlet temperature results

The discharge temperatures obtained from the simulations and the experimental measurements for the different operating conditions have been presented and compared as shown in figure 4.20. It shows that the simulation result was consistent with the measurements. Also, this figure

shows that the Outlet temperature of the Roots blower increased when outlet pressure rises. It is because the effects of backflow lead to higher pressure at the discharge port, which increases the temperature on the outlet.

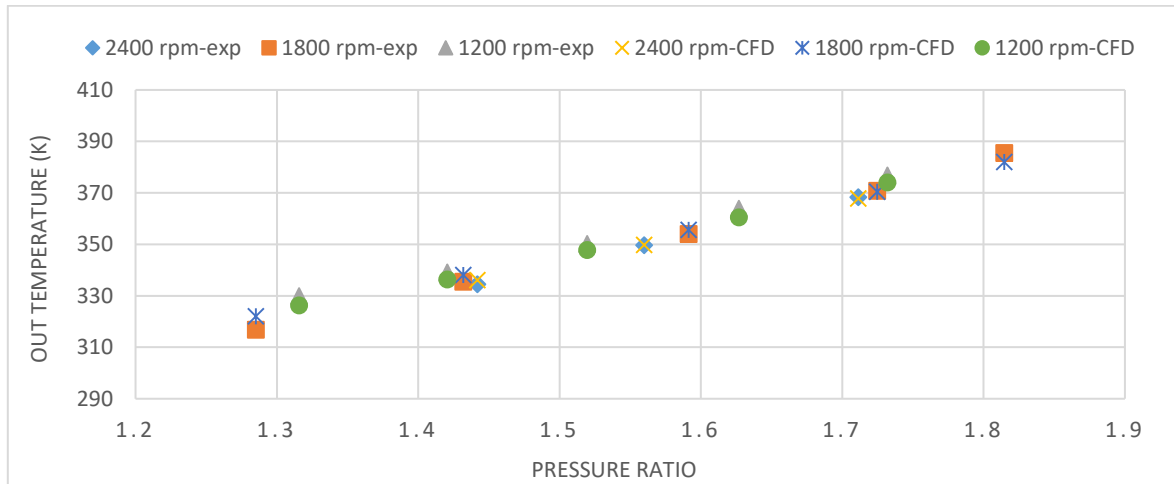


Figure 4.20: Validation of out temperature as f (pressure ratio across the blower)

Figure 4.20 represents the differences in the measurements and CFD findings concerning the outlet temperature of the blower for different operational speeds and pressure loads. It can be seen that the difference between the numerical and the measurement outcomes is small. However, as the pressure increases, the difference between the results start to grow. The maximum variance between the CFD and the measurement results has been observed for the outlet temperature of the blower is about a value of 4% per cent.

Moreover, according to the measurement results, during the first time of operation, fluid temperature values at the outlet of blower grows quickly and after that, the growth rate stabilises. A similar trend has been observed for the CFD numerical investigation as shown early in figure 4.17.

It is likely to have minor differences between the measurement and CFD numerical results because the numerical methods do not take into consideration all the forms of losses in the blower system. Such as the effect of ambient temperature on Roots blower temperature, which in the numerical modelling, the ambient temperature is kept constant. Thus, the variation in the ambient temperature during the measurement will also affect the outcome. Also, in CFD ideal gas conditions were considered, while in experiments, there are some losses, such as mechanical losses arising by the contact between the shaft and bearings and between the shaft

and the seal. Despite the reasons mentioned above, a minor differences has been observed between the CFD and the measurement results. The maximum difference between the CFD and the experimental results for the mass flow rate of operating fluid in the Roots blower is about 3% per cent. The outlet temperature variation is about 4% per cent. Hence, this numerical model can be considered an appropriate and reliable model for representing the Roots blower

#### **4.2.5. Roots blower internal flow characteristics**

Before analysing the influence of the blower's geometrical parameters such as rotor profile, rotor diameter, and internal clearances on the performance output of the Roots blower under different operating conditions which will be analysed and discussed in detail in the next chapter, it is essential first to investigate and analyse the structure of the flow in the Roots blower. So related flow features can be described, as well a general knowledge of the local flow structure can be established. In the next sections of this thesis, the effect of rotational speed and pressure difference on different Roots blower performance parameters such as mass flow rate, power consumption, efficiencies, pressure distribution, velocity distribution, and temperature distribution within a blower has been investigated and analysed.

The analysis of numerical results carried out on the Roots blower system represents the backflow phenomena, the distribution of pressure, temperature and velocity of working fluid inside the blower model.

In order to understand the working fluid behaviour inside the Roots blower system many numerical simulations are performed under different rotational speed and pressure loading conditions.

Contours and curves of pressure have been used to investigate the pressure of the fluid inside Roots blower. Figure 4.21 presents the pressure contours where rotors are meshing at 1800 rev/min after five rotations. The pressure increase as the impellers move from inlet to outlet, as presented in Figure 4.21 (A). The maximum and the minimum pressure areas are found in rotors meshing region, as shown in Figure 4.21 (B). The chamber of high-pressure consists the maximum pressure and the chamber of low-pressure consists of low-pressure. The clearances are found at different places around the chambers, the dynamic pressures were formed inside clearances as shown in Figure 4.21 (C, D).

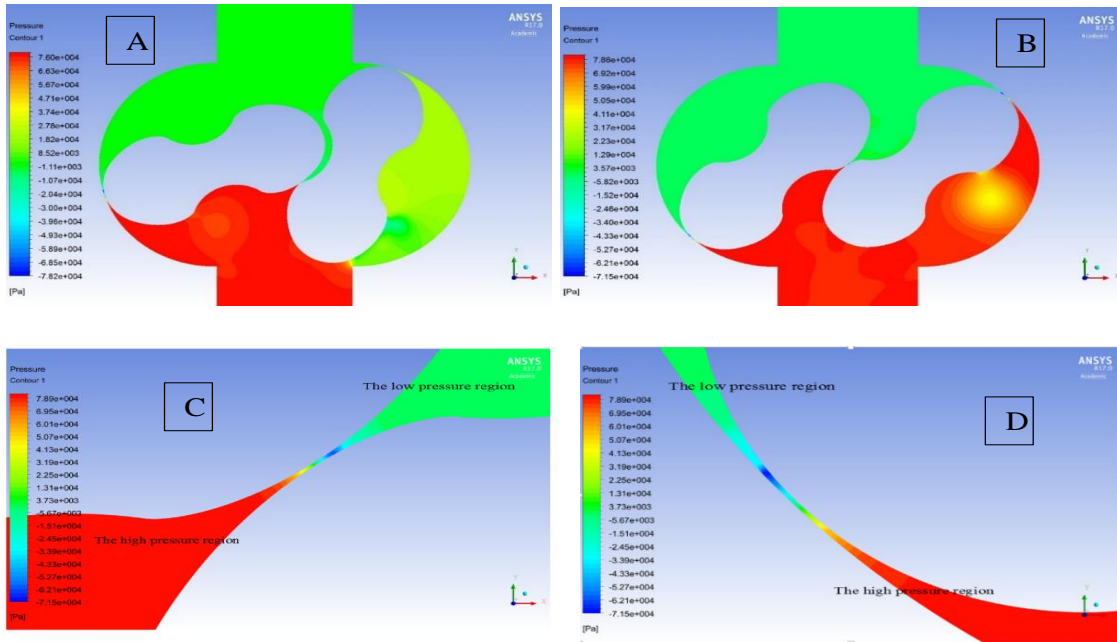


Figure 4.21: Pressure contour at speed 1800 rev/min at  $15^\circ$  and  $45^\circ$

The fluid velocities have been investigated in order to represent the state of internal flow behaviour inside the Roots blower, as shown in Figure 4.22. The clearances in the impellers meshing zone between the blower shell and tip rotors, between the two impellers, and between the end blower plates and the rotors leads to flow leakage from high-pressure zone to low-pressure zone. Also, the structure of the involute profile of the rotor are the main causes of the vortices inside the chambers, which leads to energy dissipation and therefore decreases the efficiency of the Roots blower (Kang & Vu, 2014; Y. Kang, H. Vu, & C. Hsu, 2012).

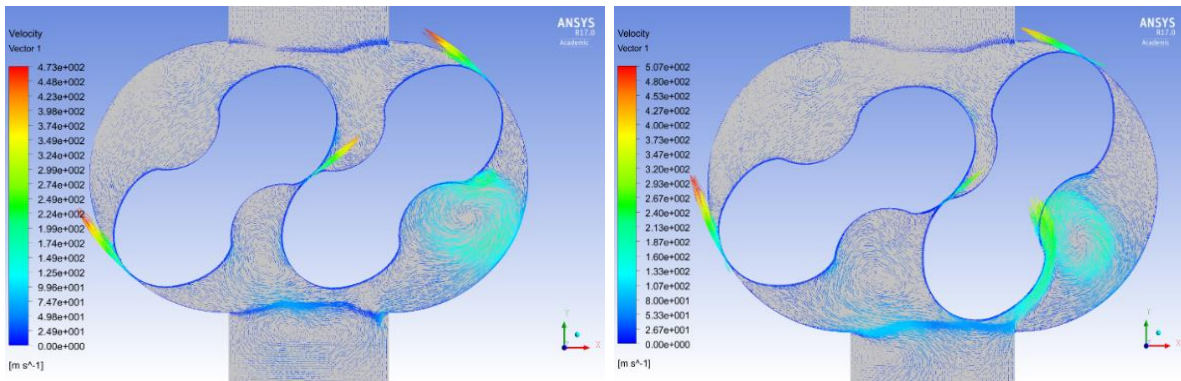


Figure 4.22: Velocity and vector contours at speed 1800 rev/min at different time steps

(Fluctuation of pressure, recirculation zones and velocity are much more significant in the outlet zone than at the inlet zone. The high pressure at the outlet will influence the velocity distribution, making the gaps filled with high-speed backflow and lead to significant energy dissipation).

For more depth and quantitative analysis of the internal flow behaviour inside the Roots blower, numbers of monitoring points have been chosen in the fluid area around the impellers and inside the clearances between rotors and also between the rotors and the casing as shown in figure 4.23. These points have been chosen to investigate almost zones within the blower; the inlet zone (P1 and P2), the outlet zone (P10 and P11), the suction and the discharge edges (P3 and P9), and the clearances and the other areas from inlet to outlet of the blower (P0, P4, P5, P6, P7 and P8).

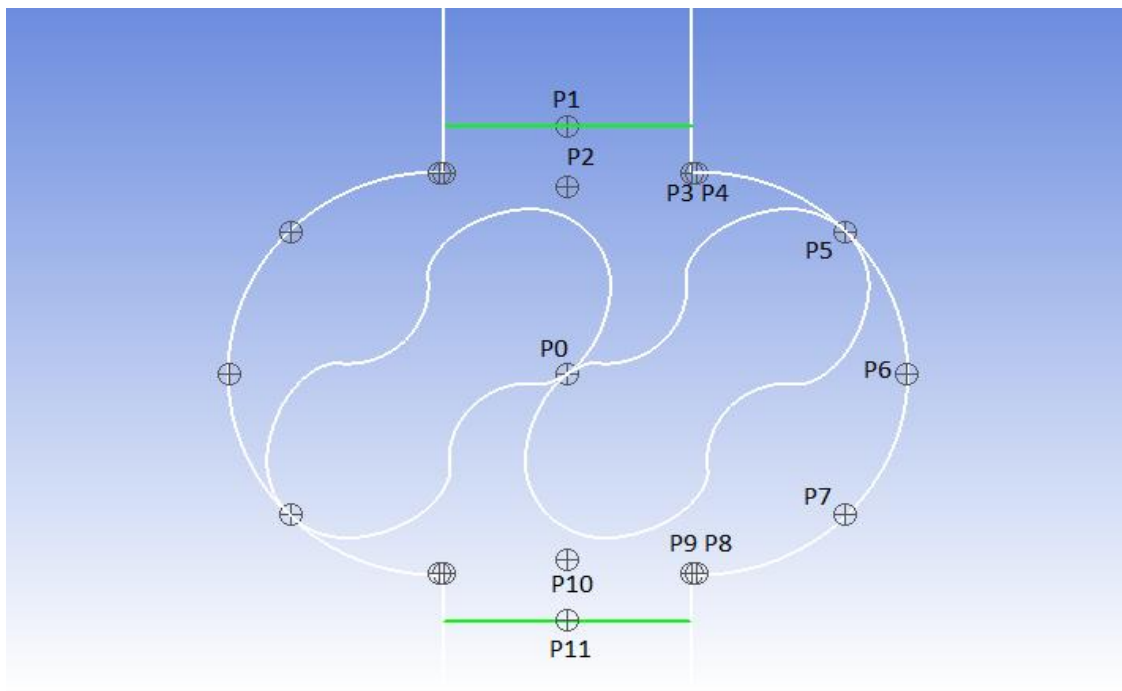


Figure 4.23: Number of points has been chosen inside the blower for more depth analysis

#### 4.2.6 Effect of pressure difference on Roots blower performance characteristics

The pressure differences of 300, 500, 700 millibars and the rotational speed of 1800 rev/min have been chosen to study the effect of pressure difference on blower performance characteristics. Furthermore, for more understanding and in-depth local analysis of the variation and the distribution of different performance parameters inside the blower,

investigations using different statistical features such as average, minimum and maximum value, root mean square (RMS), and amplitude has been carried out. Also, to simplify and parameterise the performance characterisation of Roots blower, non-dimensional analysis has been used.

#### **4.2.6.1 Effect of the pressure difference on pressure field characteristics**

In order to study the static pressure characteristics inside the blower, pressure variation inside the blower has to be understood. Further, it provides the possibility to trace areas of low pressure that might be exposed to high velocity and backflow

The contours and the distribution of pressure on middle plane of the blower for the last revolution of a case study at different angles obtained through numerical simulation at speed 1800 rev/min and pressure differences of 300, 500, 700 millibars are shown in Figure 4.24.

Figure 4.24 depicts the variations of static pressure contours in the Roots blower having two rotors and two lobes for every rotor. It is evident that the pressure is gradually increased from the inlet area to the outlet area of the blower. It can be seen from this figure that the lower pressure occurs inside clearances at the inlet side of the impeller. Also, it is evident that the distributions of static pressure at same rotational speed and under different pressure difference conditions have the same trend for all the cases under investigation.

The appearance of recirculation zones in some areas within the blower could account for local pressure loss phenomenon. Recirculation zones are often the turbulent flow of fluid and often exhibits a very low pressure at the centre. It can be seen from the figure that the location of the recirculation zones are changing from impeller outlet region close to impeller wall towards impeller inlet region as pressure difference increase. Therefore, it accounts for more local pressure loss and energy dissipation as pressure difference increases.

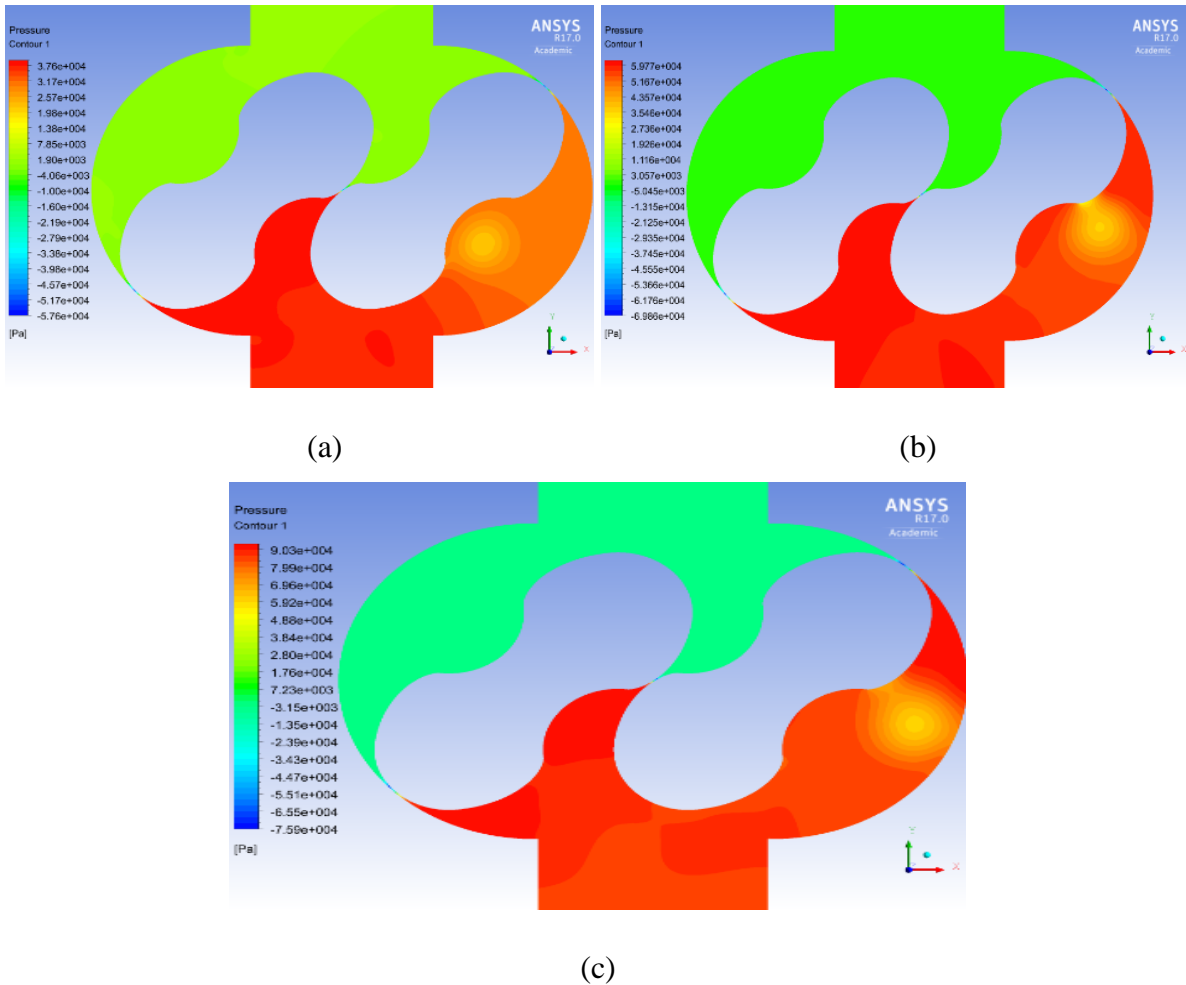


Figure 4.24: The variations of static pressure contour at a speed of 1800 rev/min and for different pressures of (a)- 300 millibar, (b)- 500 millibars, (c)- 700 millibar

Studying the fluctuation and distribution of the pressure are essential to understand and predict the unsteady flow and noise generation mechanisms in the Roots blower. Figures 4.25 and 4.26 show the instantaneous variation of static pressure at the inlet and the outlet of the blower of two-lobe over one revolution/cycle at different discharge pressures respectively. It can be seen from Figures 4.25 and 4.26 that the pressure and the fluctuation in the discharge zone are higher than that in the suction zone and it increases as the pressure difference increases. There are two possible reasons behind that; the first one is the flow is complex and existing of clearances inside the blower, and the second reason is due to the high interaction and the sudden open between the impeller and outlet region. Therefore, this will lead to pressure increase and backflow from the high-pressure side to low-pressure side.

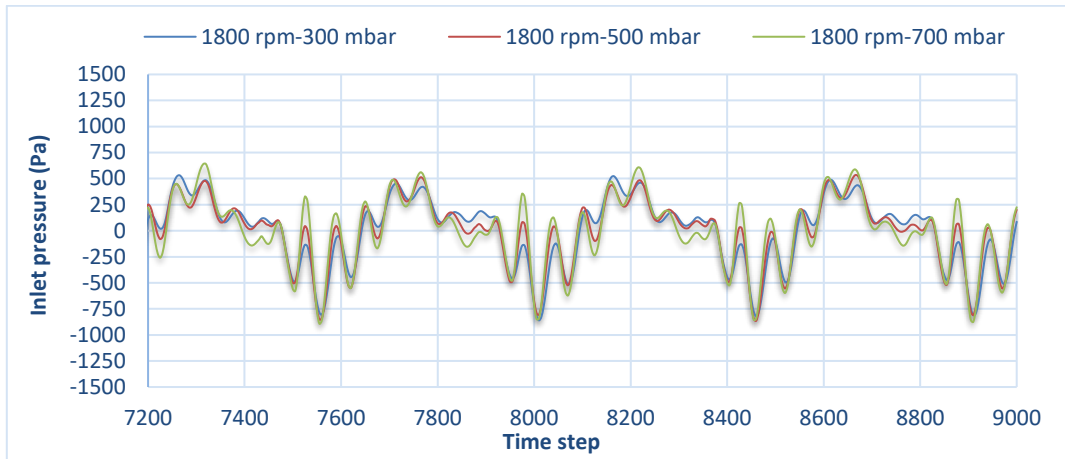


Figure 4.25: Pressure fluctuations at blower inlet at 1800 rev/min and for different pressures

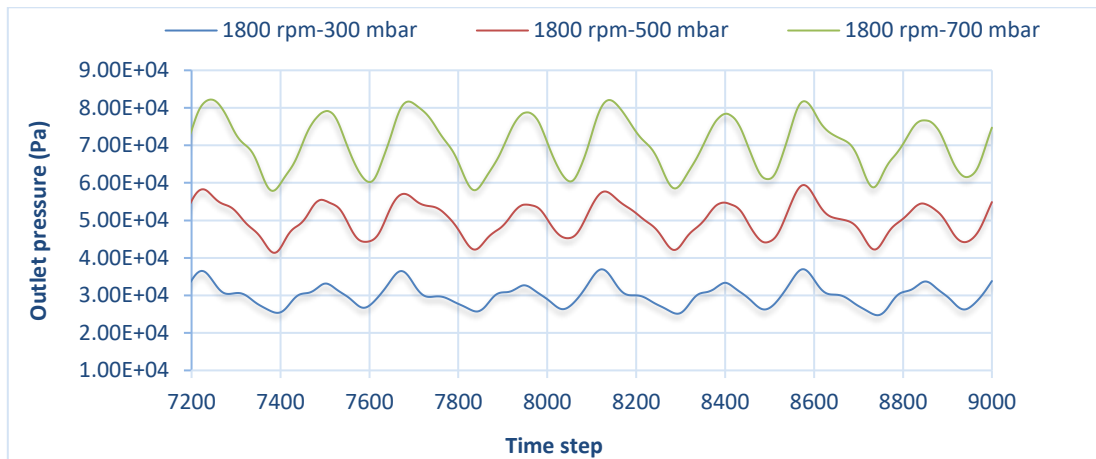


Figure 4.26: Pressure fluctuations at blower outlet at 1800 rev/min and for different pressures

Figure 4.27 shows the behaviour of pressure fluctuations from the inlet to the outlet of the blower for one rotation. It can be seen that the pressure in the mixing zone between rotors and casing fluctuates, varying from peak to the valley changing their shape of fluctuations through different positions from the inlet to outlet of the blower. The pressure and their amplitude increase slightly from point 1 to point 4 and after that rise significantly at points 5 and 6. This figure showed that the maximum amplitudes and the maximum negative pressures are at points 7 and 8. After point 8 the pressure starts to increase and their amplitude starts to decrease until the pressure and their amplitude approaching equilibrium at the outlet of the blower.

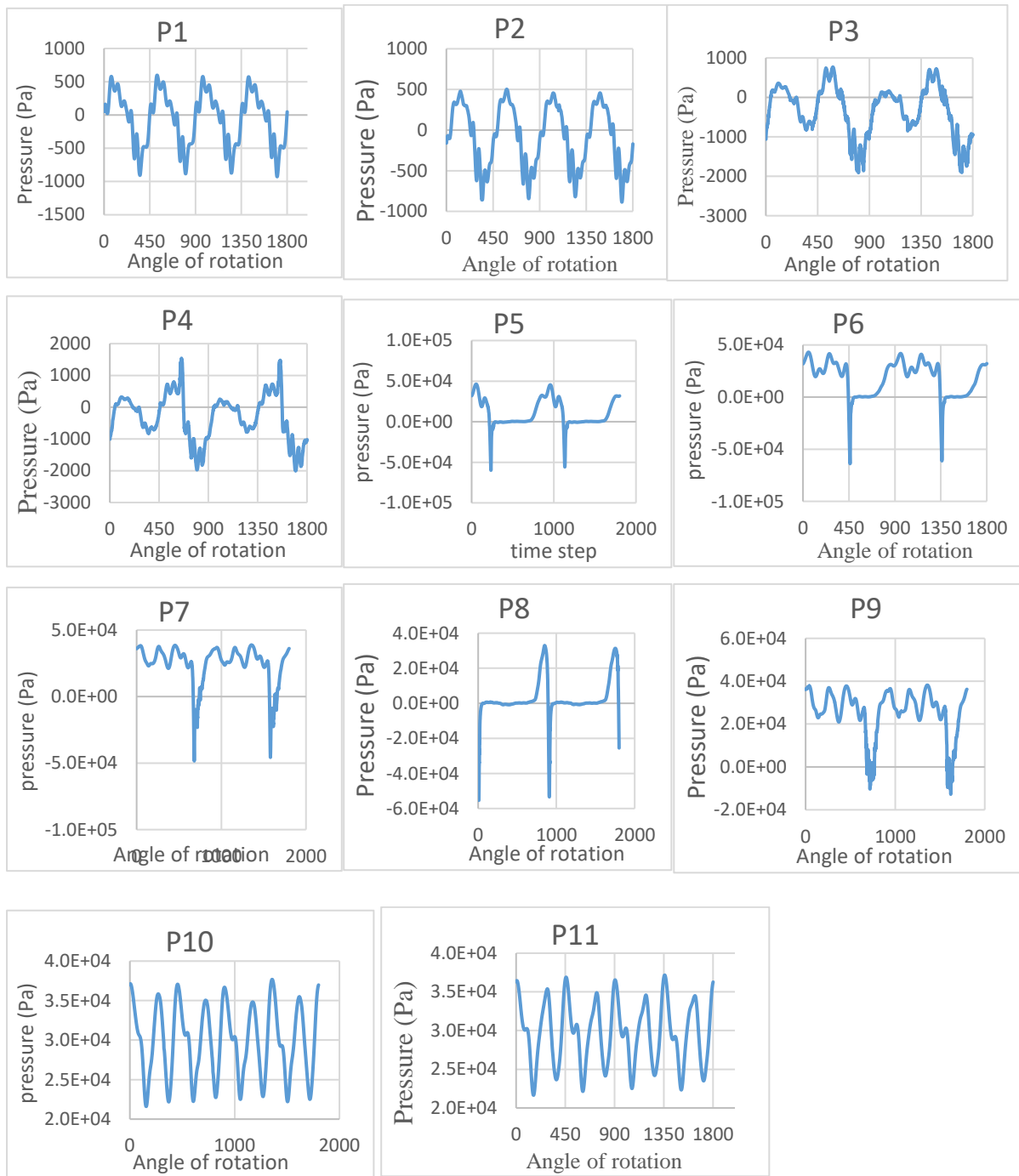


Figure 4.27: The behaviour of pressure fluctuations from the inlet to the outlet of the blower for one rotation

Furthermore, it can be concluded from figures 4.28 that the maximum positive pressure value is approximately between  $45^{\circ}$  and  $60^{\circ}$  angles of degrees at the high-pressure zone as a result from the effect of backflow pressure at discharge zone. Also, the maximum positive pressure

and their amplitude are increase with the increase in pressure difference. Moreover, the behaviour of pressure fluctuations is repeated every  $90^{\circ}$  degrees.

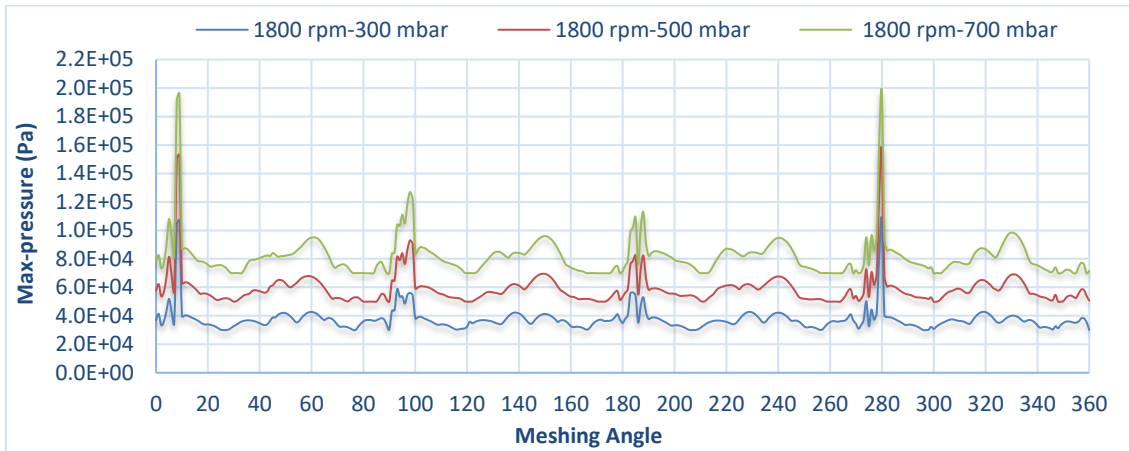


Figure 4.28: The variation of maximum-pressures at 1800 rev/min and under different discharge pressures

On the other hand, it can be concluded from figure 4.29 that the maximum negative pressure value is approximately between  $45^{\circ}$  and  $60^{\circ}$  degrees inside the clearance at the low-pressure zone as a result from the effect of backflow pressure at discharge zone. Also, the maximum negative pressure and their amplitude are increase with the increase in pressure difference. Moreover, the behaviour of pressure fluctuations is repeated every  $90^{\circ}$  degrees. (All the angles with respect to the vertical line at the centre of the rotor within the blower).

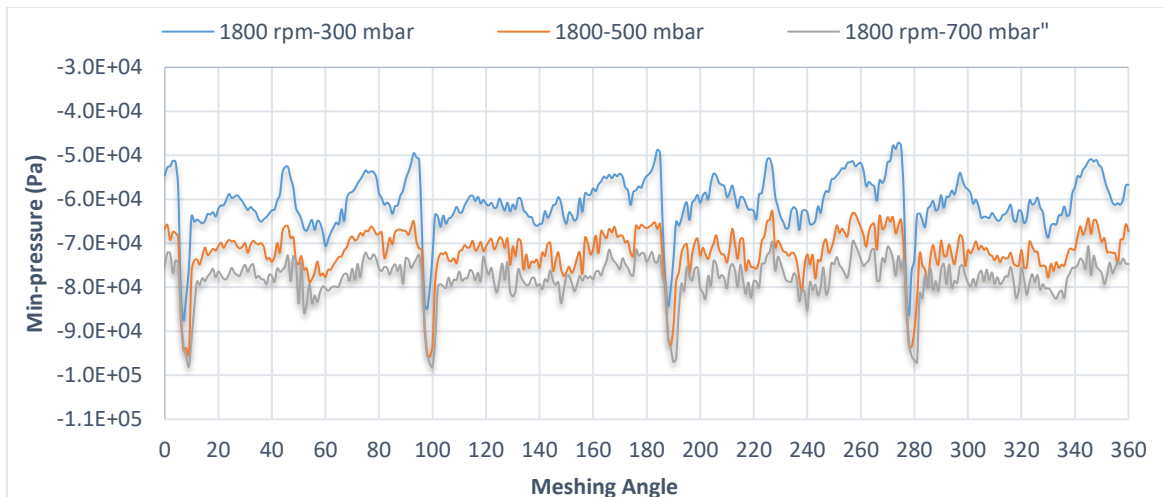


Figure 4.29: The variation of maximum negative-pressures at 1800 rev/min and under different discharge pressures

The variation and the distribution of pressure at the same speed and under different discharge pressures at various locations inside the blower from the inlet to outlet are presented in Table 4.9, figure 4.30 and figure 4.31.

Table 4.9: The maximum and minimum pressures at 1800 rev/min and under different discharge pressures in Pascal.

Positions	$P_{in}$ Pa	$P_{max}$ at 30 kPa	$P_{max}$ at 50 kPa	$P_{max}$ at 70 kPa	$P_{min}$ at 30 kPa	$P_{min}$ at 50 kPa	$P_{min}$ at 70 kPa
P1	1.0E+05	6.0E+02	6.8E+02	8.0E+02	-9.3E+02	-9.4E+02	-1.0E+03
P2	1.0E+05	5.0E+02	5.2E+02	5.4E+02	-8.9E+02	-8.5E+02	-9.0E+02
P3	1.0E+05	7.7E+02	9.1E+02	1.1E+03	-1.9E+03	-1.9E+03	-2.3E+03
P4	1.0E+05	1.5E+03	1.7E+03	1.7E+03	-2.0E+03	-2.1E+03	-2.4E+03
P5	1.0E+05	3.3E+04	5.2E+04	7.2E+04	-5.5E+04	-7.1E+04	-7.8E+04
P6	1.0E+05	4.6E+04	7.9E+04	1.1E+05	-6.0E+04	-7.0E+04	-6.6E+04
P7	1.0E+05	4.3E+04	7.2E+04	1.1E+05	-6.4E+04	-7.2E+04	-6.8E+04
P8	1.0E+05	3.9E+04	6.7E+04	9.8E+04	-4.8E+04	-5.9E+04	-6.4E+04
P9	1.0E+05	3.8E+04	6.6E+04	9.6E+04	-1.3E+04	-1.4E+04	-1.4E+03
P10	1.0E+05	3.8E+04	6.2E+04	9.0E+04	2.2E+04	3.6E+04	4.9E+04
P11	1.0E+05	3.7E+04	6.1E+04	9.0E+04	2.2E+04	3.6E+04	5.0E+04

It can be seen that there is a significant difference in maximum pressure at different discharge pressure under the same rotational speed. The maximum pressure increase from the inlet to outlet until approaches the maximum values when the tip of impeller is approximately at the middle region of the blower ( $90^0$ ) at point 6 which recorded 1.542 times, 1.58 times and 1.6 times the rated pressures of 30 kPa, 50 kPa, and 70 kPa respectively as highlighted and shown in table 4.9. Moreover, the maximum pressure after point 6 starts to decline slightly towards the outlet zone till stabilising. Furthermore, it can be concluded that the maximum pressure is increased with the increase in pressure difference.

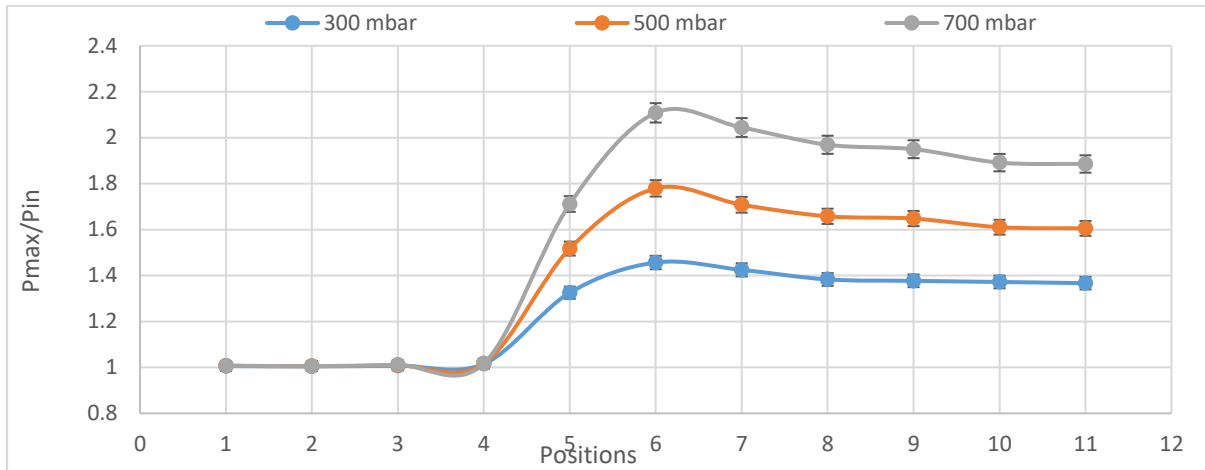


Figure 4.30: The distribution of maximum-pressures at 1800 rev/min and under different discharge pressures

On the other hand, there are small differences in maximum negative pressure as we can see in figure 4.31. Also, it can be seen in this figure that the minimum pressure increase from the inlet to outlet until approaches the maximum negative values at point 5 which approximately at the angle of  $(45^{\circ})$ . The maximum negative pressure after that declines and rises slightly between  $45^{\circ}$  (point 5) to  $135^{\circ}$  (point 7) and after this decreases towards the outlet zone until stabilize. Moreover, the maximum negative pressure value is approximately between  $45^{\circ}$  and  $180^{\circ}$  degrees inside the clearance at the low-pressure zone as a result from the effect of backflow pressure at discharge zone. The maximum negative pressure values are found at point 7 ( $135^{\circ}$  degrees of rotation) as highlighted and shown in table 4.9. Furthermore, it can be concluded that the maximum negative pressure is increased with the increase in pressure difference.

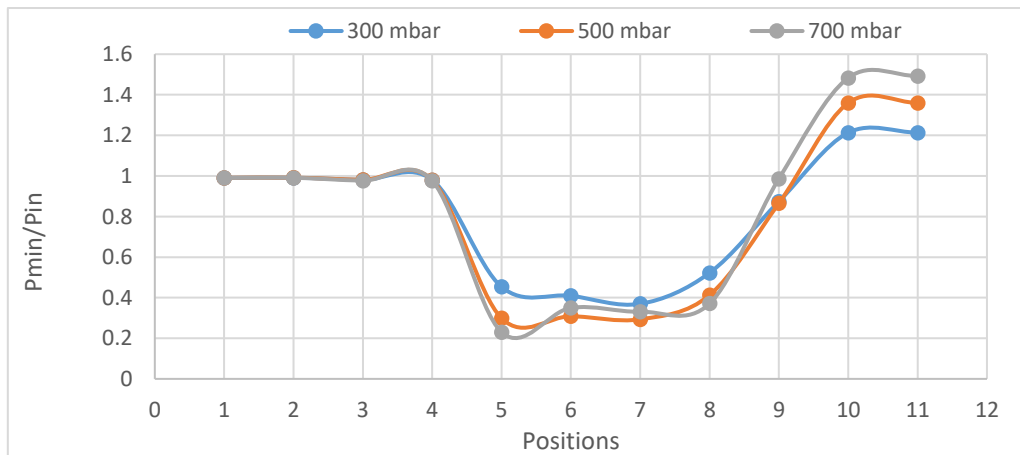


Figure 4.31: The distribution of maximum negative pressures at 1800 rev/min and under different discharge pressures.

Root mean square (RMS) refers to the arithmetic mean of the squares of a set of numbers. RMS is a meaningful way of calculating the average of values over a period of time. Figure 4.32 expresses the relation between effective pressure zones and RMS. It can be seen that the RMS increases from the inlet to outlet of the blower, which the maximum values are recorded at the discharge zones. Also, these values rise with an increase of pressure difference.

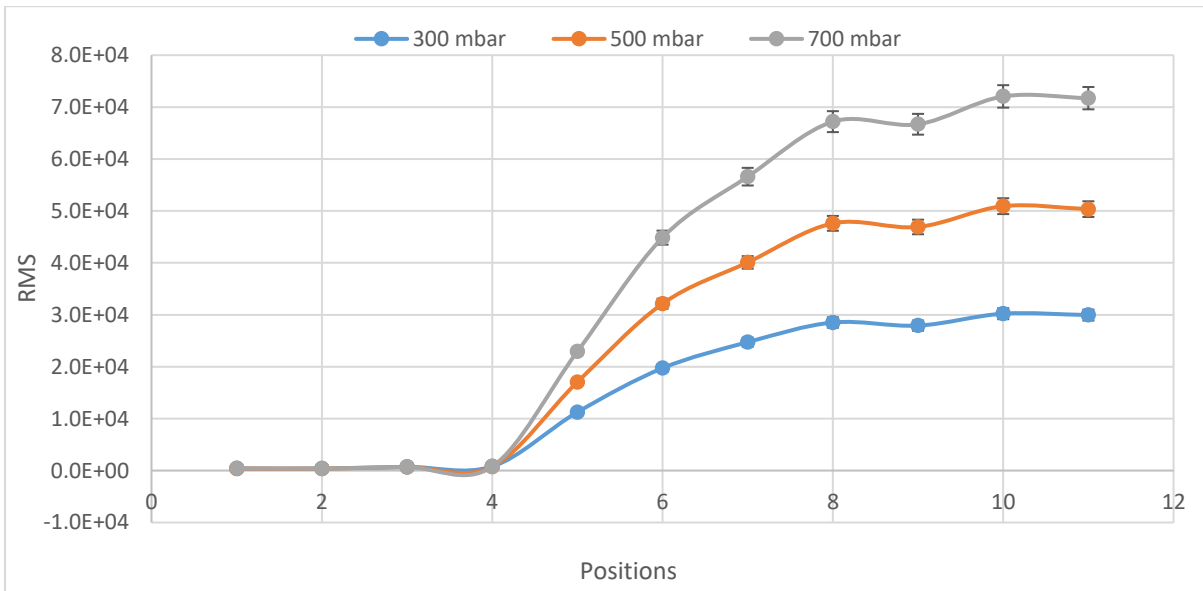


Figure 4.32: Root Mean Square (RMS) of effective pressure zones at 1800 rev/min and for different pressure difference.

The peak to peak amplitudes ( $A_{pk-pk}$ ) is the difference between the maximum positive and the maximum negative amplitudes of a waveform) divided by pressure difference are presented in Figures 4.33. It is clear to conclude that there is a small difference of the peak to peak a magnitudes at different discharge pressure under the same rotational speed at the inlet zone or the outlet regions. On the other hand, these differences increase inside the meshing region in the blower. Also, the maximum amplitude values are recorded at points 6 and 7 where the effect of pressure and backflow are high in this zone. Moreover, it can be seen that the amplitudes are increased with the increase of pressure difference and are more prominent at outlet zone than an inlet zone because the pressure and their fluctuations are higher in this area.

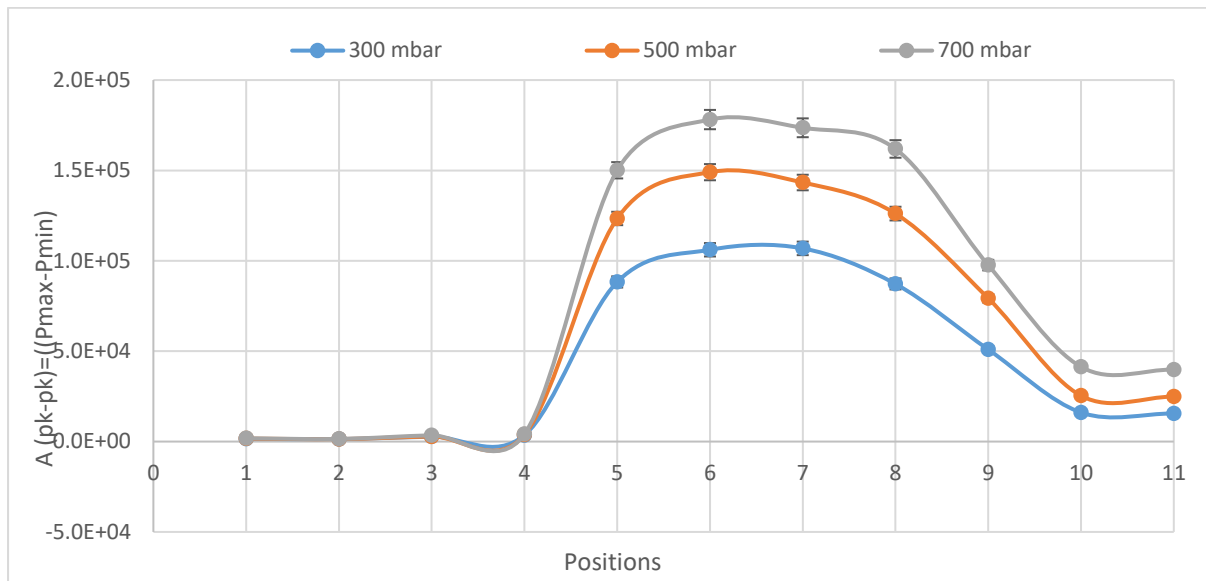


Figure 4.33: The peak-peak amplitudes at speed 1800 rev/min and for different discharge pressures.

The result shows that when the blower operates at higher pressure difference, the pressure in the outlet chamber will increase. However, the pressure decreases in the clearances within the blower at the inlet chamber causing the velocity to increase. It develops further the backflow that leads to the decline of flow rate. There are some causes why the changes in the static pressure distribution in the blower arise. The flow inside the blower is known to be very complicated, fully turbulent and unsteady due to the high interaction that occurs between the lobes of rotors, stator and fluid within the blower especially at edges of the discharge zone. Also, the rotating impellers with highly complex curvature have a considerable effect on the complex flow field developed inside the blower.

#### 4.2.6.2. Effect of the pressure difference on flow rate and pulsation characteristics

The average mass flow rate for the last revolution of case study obtained through numerical simulation at a speed 1800 rev/min and for pressure differences of 300, 500, and 700 millibars are shown below in Figure 4.34. It can be concluded that there is a small difference in the average mass flow rate, which average mass flow rate declines as the pressure difference increases. It is because higher pressure can result in more flow leakage in the gaps from high-pressure region to low pressure region and a decrease in the actual flow rate and therefore in the volumetric efficiency of the Roots blower.

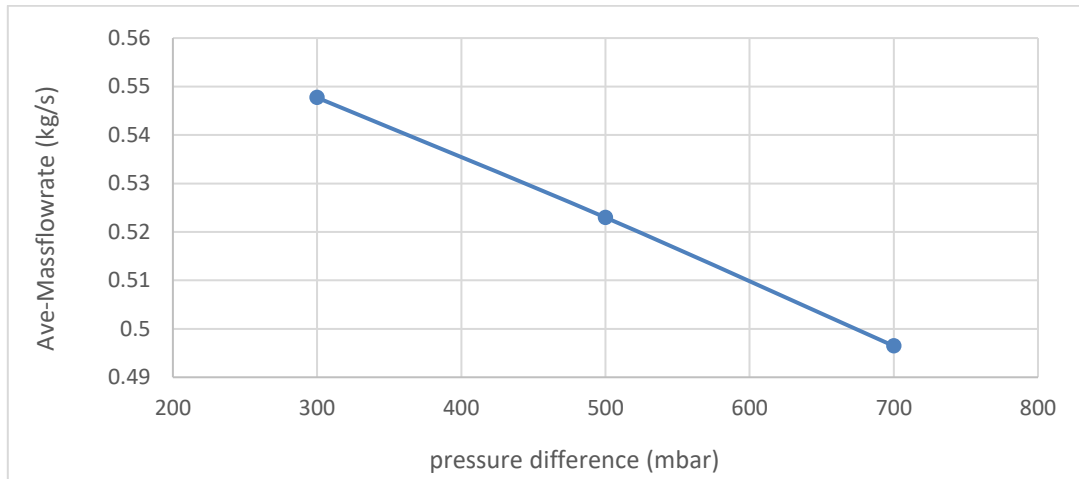


Figure 4.34: The average mass flow rate at the speed 1800 rev/min and for different discharge pressures.

The fluctuations of mass flow rate for the last revolution of case study obtained through numerical simulations at a speed 1800 rev/min and for pressure differences of (300, 500, and 700) millibars are shown below in Figure 4.35 and 4.36. It can be concluded that the amplitude of mass flow at the blower suction grows up as the pressure difference decreases, meanwhile, the amplitude of mass flow at the blower discharge rises with the increases of pressure difference. This phenomenon is apparent in figure 4.37, which illustrates the mass flow rate fluctuation coefficient (Mf) at both inlet and outlet of the blower (K. J. Huang & Lian, 2009).

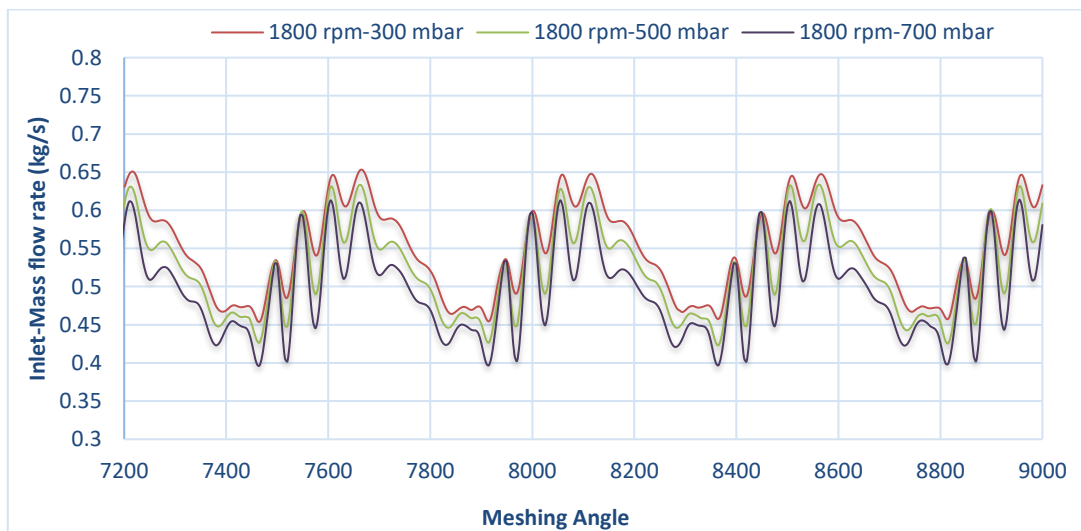


Figure 4.35: The fluctuations of the inlet mass flow rate at 1800 rev/min and for different pressure loads

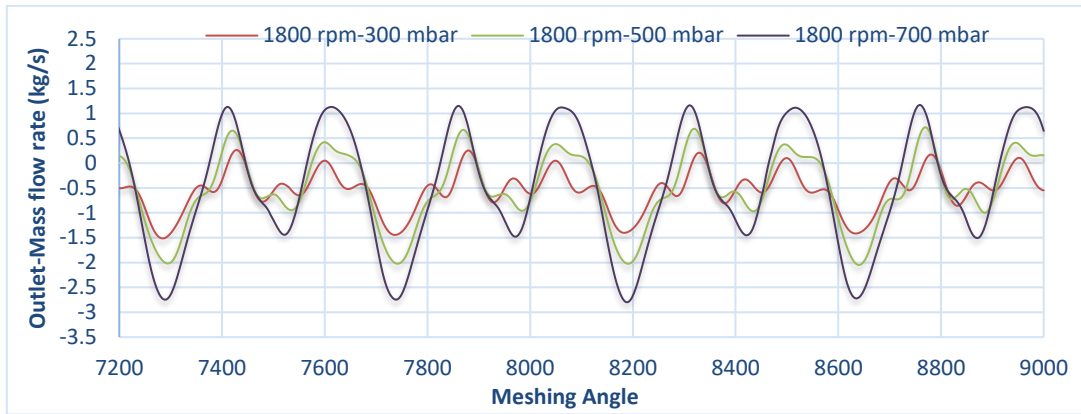


Figure 4.36: The fluctuations of the outlet mass flow rate at 1800 rev/min and for different pressure loads

Furthermore, the flow rate pulsation is generally represented by the amplitude of relative flow pulsation or the fluctuation coefficient of the flow rate ( $M_F$ ), which is defined by the equation (4.18). This can be applied as a performance guide associated with vibration and noise (K. J. Huang & Lian, 2009).

$$M_F = (\dot{m}_{max} - \dot{m}_{min}) / \dot{m}_{ave} \dots\dots\dots (4.28)$$

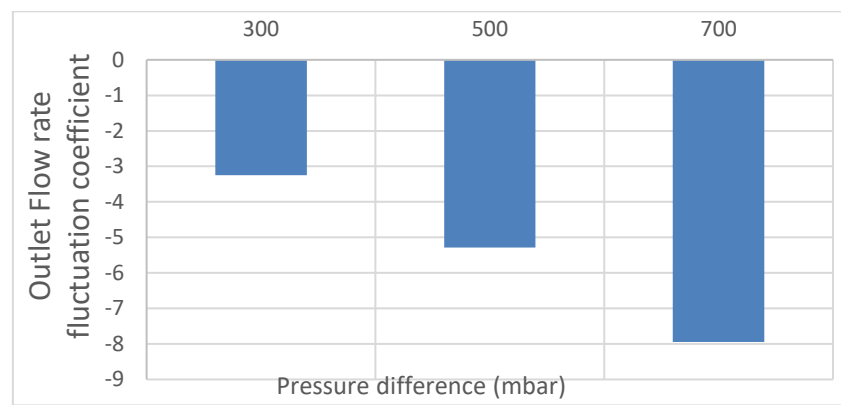
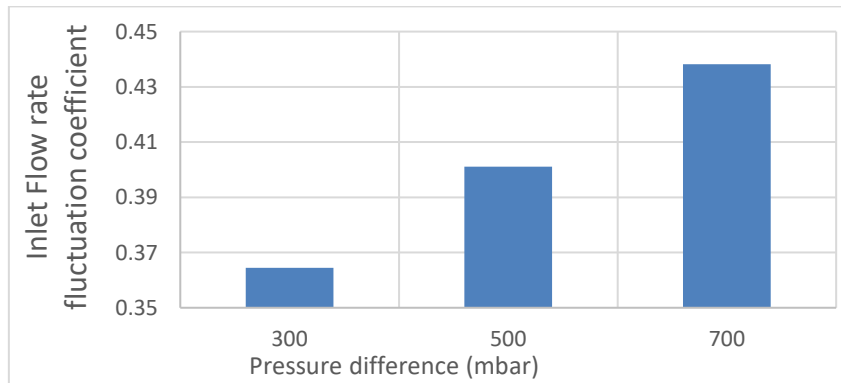


Figure 4.37: Mass flow rate fluctuation coefficient (Mf) at 1800 rev/min and for different pressure loads at the inlet (left) and an outlet (right).

#### 4.2.6.3. Effect of the pressure difference on temperature characteristics and distribution

The contours and distribution of the temperature for the last revolution of a case study obtained through numerical simulation at a speed 1800 rev/min and for pressure differences of (300, 500, and 700) millibars from left to right respectively are shown below in Figure 4.35.

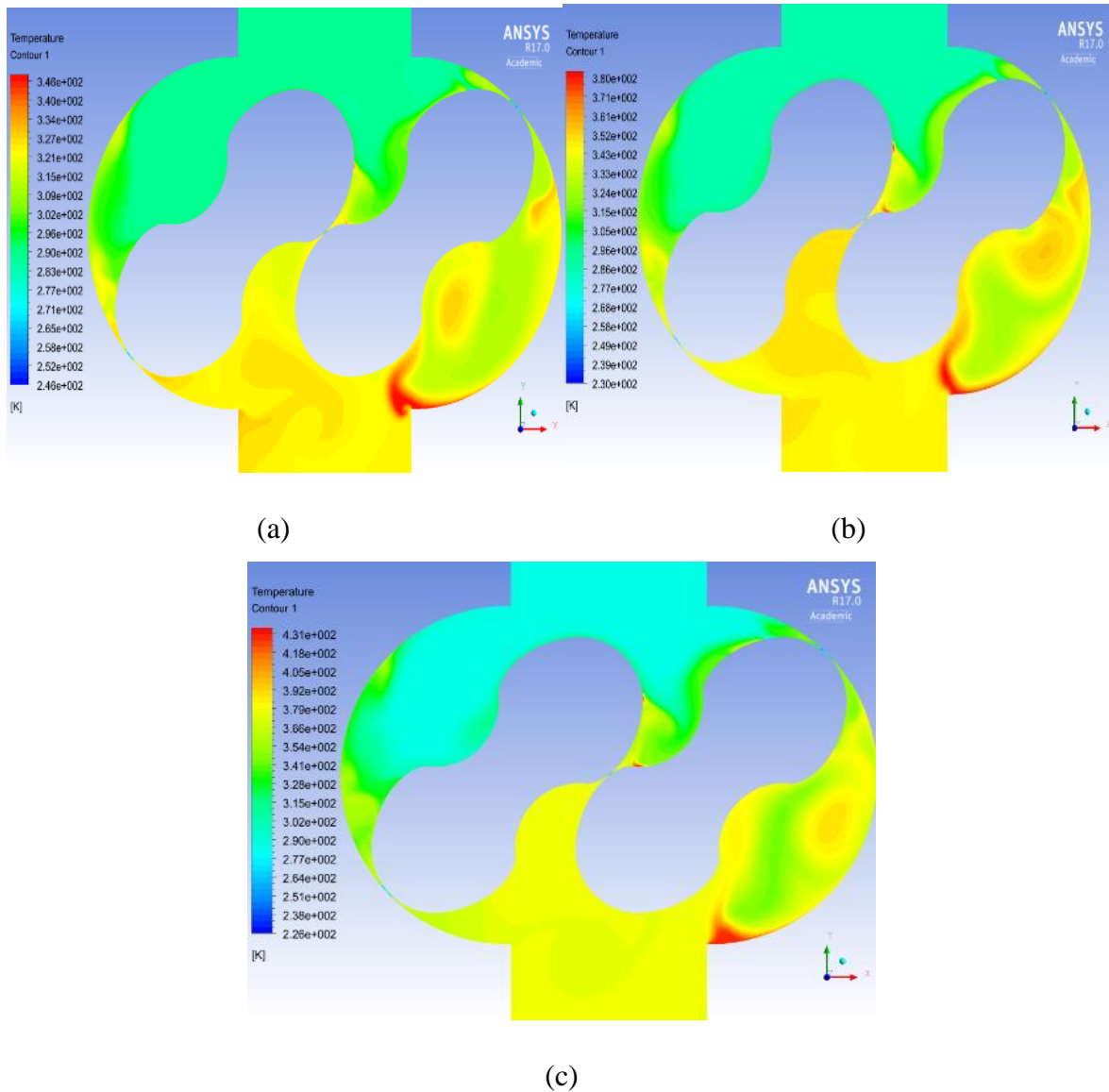


Figure 4.38: The temperature contours and distribution for the last revolution and at 45° rotation degrees, 1800 rev/min and for pressures loads of (a) - 300 millibars, (b) - 500 millibars, and (c) - 700 millibars.

Figure. 4.38 depicts the effect of unsteady flow on temperature distribution and the location of the high-temperature area in the Roots blower. It is obvious to conclude that the distribution of temperature is non-uniform and the position of high-temperatures are close to rotor wall and casing wall at the outlet zone. Also, there are big high- temperature area like vortex which changing their location and shape as rotors rotating and pressure difference change. Moreover, the temperature increase inside the blower with an increase of pressure difference and as a result of backflow effect.

The variation of outlet temperature with the rotation angle for five rotations is shown in Figure 4.39 (every full rotation is 1800 because the calculations have been performed every  $0.2^{\circ}$  degree as mentioned before). It can be seen that during the process of rotation, the gas temperature which is low before the compression process begins to rise quickly after the compression process finishes, and starts to stabilise after the third rotors meshing cycle. Also, it has been found that the temperature and their fluctuations and the maximum temperature increase as pressure difference increases.

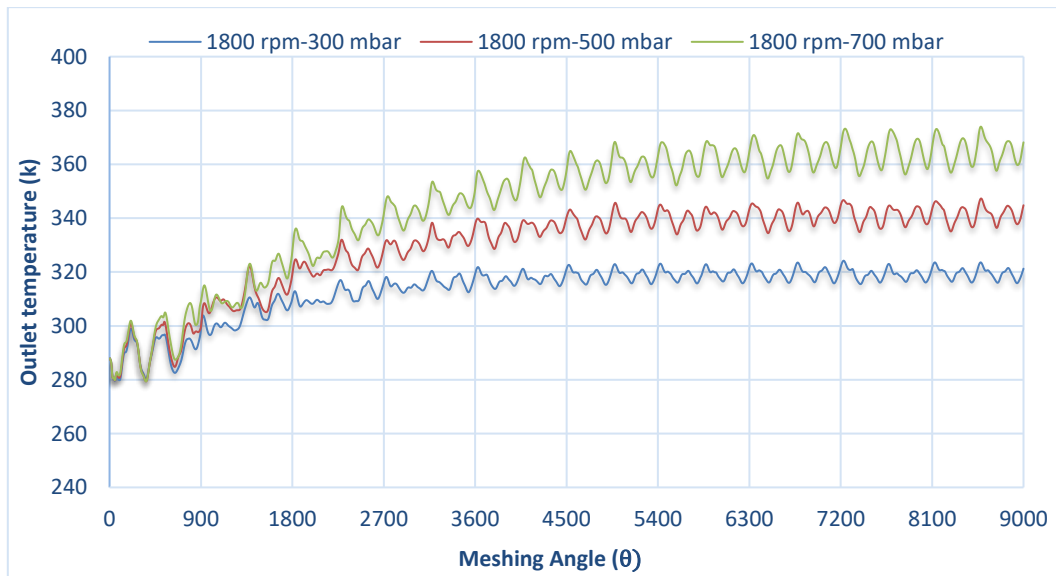


Figure 4.39: Outlet temperature at 1800 rev/min and for different pressure loads for full five rotations in the Roots blower

The variation of the maximum outlet temperature with the rotation angle for last rotation is shown in Figure 4.40. It can be conclude that the maximum temperature and their fluctuation increases as pressure difference increases. Also, the same behaviour of temperature variation is presented for different pressure loads and for every  $90^{\circ}$  degree of rotation.

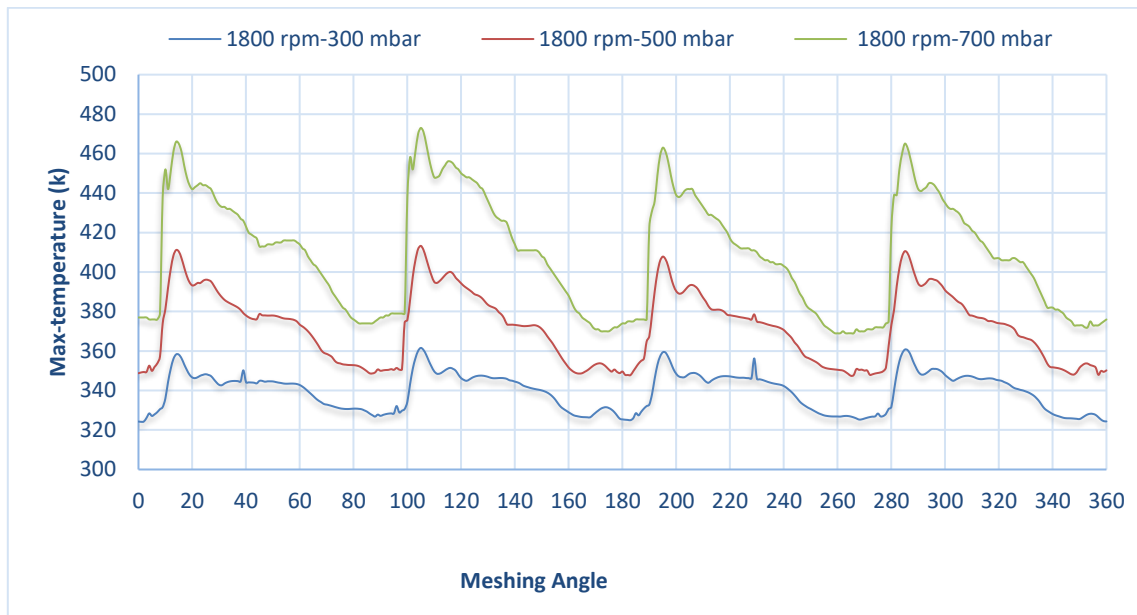


Figure 4.40: The maximum outlet temperature at a speed 1800 rev/min and for different pressure loads for the last rotation in the Roots blower

Investigations through the use of various statistical features such as the average, minimum and maximum value of temperature fluctuations have been used. This is aimed at more in-depth local analysis of the temperature variation and distribution within the blower.

The distribution and the variation of the temperature at a constant speed and under different discharge pressures inside the blower from the inlet to outlet are presented in Table 4.10 and figure 4.41. It can be seen that there is a considerable variance of maximum temperature at different discharge pressure which recorded 345.63 K<sup>0</sup>, 383 K<sup>0</sup>, and 429.79 K<sup>0</sup> for pressures of 30 kPa, 50 kPa, and 70 kPa respectively. Also, the maximum temperature increases from the inlet to the outlet of the blower. Moreover, the maximum temperature after point 6 declines slightly between angle 90<sup>0</sup> and angle 135<sup>0</sup> and after that increases until the maximum value at angle 180<sup>0</sup> (point 8). Furthermore, after point 8, the maximum temperature begins to drop towards the outlet zone till finally stabilising. (All the angles with respect to the vertical line at the centre of the rotor).

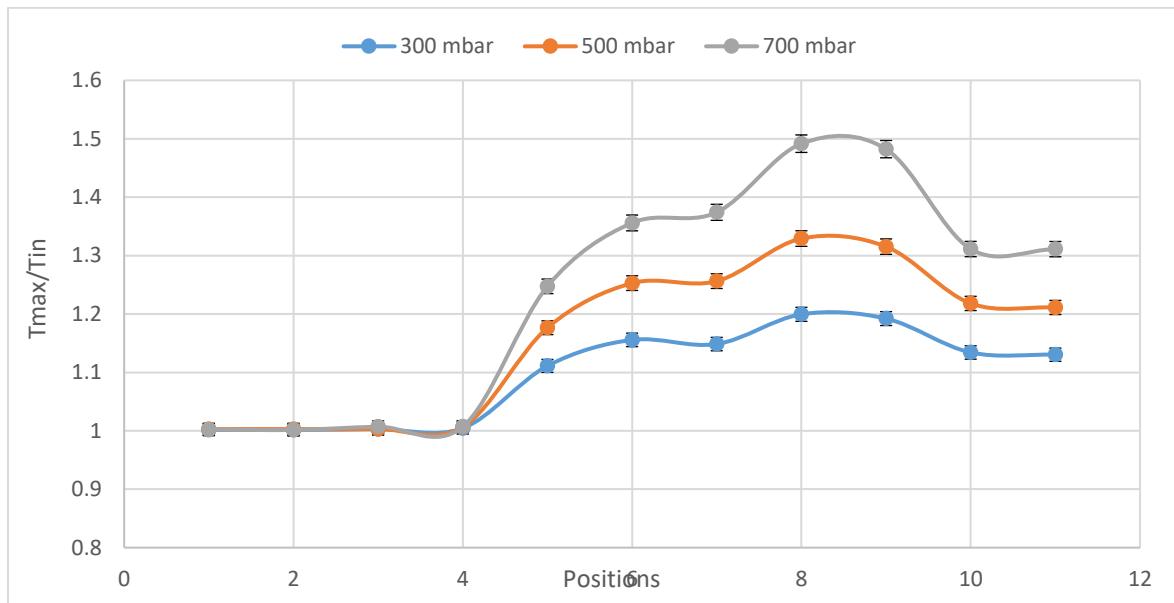


Figure 4.41: The distribution and the variation of maximum temperature at 1800 rev/min and for different pressure loads

Table 4.10: The distribution and the variation of the temperature at speed 1800 rev/min and for different discharge pressures

Positions	$T_{\max}(K^0)$ at 30 kPa	$T_{\max}(K^0)$ at 50 kPa	$T_{\max}(K^0)$ at 70 kPa	$T_{\min}(K^0)$ at 30 kPa	$T_{\min}(K^0)$ at 50 kPa	$T_{\min}(K^0)$ at 70 kPa
P1	288.64	289.00	288.80	287.40	287.00	287.34
P2	288.56	289.00	288.60	287.43	287.00	287.43
P3	289.02	289.00	290.16	286.80	287.00	286.64
P4	289.45	290.00	290.22	286.72	287.00	286.92
P5	320.18	339.00	359.43	242.15	222.00	205.36
P6	333.01	361.00	390.72	249.05	241.00	254.46
P7	330.95	362.00	395.95	246.10	238.00	247.69
P8	345.63	383.00	429.79	264.30	263.00	265.05
P9	343.52	379.00	427.11	289.73	306.00	332.46
P10	326.80	351.00	377.83	309.98	329.00	350.41
P11	325.71	349.00	377.78	312.24	331.00	351.92

On the other hand, there are apparent differences in minimum temperature as we can see in Table 4.10 and figures 4.42 and 4.43. It can be noticed that the minimum temperature decreases as the pressure difference increase which recorded 242.15 K<sup>0</sup>, 222 K<sup>0</sup>, and 205.36 K<sup>0</sup> for pressures of 30 kPa, 50 kPa, and 70 kPa respectively. Also, it can be seen in this figure that the minimum temperature increase from the inlet to outlet until it approaches the minimum value, when the tip of the impellers is approximately at the angle of (45<sup>0</sup>) with respect to the vertical line at the centre of the impeller (point 5), the minimum temperature after that declines and rises slightly when tip is in between 45<sup>0</sup> and 135<sup>0</sup> angles with respect to the vertical line at the centre of the impeller. However, the minimum temperature after angle 135<sup>0</sup> (point 7) increases towards the outlet zone until stabilise.

Furthermore, according to previous analysis, concerning the temperature variations in the blower, the outcomes have presented that pressure difference has a considerable influence on variation and distribution of the temperature which the maximum temperatures increase and the minimum temperature decrease as pressure difference rise. The physical significance of the temperature in the blower that any increase of the temperature above the acceptable level will affect the reliability and performance of the blower which may lead to failure of some components of the blower system like bearing and sealing. Also, this increase of temperature may affect the clearances size within the blower as a result from extreme thermal expansion of rotors and casing materials which may lead to contact and failure of the blower (these are not included in this study because pressure differences that have been investigated are in acceptable level and therefore the temperatures have been increased to acceptable level too). Moreover, the pressure difference is one of the main factors affect the temperature, any increase of pressure above the acceptable level will lead to excessive temperature.

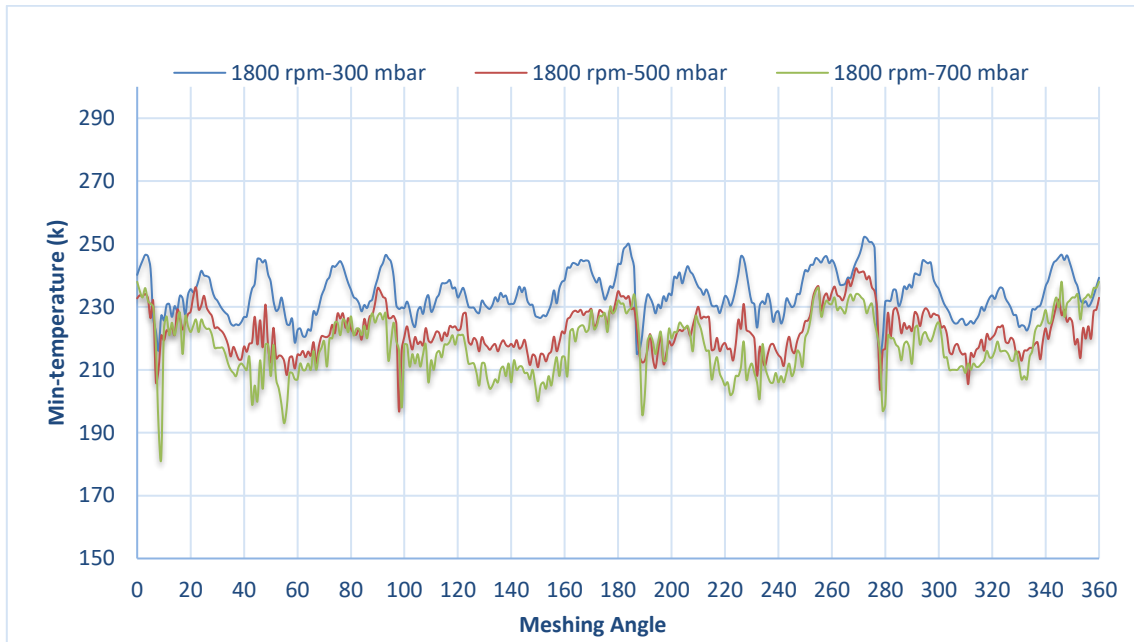


Figure 4.42: The variation of minimum temperature at rotational speed 1800 rev/min and for different pressure loads

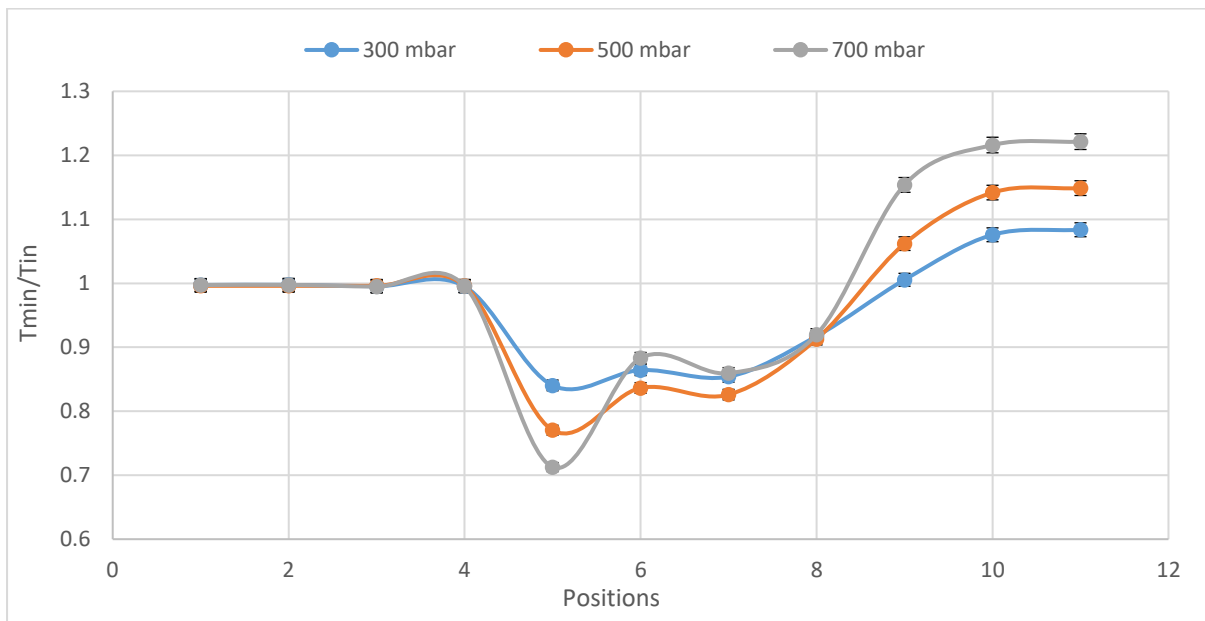


Figure 4.43: The distribution and the variation of minimum temperature at 1800 rev/min and for different pressure loads

#### 4.2.6.4. Effect of the pressure difference on velocity characteristics and distribution

The variation and the distribution of velocity for the last revolution of a case study at different time steps obtained through numerical simulation at a rotational speed 1800 rev/min and for pressure differences of (300, 500, and 700) millibars are shown in Figure 4.44. It shows that the pressure difference will affect the distribution of the velocity inside the Roots blower.

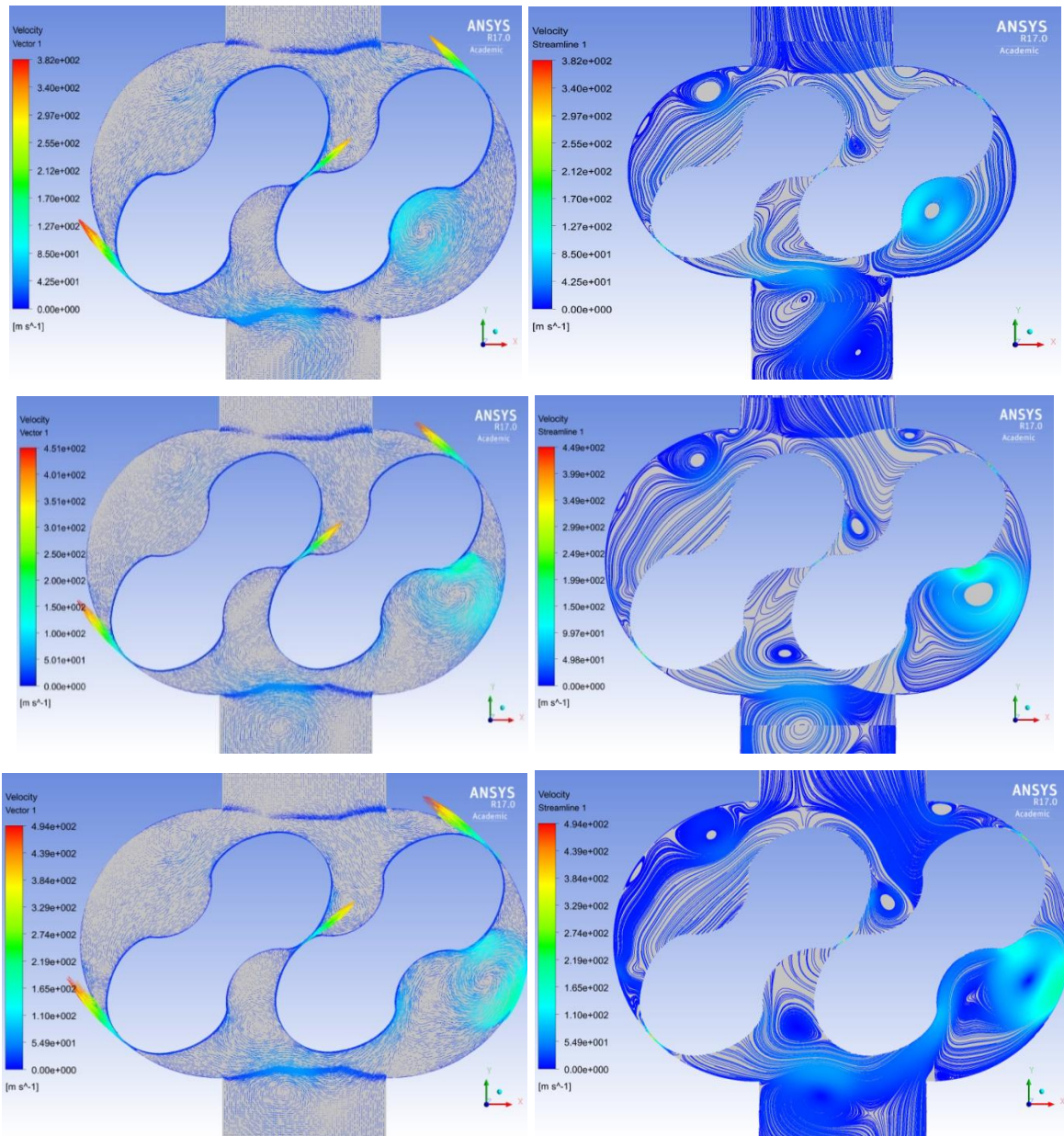


Figure 4.44: The velocity vector and streamline contours at a rotational speed 1800 rev/min, meshing angle at  $45^{\circ}$  and for pressure differences of (300, 500, and 700) millibar from up to down respectively.

The high and low velocities are existed in the flow mixing regions as recirculation zones. These zones occur when the rotors sudden cross the edges of the suction or the discharge zones which the core of these areas consists of the low velocity. Figure 4.44 shows the two rotors formed two chambers; three recirculation zones occurred near the inlet region and other three at the outlet region. It can be seen from this figure that the location of recirculation zones are changing as the pressure difference change which the distance between the centre of recirculation zone and the outlet zone increase with the increase of pressure difference. Moreover, these recirculation areas of high and low velocities may lead to further vibration and energy losses as pressure difference increases. Furthermore, the maximum velocities are found inside the clearances and it increases with the increase in pressure difference as shown in figure 4.44. The rotation role of these recirculation zones that the component of vertical velocity is become negative in these areas, with the opposite direction of the flow regarding to the outlet zone in the blower. It indicates that the existence of recirculation zones reduces the outlet flow and plays an adverse effect on the flow rate. The change of the internal flow velocity shows that the high pressure at the outlet has a strong influence on velocity distribution of the whole region within the Roots blower, making the gaps filled with high-speed backflow, which will inevitably lead to significant energy dissipation.

Table 4.11: The distribution and the variation of the velocity at a speed 1800 rev/min and under different discharge pressure conditions inside the blower from the inlet to the outlet.

Positions	$V_{ave}$ (m/s) at 30 kPa	$V_{ave}$ (m/s) at 50 kPa	$V_{ave}$ (m/s) at 70 kPa	$V_{max}$ (m/s) at 30 kPa	$V_{max}$ (m/s) at 50 kPa	$V_{max}$ (m/s) at 70 kPa
P1	13.25	12.86	12.45	11.48	11.09	10.67
P2	15.05	14.61	14.19	17.62	17.06	16.47
P3	16.40	14.13	14.12	48.29	49.02	57.20
P4	7.19	6.83	5.95	27.98	30.81	31.87
P5	19.17	22.03	27.12	351.16	463.21	528.91
P6	16.03	21.57	25.05	347.35	423.83	449.87
P7	27.12	39.82	49.38	385.48	427.36	470.74
P8	39.97	49.51	60.36	335.03	398.80	462.02
P9	49.91	60.71	68.25	243.72	259.50	266.54
P10	38.76	37.53	37.78	54.64	51.79	67.05
P11	41.45	40.47	38.33	42.63	45.17	41.73

Investigations through the use of various statistical features such as the average and maximum value of velocity fluctuations have been used. This is aimed at more in-depth local analysis of the velocity variation and distribution within the blower.

The distribution and the variation of the average velocity at a constant speed 1800 rev/min and under different discharge pressures inside the blower from the inlet to outlet are presented in Table 4.11 and figure 4.45. It can be seen that there is a considerable variance of average velocity at different discharge pressure which recorded 49.91 m/s, 60.71 m/s, and 68.25 m/s for pressures of 30 kPa, 50 kPa, and 70 kPa respectively. Also, the average velocity increases from the inlet to outlet of the blower. Moreover, the average velocity after point 5 declines slightly between angle  $45^{\circ}$  and angle  $90^{\circ}$  and after that increases until approaching the maximum value at the edges of the discharge zone (point 9). Furthermore, after point 9, the average velocity declines towards the outlet zone till finally stabilising. (All the angles with respect to the vertical line at the centre of the impeller).



Figure 4.45: The variation of average velocity at 1800 rev/min and different pressure loads

Table 4.11 and figure 4.46 show that there are apparent differences in the maximum velocity. It can be noticed that the maximum velocity increases as pressure difference increase which recorded 351.16 m/s, 463.21 m/s, 528.91 m/s for pressures of 30 kPa, 50 kPa, and 70 kPa respectively. Also, it can be seen in this figure that the maximum velocity increase from the inlet to outlet until it approaches the maximum value, when the tip of the impeller is

approximately at the angle of  $(45^\circ)$  with respect to the vertical line at the centre of the impeller (point 5), the maximum velocity after that declines and rises slightly when the tip is in between  $45^\circ$  and  $135^\circ$  angles with respect to the vertical line at the centre of the impeller in the blower. However, the maximum velocity after angle  $135^\circ$  (point 7) increases towards the outlet zone until stabilise.

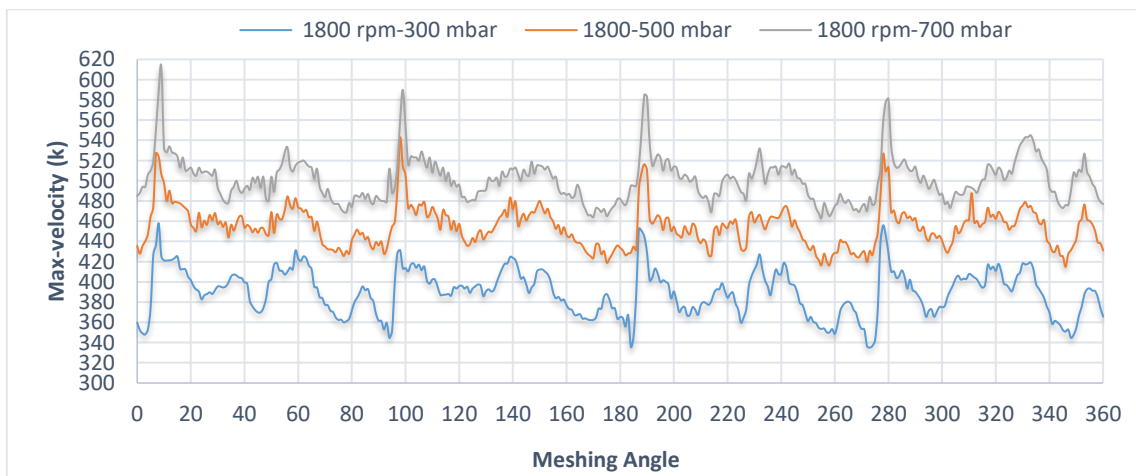
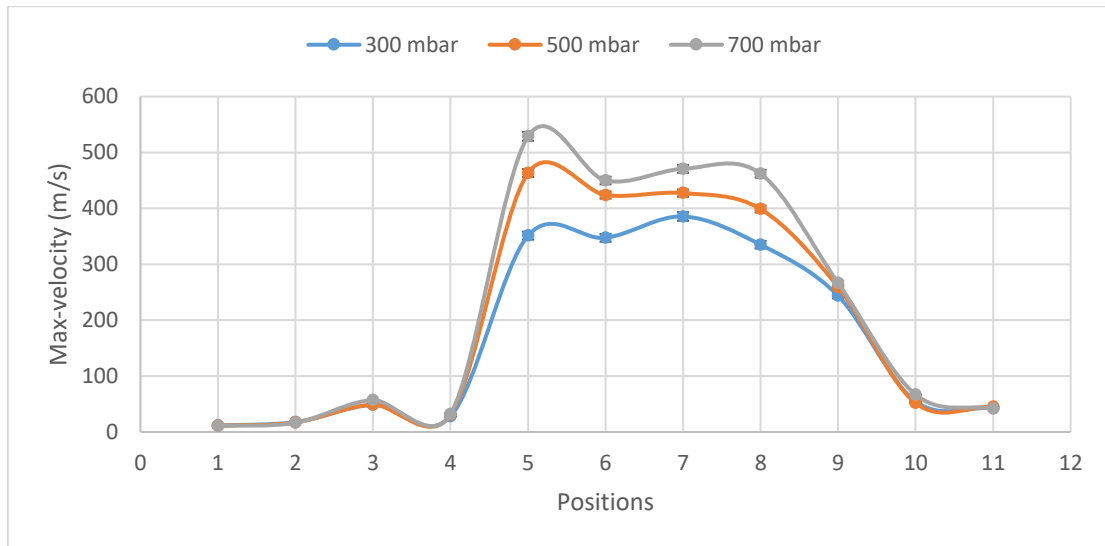


Figure 4.46: The distribution and the variation of Maximum velocity at 1800 rev/min and different pressure loads

On the other hand, the velocity varies rapidly with the change of angle. According to the comparison between the different positions of rotors meshing angle, it is found that the fluctuation of velocity repeats itself every  $90^\circ$  angles with respect to the vertical line at the centre of the impeller in the blower. Also, the high and the low values of velocity start at about

$6^{\circ}$  - $9^{\circ}$  angles with respect to the vertical line at the centre of the impeller in the blower as shown in figure 4.46.

Furthermore, according to previous analysis, concerning the velocity variations in the blower, the results have presented that pressure difference has a considerable influence on variation and distribution of the velocity which the average and the maximum velocities increase as pressure difference increase. Moreover, it has been found that the positions of the minimum pressures and minimum temperatures are very close to the locations of maximum velocities.

The physical significance of the velocity in the blower that any increase of the velocity above the acceptable level will affect the reliability and performance of the blower which may lead to increase of vibration and noise in the blower system. Also, an extreme increase of velocity may affect the foundation of the blower system which may lead to failure of the blower system. Moreover, the pressure difference is one of the main factors affect the velocity, any increase of pressure above the acceptable level will lead to excessive velocity within the blower.

#### **4.2.7. Effect of the rotational speed on the Roots blower performance characteristics**

The main observation from the earlier sections is that the performance of the blower is influenced by the change of operational conditions. Consequently, the flow behaviour such as pressure and velocity, as well as unsteadiness of the internal flow in the Roots blower are expected to be different as the change of working conditions taking place. Hence, all of these parameters can affect the flow characteristics and the performance of the blower. Also, the blower performance under different blower rotating speeds can vary appreciably. Therefore, for further investigation, this section would include studying the effect of the rotational speed of blower on the pressure variations, velocity variations and temperature variations within a Roots blower, and also their performance. The rotational speeds of 1200, 1800, 2400 rev/min and the differential pressure of 700 millibars have been chosen in the CFD numerical model to study the effect of speed change on blower performance because these speeds 2400, 1800, and 1200 are maximum, medium, and minimum design speeds of Roots blower under investigation respectively. Also, the pressure difference 700 millibars is the maximum design pressure difference of Roots blower under research. Additionally, for more understanding and in-depth local analysis of the influence of rotational speed on the variation and the distribution of different performance parameters inside the blower, investigations with different statistical

features such as average, minimum and maximum value, root mean square (RMS), and amplitude has been carried out. Also, to simplify and parameterise the performance characteristics of Roots blower, non-dimensional analysis has been used.

#### 4.2.7.1. Effect of the rotational speed on pressure field characteristics

In the present study, the influence of rotational speed of the rotors on pressure variation and distribution has been established through the use of ANSYS FLUENT code and dynamic mesh technique (DMT).

The contours and distribution of the pressure for the last revolution of a case study obtained through numerical simulation at speeds of (1200, 1800, and 2400) rev/min and of 700 millibar pressure difference are shown below in Figure 4.47.

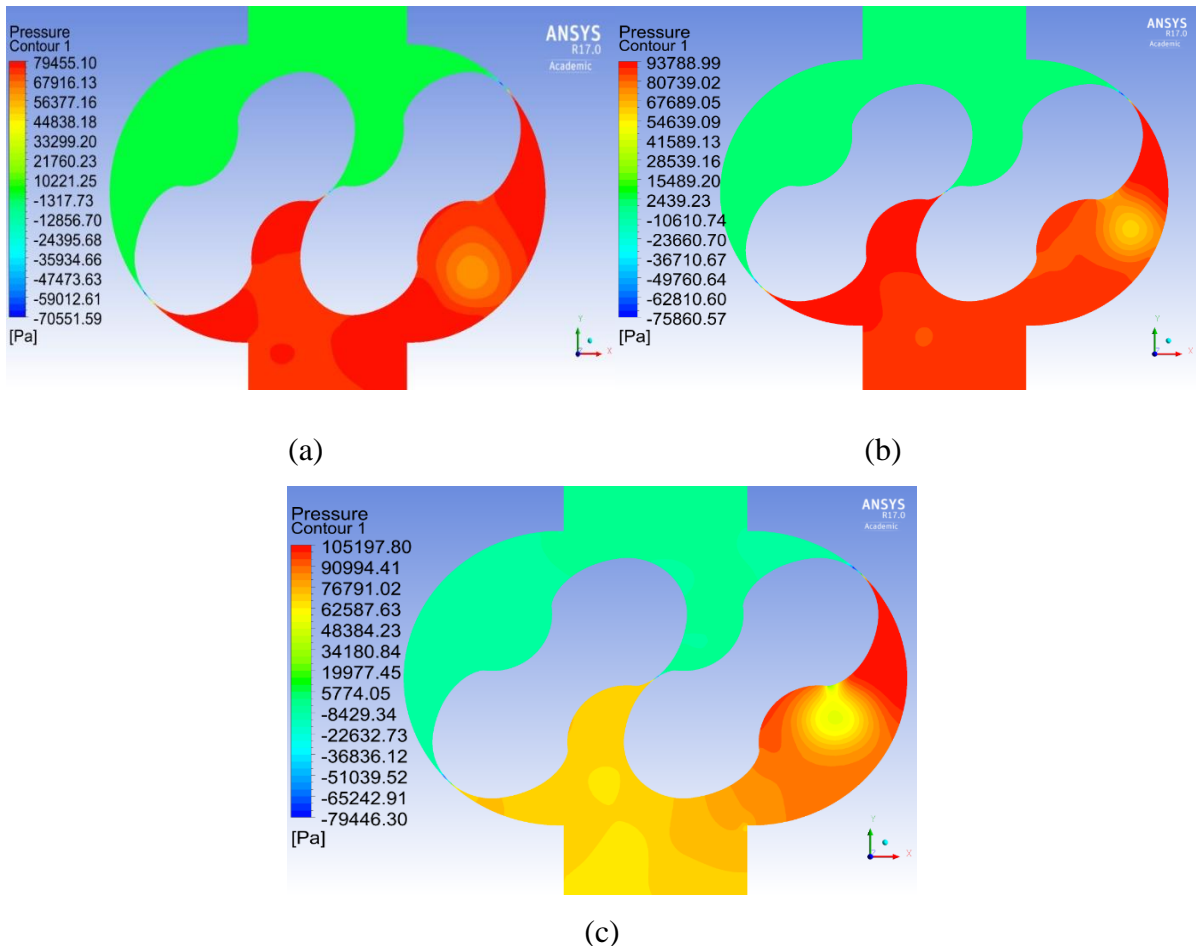


Figure 4.47: The distribution and the variations of static pressure at 700 millibar and for rotational speed of (a) - 1200 rev/min, (b) - 1800 rev/min, (c) - 2400 rev/min

Figure 4.47 depicts the variations and the distribution of static pressure contours in the Roots blower. It is evident that the distributions of static pressure at different rotational speed and under same pressure difference have the same trend for all the cases under investigation which the pressure is gradually increased from the inlet area to the outlet area of the blower. It can be seen from this figure that the lower pressure occurs inside clearances at the inlet side of the rotor. However, there are apparent differences in the variation and the distribution of static pressure as the rotational speed increase. It can be seen that the positive and the negative static pressure in figure 4.47 (c) is higher than other figures. Also, the areas of recirculation are bigger and more obvious in figure 4.47 (c) than other figures. Moreover, the appearance of recirculation zones in some regions within the blower could account for local pressure loss phenomenon. A recirculation zones are often the turbulent flow of fluid and exhibits a very low pressure at the centre. It can be seen from the figure that the location of the recirculation zones are changing as a change of rotational speed. Therefore, the pressure loss will increase with the increase of rotational speed.

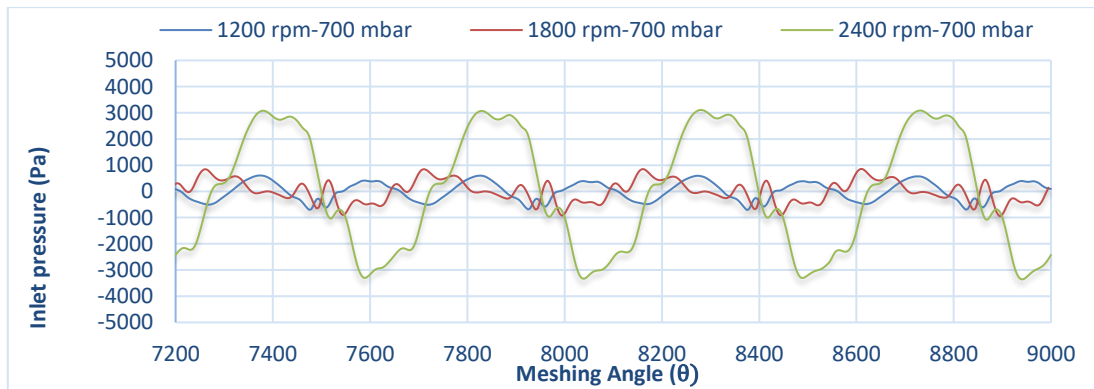


Figure 4.48: Pressure fluctuations at blower inlet at 1800 rev/min and for different pressures

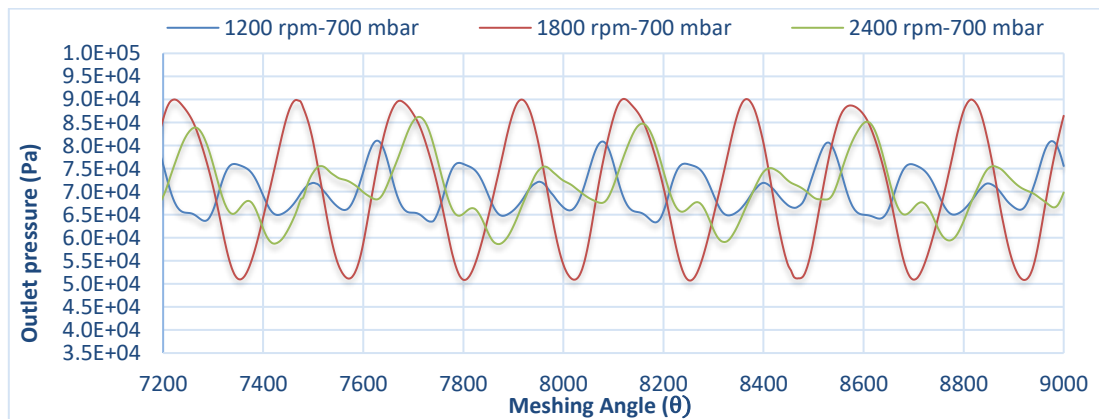


Figure 4.49: Pressure fluctuations at blower inlet at 1800 rev/min and for different pressures

Studying the fluctuation of the pressure are essential to understand and predict the unsteady flow and noise generation mechanisms in the Roots blower. Figures 4.48 and 4.49 show the instantaneous variation of static pressure at the inlet and outlet of the two-lobe Roots blower over one revolution/cycle at the different rotational speed. It can be seen from these figures that the pressure and the amplitude of fluctuation in the discharge zone are higher than that in the suction zone and it increases as the rotational speed increase. However, at the outlet the pressure and their amplitude at a speed 1800 rev/min is higher than the pressure and their amplitude at a speed 2400 rev/m, this is because the effect of high pressure on one hand and the effect of high speed on the other hand or in other words the effect of interaction between the high-pressure difference and the rotational speed.

Table 4.12: The max-pressures and the min-pressures at 700 millibars and under different rotational speeds.

Positions	$P_{in}$ Pa	$P_{max}$ (Pa) at 1200 rev/min	$P_{max}$ (Pa) at 1800 rev/min	$P_{max}$ (Pa) at 2400 rev/min	$P_{min}$ (Pa) at 1200 rev/min	$P_{min}$ (Pa) at 1800 rev/min	$P_{min}$ (Pa) at 2400 rev/min
P1	1.0E+05	5.8E+02	8.0E+02	3.0E+03	-7.3E+02	-1.0E+03	-3.4E+03
P2	1.0E+05	6.5E+02	5.4E+02	3.3E+03	-8.1E+02	-9.0E+02	-3.6E+03
P3	1.0E+05	7.6E+02	1.1E+03	3.3E+03	-9.3E+02	-2.3E+03	-5.3E+03
P4	1.0E+05	1.8E+03	1.7E+03	3.3E+03	-9.5E+02	-2.4E+03	-5.3E+03
P5	1.0E+05	9.0E+04	7.2E+04	9.5E+04	-7.3E+04	-7.8E+04	-7.7E+04
P6	1.0E+05	8.4E+04	1.1E+05	1.1E+05	-7.0E+04	-6.6E+04	-6.9E+04
P7	1.0E+05	8.2E+04	1.1E+05	9.4E+04	-7.2E+04	-6.8E+04	-7.1E+04
P8	1.0E+05	8.3E+04	9.8E+04	8.7E+04	-6.3E+04	-6.4E+04	-6.3E+04
P9	1.0E+05	8.2E+04	9.6E+04	8.7E+04	-1.3E+04	-1.4E+03	-1.3E+04
P10	1.0E+05	8.2E+04	9.0E+04	8.5E+04	6.3E+04	4.9E+04	5.6E+04
P11	1.0E+05	8.1E+04	9.0E+04	8.5E+04	6.3E+04	5.0E+04	5.7E+04

The variation and distribution of pressure at same discharge pressure and under different rotational speeds of the blower from the inlet to outlet are presented in Table 4.12 and Figures 4.50, 4.51. It can be seen that there is a significant difference in maximum pressure at different rotational speeds and under the same discharge pressure. The maximum pressure increases

from the inlet to outlet until approaches the maximum values when the tip of impeller is approximately at the middle region of the blower ( $90^{\circ}$  or point 6) which recorded  $8.44E+04$  Pa,  $1.12E+05$  Pa, and  $1.05E+05$  Pa of speeds 1200 rev/min, 1800 rev/min, and 2400 rev/min respectively as highlighted and shown in table 4.12. Also, the pressure value declines slightly towards the outlet zone after point 6 until stabilise.

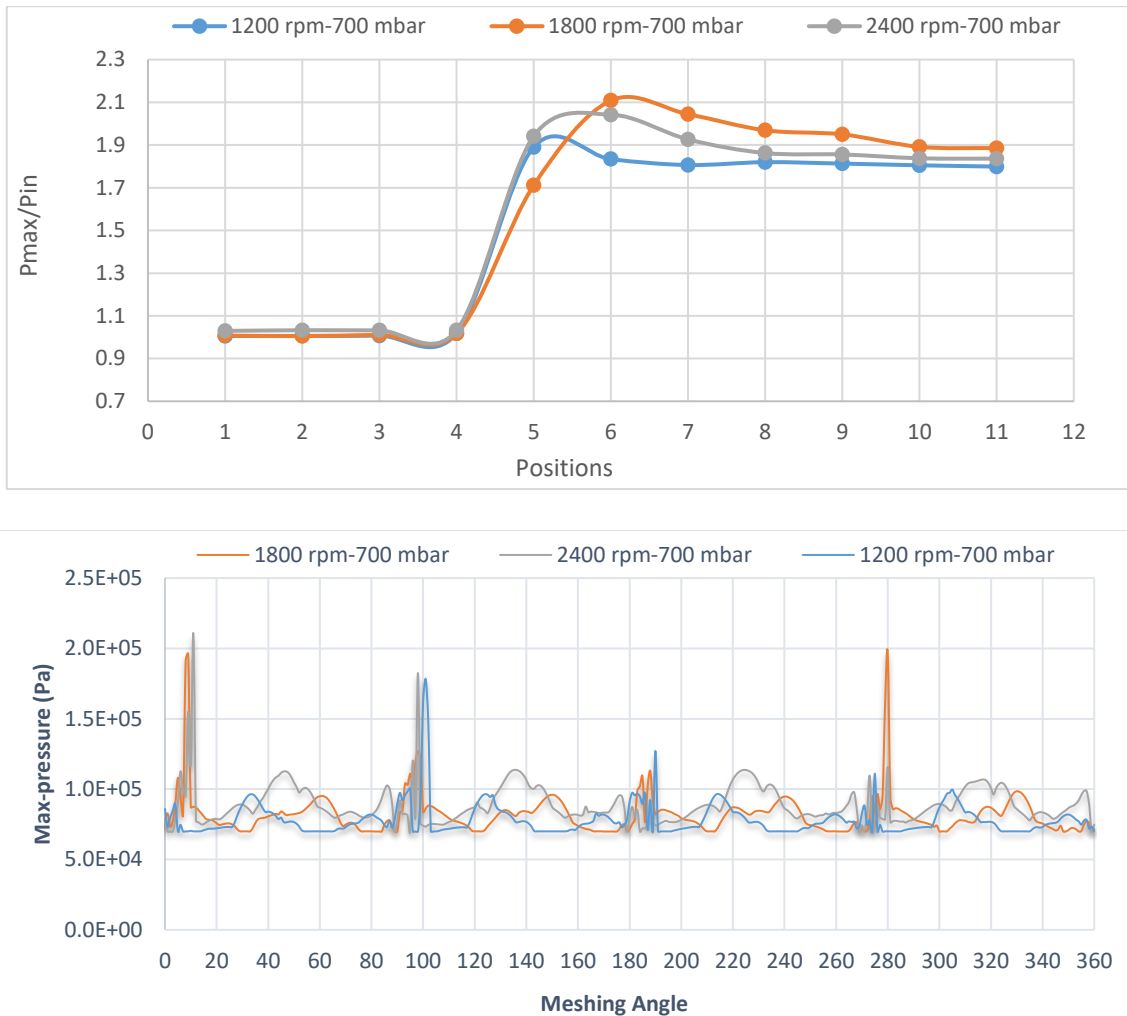


Figure 4.50: The distribution of max-pressures at 700 millibars and under different rotational speeds.

Furthermore, it can be concluded from figures 4.50 that the maximum positive pressure value is approximately between  $45^{\circ}$  and  $60^{\circ}$  angles of degrees at the high-pressure zone as a result from the effect of backflow pressure at discharge zone. Also, the behaviour of pressure fluctuations is repeated every  $90^{\circ}$  degrees. Moreover, the maximum positive pressure and their amplitude are increase with the increase of rotational speed. However, the maximum pressure and their amplitude at the speed of 1800 rev/min are higher than the maximum pressure and

their amplitude at the speed of 2400 rev/min. This is because of the effect of high pressure at the outlet zone on one hand and the effect of high speed and high velocity inside the clearances in the blower on another hand.

(All the angles with respect to the vertical line at the centre of the rotor within the blower).

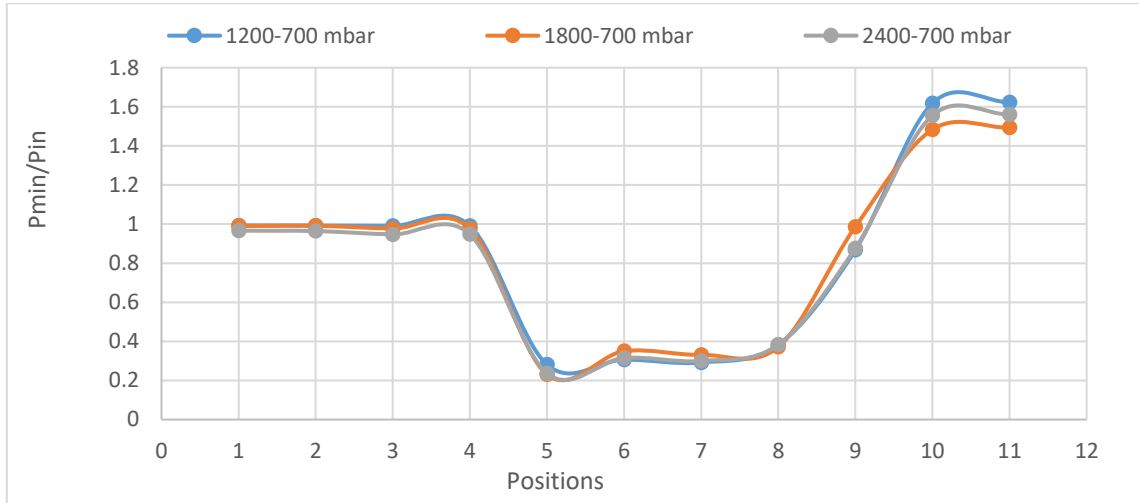


Figure 4.51: The distribution of min-pressure at 700 millibars and under different rotational speeds.

Figure 4.51 and table 4.12 show that there are small differences in maximum negative pressure which recorded  $-7.3E+04$  Pa,  $-7.8E+04$  Pa,  $-7.7E+04$  Pa of speeds 1200 rev/min, 1800 rev/min, and 2400 rev/min respectively as highlighted and shown in table 4.12. It can be seen in this figure that the maximum negative pressure increases from the inlet to outlet until it approaches the maximum values when the tip of impeller is approximately at the angle of  $(45^{\circ})$  with respect

to the vertical line at the centre of the rotor and after that it declines toward the outlet zone until stabilise.

On the other hand, it can be concluded from figure 4.51 that the maximum negative pressure value is approximately between  $45^{\circ}$  and  $60^{\circ}$  degrees inside the clearance at the low-pressure zone as a result from the effect of backflow pressure at discharge zone. Also, the behaviour of pressure fluctuations is repeated every  $90^{\circ}$  degrees. Moreover, the maximum negative pressure and their amplitude are increase with the increase of rotational speed. However, the maximum negative pressure and their amplitude at the speed of 1800 rev/min are higher than the maximum negative pressure and their amplitude at the speed of 2400 rev/min. This is because of the effect of high pressure at the outlet zone on one hand and the effect of high speed and high velocity inside the clearances in the blower on the other hand.

(All the angles with respect to the vertical line at the centre of the rotor within the blower).

Root mean square (RMS) refers to the arithmetic mean of the squares of a set of numbers. RMS is a meaningful way of calculating the average of values over a period of time. Figure 4.52 expresses the relation between effective pressure zones and RMS. It can be seen that the RMS increases from the inlet to outlet of the blower, which the maximum values are recorded at the discharge zones. Also, these values rise with an increase of rotational speed.

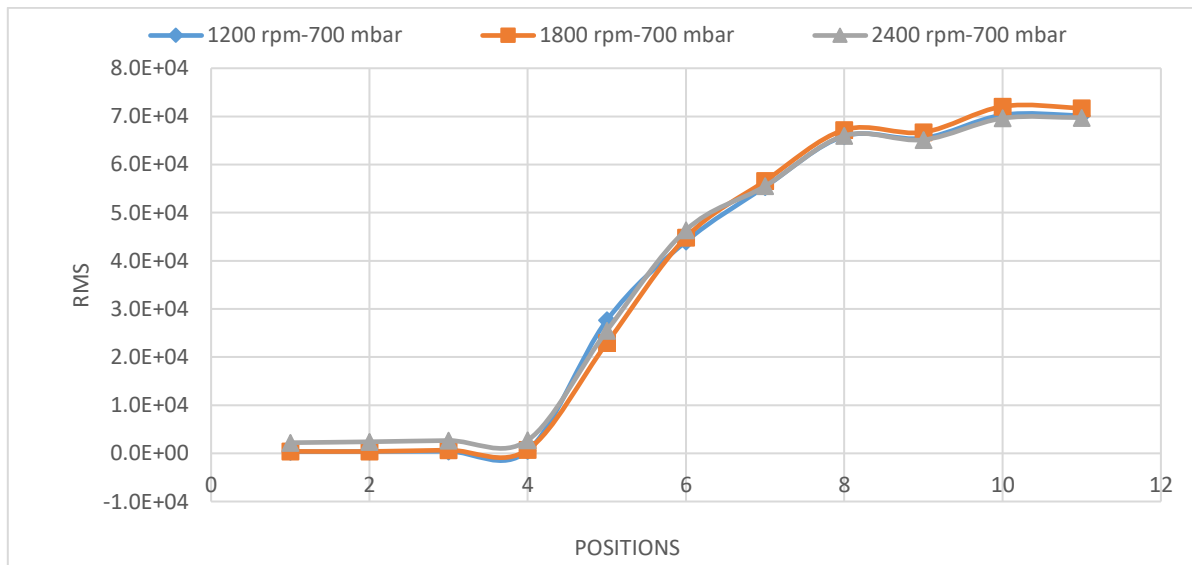


Figure 4.52: Root Mean Square (RMS) of effective pressure zones at 700 millibars and different rotational speed.

The peak-to-peak amplitudes at different rotational speeds under the same discharge pressure are presented in Figure 4.53. It is clear to conclude that there is a small difference of amplitudes when the tip of impellers is at the inlet or the outlet regions. On the other hand, the differences of amplitudes are increased when the tip of rotors starts to move away from these zones.

These differences increase inside the meshing region in the blower. Also, the maximum amplitude values are recorded at points 6 and 7 where the effect of pressure and backflow are high in this zone. Moreover, it can be seen that the amplitudes are increased with the increase of rotational speed and are more prominent at outlet zone than an inlet zone because the pressure and their fluctuations are higher in this area. However, pressure amplitude at the speed of 1800 rev/min is higher than the pressure amplitude at the speed of 2400 rev/min. This is because of the effect of high pressure at the outlet zone on one hand and the effect of high speed and high velocity inside the clearances in the blower on the other hand.

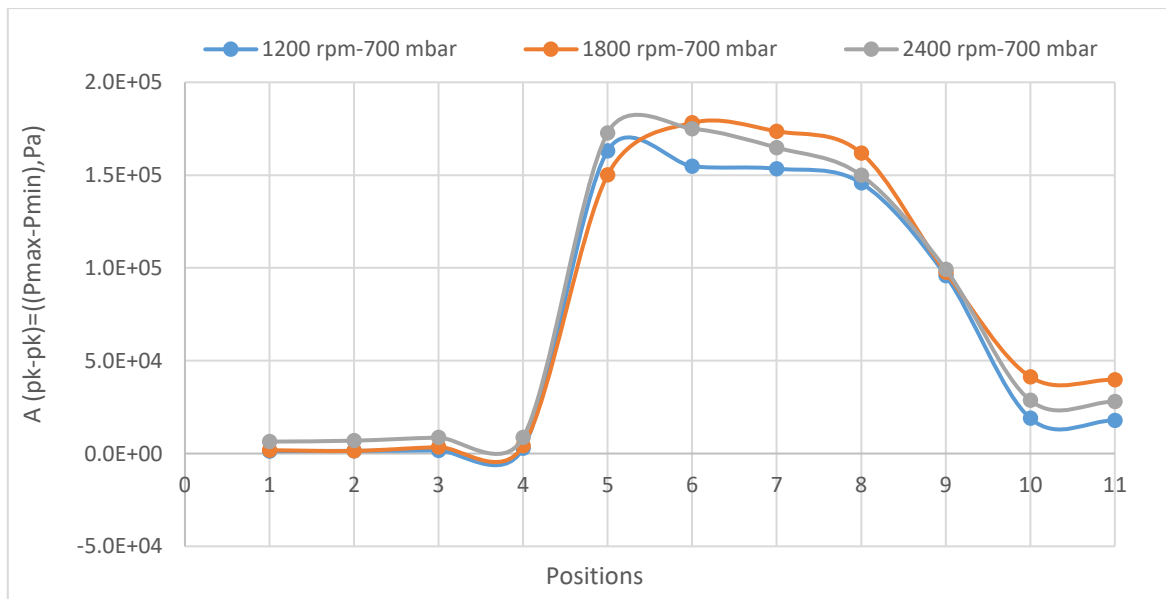


Figure 4.53: The peak-peak amplitudes at different speeds and 700-millibars discharge pressure.

Additionally, according to previous analysis, concerning the pressure variations in the blower, the outcomes have presented that the rotational speed of the blower has a considerable influence on variations and distribution of the pressure.

#### 4.2.7.2. The effect of the rotational speed on flow rate characteristics

The average mass flow rate for the last impeller meshing rotation cycle of the Roots blower of case study obtained through numerical simulation at rotational speeds of (1200, 1800, and 2400) rev/min and for pressure difference 700 millibars are shown in table 4.13 and figure 4.54. It can be observed that the average mass flow rate increase linearly with the increase of the blower rotors speeds.

Figure 4.13: The average and the fluctuation coefficient of the mass flow rate at different speeds and 700 millibars pressure difference

Rotational speed (rev/min)	$\dot{m}_{ave}$ (kg/s) at	$M_F$ at inlet	$M_F$ at the outlet
1200	0.2681	0.4383	-6.320
1800	0.4950	0.4393	-7.969
2400	0.7301	0.8528	-4.142

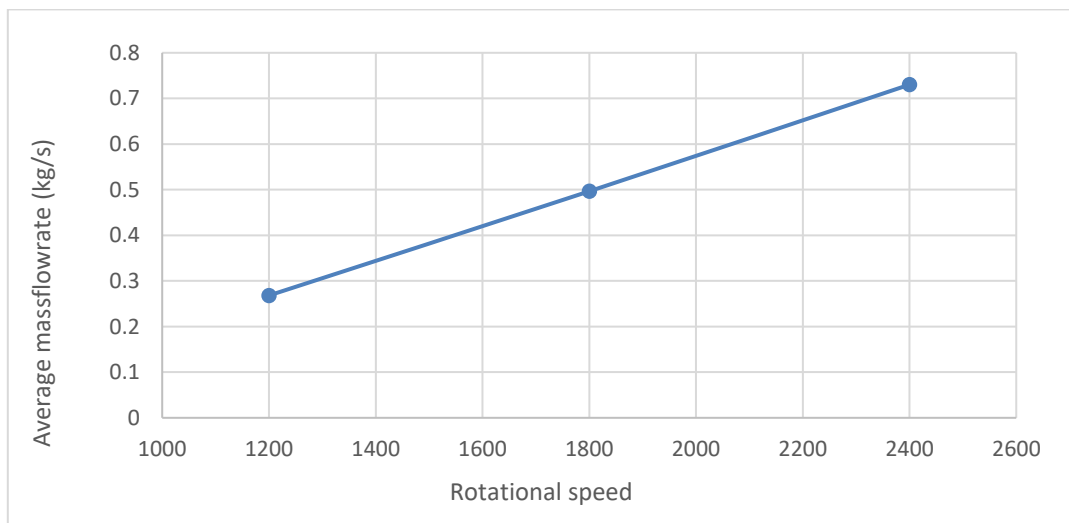


Figure 4.54: The average mass flow rate at different speeds and 700 millibars pressure difference

The fluctuations of mass flow rate for the last impeller meshing rotation cycle of the Roots blower of case study obtained through numerical simulation at rotational speeds of (1200, 1800, and 2400) rev/min and for pressure difference 700 millibars are shown in figure 4.55. It can be concluded that there are a small difference of the amplitude and the fluctuation coefficient ( $M_f$ ) of inlet mass flow rate between that from a speed of 1200 rev/min and that from the speed of

1800 rev/min. However, the difference rises considerably at a speed of 2400 rev/min. The reason behind that because of the effect of high speed and high-pressure difference which result in an increase of velocity and backflow.

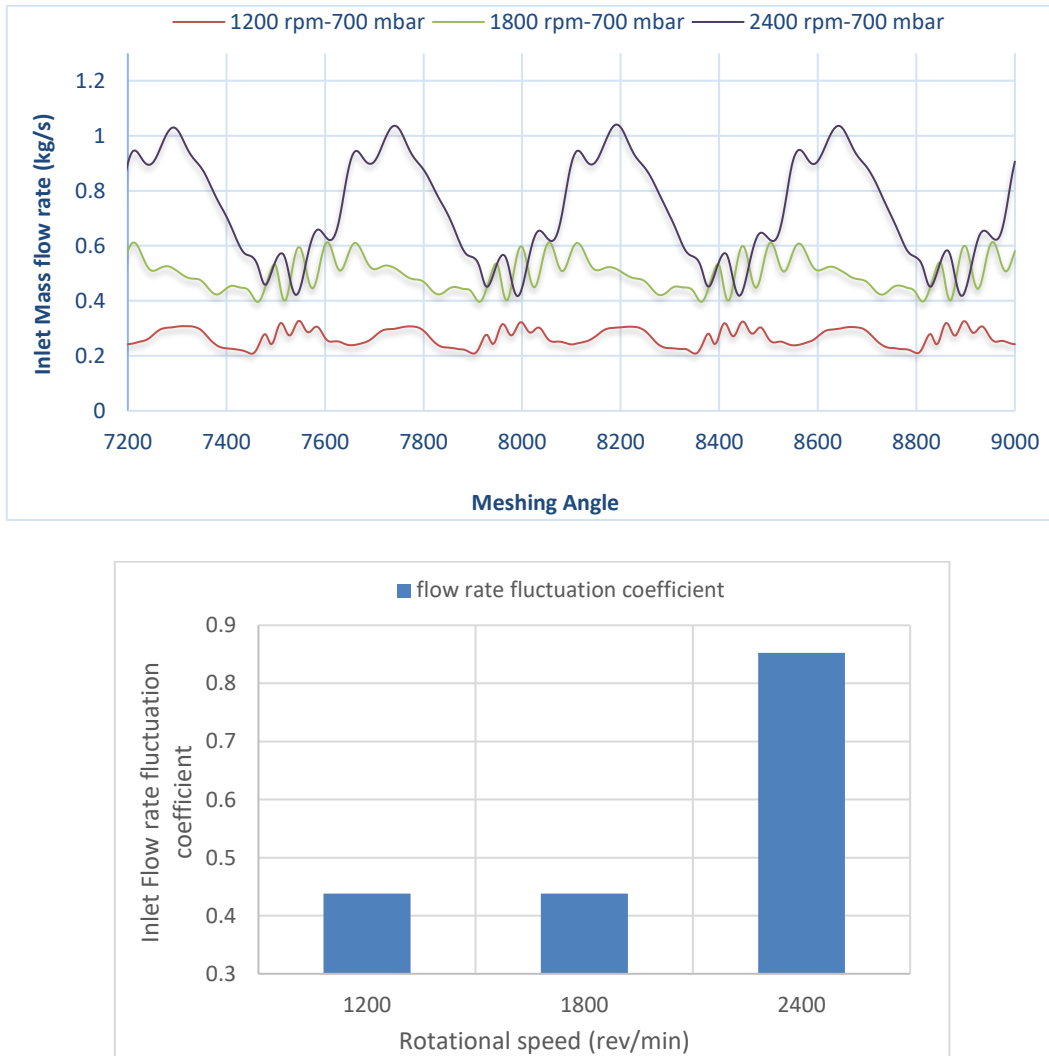


Figure 4.55: The fluctuations of the inlet mass flow rate at 1800 rev/min and different pressure loads

Moreover, the amplitude of the outlet mass flow rate at a speed 1800 rev/min is higher than the amplitude at a speed 2400 rev/m as shown in figure 4.55. Also, figure 4.56 illustrates the mass flow rate fluctuation coefficient (Mf) at the outlet of the blower which the outlet mass flow rate fluctuation coefficient at a speed 1800 rev/min is higher than that at a speed 2400 rev/m. This is because of the effect of high pressure on one hand and the effect of high speed on the other hand or in other words the effect of interaction between the high-pressure difference and the

rotational speed. These can be found in applications where high mass flow rate is needed at high pressure difference.

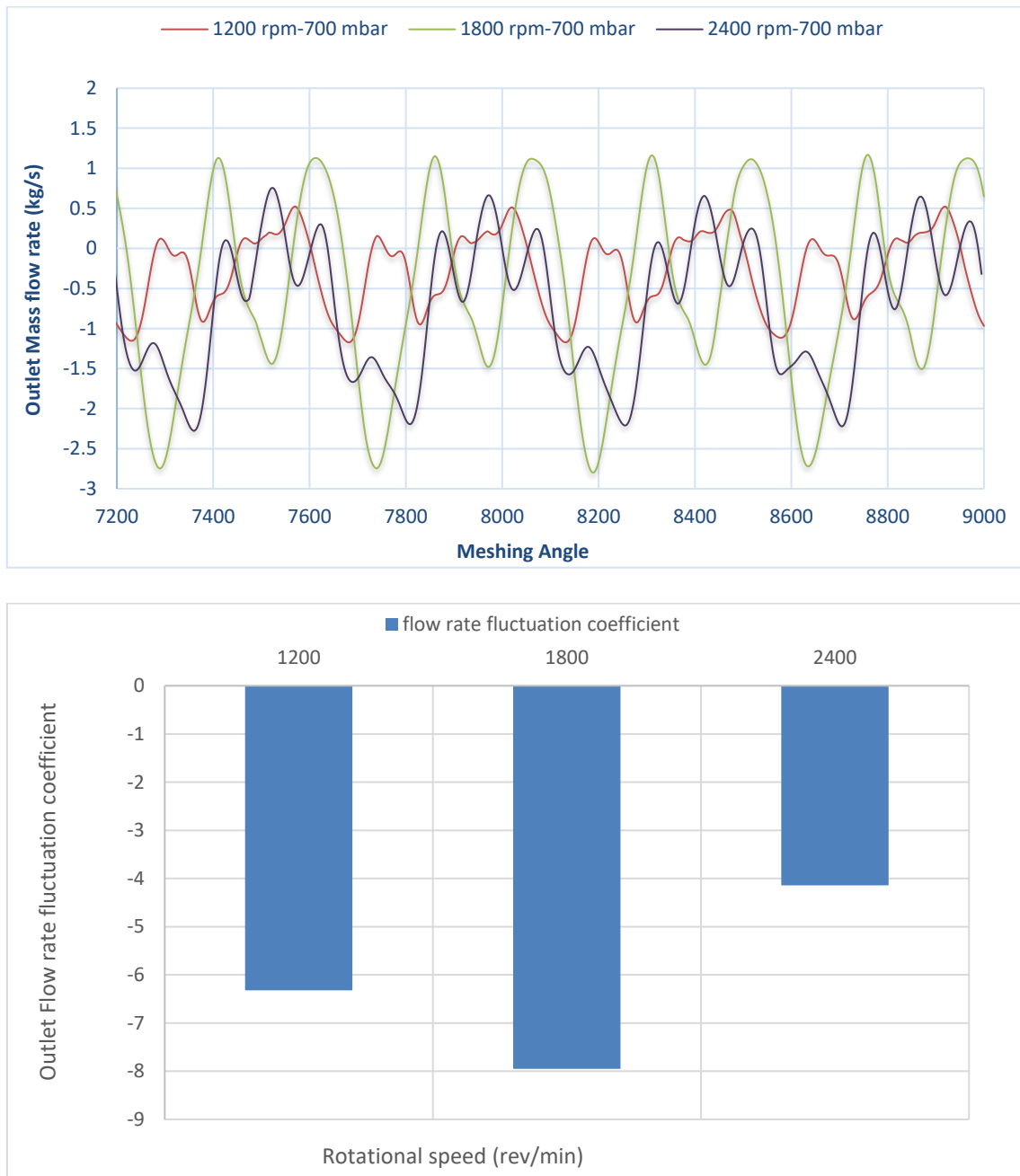
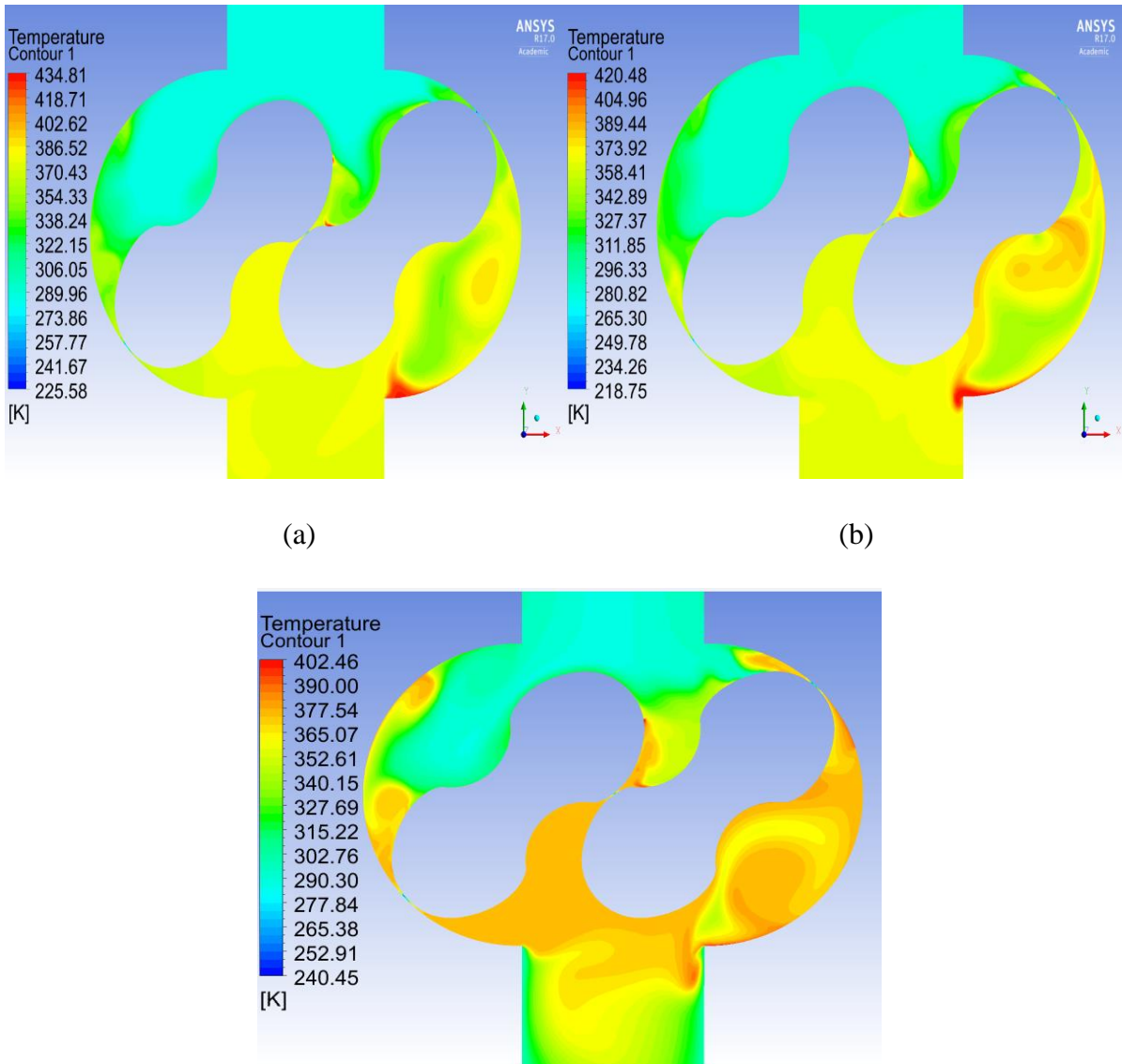


Figure 4.56: The amplitude of fluctuations of the mass flow rate at 700 millibars pressure difference and different rotational speeds

### 4.2.7.3. Effect of the rotational speed on distributions and characteristics of temperature

The temperature contour for the last revolution of a case study at different time steps obtained through numerical simulation at speeds of 1200, 1800, and 2400 rev/min at a constant pressure rise are shown below in Figure 4.57.



(c) Figure 4.57: The temperature contours for the last revolution and at  $45^\circ$  rotation degrees, 700 mbar and for rotational speeds of (a) 1200 rev/min, (b) 1800 rev/min, and (c) 2400 rev/min.

Figure. 4.57 shows the influence of unsteady flow on temperature distribution and the location of the high-temperature area inside the Roots blower. It is apparent to conclude that the distribution of temperature is non-uniform and the position of high-temperatures are close to

rotor wall and casing wall at the outlet zone. Also, there are high- temperature areas inside the chamber between the rotor and the casing at discharge zone which changing their location and shape as rotors rotating and with a change of rotational speed. Moreover, the temperature increase inside the blower with a decrease of rotational speed and at high-pressure difference as a result of backflow effect.

However, the high-pressure difference increasing the effect of backflow while the high rotational speed decreasing the effect of backflow. This is explaining why the effect of backflow at low speed and high-pressure difference is higher and therefore temperature is higher.

The variation of the outlet temperature with the rotation angle for last rotation is shown in Figure 4.58. It can be concluded that the temperature and their amplitude increases as rotational speed increases.

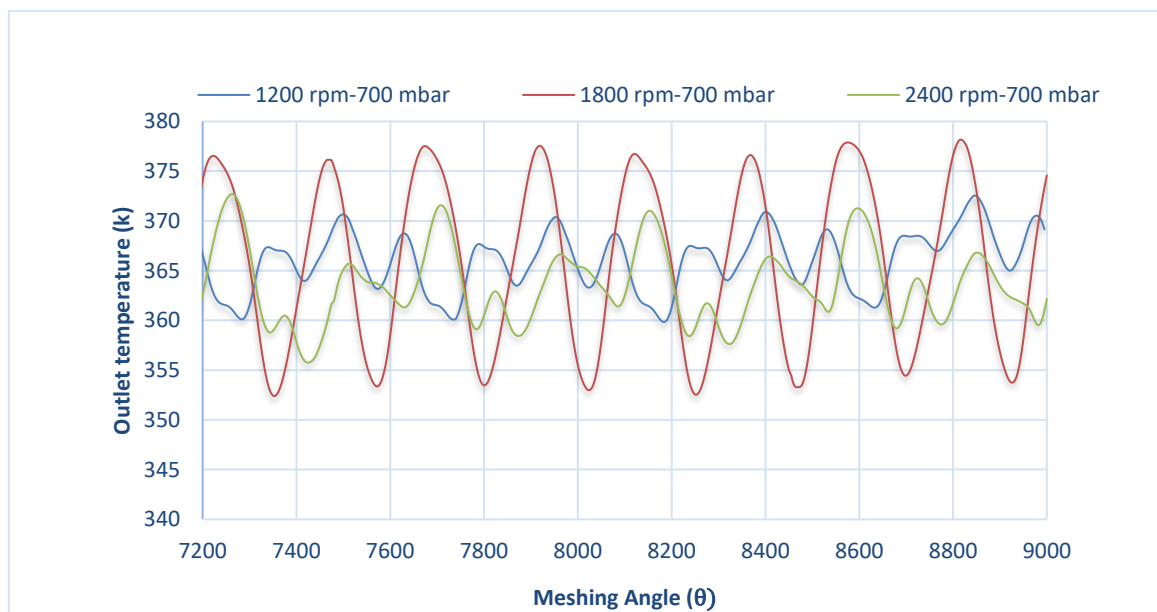


Figure 4.58: Outlet temperature at a pressure difference 700 millibars and for different rotational speeds

Table 4.14: The distribution and the variation of the temperature inside the blower from the inlet to the outlet at a discharge pressure of 700 millibars and under different rotational speeds

Positions	$T_{in}$ $K^0$	$T_{max}$ ( $K^0$ ) at 1200 rev/min	$T_{max}$ ( $K^0$ ) at 1800 rev/min	$T_{max}$ ( $K^0$ ) at 2400 rev/min	$T_{min}$ ( $K^0$ ) at 1200 rev/min	$T_{min}$ ( $K^0$ ) at 1800 rev/min	$T_{min}$ ( $K^0$ ) at 2400 rev/min
P1	288.15	288.83	288.80	290.56	287.70	287.34	285.34
P2	288.15	290.41	288.59	290.82	287.67	287.42	285.17
P3	288.15	313.57	290.15	291.15	294.02	286.64	284.38
P4	288.15	315.89	290.22	291.35	294.62	286.92	284.22
P5	288.15	385.24	359.43	353.60	244.31	205.36	207.46
P6	288.15	390.02	390.72	386.01	255.56	254.45	242.75
P7	288.15	391.80	395.94	377.88	236.49	247.69	235.77
P8	288.15	437.01	429.79	420.32	241.43	265.05	258.61
P9	288.15	436.27	427.10	417.77	283.70	332.45	316.49
P10	288.15	378.4381	377.82	376.44	364.82	350.40	351.72
P11	288.15	372.4017	377.78	371.89	359.73	351.92	354.51

Investigations through the use of various statistical features such as the average, minimum and maximum value of temperature fluctuations have been used. This is aimed at more in-depth local analysis of the temperature variation and distribution within the blower.

The distribution and the variation of the temperature at a constant discharge pressure and under different rotational speeds in the blower from the inlet to outlet are presented in Table 4.14.

Figure 4.59 depicts that there is a considerable variance of maximum temperature at different rotational speeds which recorded 437.01  $K^0$ , 429.79  $K^0$ , and 420.32  $K^0$  for speeds of 1200 rev/min, 1800 rev/min, and 2400 rev/min respectively. Also, the maximum temperature increases from the inlet to the outlet of the blower. Moreover, the maximum temperature after point 6 declines slightly between angle 90° (P6) and angle 135° (P7) and after that increases until the maximum value at angle 180° (P8). Furthermore, after P8, the maximum temperature begins to drop towards the outlet zone till finally stabilising.

(All the angles with respect to the vertical line between the inlet and the outlet of the blower).

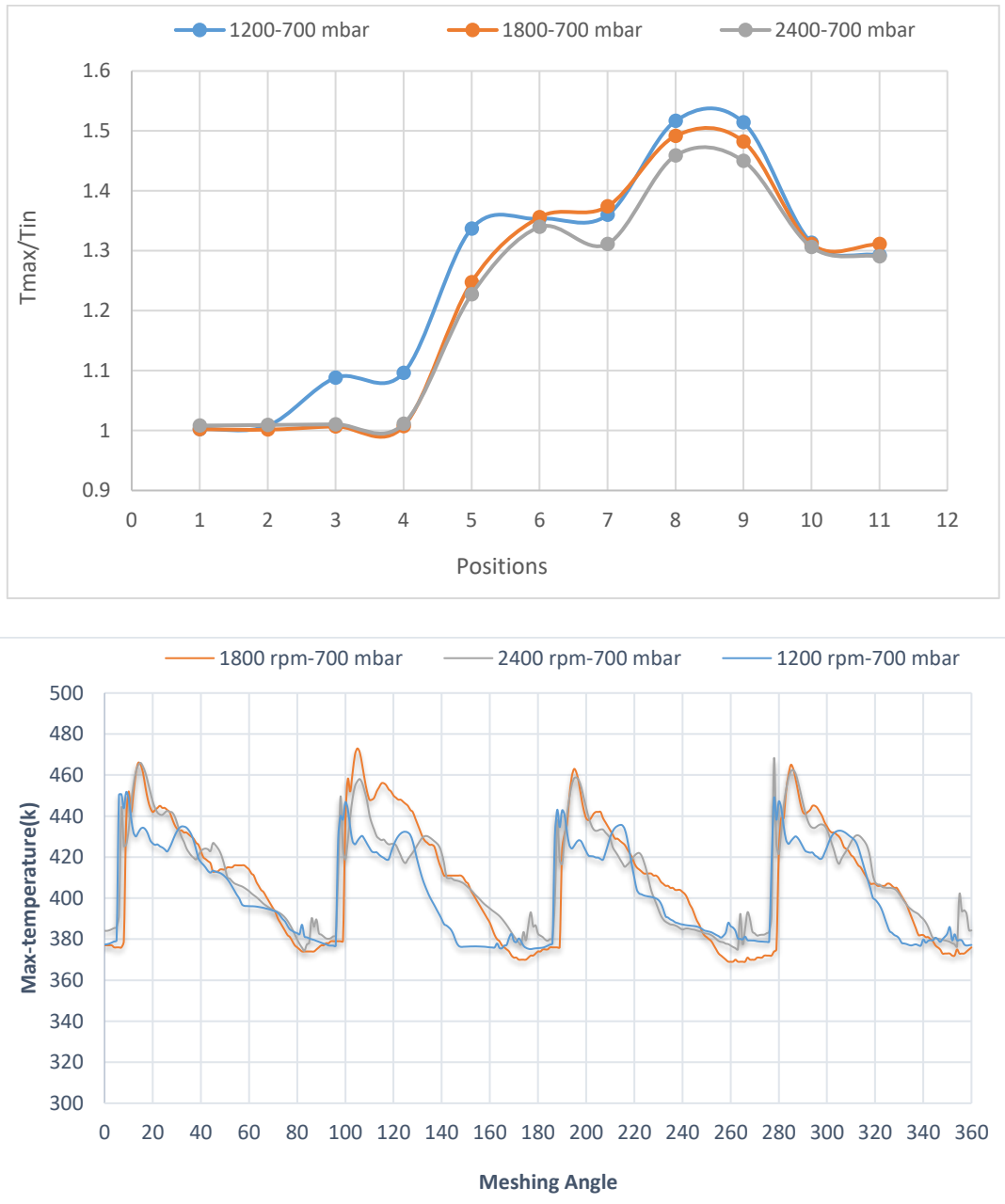


Figure 4.59: The distribution and the variation of minimum temperature at same discharge pressure 700 millibars and under different rotational speeds.

Table 4.14 and figure 4.60 show that there are apparent differences in minimum temperature. It can be seen that the minimum temperature decreases as rotational speeds increase which recorded 236.49 K<sup>0</sup>, 205.36 K<sup>0</sup>, and 207.46 K<sup>0</sup> for rotational speeds of 1200 rev/min, 1800 rev/min, and 2400 rev/min respectively. Also, it can be seen in this figure that the minimum temperature increase from the inlet to outlet until it approaches the minimum value, when the tip of the impellers is approximately at the angle of (45<sup>0</sup>) with respect to the vertical line at the

centre of the impeller, the minimum temperature after that declines and rises slightly when tip is in between  $45^{\circ}$  and  $135^{\circ}$  angles with respect to the vertical line at the centre of the impeller. However, the minimum temperature after angle  $135^{\circ}$  (P7) increases towards the outlet zone until stabilise.

Furthermore, according to previous analysis, concerning the temperature variations in the blower, the outcomes have presented that rotational speed has a significant influence on the variation and the distribution of the temperature which the maximum temperatures decreases and the minimum temperature decrease as rotational speed increase. However, the effect of pressure difference on the variation and the distribution of the temperature is more apparent than rotational speed.

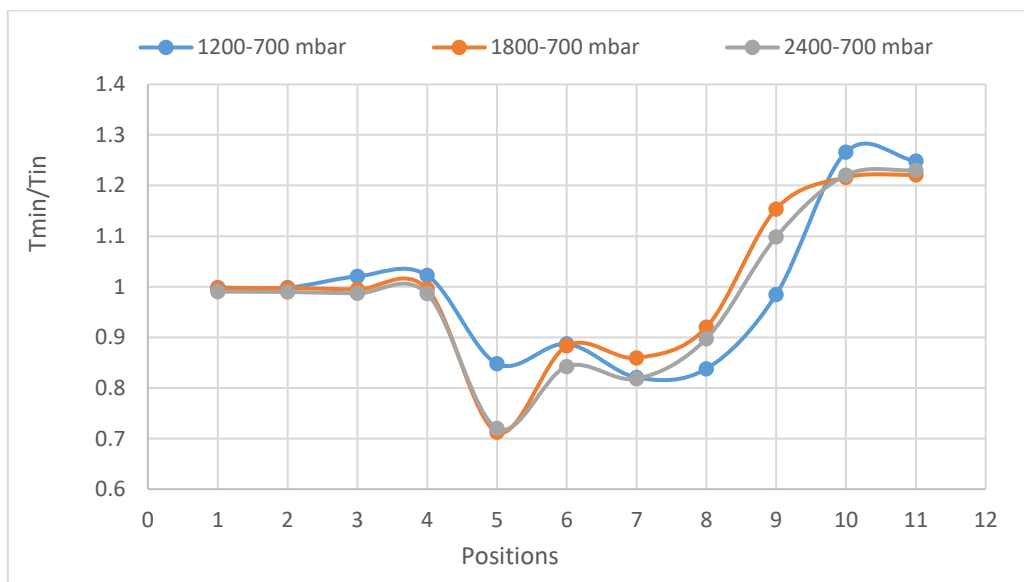


Figure 4.60: The distribution and the variation of minimum temperature at a discharge pressure of 700 millibars and under different rotational speeds

#### 4.2.7.4. Effect of the rotational speed on the distribution and characteristics of velocity

The velocity and vector contours for the last revolution of a case study at different time steps obtained through numerical simulation at speed (1200, 1800, and 2400) rev/min are shown below in Figure 4.61. It shows that the pressure difference will affect the distribution of the velocity inside of the positive displacement blower

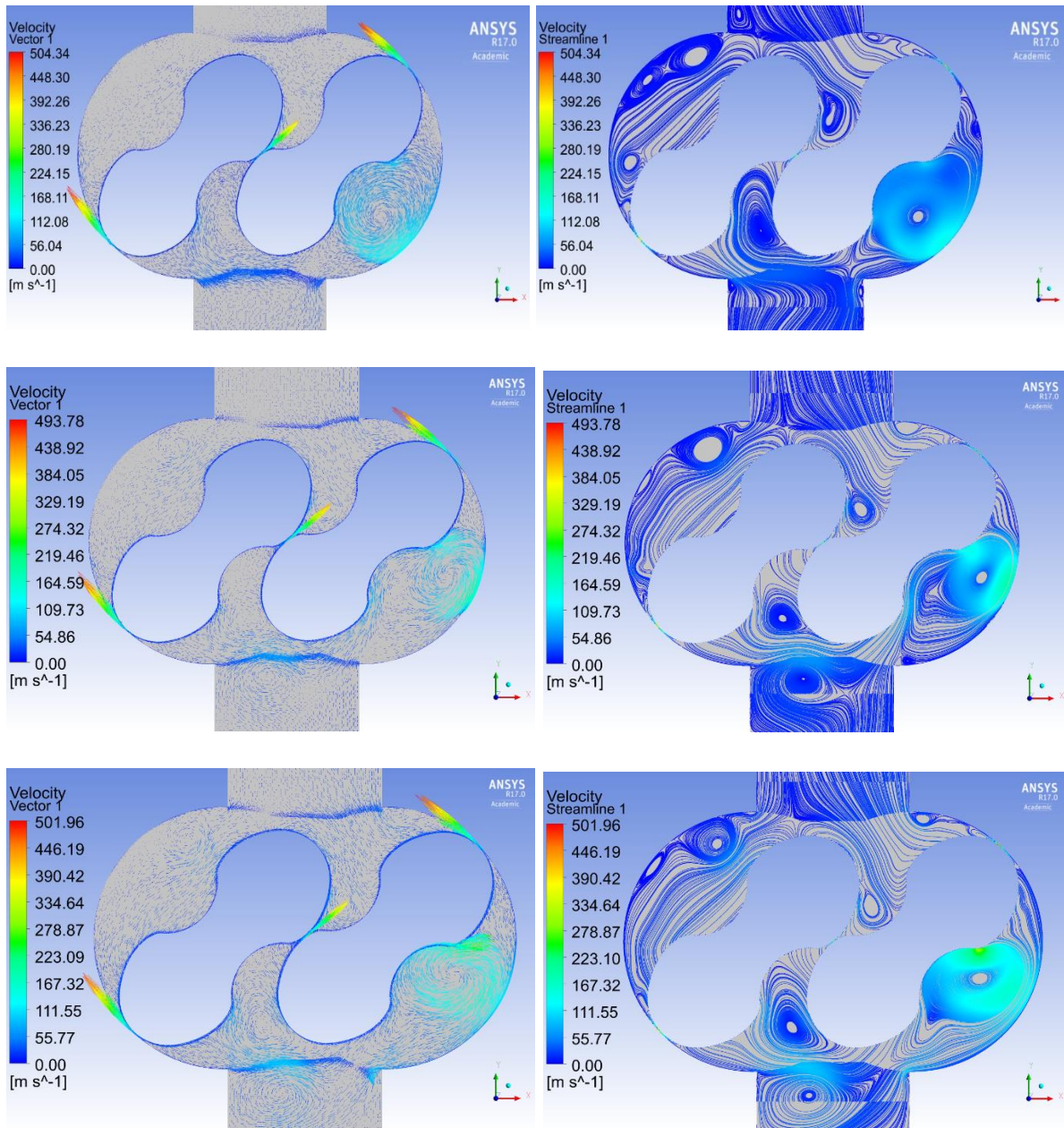


Figure 4.61: The velocity vectors and streamline contours at a pressure difference of 700 millibars, meshing angle of  $45^{\circ}$  and for rotational speeds of (1200, 1800, and 2400) rev/min from up to down respectively.

The high and low velocities are existed in the flow mixing regions as recirculation zones. These zones occur when the rotors sudden cross the edges of the suction or the discharge zones which the core of these areas consists of the low velocity. Figure 4.61 shows the two rotors formed two chambers; some recirculation zones occurred near the inlet region and other at the outlet region. It can be seen from this figure that the location and the shape of recirculation zones are changing as the rotational speeds changing. Moreover, these recirculation areas of high and low velocities may lead to further vibration and energy losses as rotational speeds increases. Furthermore, the maximum velocities are found inside the clearances and it increases with the increase of rotational speeds as shown in figure 4.61. The rotation role of these recirculation zones results in the vertical velocity component being negative in these areas, with the flow moving in the opposite direction to the outlet. It indicates that the existence of recirculation zones reduces the outlet flow and plays an adverse effect on the flow rate. However, the increase of rotational speed commonly plays a positive effect on the outlet flow which may decrease the influence of backflow. The variation of the internal flow velocity shows that the rotational speed and high pressure at the outlet has a strong influence on the velocity distribution of the whole region within the Roots blower.

Investigations through the use of various statistical features such as the average and maximum value of velocity fluctuations have been used. This is aimed at more in-depth local analysis of the velocity variation and distribution within the blower.

Table 4.15 and figure 4.62 depict that average velocity generally increases with the increase of rotational speed. Also, it can be seen that there is obvious variance of average velocity at a different rotational speed which recorded 51.33 m/s, 55.03 m/s, and 68.24 m/s for rotational speeds of 1200 revs/min, 1800 revs/min, and 2400 revs/min respectively. Also, the average velocity increases from the inlet to outlet of the blower. Moreover, the average velocity after P5 declines slightly between angle  $45^{\circ}$  and angle  $90^{\circ}$  and after that increases until approaching the maximum value at the edges of the discharge zone (P9). Furthermore, after P9, the average velocity declines towards the outlet zone till finally stabilising. (All the angles with respect to the vertical line at the centre of the impeller).

Table 4.15: The distribution and the variation of the average velocity inside the blower from the inlet to the outlet at a pressure difference of 700 millibars and under different rotational speed.

Positions	$V_{ave}$ (m/s) at 1200 rev/min	$V_{ave}$ (m/s) at 1800 rev/min	$V_{ave}$ (m/s) at 2400 rev/min
P1	6.84	8.67	12.44
P2	6.51	9.91	14.19
P3	5.77	10.49	14.12
P4	4.24	5.95	5.94
P5	22.65	30.89	27.11
P6	30.72	29.98	25.05
P7	42.86	37.97	49.37
P8	47.74	50.80	60.35
P9	51.33	55.03	68.24
P10	22.38	30.65	37.77
P11	12.95	26.60	38.32

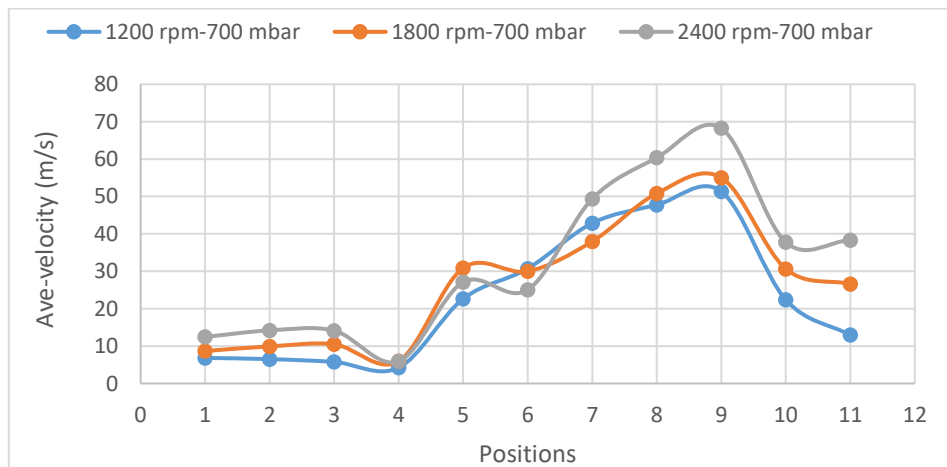


Figure 4.62: The variation of average velocity at 700 millibars pressure difference and different rotational speeds

Table 4.16: The distribution and the variation of the maximum velocity inside the blower from the inlet to the outlet at a pressure difference of 700 millibars and under different rotational speed.

Positions	$V_{\max}$ (m/s) at 1200 rev/min	$V_{\max}$ (m/s) at 1800 rev/min	$V_{\max}$ (m/s) at 2400 rev/min
P1	8.26	10.67	18.76
P2	10.70	16.46	25.28
P3	54.43	57.19	24.93
P4	37.40	31.86	21.41
P5	503.64	528.90	504.75
P6	460.19	449.87	422.42
P7	504.68	470.74	459.53
P8	430.49	462.01	433.27
P9	258.71	266.54	260.76
P10	42.06	67.05	82.94
P11	21.93	41.73	63.73

Table 4.16 and figure 4.63 illustrate that there are apparent differences in the maximum velocity. It can be observed that the maximum velocity increases as rotational speed increases which recorded 504.68 m/s, 528.91 m/s, 504.75 m/s for rotational speeds of 1200 revs/min, 1800 revs/min, and 2400 revs/min respectively. Also, it can be seen in this figure that the maximum velocity increase from the inlet to outlet until it approaches the maximum value, when the tip of the impeller is approximately at the angle of  $(45^{\circ})$  with respect to the vertical line at the centre of the impeller (P5), the maximum velocity after that declines and rises slightly when the tip is in between  $45^{\circ}$  and  $135^{\circ}$  angles with respect to the vertical line at the centre of the impeller in the blower. However, the maximum velocity after angle  $135^{\circ}$  (P7) decreases towards the outlet zone until stabilising.

On the other hand, the velocity varies rapidly with the change of angle. According to the comparison between the different positions of rotors meshing angle, it is found that the fluctuation of velocity repeats itself every  $90^{\circ}$  angles with respect to the vertical line at the centre of the impeller in the blower. Also, the high and the low values of velocity start at about

$6^0$  - $9^0$  angles with respect to the vertical line at the centre of the impeller in the blower as shown in figure 4.63.

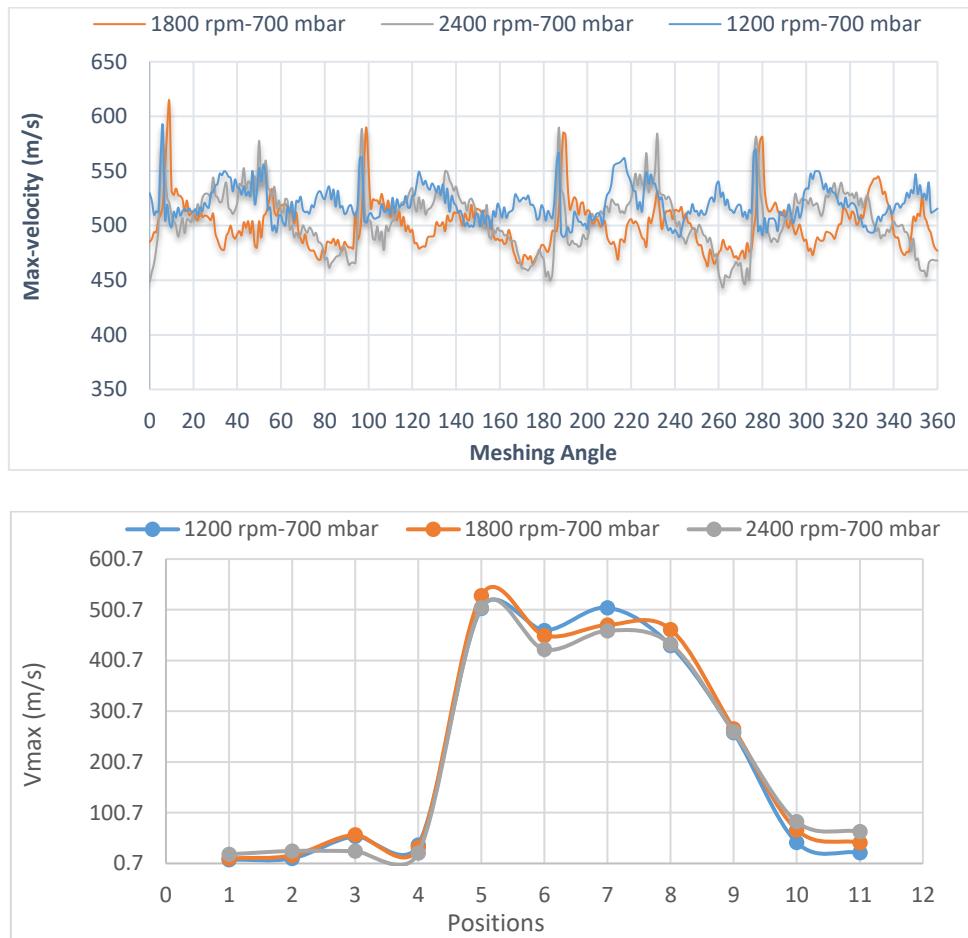


Figure 4.63: The distribution and the variety of maximum velocity at 700 millibars pressure difference and different rotational speeds

Furthermore, according to previous analysis, concerning the velocity variations in the blower, the results have presented that rotational speed has a considerable influence on variation and distribution of the velocity which the average and the maximum velocities increase as rotational speed increase.

The physical significance of the velocity in the blower that any increase of the velocity above the acceptable level will affect the reliability and performance of the blower which may lead to increase of vibration and noise in the blower system. Also, an extreme increase of velocity may affect the foundation of the blower system which may lead to failure of the blower system. Moreover, the rotational speed is one of the main factors affect the velocity, any increase of rotational speed above the acceptable level will lead to extreme velocity within the blower.

#### 4.2.8 Conclusion summary

According to the previous in-depth analysis regarding the effect of pressure difference and rotational speed on the flow field in Roots blower. It can be concluded that both rotational speed and pressure difference have a significant influence on the variation and the distribution of the pressure, the temperature, mass flow rate, and velocity. It can be concluded that:

- The mass delivery, specific power and efficiencies decrease with the increase of pressure ratio because the high levels of pressure ratios increase the gas leakage which declines the volumetric efficiency.
- The result depicts that increasing the rotational speed will improve the volumetric efficiency.
- The losses dependence on rotational speed and pressure ratio
- The volumetric and adiabatic-efficiency characteristics are influenced by the internal leakage which increases with the increase of the pressure ratio and also decreases of rotational speed.
- The pressure is gradually increased from the inlet area to the outlet area of the blower. Also, the lower pressure occurs inside clearances at the inlet side of the impeller.
- The pressure and their amplitude of fluctuation in the discharge zone are higher than that in the suction zone and it increases as the pressure difference increase. Also, the behaviour of pressure fluctuations is repeated every  $90^0$  degrees. Moreover, the maximum positive and negative pressures and their amplitudes are increase with the increase of pressure difference.
- The average mass flow rate declines as the pressure difference increase, because flow leakage increases with increases of pressure difference. Also, the amplitude of mass flow at the blower suction grows up as the pressure difference decreases (velocity increase), meanwhile the amplitude of mass flow at the blower discharge rises with the increase of pressure difference (backflow velocity increase).
- The temperature and their amplitude of fluctuations increase as pressure difference increases. Also, the same behaviour of temperature variation is presented for different pressure loads and for every  $90^0$  degrees of rotation with respect to the vertical line at the centre of the impeller in the blower. Moreover, the maximum temperatures increase and minimum temperature decrease as pressure difference rise.

- The average and the maximum velocities increase as pressure difference increase. Also, the fluctuation of velocity repeats itself every  $90^{\circ}$  angles with respect to the vertical line at the centre of the impeller in the blower.
- There are apparent differences in the variation and the distribution of static pressure as rotational speed increase. Also, the pressure and the amplitude of fluctuation in the discharge zone is higher than that in the suction zone and it increases as the rotational speed increase. Moreover, the maximum positive and negative pressures and their amplitudes are increase with the increase of rotational speed.
- The average mass flow rate increase linearly with the increase of the blower rotors speed. Also, the amplitude of mass flow at the blower suction rise as the rotational speed increases, meanwhile the amplitude of mass flow at the discharge of the blower rises with the increase of rotational speed.
- The temperature increase inside the blower with a decrease of rotational speed. Also, the maximum temperature and their amplitude decreases and the minimum temperature decrease as rotational speed increase.
- The average and the maximum velocities increase as rotational speed increase. Moreover, the amplitudes are increased with the increase of rotational speed and are more prominent at outlet zone than an inlet zone.

Furthermore, from the above numerical analysis, it can be seen that with the establishment of a relationship between velocity field, temperature field and pressure field it has been found that the positions of the minimum pressures and minimum temperatures are very close to the locations of maximum velocities as shown below in figure 4.56. Based on above discussion, it can be concluded that the analysis of transient numerical simulation results using the CFD approach with dynamic mesh technique (DMT) can predict an accurate result and provide useful information regarding the flow field and the performance of the Roots blower.

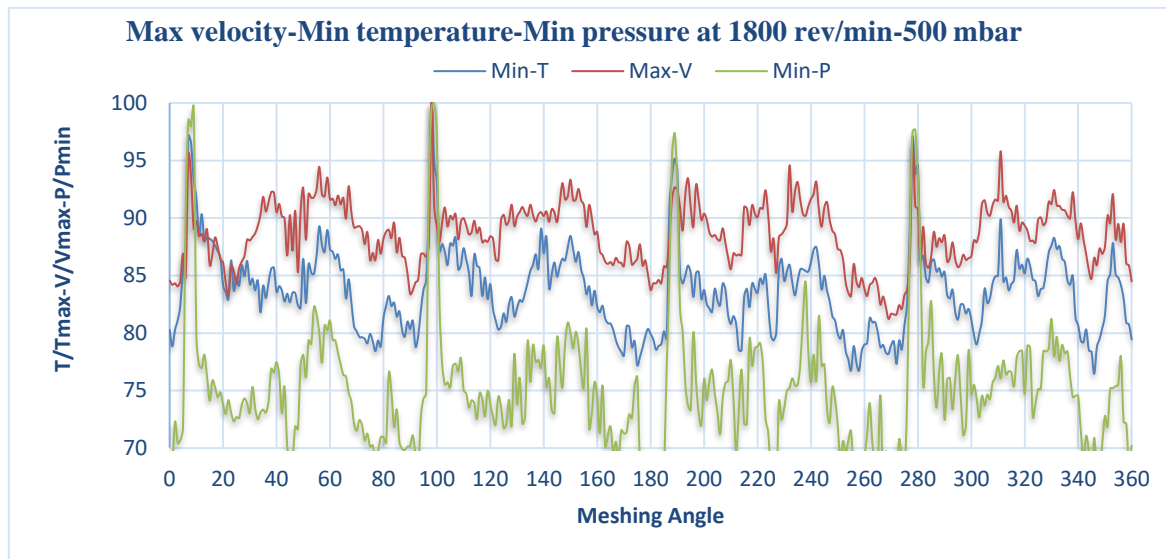


Figure 4.64: The relationship between the velocity field, temperature field and pressure field

The qualitative and the quantitative analysis of the experimental and the numerical results have been conducted in this chapter, regarding the Roots blower performance characterisation. The analysis carried out for in-depth understanding the influence of different operating parameters such as pressure difference and rotational speed on the variation and the distribution of flow-related parameters within Roots blower such as pressure, temperature, and velocity and therefore on Roots blower performance. In addition, the prediction models have been developed for outlet temperature, mass flow rate, efficacy, and power which dictate the design process of Roots blower. Moreover, analysis and discussions in detail of the influence of different geometrical parameters on flow field behaviour and blower performance will be included in the next chapter.

## **Chapter 5**

### **Quantitative evaluation of Roots blower performance undergoing geometrical changes**

The flow working domain of a Roots blower is complex because it continuously deforms during each rotation of the two rotors. Therefore, it is difficult to understand the physical phenomena occurring in such a domain. The most reliable information about physical phenomena is usually obtained by experiment. However, using the experimental investigation to study the flow characteristics and their behaviour inside the blower through different geometric parameters might be time-consuming and expensive because of various limitations and difficulties in measurements.

The computational fluid dynamics (CFD) codes have been developed to become an effective and applicable approach for flow field investigations. In comparison with the experimental measurement that may be required in the majority of engineering applications, CFD techniques generally provide all related flow information of the domain under investigation, which often cannot be achieved by experimental procedures due to the limitations related to equipment of measurement. Therefore, a numerical investigation using CFD techniques to study and analyse the influence of different geometrical parameters on flow field behaviour and on blower performance will be presented in the next sections.

The result obtained from CFD simulations that have been conducted for different Roots blower models with different clearance sizes which have been summarised in chapter 3, are presented in this chapter. In order for more in-depth understanding of the internal flow behaviour and the complex flow structure within a Roots blower, a qualitative and a quantitative analysis have been conducted using geometrical variations. The effect of various geometric parameters on the Roots blower system performance has been examined under different rotational speeds and pressure loading conditions. Moreover, pressure fluctuations in both time and frequency domain, at chosen points inside the blower, have been investigated and analysed. Furthermore, semi-empirical expressions have been developed as a function of the geometrical parameters and operating conditions to predict some performance factors of the Roots blower.

## 5.1 Roots blower geometrical models

The geometrical models of Roots blower have been used in this chapter with their specifications are summarised in Table 5.1. The operating speeds have been used in these models are (1200, 1800 and 2400) rev/min. Also, the pressure differences are (300, 5000, 700). These models with their specifications and operating condition are presented in detail earlier in chapter 3. All specifications that are not mentioned in the table below are the same as in the baseline Roots blower model.

Table 5.1: Roots blower models specifications.

Casing-Rotor gap or Tip clearance (TC) models	Rotor radius (mm)	Rotor waist (mm)	Tip clearance (TC) (mm)	Centre clearance (CC) (mm)
Model TC1	123.681	56.7	0.22	0.34
Model TC2 (Baseline model)	123.66	56.7	0.24	0.34
Model TC3	123.641	56.7	0.26	0.34
Rotor-Rotor gap models Centre clearance (CC)	Rotor radius (mm)	Rotor waist (mm)	Tip clearance (TC) (mm)	Centre clearance (CC) (mm)
Model CC1	123.66	56.726	0.24	0.3
Model CC2 (Baseline model)	123.66	56.7	0.24	0.34
Model CC3	123.66	56.683	0.24	0.38

## 5.2 Effect of Geometrical Parameters

The characteristics of internal flow and the performance of the Roots blower under different operation conditions have been investigated and analysed in the previous chapter. It can be concluded that there are different operational conditions considerably have influences on the distribution and the behaviour of the flow field and therefore the performance of the blower. For additional analysis, the 2D/3D Roots blower models considered in the present study have been analysed with different clearance sizes, because the size of clearance play an important role in the performance of the Roots blower. The main objective of this investigation is to carry out extensive numerical calculations using advanced CFD code in order to determine and study the effect of some geometrical parameters such as the rotor profile, rotor diameter, and clearance size on the characteristic of the blower performance under different conditions.

The Roots blower model considered in the current study has been analysed with a different shape of impeller profiles, rotor diameters and clearances. The subsequent sections will illustrate the influence of rotor profile, rotor diameter and clearance change on the Roots blower's performance characteristics comprehensively.

One of the most critical factors, which have significant effects on the Roots blower performance characteristics is the profile of the blower rotor. In order to estimate the optimum profile of the impeller, many studies have been conducted (Hsieh & Hwang, 2007, 2008; Hwang & Hsieh, 2006; Kun, Dechun, Zhenhou, Guangyu, & Naiheng, 2007; Litvin & Feng, 1996; H.-C. Liu, Tong, & Yang, 2000; Mimmi & Pennacchi, 1997; Niimura, Kikuta, & Usui, 1990; Tong & Yang, 2005; Wang, Fong, & Fang, 2002; Yang & Tong, 2002; Yao, Ye, Dai, & Cai, 2005).

The majority of these studies have been shown that there is no optimum profile yet, but depending on which the essential parameter in the application, for example, mass flow rate, differential pressure or noise. In the present study, the profile of the rotor in the baseline model of Roots blower has been modified. The modifications have been done by stretching and contracting of both rotors in the impeller diameter direction to decrease and increase the tip clearance respectively. Also, to decrease and increase the centre clearance, stretch and contraction of the two rotors have been done in rotor waist direction as illustrated in figure 5.1. Therefore, the effect of the rotor profile on the Roots blower performance characteristics will be included with clearance effect investigations in the next sections.

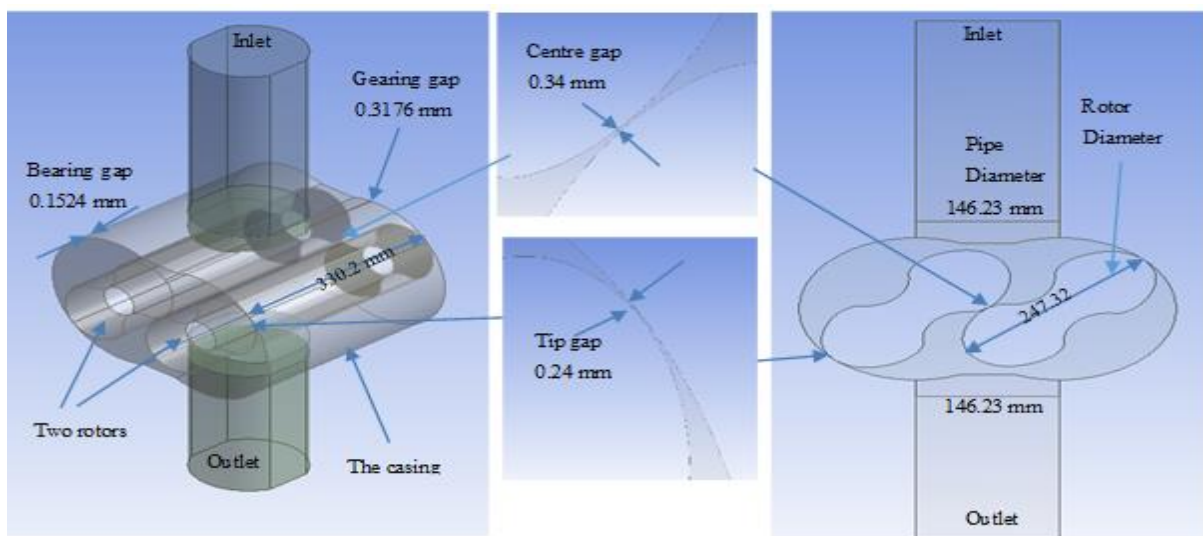


Figure 5.1: The 3D/2D geometry of Roots blower model

### **5.3 Effect of the clearance size on the performance of Roots blower**

The literature review revealed that material interferences may occur between different parts of Roots blower during the process of operation, because of high rotational speed of blower impellers (Burmistrov et al., 2015; Houzeaux & Codina, 2007; Mimmi & Pennacchi, 1999). Therefore, appropriate sizes of clearances must be provided between these parts to avoid such interferences. Consequently, the drop in the volumetric efficiency of the blower may arise. The phenomenon of local pressure losses mentioned in previous chapter in this study could explain this drop. The backflow has been found at the clearances inside the blower, and thus this is one of the reasons causing a pressure loss that affects the performance of the blower.

The following section of this chapter will illustrate the effect of the rotor diameter and hence clearance on the performance of Roots blower. It has been conducted based on numerical results obtained from the different configurations. Based on 2-D CFD model for a chosen set of boundary conditions, the detailed numerical results regarding speed, temperature, pressure, and the velocity have been analysed and described. Five revolutions have been simulated to ensure the simulation of the case reached the stable state. In the following, the contours for the last working period will be visually analysed to explain these differences.

### **5.4 Establish the effect of the gap between the rotor and the casing (Tip clearance) on the Roots blower performance**

As discussed in the previous chapter, the backflow through the gap between rotor and casing plays an essential role in pressure loss in the blower. It is apparent that the adjustment of the clearances could enhance the performance of the blower. In a study on lobe pump, Prakash et al proved that an increase in the clearance width could cause an unexpected decrease in the pump efficiency. The efficiency declines to about 43% when the clearance width is 2.0mm and as low as 24% for the 4.0mm clearance width in comparison with the 1.0mm clearance width case (Prakash, Stokes, Bertolini, Tatford, & Gomme, 2003). Our research proposes a tip clearance (located between the rotors and the casing) size of 0.24 mm for the blower with an involute profile, and conducts analysis for two other tip clearance sizes 0.22 mm and 0.26 mm for a range of speeds from 1200 rev/min to 2400 rev/min. The numerical analysis is expected

to provide significant results suggesting an explanation about the effect of the finer gap on performance characteristics.

### 5.4.1 Effect of Gap between Rotor and Casing on pressure distributions

The instantaneous pressure field on middle plane of the blower for the last revolution of a case study at different angles obtained through numerical simulation at a speed 2400 rev/min, a pressure difference 700 millibars and for clearances of 0.22 mm, 0.24 mm (baseline model), and 0.26 mm are shown in Figure 5.2.

Figure 5.2 presents the variation and the distribution of the static pressure. It is apparent that the pressure is gradually increased from the inlet zone towards the outlet zone within the blower. However, it can be seen from this figure that the lower pressure occurs inside clearances between the low-pressure region at the inlet side and the high-pressure region at the outlet side in the blower. Also, it is noticeable that the distributions of static pressure at same rotational speed and under different clearances have the same trend for all cases under investigation, but the effect of recirculation zones are increased as the tip gap increase.

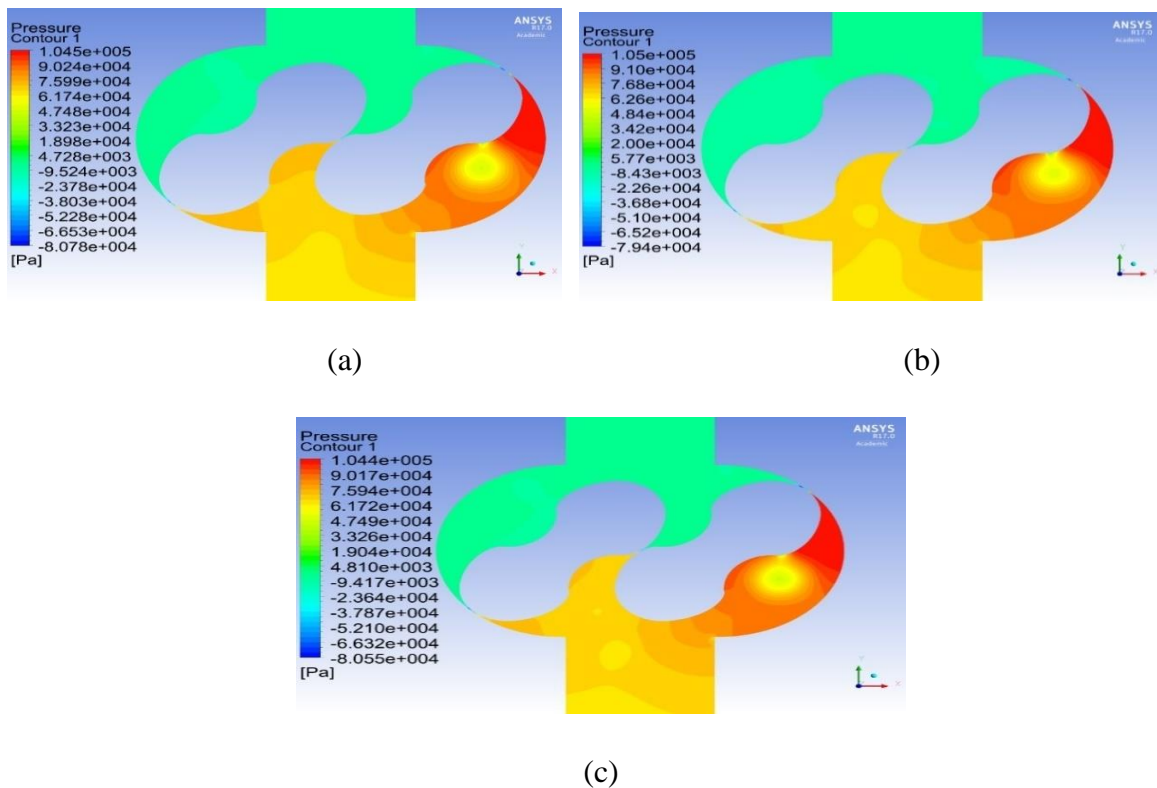


Figure 5.2: The static pressure contours at a speed of 2400 rev/min, a pressure difference of 700 millibars, and for tip clearances of (a) 0.22 mm, (b) 0.24 mm, and (c) 0.26 mm.

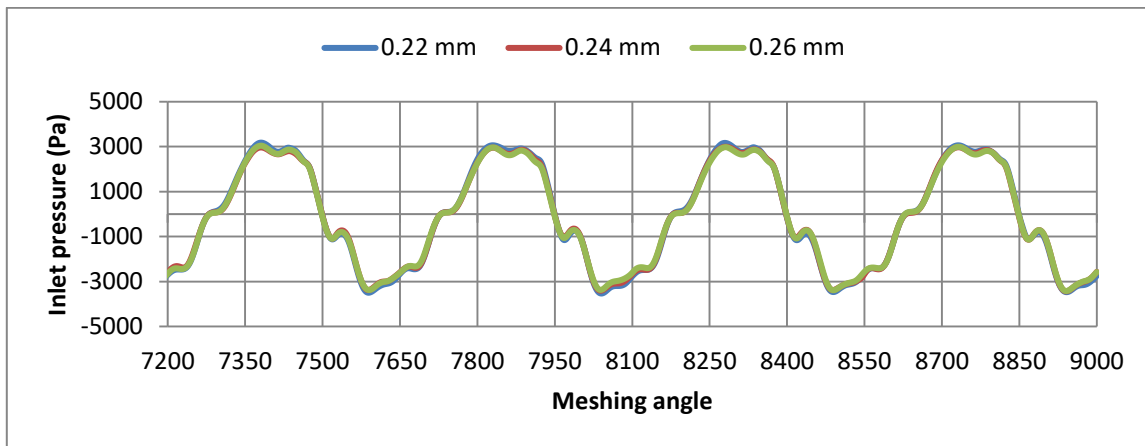


Figure 5.3: Pressure fluctuations at blower inlet at 2400 rev/min, 700 millibars, and for different tip clearances.

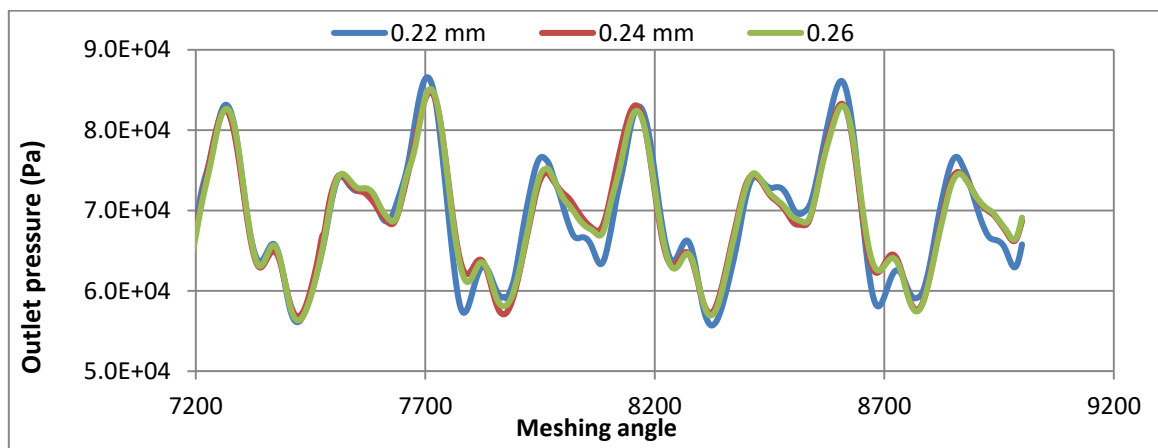


Figure 5.4: Pressure fluctuations at blower outlet at a speed 2400 rev/min, a pressure difference 700 millibars, and for different tip clearances.

Moreover, it can be seen from figures 5.3 and 5.4 that amplitudes and fluctuates of the pressure in outlet zone are higher than that in the inlet zone. These amplitudes and fluctuations increase as tip clearance decreases (diameter increase).

The statistical analysis of the variation and the distribution of the pressure at a speed 2400 rev/min, a discharge pressure 700 millibars, and for different tip clearances inside the blower from the inlet to outlet are presented in Tables 5.2 and 5.3 It can be seen that there is a slight difference of the average, the maximum positive and the maximum negative pressures, which the average pressure decrease as tip clearance decrease and both the maximum positive and the maximum negative pressures rise as tip clearances decrease. Therefore, the pressure losses increase with the decrease of tip clearances.

Table 5.2: The average pressure at a speed 2400 rev/min, a pressure difference 700 millibars, and for different tip clearances.

Positions	$P_{ave}$ at 0.22 mm	$P_{ave}$ at 0.24 mm	$P_{ave}$ at 0.26 mm
P1	-8.71E+01	-8.82E+01	-8.79E+01
P2	-1.26E+02	-1.27E+02	-1.28E+02
P3	-7.39E+02	-7.80E+02	-7.18E+02
P4	-8.18E+02	-7.90E+02	-7.99E+02
P5	6.98E+03	7.26E+03	7.02E+03
P6	2.56E+04	2.57E+04	2.56E+04
P7	4.18E+04	4.15E+04	4.17E+04
P8	5.84E+04	5.85E+04	5.84E+04
P9	6.14E+04	6.09E+04	6.17E+04
P10	6.91E+04	6.92E+04	6.92E+04
P11	6.92E+04	6.94E+04	6.93E+04

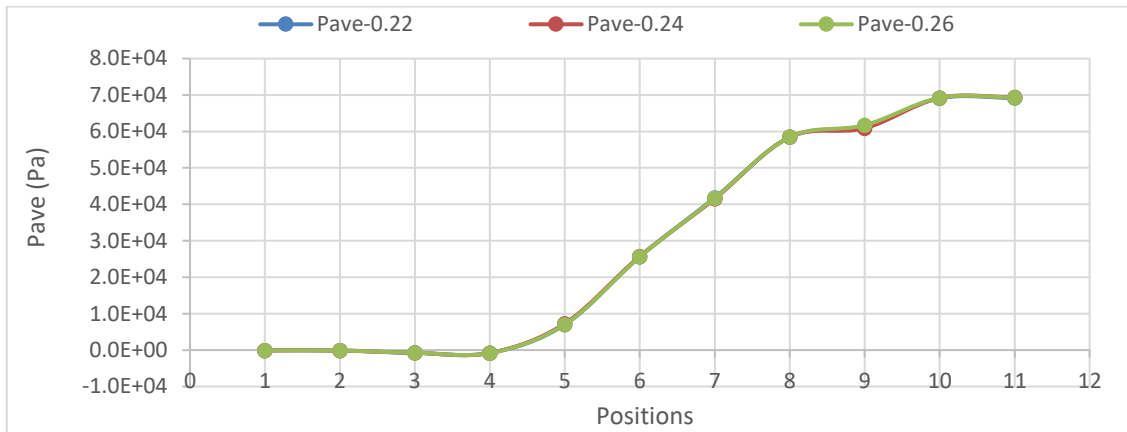


Figure 5.5: The distribution of average-pressures at a speed 2400 rev/min, a pressure difference 700 millibars and for different tip clearances.

The data in table 5.2 and figure 5.5 present that the average pressures are increase gradually from the inlet region until rich the maximum values at the outlet of the blower (P11). The average pressures at the outlet zone are 6.91E+04 Pa, 6.93E+04 Pa, and 6.93E+04 Pa for clearances 0.22 mm, 0.24 mm and 0.26 mm respectively which the average pressure increased as clearance increase (diameter decrease).

Table 5.3: The maximum and the minimum pressure at 2400 rev/min, 700 millibars, and for different tip clearances in Pascal.

Positions	P <sub>max</sub> at 0.22 mm	P <sub>max</sub> at 0.24 mm	P <sub>max</sub> at 0.26 mm	P <sub>min</sub> at 0.22 mm	P <sub>min</sub> at 0.24 mm	P <sub>min</sub> at 0.26 mm
P1	3.18E+03	2.99E+03	3.04E+03	-3.53E+03	-3.43E+03	-3.42E+03
P2	3.52E+03	3.31E+03	3.38E+03	-3.73E+03	-3.63E+03	-3.53E+03
P3	3.40E+03	3.25E+03	3.36E+03	-5.65E+03	-5.34E+03	-5.33E+03
P4	3.41E+03	3.26E+03	3.28E+03	-5.67E+03	-5.33E+03	-5.38E+03
P5	9.04E+04	9.54E+04	9.11E+04	-8.00E+04	-7.74E+04	-7.78E+04
P6	1.03E+05	1.06E+05	1.03E+05	-6.99E+04	-6.94E+04	-6.88E+04
P7	9.52E+04	9.39E+04	9.45E+04	-7.51E+04	-7.09E+04	-7.43E+04
P8	9.05E+04	8.74E+04	8.78E+04	-6.27E+04	-6.25E+04	-6.24E+04
P9	8.95E+04	8.67E+04	8.70E+04	-7.89E+03	-1.25E+04	-5.71E+03
P10	8.66E+04	8.49E+04	8.53E+04	5.54E+04	5.63E+04	5.57E+04
P11	8.66E+04	8.47E+04	8.51E+04	5.57E+04	5.68E+04	5.63E+04

The data in table 5.3 and figure 5.6 show that the maximum pressures are found in the outlet zone at point 6 (P6) which are 1.03e+05 Pa for clearance 0.22 mm, 1.05E+05 Pa for clearance 0.24 mm and 1.03E+05 Pa for clearance 0.26 mm respectively. The reason for that because these points are very close to the outlet zone which is affected by the high pressure and backflow in this region, which the maximum pressure increased as clearance decrease (diameter increase).

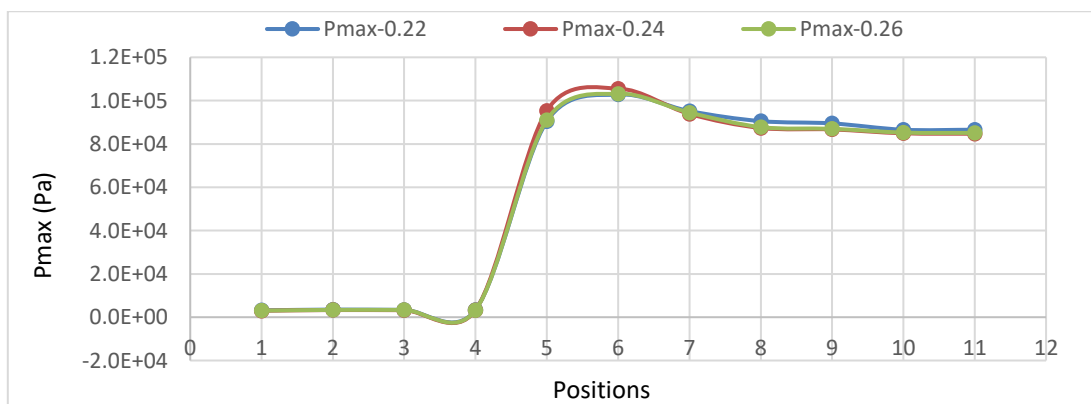


Figure 5.6: The distribution of maximum-pressure at 2400 rev/min, a pressure difference 700 millibars and for different tip clearances.

The data in table 5.3 and figure 5.7 illustrate that the maximum negative pressures are found inside the clearances in the inlet zone at point 5 (P5) which are  $-8.00E+04$  Pa for clearance 0.22 mm,  $-7.74E+04$  Pa for clearance 0.24 mm and  $-7.78E+04$  Pa for clearance 0.26 mm respectively. The reason for that because these points are very close to the outlet zone which is affected by the high pressure and backflow in this region, which the maximum negative pressure increased as clearance decrease (diameter increase).

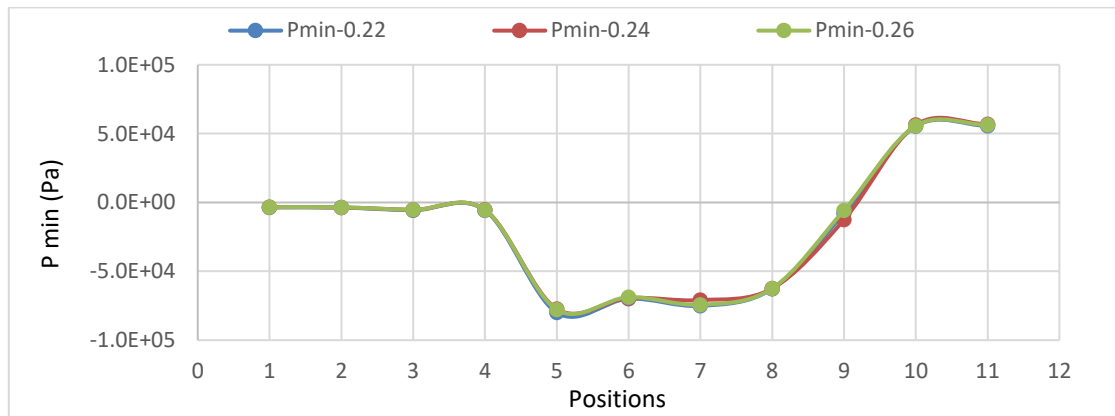


Figure 5.7: The distribution of maximum negative pressures at a speed 2400 rev/min, a pressure difference 700 millibars and for different tip clearances.

Root mean square (RMS) refers to the arithmetic mean of the squares of a set of numbers. RMS is a meaningful way of calculating the average of values over a period of time. Figure 5.8 expresses the relation between effective pressure zones and RMS. It can be seen that the RMS increases from the inlet to outlet of the blower, which the maximum values are recorded at the discharge zones. Also, these values rise with a decrease of tip clearance.

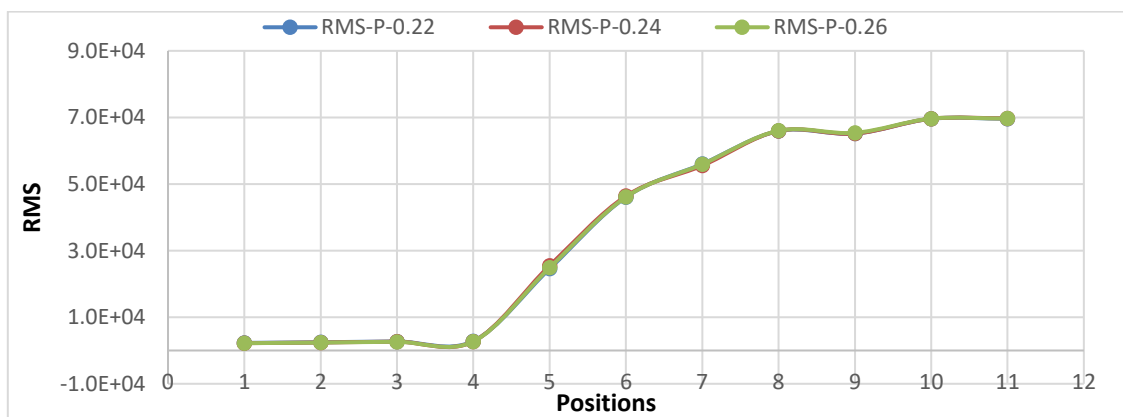


Figure 5.8: Root Mean Square (RMS) of effective pressure zones at 1800 rev/min and different pressure difference.

The peak to peak amplitudes ( $A$  (pk-pk)) is the difference between the maximum positive and the maximum negative amplitudes of a waveform) are presented in Figures 5.9. It is clear to conclude that there is a small difference of amplitude at different tip clearances under the same rotational speed and same pressure, which starts to increase from inlet until approach the maximum values at about  $45^{\circ}$  angle of degrees (point 5) and after that, it declines. Also, it can be seen that the amplitudes are decreased with the increase of tip clearances and are bigger at the outlet zone than an inlet zone because the pressure and their fluctuations are higher in this area.

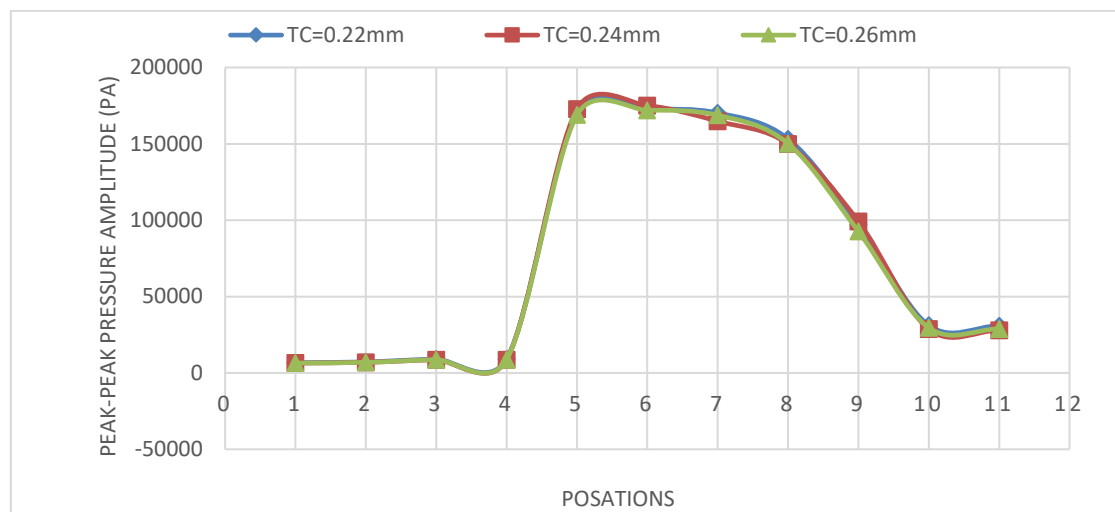


Figure 5.9: The peak-peak amplitudes at a speed 2400 rev/min, a pressure difference 700 millibars and for different tip gaps

The result shows that when the blower operates at small tip clearance, the pressure decreases in the clearances within the blower at the inlet chamber causing the velocity to increase. It develops further the backflow leads to the decline of flow rate. On the other hand, the high velocity inside the small gap will force the flow to move from inlet to outlet which finally leads to an increase in flow rate.

Furthermore, according to previous analysis, concerning the pressure variations in the blower, the outcomes have presented that clearance has a considerable influence on variation and distribution of the pressure which the average pressure is mostly remaining the same, the maximum negative pressures mostly decrease as rotor diameter decreases or tip clearance

increases. However, the maximum positive pressures mostly increase as rotor diameter decreases or tip clearance increases as shown in figure 5.10.

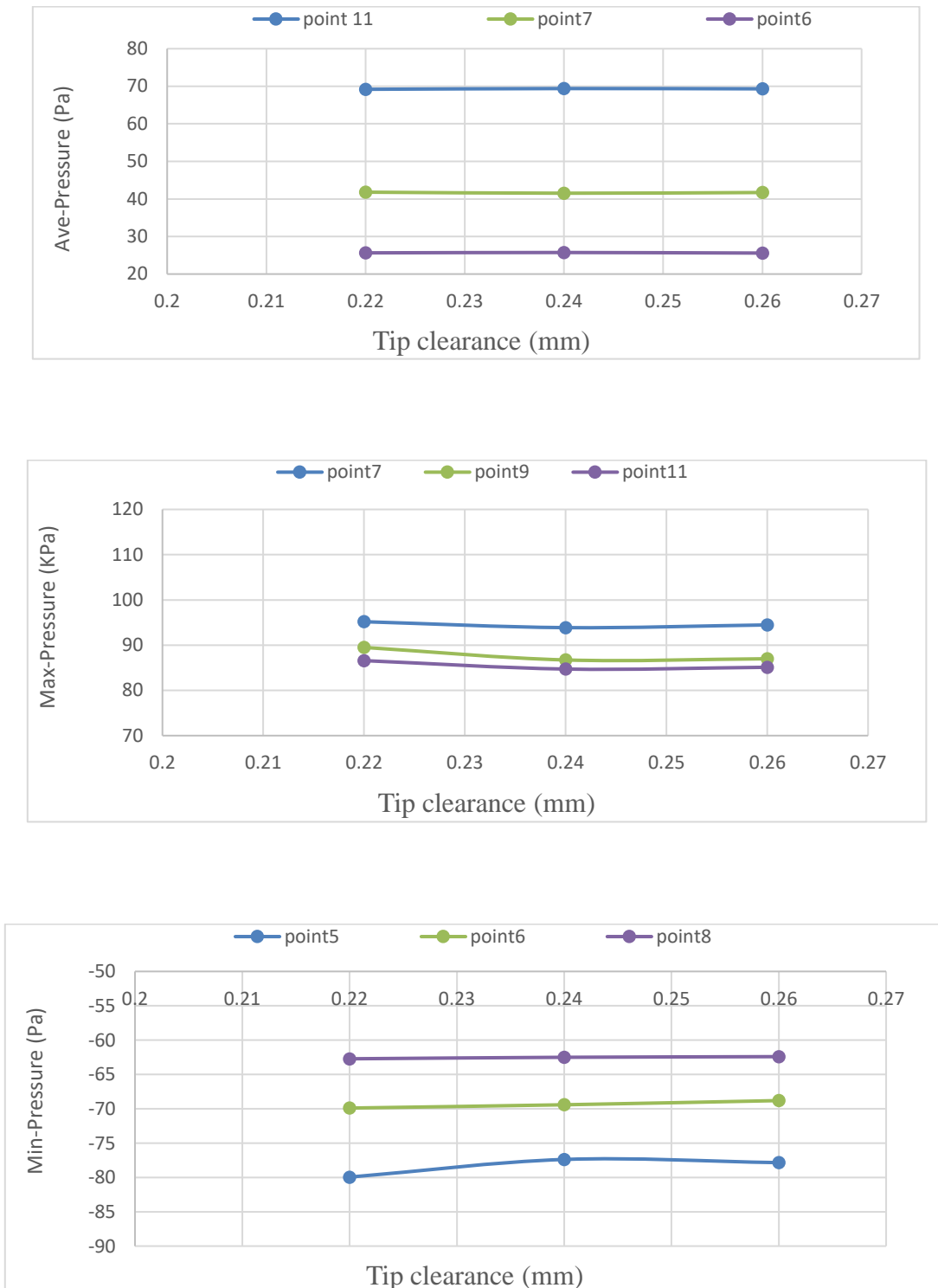


Figure 5.10: the relation between the impeller diameter and tip clearance with the pressure variation in the blower

### 5.4.2 The Effect of clearance between rotor and casing on the mass flow rate

The average mass flow rate for the last revolution of case study obtained through numerical simulation at a speed 2400 rev/min, a pressure difference 700 millibars, and for different tip clearances are shown below in Figure 5.11. It can be concluded that there is a small difference in the average mass flow rate, which declines as the tip gap increase. So it is because the smaller gap can result in a higher velocity of the medium, which will lead to more resist of the leakage in the gap and therefore increase the actual flow rate and volumetric efficiency of the Roots blower.

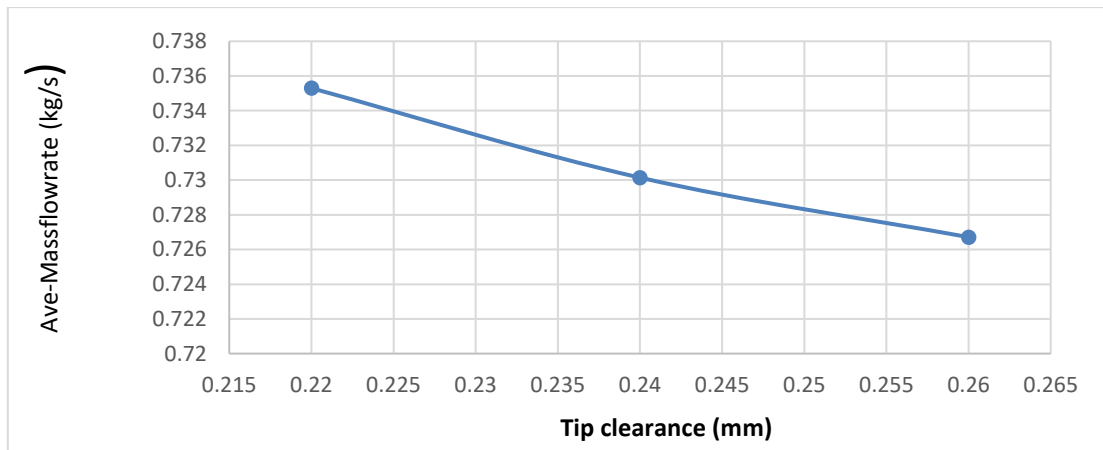


Figure 5.11: The average mass flow rate at speed 2400 rev/min, pressure differences 700 millibars, and different tip clearances.

The flow rate pulsation is usually defined by relative amplitude of flow fluctuation or the coefficient of flow rate fluctuation  $M_F$ , which is represented by the Equation (4.18). This can be used as a performance index associated with the vibration and the noise, as defined in [23]:

The fluctuations of mass flow rate for the last revolution of case study obtained through numerical simulations at a speed 1800 rev/min and for pressure differences of (300, 500, and 700) millibars are shown below in Figure 5.12 and 5.13. It can be concluded that the amplitude of mass flow at the blower suction grows up as the pressure difference decreases, meanwhile, the amplitude of mass flow at the blower discharge rises with the increase of pressure difference. This phenomenon is apparent in figure 5.14, which illustrates the mass flow rate fluctuation coefficient ( $M_F$ ) at both the inlet and the outlet of the blower

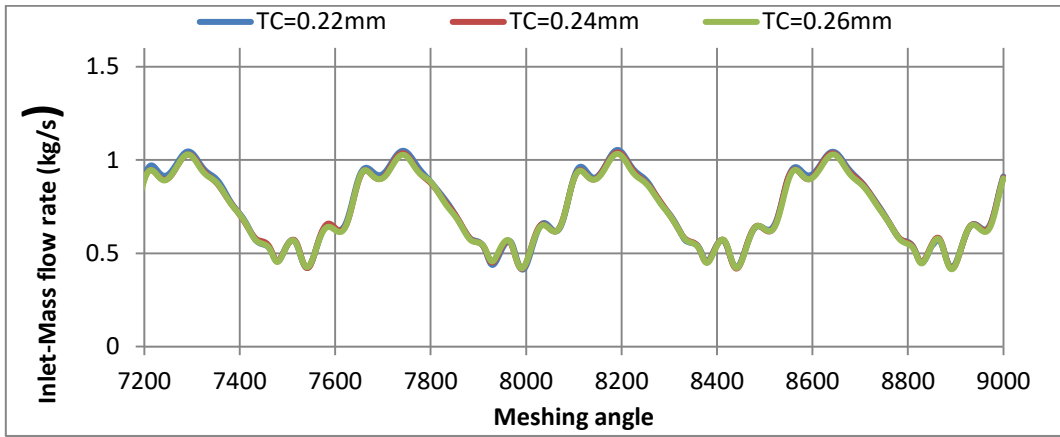


Figure 5.12: Mass flow rate fluctuation at 2400 rev/min, 700 mbars and different tip gaps at the inlet

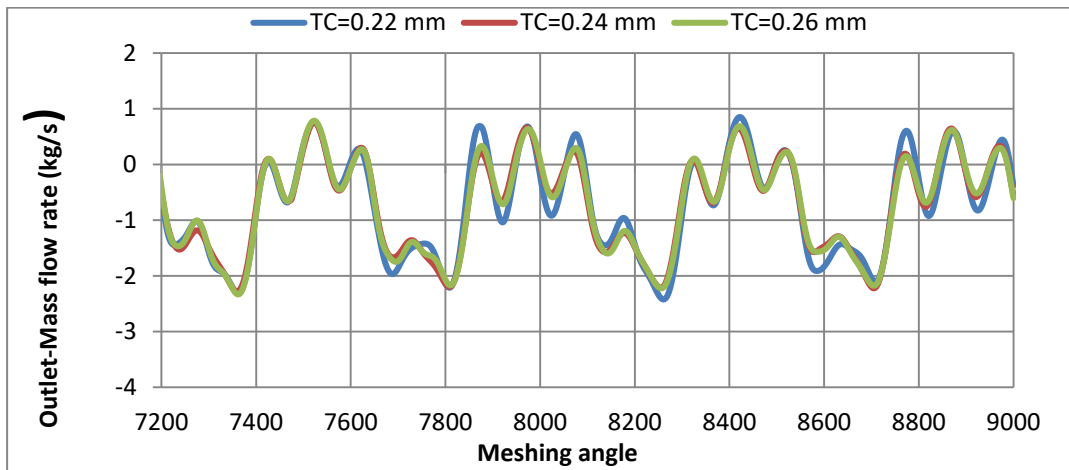


Figure 5.13: Mass flow rate fluctuation at 2400 rev/min, 700 millibars and for different tip gaps at inlet and outlet.

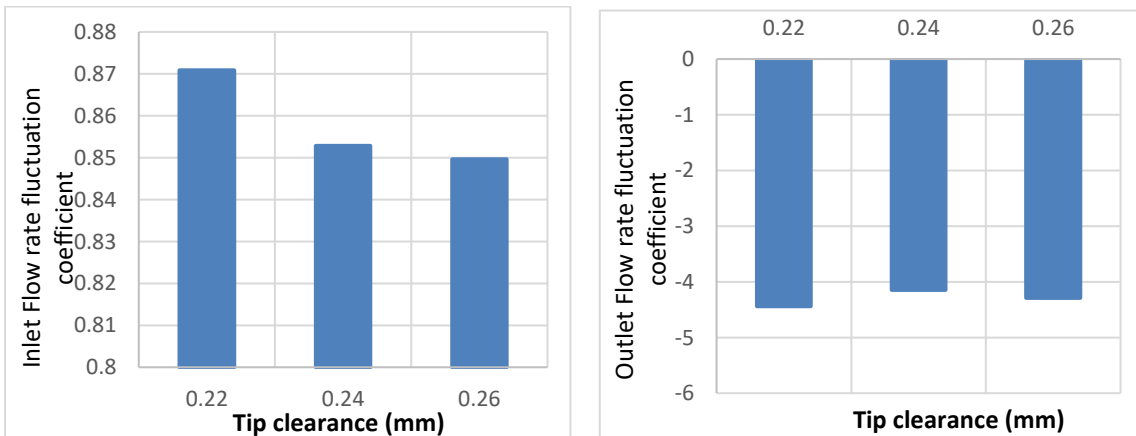


Figure 5.14: Mass flow rate fluctuation coefficient ( $M_F$ ) at 2400 rev/min, 700 millibars and for different tip clearances at the inlet (left) and the outlet (right) of the blower.

### 5.4.3 Effect of clearance between rotor and casing on temperature distributions

The temperature contours for the last revolution of a case study obtained through numerical simulations at a speed 2400 rev/min, a pressure difference 700 millibars and for different tip gaps from left to right respectively are shown in Figure 5.15.

Figure. 5.15 represents the effect of unsteady flow on temperature distribution and the location of the high-temperature area in the Roots blower. It is obvious to conclude that the distribution of temperature is non-uniform and the position of high-temperatures are close to rotor wall and casing wall at the outlet zone. Also, there is a big high- temperature recirculation area which changing their shape as rotors rotating and tip clearance change. Moreover, the temperature increase inside the blower with an increase of tip clearance and as a result of backflow effect.

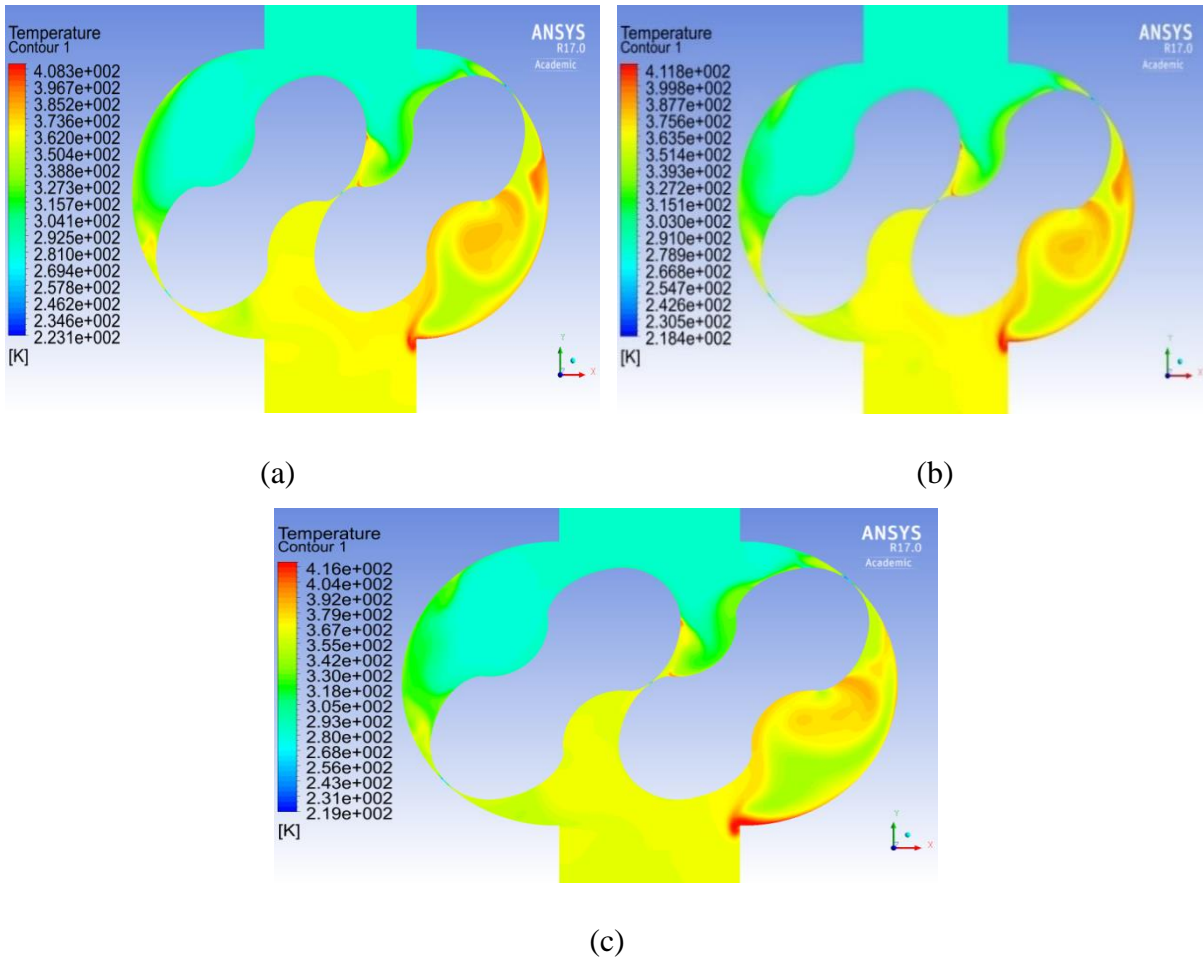


Figure 5.15: The temperature contours and distribution for the last revolution and at 45° rotation degrees, 2400 rev/min, a difference pressure 700 millibars, and for tip gaps of (a) 0.22 mm, (b) 0.24 mm, and (c) 0.26 mm.

The variation of outlet temperature with the rotation angle for the last rotation is shown in Figure 5.16 (every full rotation is 1800 because the calculations have been performed every 0.2 degree as mentioned before). It can be seen that the temperature, their amplitude of fluctuations generally rises as tip clearance increases.

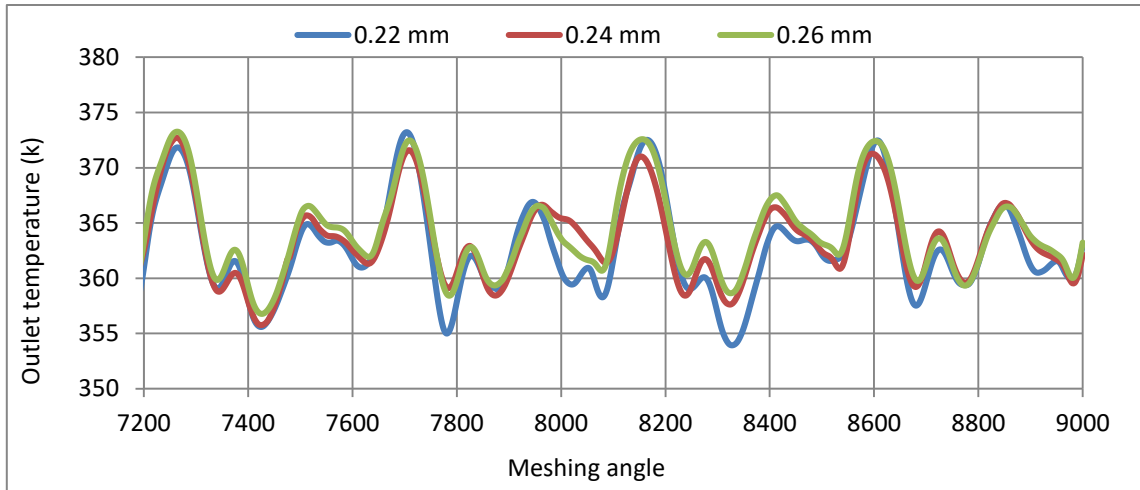


Figure 5.16: Outlet total temperature at 2400 rev/min, different pressure 700 millibars and different tip clearances.

Aim to more depth of local analysis of the temperature variation and distribution within the blower, investigations through the use of different statistical features such as the average, minimum and maximum value of temperature fluctuations have been used.

The statistical analysis of the distribution and the variation of the temperature at a speed 2400 rev/min, a discharge pressure 700 millibars and for different tip gaps inside the blower from the inlet to outlet of the blower are presented in Tables 5.4 and 5.5. It can be seen that there are small variances of the temperature with different tip clearances.

The data in table 5.4 and figure 5.17 show that the average temperatures increase gradually from the inlet to outlet of the blower. Also, it can be seen that the maximum values of the average temperatures are found at the outlet of the blower which are 362.25 K<sup>0</sup> for clearance 0.22 mm, 363.390 K<sup>0</sup> for clearance 0.24 mm and 363.70 K<sup>0</sup> for clearance 0.26 mm respectively. The reason for that because these points are very close to the outlet zone which affected by high pressure and backflow in this region. Also, it can be seen that the maximum temperature increases as the clearance increases (diameter decreases).

Table 5.4: The distribution, and the variation of the average temperature at a speed 2400 rev/min, a discharge pressure 700 millibars, and for different tip clearances.

Positions	$T_{ave}$ (K <sup>0</sup> ) at 0.22 mm	$T_{ave}$ (K <sup>0</sup> ) at 0.24 mm	$T_{ave}$ (K <sup>0</sup> ) at 0.26 mm
P1	288.0	288.07	288.07
P2	288.04	288.04	288.05
P3	287.89	287.98	287.90
P4	287.94	287.91	287.92
P5	333.03	328.82	331.26
P6	339.30	340.11	341.16
P7	352.17	354.88	351.15
P8	360.27	360.65	359.31
P9	358.37	359.30	357.76
P10	362.25	363.39	363.70
P11	361.89	362.68	363.32

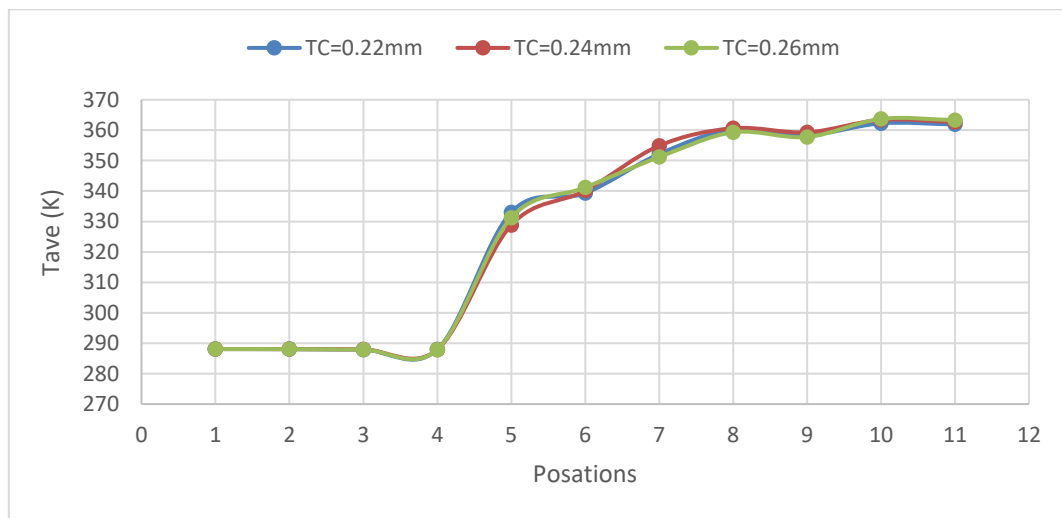


Figure 5.17: The distribution and the variation of average temperature at 2400 rev/min, 700 millibars pressure load and different tip clearances.

The data in table 5.5 and figure 5.19 show that the maximum temperatures are found at point 8 which are 414.96 K<sup>0</sup> for clearance 0.22 mm, 420.32 K<sup>0</sup> for clearance 0.24 mm and 422.59 K<sup>0</sup> for clearance 0.26 mm respectively. The reason for that because these points are very close to

the outlet zone which affected by high pressure and backflow in this region. Also, it can be seen that the maximum temperature increases as the clearance increases (diameter decreases).

Table 5.5: The distribution, and the variation of the maximum and the minimum temperatures at a speed 2400 rev/min, a discharge pressure 700 millibars, and for different tip clearances.

Positions	$T_{\max}$ (K <sup>0</sup> ) at 0.22 mm	$T_{\max}$ (K <sup>0</sup> ) at 0.24 mm	$T_{\max}$ (K <sup>0</sup> ) at 0.26 mm	$T_{\min}$ (K <sup>0</sup> ) at 0.22 mm	$T_{\min}$ (K <sup>0</sup> ) at 0.24 mm	$T_{\min}$ (K <sup>0</sup> ) at 0.26 mm
P1	290.71	290.56	288.82	285.26	285.34	287.27
P2	290.98	290.82	288.64	285.10	285.17	286.52
P3	291.30	291.15	289.35	283.79	284.38	286.45
P4	291.82	291.35	289.96	283.78	284.22	286.78
P5	352.40	353.60	354.48	189.74	207.46	211.85
P6	383.39	386.01	389.41	230.16	242.75	237.45
P7	378.79	377.88	401.36	231.53	235.77	224.76
P8	414.95	420.32	422.58	260.54	258.61	254.79
P9	411.64	417.77	419.81	314.58	316.49	327.98
P10	374.66	376.44	375.43	352.45	351.72	349.18
P11	372.15	371.89	374.19	352.59	354.51	349.99

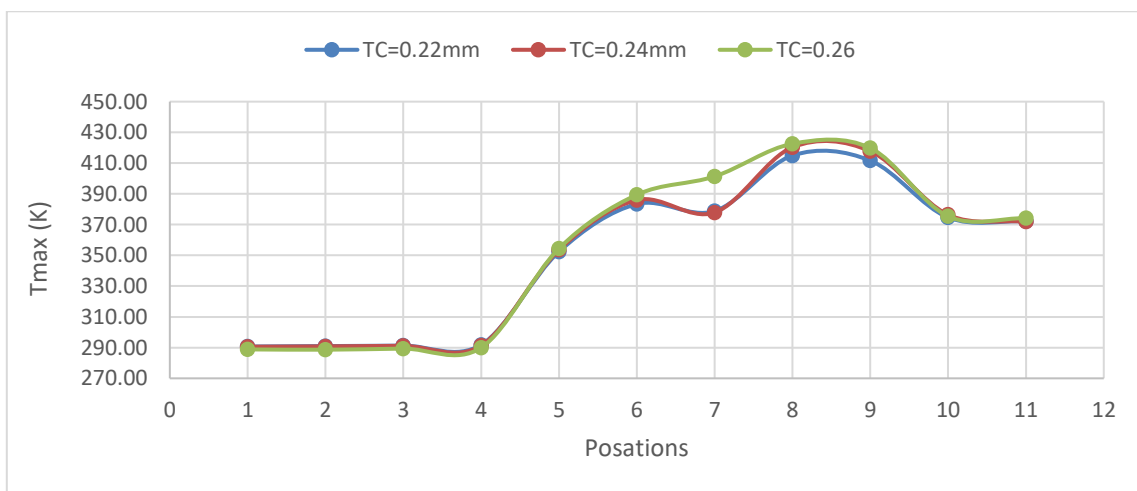


Figure 5.18: The distribution and the variation of maximum temperature at 2400 rev/min, 700 millibars pressure load and for different tip clearances.

On the other hand, there are slight differences in the maximum negative temperature as we can see in figure 5.19 and Table 5.5. Also, it can be seen in this figure that the minimum temperature increase as a tip clearance decreases. Moreover, the minimum temperatures for the cases under investigation are located at point 5 inside the clearance at inlet zone as a result from low pressure and high velocity in the clearances. These temperatures are 189.74 K<sup>0</sup> for clearance 0.22 mm, 207.46 K<sup>0</sup> for clearance 0.24 mm and 211.85 K<sup>0</sup> for clearance 0.26 mm respectively.

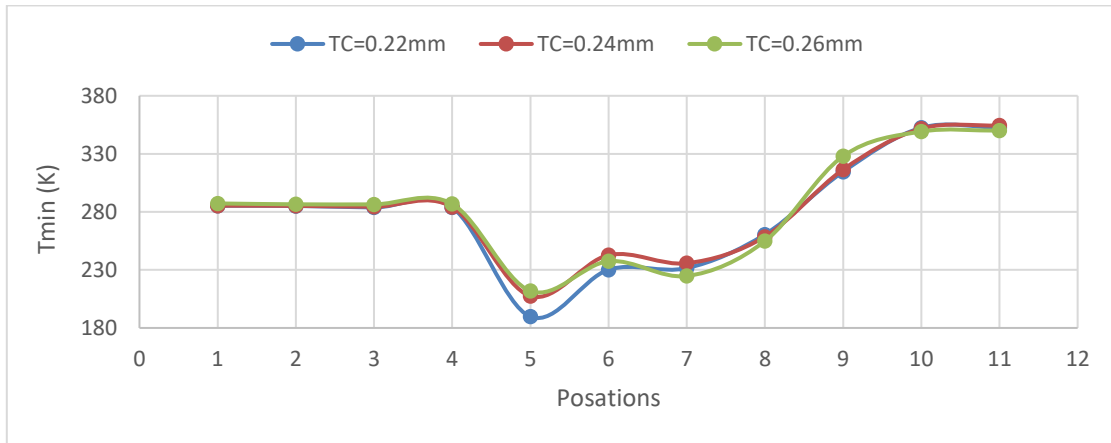


Figure 5.19: The distribution and the variation of maximum negative temperature at 2400 rev/min, a pressure load 700 millibars and for different tip clearances.

Furthermore, according to previous analysis, concerning the temperature variations in the blower, the outcomes have presented that tip clearance difference has a considerable influence on the variation and the distribution of the temperature, which the average temperature, maximum positive and negative temperatures mostly increases as rotor diameter decreases, or tip clearance increases as shown in figure 5.20.

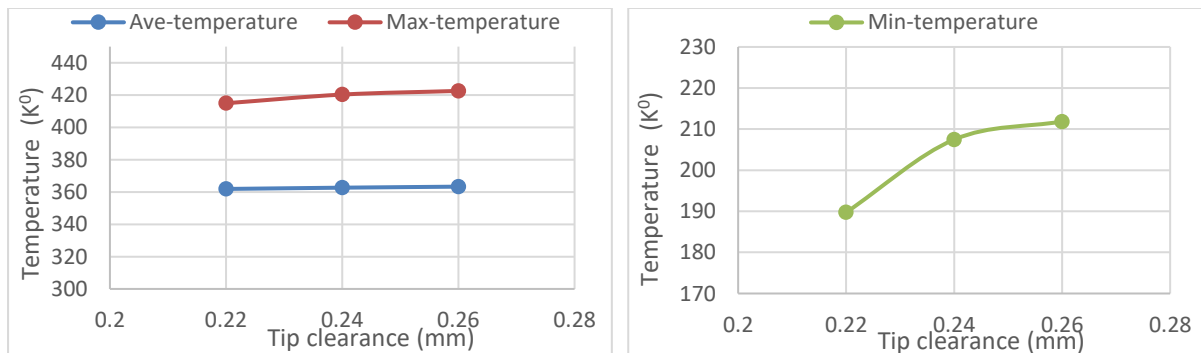


Figure 5.20: The relation between the tip clearance and the maximum and minimum-recorded points of temperature in the blower

#### 5.4.4. Effect of the gap between rotor and casing on velocity distributions

The variation and the distribution of velocity for the last revolution of case study obtained through numerical simulations at a rotational speed 2400 rev/min, a pressure difference 700 millibars, and for tip clearances of 0.22 mm, 0.24 mm (baseline model), and 0.26 mm are shown below in Figure 5.21 as velocity vectors and streamline contours. It shows that the clearance difference will affect the distribution of the velocity inside of the positive displacement blower.

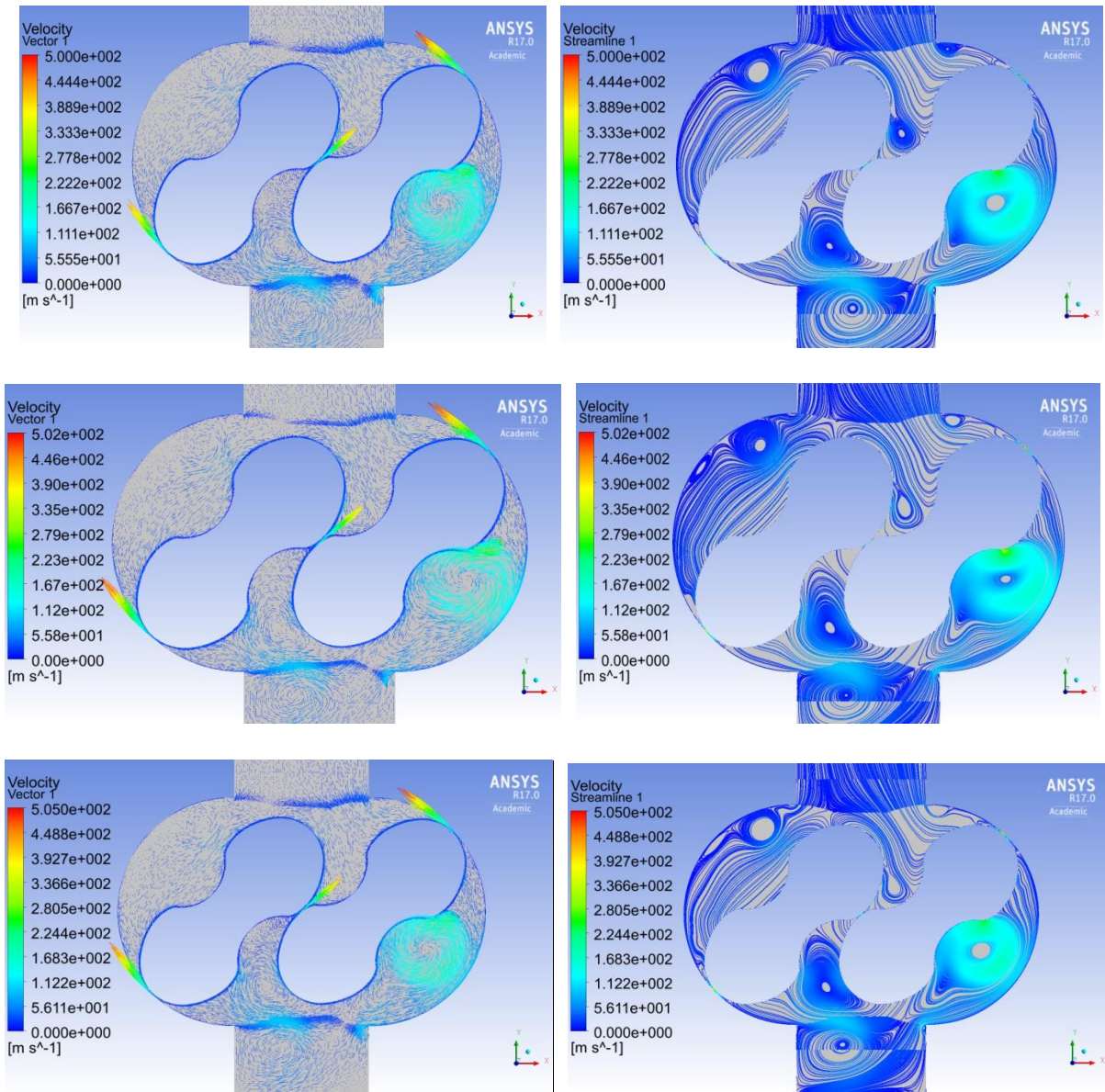


Figure 5.21: The velocity vectors and streamline contours at a rotational speed 2400 rev/min, meshing angle at  $45^{\circ}$  degrees, a pressure difference 700 millibars and for tip clearances of (0.22 mm, 0.24 mm, and 0.26 mm from up to down respectively).

The high and low velocities exist in the flow mixing regions as recirculation zones. These zones occur when the rotors suddenly cross the edges of the suction or the discharge zones which the core of these areas consists of the low velocity. Figure 5.21 shows the two rotors formed two chambers; some recirculation zones occurred near the inlet region and other at the outlet region. It can be seen from this figure that the shape of recirculation zones are changing as the tip clearance changes. Moreover, these recirculation areas of high and low velocities may lead to further vibration and energy losses as tip clearance increases. Furthermore, the maximum velocities are found inside the clearances and it increases with the increase of tip clearance, but sometimes these velocities are higher with an increase of tip clearance because of the effect of the backflow as shown in figure 5.21 as a result from the effect of these recirculation zones the component of the vertical velocity in these areas and inside the clearances being negative, so the flow moving back to the inlet direction. It indicates that the existence of recirculation zones reduces the outlet flow and plays an adverse effect on the flow rate. However, the decrease of tip clearance commonly plays a positive effect on the outlet flow which may decrease the influence of backflow. The variation of the internal flow velocity shows that the tip clearance has a considerable influence on the velocity distribution of the whole region within the Roots blower.

Usually, the maximum speed of the rotational flow is at the tip of the impeller and often takes place at the clearance between the impellers and the casing as shown in Figure 5.21. This high speed leads to low-pressure and high-velocity regions that might produce a force to attract the fluid back to the inlet zone and may generate a backflow.

Table 5.6 provides the statistical analysis of the velocity variation within the blower through distributed points from the inlet to outlet of the Roots blower. The results represent that there is a slight deviation of the average velocities at different tip clearances. These velocities increase at outlet zone with a finer gap. Also, the differences between the maximum velocities at different tip clearances are small which rise mostly as tip gap decreases.

Table 5.6: The distribution and the variation of the velocity at a rotational speed 2400 rev/min, a pressure difference 700 millibars and for different clearances

Positions	$V_{ave}$ (m/s)	$V_{ave}$ (m/s)	$V_{ave}$ (m/s)	$V_{max}$ (m/s)	$V_{max}$ (m/s)	$V_{max}$ (m/s)
	at 0.22mm	at 0.24mm	at 0.26mm	at 0.22mm	at 0.24mm	at 0.26mm
P1	12.56	12.44	12.43	18.89	18.76	18.70
P2	14.44	14.19	14.30	24.91	25.28	24.90
P3	16.88	14.12	16.20	31.25	24.94	28.68
P4	6.70	5.94	6.72	25.06	21.41	25.31
P5	23.45	27.11	23.80	543.42	504.75	514.60
P6	22.36	25.05	23.02	440.63	422.42	444.94
P7	44.37	49.37	46.81	447.20	459.53	457.66
P8	58.10	60.35	59.40	419.06	433.27	422.55
P9	70.88	68.24	69.70	269.54	260.76	269.06
P10	40.66	37.77	38.49	96.06	82.94	85.22
P11	40.66	38.32	39.62	65.31	63.73	64.02

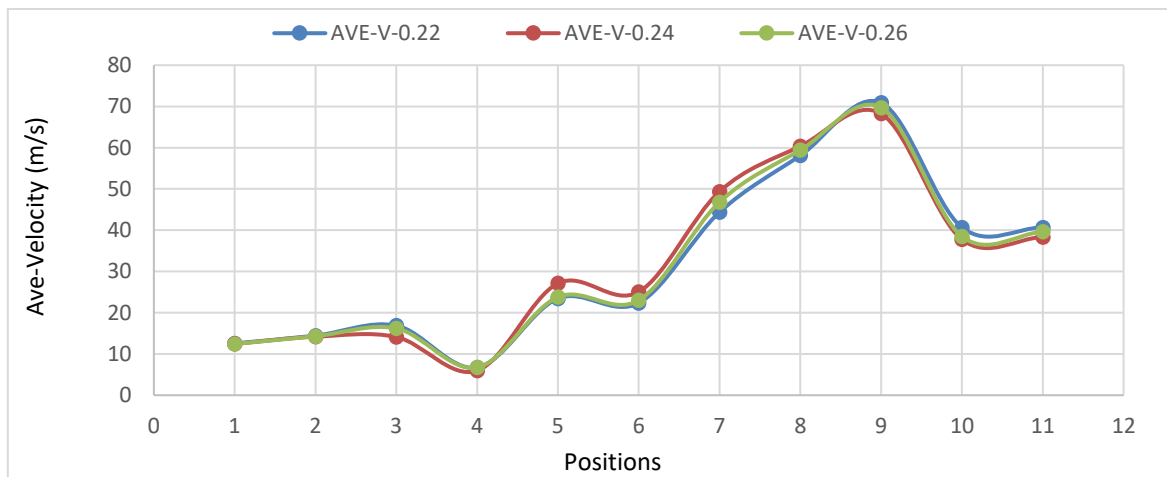


Figure 5.22: The average velocity distribution at rotational speed 2400 rev/min, pressure differences 700 millibars and for clearances of (0.22 mm, 0.24 mm, and 0.26 mm).

The data in the table and figure 5.22 show that the maximum velocities are found at point 5 which are 543.42 m/s for clearance 0.22 mm, 504.75 m/s for clearance 0.24 mm and 514.6 m/s for clearance 0.26 mm respectively. The reason for that because this point located inside the

gap in the area between inlet zone and outlet zone which affected by the increase of high-pressure area and high speed of backflow in this region, which the maximum velocity usually increased as tip clearance decrease (diameter increase).

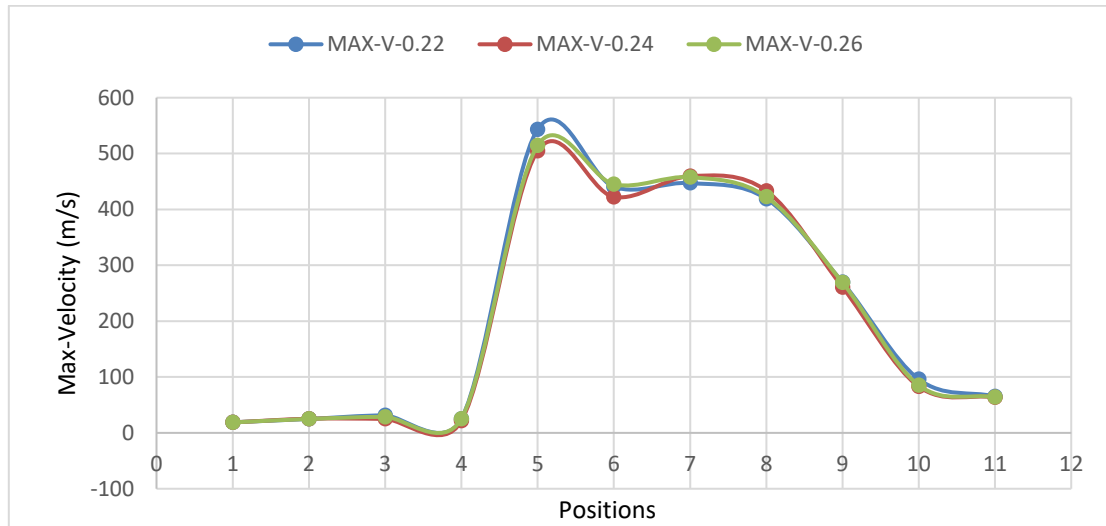


Figure 5.23: The Maximum velocity distribution at rotational speed 2400 rev/min, pressure differences 700 millibars and for clearances of (0.22 mm, 0.24 mm, and 0.26 mm).

Furthermore, according to previous analysis, concerning the velocity variations in the blower, the outcomes have presented that clearance difference has a considerable influence on variants and distribution of the velocity that the average velocity, the maximum positive velocity mostly increases as rotor diameter increases or tip clearance decreases as shown in figure 5.23.

Furthermore, according to previous analysis, regarding the velocity variations in the blower, the results have presented that tip clearance has a significant influence on variation and distribution of the velocity which the average and the maximum velocities increase as tip clearance increase. Moreover, it has been found that the positions of the minimum pressures and minimum temperatures are very close to the locations of maximum velocities.

The physical significance of the velocity in the blower that any increase of the velocity above the acceptable level will affect the reliability and performance of the blower which may lead to increase of vibration and noise in the blower system. Also, an extreme increase of velocity may affect the foundation of the blower system which may lead to failure of the blower system. Moreover, the tip clearance size is one of the main factors affect the velocity, any increase or decrease of tip clearance size above the acceptable level will lead to extreme velocity within the blower.

## 5.5 Effect of clearance between two rotors (centre clearance) on Roots blower performance

In order to investigate the influence of clearance size between two rotors on the performance of the Roots blower, the analysis with centre clearances of 0.3 mm, 0.34 mm (baseline model), and 0.38 mm at a rotational speed 2400 rev/min and a pressure difference 700 millibars have been conducted and compared. In the present study, the influence of centre clearance in the blower on pressure variation and distribution has been established through the use of ANSYS FLUENT code and dynamic mesh technique (DMT).

### 5.5.1. Effect of the gap between two rotors on pressure characteristics

The distribution and the variation of pressure in the Roots blower model for the last revolution at a discharge pressure 700 millibars, a speed 2400 rev/min and for centre clearances of 0.3 mm, 0.34 mm, and 0.38 mm are shown in Figure 5.24.

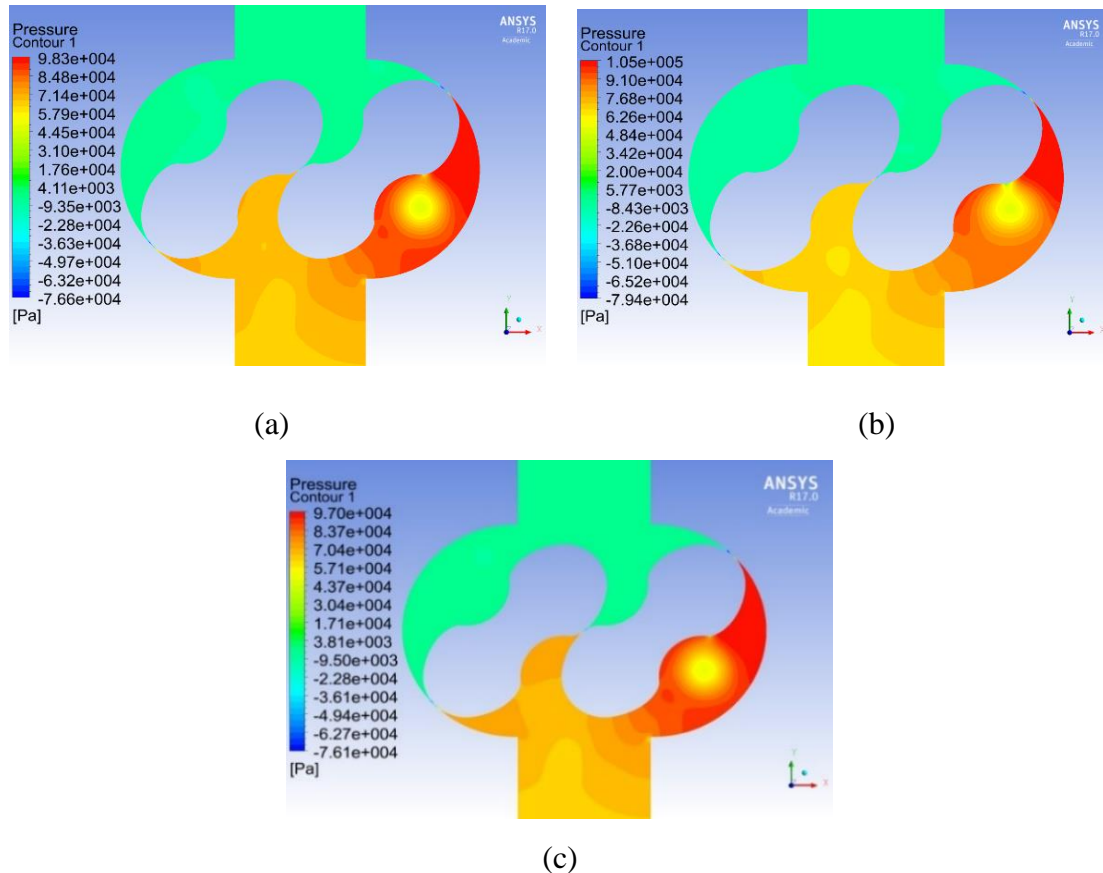


Figure 5.24: The static pressure contours at a speed 2400 rev/min, a pressure difference 700 millibars, and for centre clearances of (a) 0.3 mm, (b) 0.34 mm, (c) 0.38 mm.

Similarly, as discussed in the case of tip clearance effect on pressure variation and distribution, It can be seen from this figure that the lower pressure occurs inside clearances at the inlet side of the impeller. Also, it is evident that the distributions of static pressure at a constant rotational speed, the same discharge pressure and under different centre clearances have the same trend for all cases in the investigation.

Figure 5.24 depicts the variations and the distribution of static pressure contours in the Roots blower. It is apparent that the pressure is gradually increased from the inlet zone to the outlet zone of the blower. Also, there are small differences in the variation and the distribution of static pressure as the centre clearance increase or decrease. It can be seen that the positive and the negative static pressure in figure 5.24 b is higher than other figures.

Figures 5.25 and 5.26 show the instantaneous variation of static pressure at the inlet and the outlet of the two-lobe Roots blower over one revolution/cycle at different centre clearances. It can be seen from these figures that the pressure and the amplitude of fluctuation in the discharge zone are higher than that in the suction zone and it increases as the centre clearance decreases. However, at the outlet, the pressure and their amplitude at a centre clearance 0.34 mm (baseline clearance) are a little higher than the pressure and their amplitude at other centre clearances.

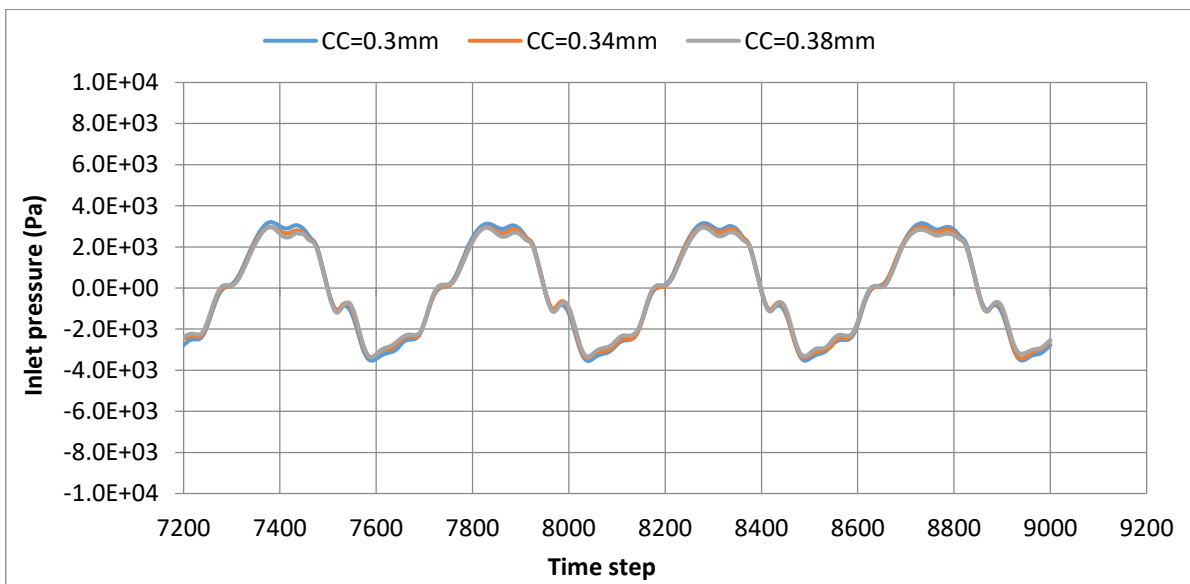


Figure 5.25: Pressure fluctuations at blower inlet at 2400 rev/min, 700 millibars, and different centre clearances (CC).

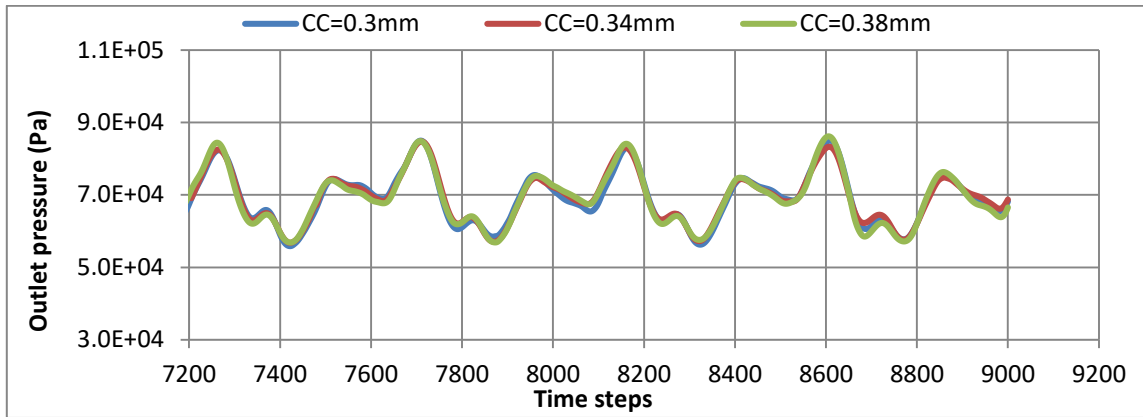


Figure 5.26: Pressure fluctuations at blower outlet at 2400 rev/min, 700 millibars, and for different centre clearances (CC).

The statistical analysis of the variation and the distribution of static pressure at a discharge pressure 700 millibars, a speed 2400 rev/min and for different centre clearances in the blower from the inlet to outlet are presented in Tables 5.7 and 5.8.

Table 5.7: The average pressure, at 2400 rev/min, 700 millibars, and under different centre clearances in Pascal.

Positions	$P_{ave}$ at 0.3 mm	$P_{ave}$ at 0.34mm	$P_{ave}$ at 0.38mm
P1	-8.79E+01	-8.82E+01	-8.50E+01
P2	-1.29E+02	-1.27E+02	-1.24E+02
P3	-7.63E+02	-7.80E+02	-6.68E+02
P4	-8.24E+02	-7.90E+02	-7.71E+02
P5	6.85E+03	7.26E+03	6.90E+03
P6	2.55E+04	2.57E+04	2.51E+04
P7	4.19E+04	4.15E+04	4.17E+04
P8	5.84E+04	5.85E+04	5.82E+04
P9	6.09E+04	6.09E+04	6.18E+04
P10	6.92E+04	6.92E+04	6.91E+04
P11	6.92E+04	6.94E+04	6.92E+04

The average pressure increases from the inlet to outlet until approaches the maximum values at the discharge of the blower ( P11) which recorded 6.92E+04 Pa, 6.93E+04 Pa, and 6.92E+04

Pa for centre clearances of 0.3 mm, 0.34 mm and 0.38 mm respectively. Also, the pressure value after P6 declines slightly towards the outlet zone until stabilize as shown in table 5.7 and figure 5.27. However, the average pressure at the centre clearance 0.34 mm is higher than the average pressure at the centre clearances of 0.3 mm. This is because of the effect of high velocity inside a smaller clearance.

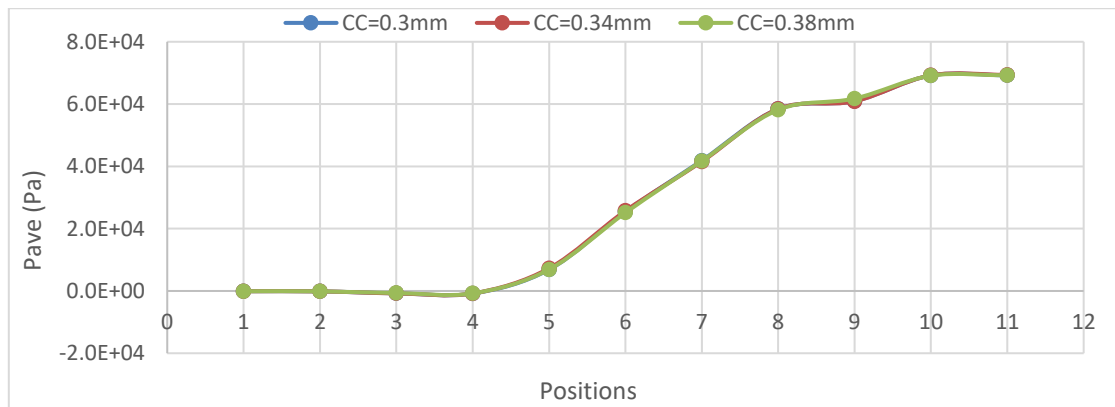


Figure 5.27: The distribution of average-pressures at 2400 rev/min, 700 millibars and under different centre clearances.

Table 5.8: The maximum positive and negative pressures, at 2400 rev/min, 700 millibars, and under different centre clearances in Pascal.

Positions	$P_{max}$ at 0.3 mm	$P_{max}$ at 0.34 mm	$P_{max}$ at 0.38 mm	$P_{min}$ at 0.3 mm	$P_{min}$ at 0.34 mm	$P_{min}$ at 0.38 mm
P1	3.20E+03	2.99E+03	2.97E+03	-3.55E+03	-3.43E+03	-3.37E+03
P2	3.53E+03	3.31E+03	3.30E+03	-3.70E+03	-3.63E+03	-3.48E+03
P3	3.52E+03	3.25E+03	3.18E+03	-5.75E+03	-5.34E+03	-5.18E+03
P4	3.51E+03	3.26E+03	3.12E+03	-5.58E+03	-5.33E+03	-5.27E+03
P5	9.33E+04	9.54E+04	9.17E+04	-8.28E+04	-7.74E+04	-8.15E+04
P6	1.02E+05	1.06E+05	1.03E+05	-6.98E+04	-6.94E+04	-7.05E+04
P7	9.46E+04	9.39E+04	9.47E+04	-7.39E+04	-7.09E+04	-7.40E+04
P8	8.73E+04	8.74E+04	9.12E+04	-6.32E+04	-6.25E+04	-6.17E+04
P9	8.66E+04	8.67E+04	9.05E+04	-1.23E+04	-1.25E+04	-1.12E+04
P10	8.57E+04	8.49E+04	8.81E+04	5.55E+04	5.63E+04	5.49E+04
P11	8.50E+04	8.47E+04	8.62E+04	5.59E+04	5.68E+04	5.68E+04

The maximum pressure increases from the inlet to outlet until approaches the maximum values when the tip of impeller is approximately at the middle region of the blower ( P6) which recorded  $1.02\text{E}+05$  Pa,  $1.06\text{E}+05$  Pa and  $1.03\text{E}+05$  Pa for centre clearances of 0.3 mm, 0.34 mm and 0.38 mm respectively as shown in table 5.8 and figure 5.28. Also, the pressure value after P6 declines slightly towards the outlet zone until stabilize. However, the maximum pressure at the centre clearance 0.34mm is higher than the maximum pressure at the centre clearances of 0.3mm. This is, because of the effect of high velocity inside a smaller clearance.

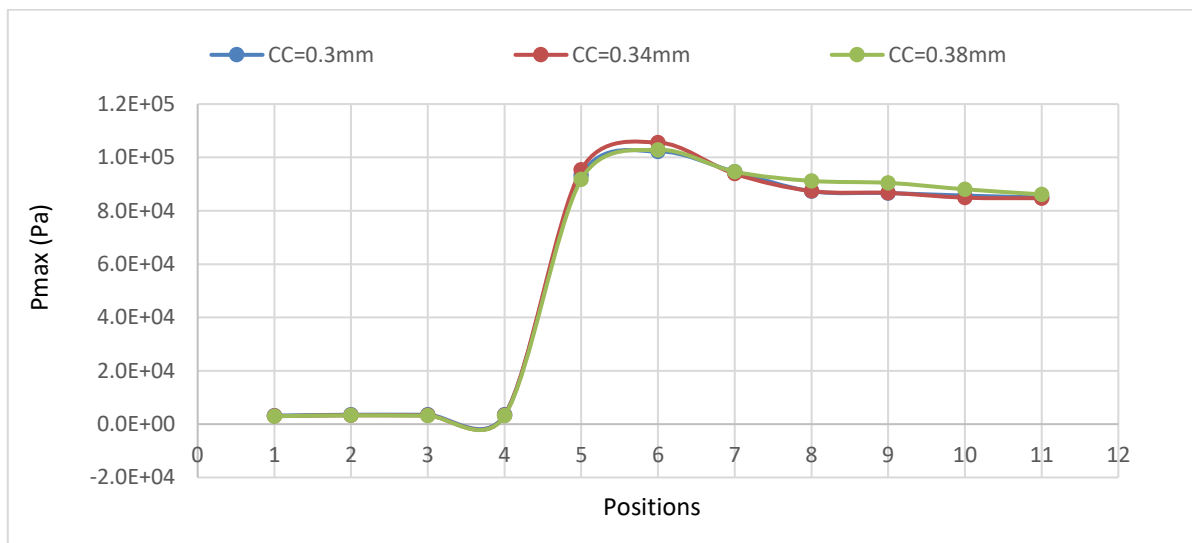


Figure 5.28: The distribution of maximum-pressures at 2400 rev/min, 700 millibars and under different centre clearances.

Figure 5.29 and Table 5.8 illustrate that there are small differences in maximum negative pressure which recorded  $-8.28\text{E}+04$  Pa,  $-7.74\text{E}+04$  Pa, and  $-8.15\text{E}+04$  Pa for centre clearances of 0.3 mm, 0.34 mm and 0.38 mm respectively as shown in table 5.8. It can be seen in this figure that the maximum negative pressure increases from the inlet to outlet until it approaches the maximum values when the tip of the impeller is approximately at the (P5) due to the high velocity in this zone, and after that, it declines toward the outlet zone until stabilise.

Moreover, the maximum negative pressure is increased with the decrease of centre clearance. However, the maximum negative pressure at the centre clearance 0.38 mm is higher than that at the centre clearance 0.34 mm. This is because of the effect of high pressure and high velocity at this point (P5).

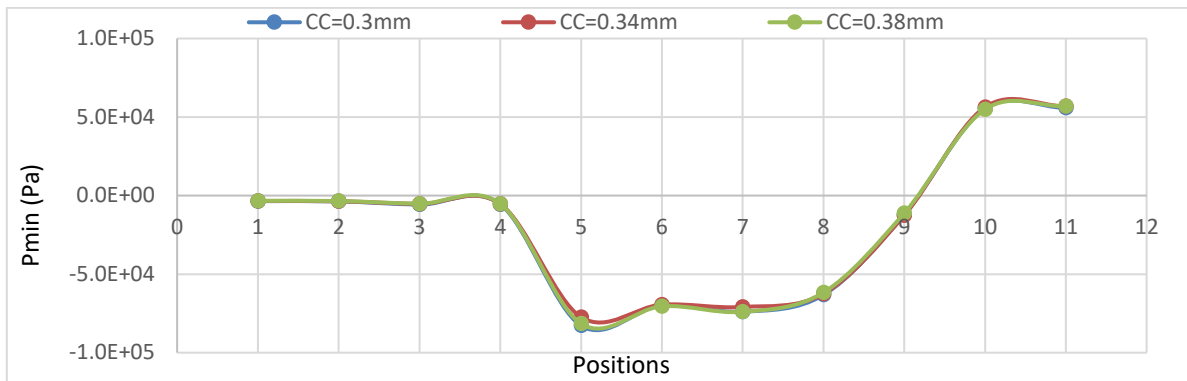


Figure 5.29: The distribution of maximum negative pressures at 2400 rev/min, 700 millibars and under different centre clearances.

Root mean square (RMS) refers to the arithmetic mean of the squares of a set of numbers. RMS is a meaningful way of calculating the average of values over a period of time. Figure 5.30 expresses the relation between effective pressure zones and RMS. It can be seen that the RMS increases from the inlet to outlet of the blower, which the maximum values are recorded at the discharge zones. Also, these values generally rise with a decrease of centre clearances.

Table 5.9: The Root Mean Square (RMS) and the peak to peak amplitudes of the pressure at a speed 2400 rev/min, a pressure difference 700 millibars and for different centre clearances.

Positions	RMS at 0.3 mm	RMS at 0.34 mm	RMS at 0.38 mm	P <sub>pk-pk</sub> at 0.3 mm	P <sub>pk-pk</sub> at 0.34 mm	P <sub>pk-pk</sub> at 0.38 mm
P1	2.33E+03	2.22E+03	2.13E+03	6.75E+03	6.42E+03	6.34E+03
P2	2.52E+03	2.40E+03	2.30E+03	7.23E+03	6.94E+03	6.78E+03
P3	2.79E+03	2.66E+03	2.55E+03	9.27E+03	8.59E+03	8.36E+03
P4	2.85E+03	2.72E+03	2.63E+03	9.09E+03	8.59E+03	8.40E+03
P5	2.48E+04	2.55E+04	2.48E+04	1.76E+05	1.73E+05	1.73E+05
P6	4.58E+04	4.64E+04	4.52E+04	1.72E+05	1.75E+05	1.73E+05
P7	5.61E+04	5.55E+04	5.60E+04	1.69E+05	1.65E+05	1.69E+05
P8	6.60E+04	6.60E+04	6.60E+04	1.51E+05	1.50E+05	1.53E+05
P9	6.52E+04	6.51E+04	6.54E+04	9.89E+04	9.93E+04	1.02E+05
P10	6.96E+04	6.96E+04	6.96E+04	3.02E+04	2.86E+04	3.31E+04
P11	6.96E+04	6.97E+04	6.96E+04	2.91E+04	2.79E+04	2.93E+04

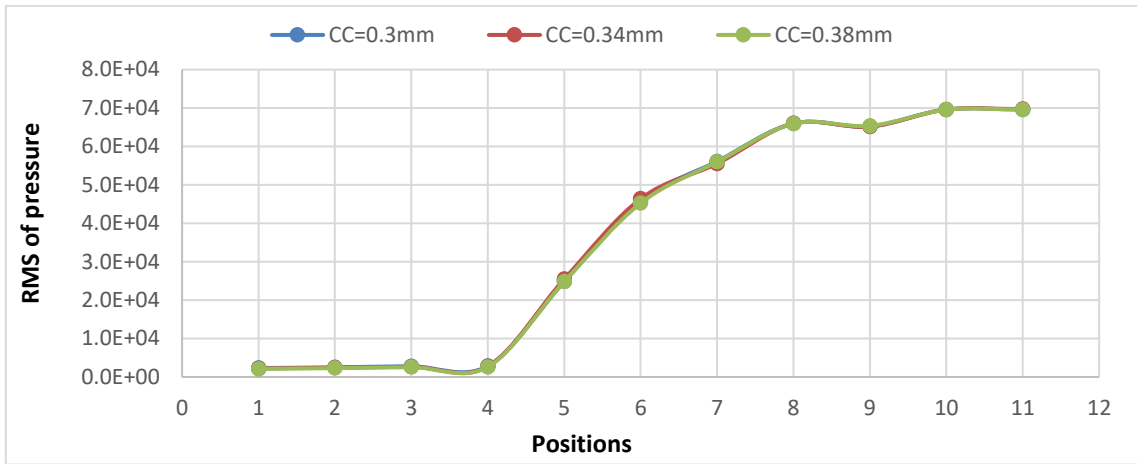


Figure 5.30: The relation between effective pressure zones and RMS

The peak-to-peak amplitudes at a rotational speed 2400 rev/min, a discharge pressure 700 millibars, and for different centre clearances are presented in Figure 5.31. It is clear to conclude that there is a small difference of amplitudes when the tip of impellers is at the inlet or the outlet regions. On the other hand, the differences of amplitudes are increased when the tip of rotors starts to move away from these zones. These differences increase inside the meshing region in the blower. Also, the maximum amplitude values are recorded at points 5 and 6 where the effect of pressure and backflow are high in this zone. Moreover, it can be seen that the amplitudes are increased with the increase of centre clearances and are more prominent at outlet zone than an inlet zone because the pressure and their fluctuations are higher in this area.

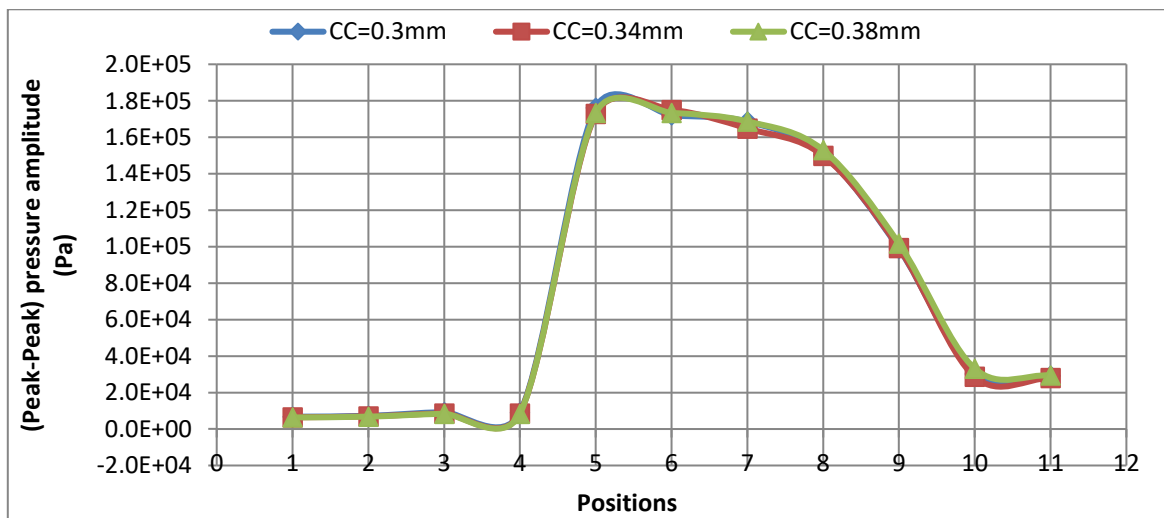


Figure 5.31: The peak-peak pressure amplitudes at speed 2400 rev/min, 700 millibars and different centre gaps

The numerical result indicates that the pressure drops in the clearances within the blower at the inlet chamber when the blower operates at small centre clearance, causing the velocity to increase. It develops further the backflow leads to the decline of flow rate. On the other hand, the high velocity inside the small gap will force the flow to move from inlet to outlet which finally leads to an increase in flow rate.

Additionally, regarding the pressure deviations in the blower, the results have presented that gap change has a significant effect on variations and distribution of the pressure which the average pressure, maximum negative pressures mostly decreases as rotor waist decreases or centre clearance increases. However, the maximum positive pressures mostly increase as the rotor waist decreases or centre clearance increases as shown in figure 5.32.

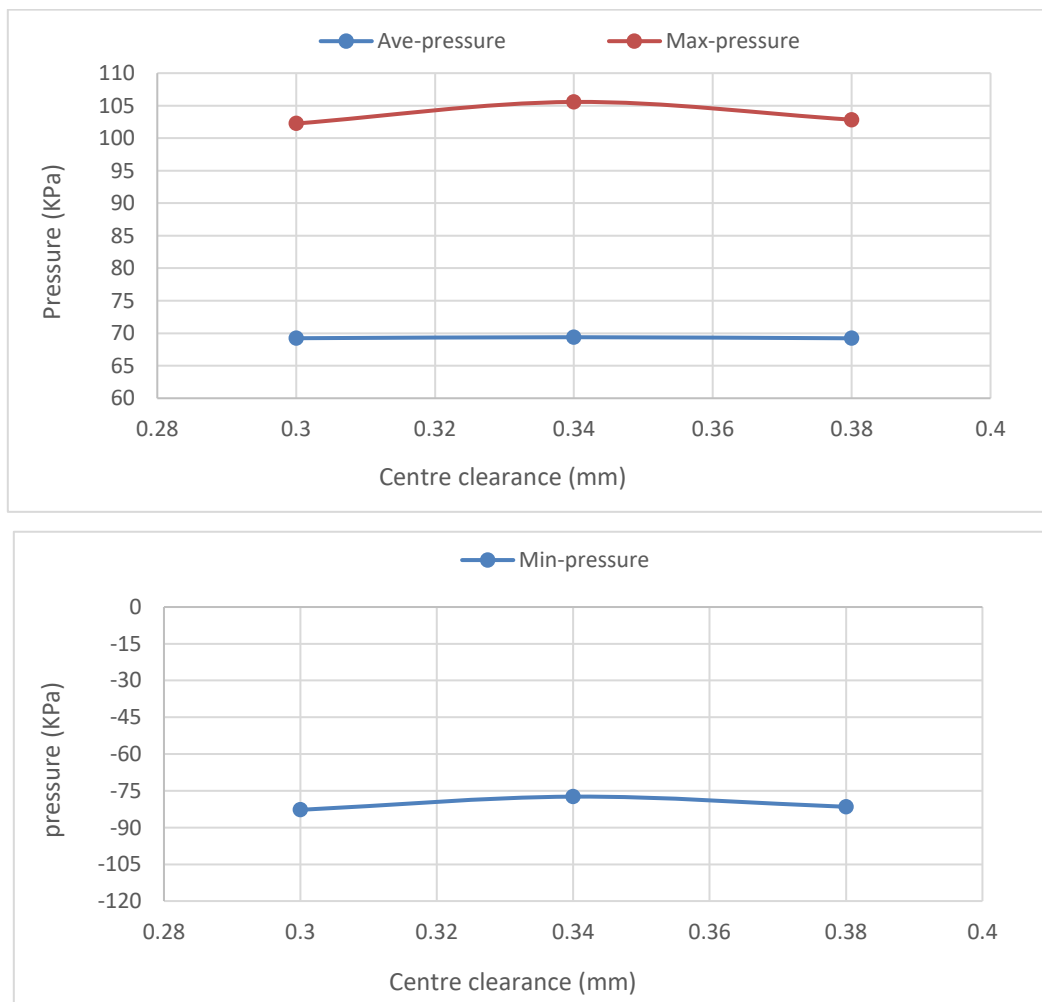


Figure 5.32: The relation between the centre clearances with the pressure in the blower

### 5.5.2 The Effect of the gap between two rotors on the mass flow rate

Figure 5.33 illustrates the relationship between the average mass flow rate and different centre clearances obtained through different numerical simulations at a speed 2400 rev/min and a pressure difference 700 millibars. It can be concluded that there is a difference in the average mass flow rate, which declines linearly as the centre gap increase.

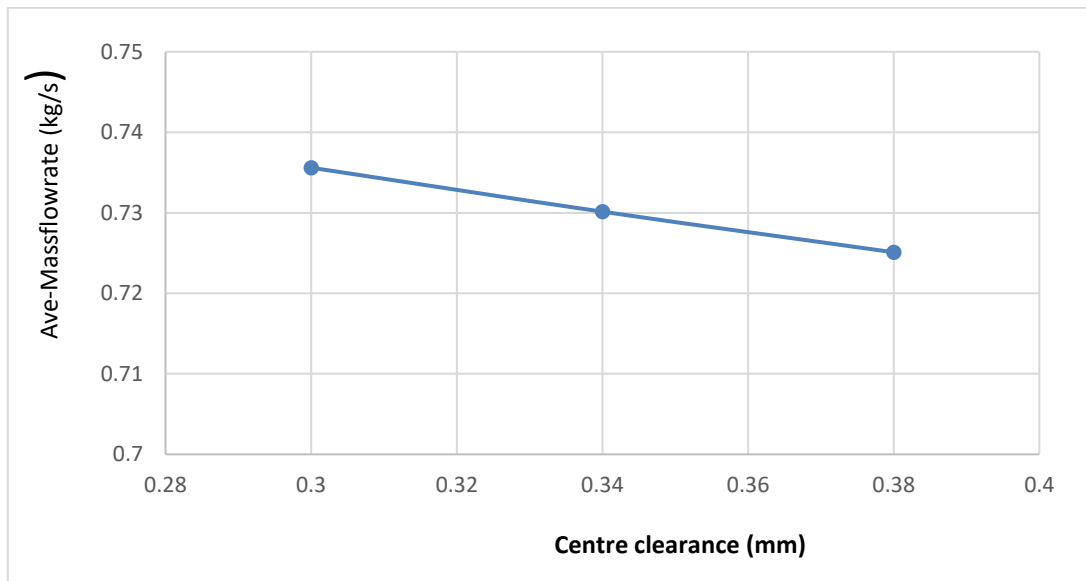


Figure 5.33: The average mass flow rate at speed 2400 rev/min, pressure difference 700 millibars, and different centre clearances

The fluctuations of mass flow rate for the last impeller meshing rotation cycle of the Roots blower of case study obtained through numerical simulations at rotational speeds 2400 rev/min, a pressure difference 700 millibars, and for different centre clearances are shown in figure 5.34. It can be concluded that there are a small difference of the amplitude and the fluctuation coefficient ( $M_F$ ) of inlet mass flow rate which both increase with the decrease of centre clearance. The reason behind that because of the effect of high velocity in the smaller gap.

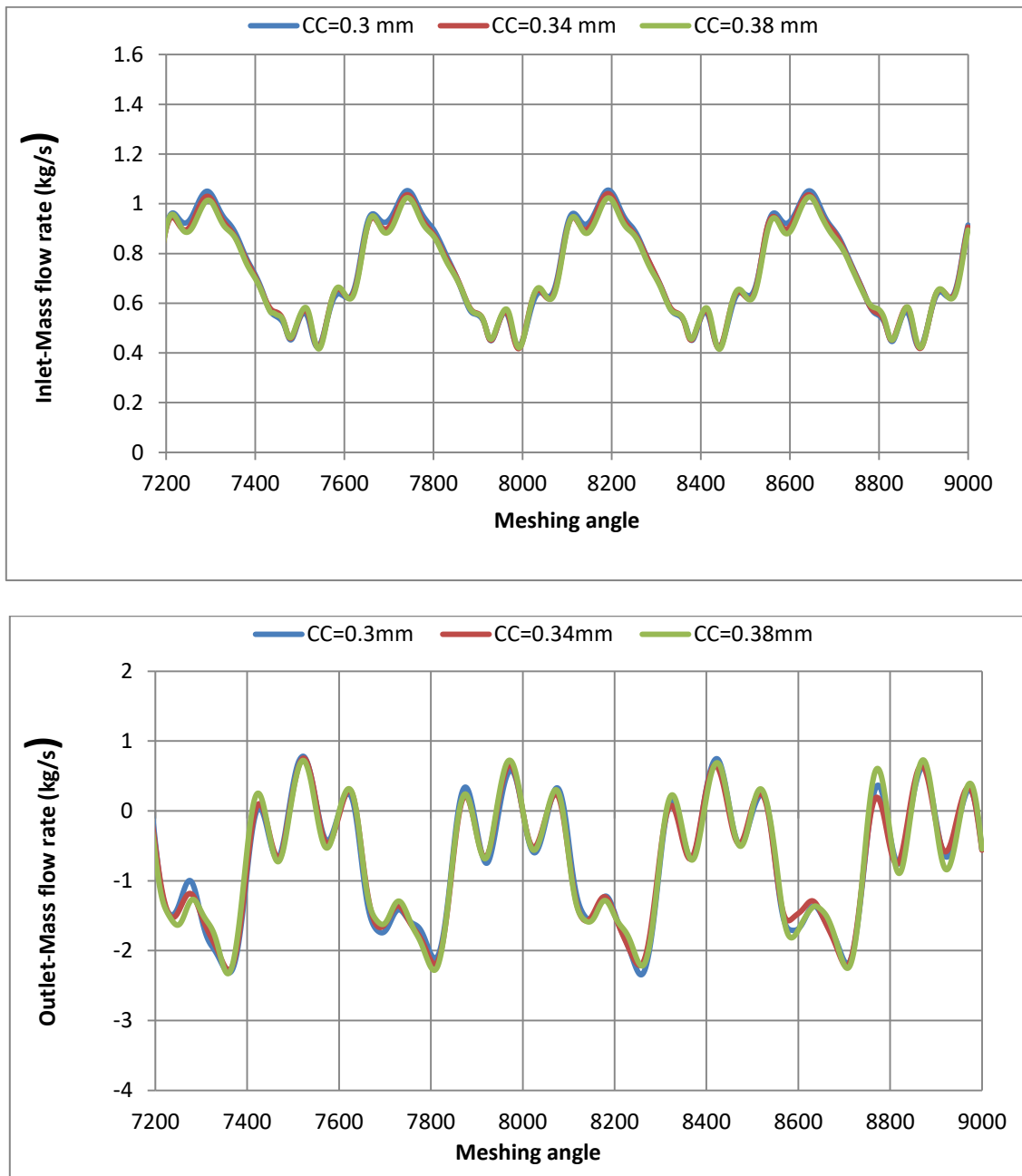


Figure 5.34: Mass flow rate fluctuation at 2400 rev/min, 700 millibars and different centre gaps at inlet and outlet of the blower

Moreover, the amplitude and the fluctuation coefficient ( $M_F$ ) of the outlet mass flow rate at both centre clearances of 0.3 mm and 0.38 mm are higher than the amplitude at a centre clearances 0.34 mm as shown in figures 5.34 and 5.35. This is because of the effect of high velocity and backflow.

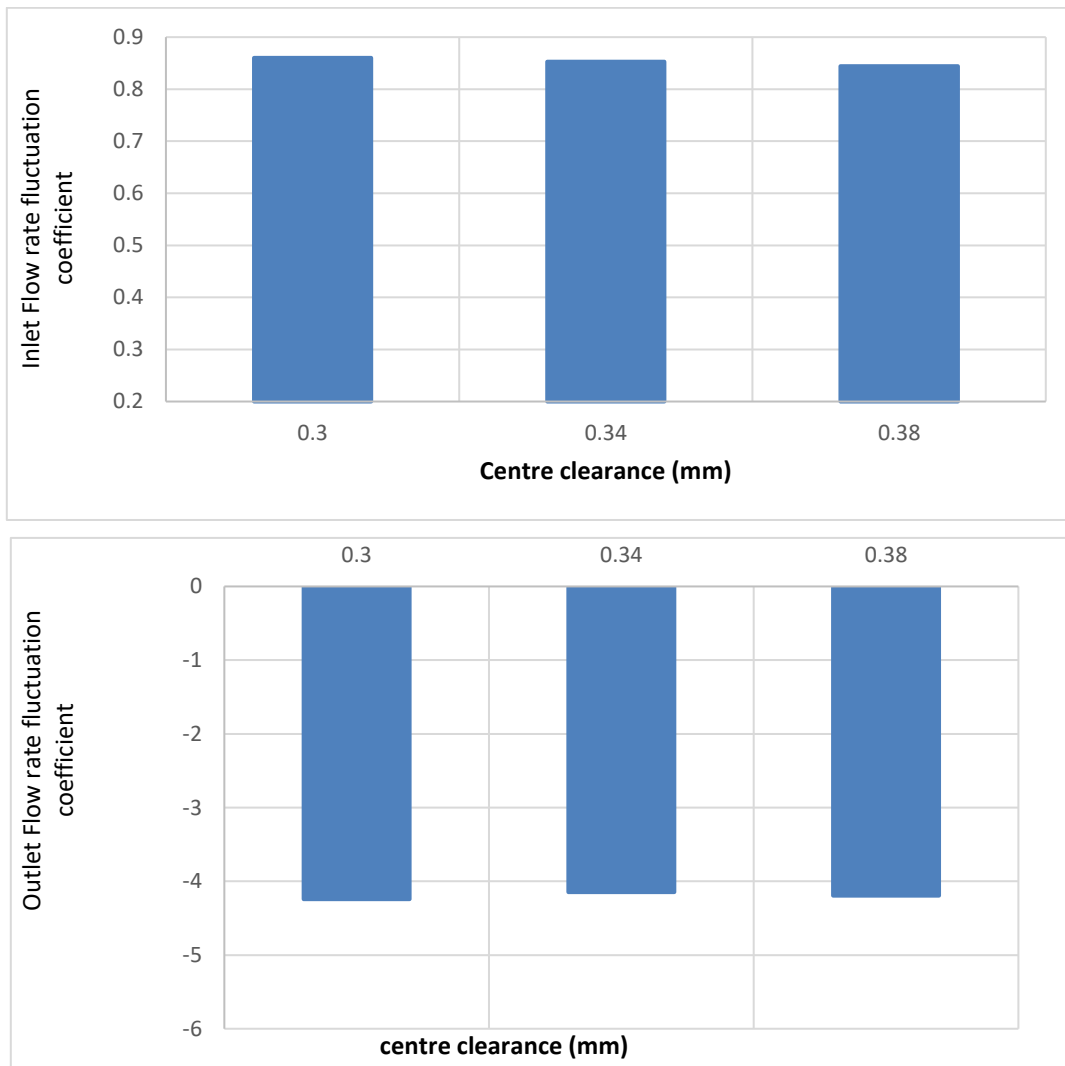
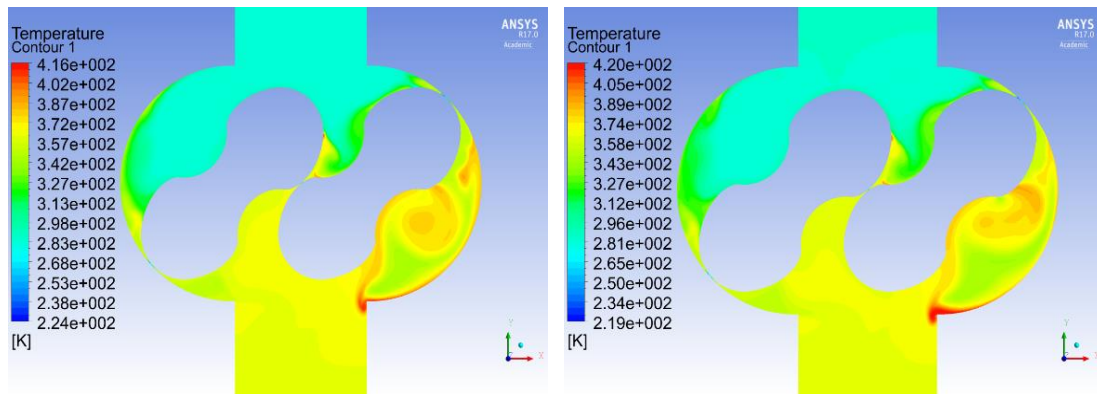


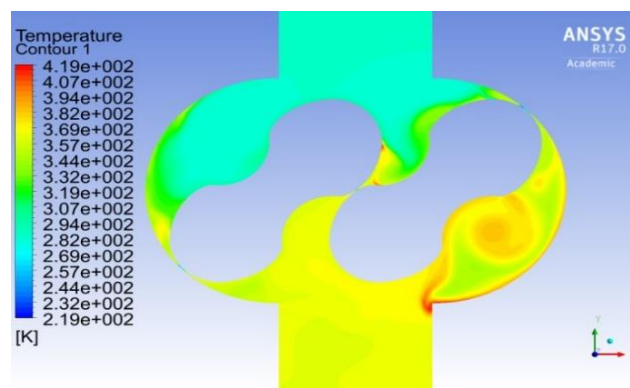
Figure 5.35: Mass flow rate fluctuation coefficient ( $M_f$ ) at 2400 rev/min, 700 millibars and different centre clearances at the inlet (left) and outlet (right).

### 5.5.3. Effect of the gap between two rotors on temperature characteristics in Roots blower

The contours and the distribution of the temperature at angle  $45^{\circ}$  degrees of rotors rotation in Roots blower as shown in figure 5.36. These contours are obtained through different numerical simulations at a speed 2400 rev/min, a pressure difference 700 millibars and for different centre clearances.



(b)



(c)

Figure 5.36: The contours of the temperature for the last revolution and at angle  $45^0$  degrees of rotation, 2400 rev/min, a difference pressure 700 millibars and for centre clearances of (a ) 0.3 mm, (b) 0.34 mm, and (c) 0.38 mm.

Figure. 5.36 shows the effect of unsteady flow on the variation and distribution of the temperature within the Roots blower. It is apparent to conclude that the distribution of temperature is non-uniform and the position of high-temperatures are close to rotor wall and casing wall at the outlet zone. Also, there are high-temperature areas inside the chamber between the rotor and the casing at discharge zone which changing their location and shape as rotors rotating and with a change of centre clearance. Moreover, the temperature increases inside the blower with increase of centre clearance.

The variation of the outlet temperature with the rotation angle for last rotation is shown in Figure 5.37. It can be concluded that the maximum temperature and their amplitude increases as rotational speed increases.

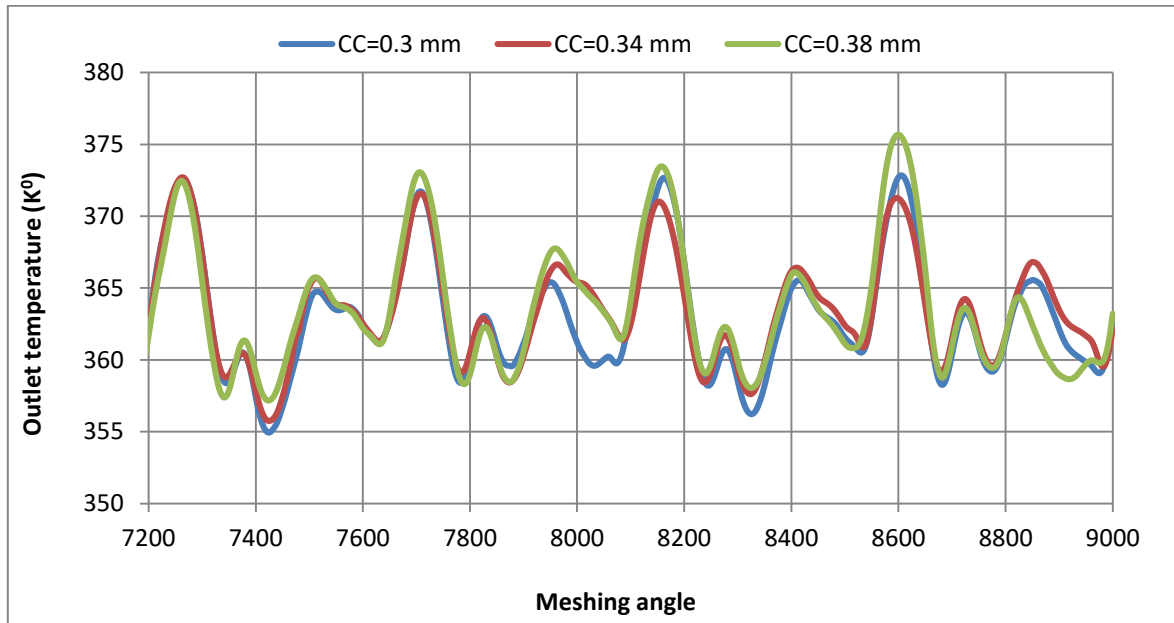


Figure 5.37: Outlet total temperature at 2400 rev/min, different pressure 700 millibars and different Centre clearances.

Investigations through the use of various statistical features such as the average, minimum and maximum value of temperature fluctuations have been used. This is aimed at more in-depth local analysis of the temperature variation and distribution within the blower.

The distribution and the variation of the average temperature at a discharge pressure 700 millibars, a speed 2400 rev/min and under different centre clearances in the blower from the inlet to outlet are presented in Table 5.10 and figure 5.38.

Table 5.10 and figure 5.38 depict that there is a little difference of the average temperature at different centre clearances which recorded  $362.34 \text{ K}^0$ ,  $363.39 \text{ K}^0$ , and  $363.18 \text{ K}^0$  for centre gaps of 0.3 mm, 0.34 mm, and 0.38 mm respectively. Also, the average temperature increases from the inlet to the outlet of the blower.

Table 5.10: The average temperature, at 2400 rev/min, 700 millibars, and under different centre clearances

Positions	$T_{ave}$ (K <sup>0</sup> ) at 0.3 mm	$T_{ave}$ (K <sup>0</sup> ) at 0.34 mm	$T_{ave}$ (K <sup>0</sup> ) at 0.38 mm
P1	288.08	288.08	288.08
P2	288.05	288.04	288.05
P3	287.86	287.99	287.88
P4	287.87	287.91	287.90
P5	328.87	328.83	326.99
P6	344.40	340.11	344.32
P7	354.97	354.89	354.72
P8	359.89	360.65	361.50
P9	358.38	359.31	359.32
P10	362.34	363.39	363.18
P11	362.11	362.68	362.68

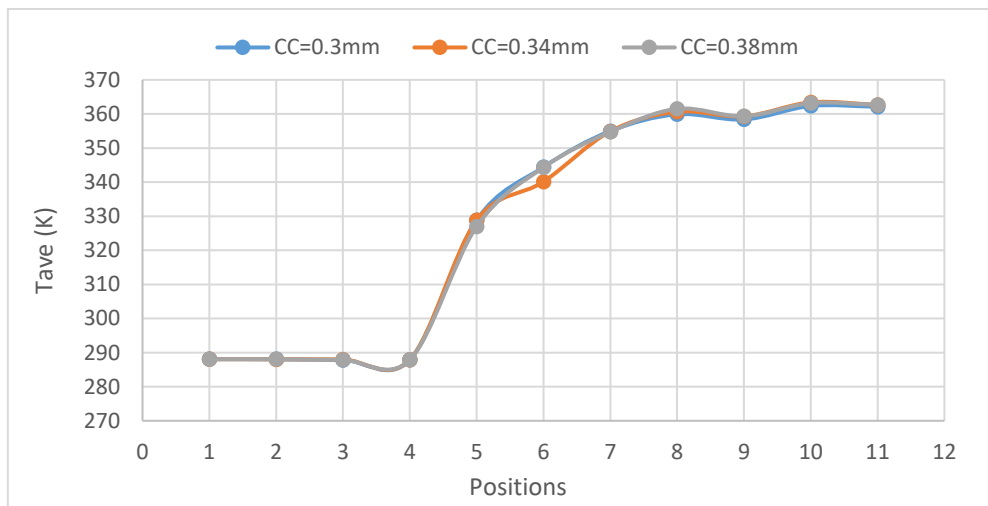


Figure 5.38: The distribution and the variation of average temperature at 2400 rev/min, 700 millibars pressure load and for different centre clearances

The distribution and the variation of the maximum temperature at a discharge pressure 700 millibars, a speed 2400 rev/min and under different centre clearances in the blower from the inlet to outlet are presented in Table 5.11 and figure 5.39.

Figure 5.39 depicts that there is an apparent variance of the maximum temperature at different centre clearances which recorded 416.42 K<sup>0</sup>, 420.33 K<sup>0</sup>, and 421.03 K<sup>0</sup> for centre gaps of 0.3 mm, 0.34 mm, and 0.38 mm respectively. Also, the maximum temperature increases from the inlet to the outlet of the blower. Moreover, the maximum temperature after point 6 declines slightly between (P6) and (P7) and after that increases until approaches the maximum value at (P8). Furthermore, after P8, the maximum temperature declines towards the outlet zone till finally stabilising. The reason for that the maximum temperature is at P8 because this point is located very close to blower discharge edge at outlet zone which affected by high pressure and backflow in this region which the maximum temperature increases as centre clearance increases

Table 5.11: The variation, and the distribution of the maximum and the minimum temperatures at a rotational speed 2400 rev/min, a discharge pressure 700 millibars, and for different centre clearances.

Positions	T <sub>max</sub> (K <sup>0</sup> ) at 0.3 mm	T <sub>max</sub> (K <sup>0</sup> ) at 0.34 mm	T <sub>max</sub> (K <sup>0</sup> ) at 0.38 mm	T <sub>min</sub> (K <sup>0</sup> ) at 0.3 mm	T <sub>min</sub> (K <sup>0</sup> ) at 0.34 mm	T <sub>min</sub> (K <sup>0</sup> ) at 0.38 mm
P1	290.73	290.57	290.55	285.25	285.34	285.40
P2	294.81	290.82	290.81	285.12	285.17	284.93
P3	291.44	291.16	291.04	283.80	284.39	284.11
P4	291.77	291.35	291.28	283.92	284.23	284.19
P5	350.82	353.60	348.61	202.42	207.46	209.18
P6	386.10	386.01	384.44	248.05	242.76	240.80
P7	383.13	377.88	386.16	232.02	235.77	231.94
P8	416.42	420.33	421.03	257.63	258.62	259.28
P9	415.93	417.77	417.45	310.96	316.49	320.39
P10	375.13	376.44	378.19	349.94	351.73	348.64
P11	371.82	371.90	374.15	353.64	354.51	355.68

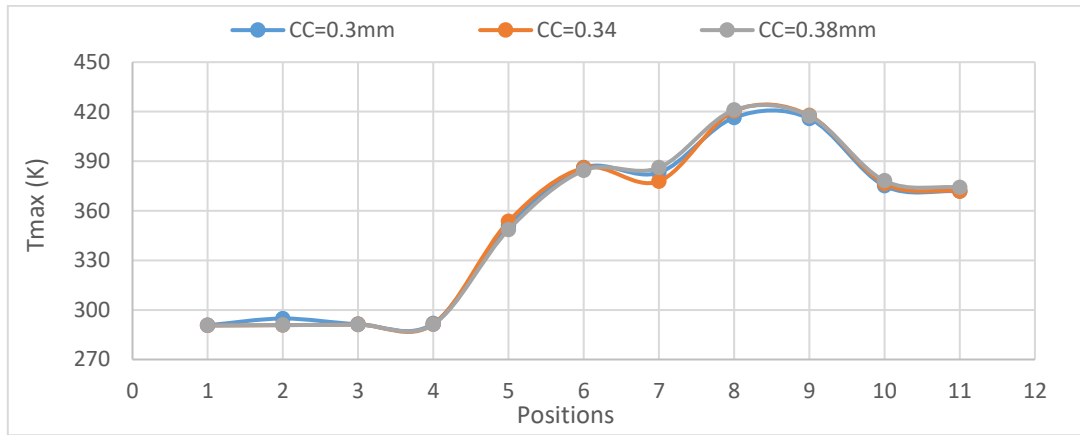


Figure 5.39: The distribution and the variation of maximum temperature at a speed 2400 rev/min, a pressure difference 700 millibars pressure load and for different centre clearances

Table 5.11 and figure 5.40 show that there are apparent differences in minimum temperature. It can be seen that the minimum temperature decreases as the centre gap decreases which recorded 202.42 K<sup>0</sup>, 207.46 K<sup>0</sup>, and 209.18 K<sup>0</sup> for centre gaps of 0.3 mm, 0.34 mm, and 0.38 mm respectively. Also, it can be seen in this figure that the minimum temperature increase from the inlet to outlet until it approaches the minimum value when the tip of the impellers is approximately at the angle of (P5), the minimum temperature after that declines and rises slightly when the tip is in between P5 and P7. Moreover, the minimum temperature after (P7) increases towards the outlet zone until stabilise. However, the pressure losses increase with the decrease of centre clearances. Also, the minimum temperatures are located at point 5 inside the clearance at suction zone due to low pressure and high velocity at this point.

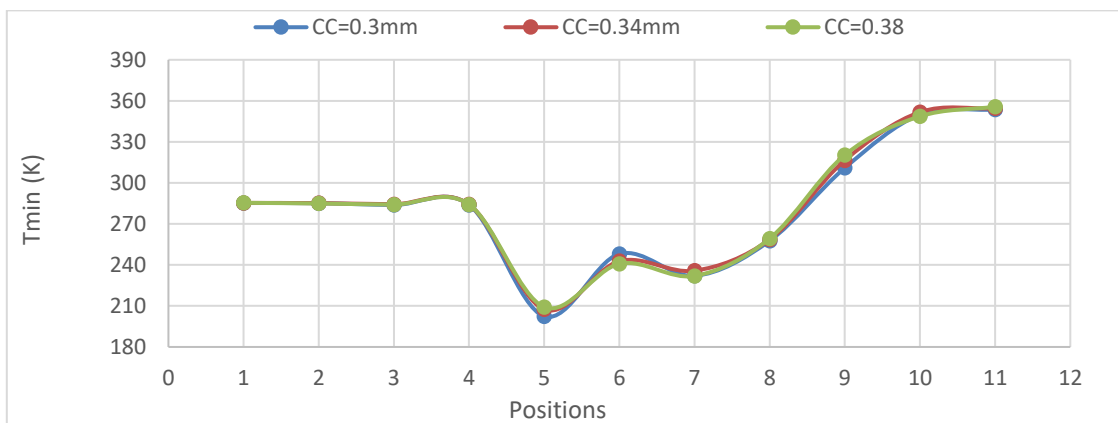


Figure 5.40: The distribution and the variation of the minimum temperature at a speed 2400 rev/min, a pressure load 700 millibars and for different centre clearances

Furthermore, according to previous analysis, regarding the temperature variations in the blower, the results have presented that centre clearance has a considerable effect on the variation and the distribution of the temperature which the maximum temperatures decreases and the minimum temperature decrease as centre clearance decreases as shown in figure 5.41

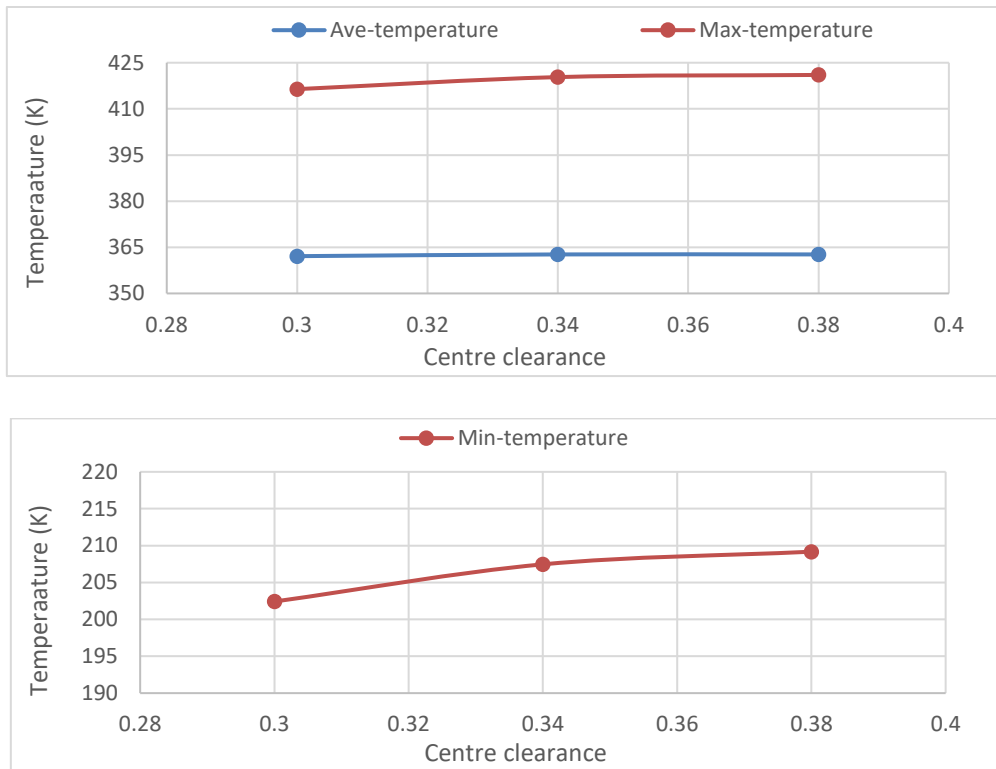


Figure 5.41: The relation between the impeller diameter and centre clearance with the temperature in the blower

#### 5.5.4. Effect of Gap between two rotors on velocity distributions

The distribution and the variation of the velocity in the Roots blower model for the last revolution at a discharge pressure 700 millibars, a speed 2400 rev/min and for centre clearances 0.3 mm, 0.34 mm, and 0.38 mm are shown in Figure 5.42 as velocity vectors and streamline contours.

It can be seen from this figure that the high velocity occurs inside clearances at the inlet side of the impeller. Also, it is evident that the distributions of velocity at the same rotational speed, the same discharge pressure and under different centre clearances have the same trend for all cases under investigation. Moreover, it shows that the change of centre clearance size will affect the distribution of the velocity inside of the blower

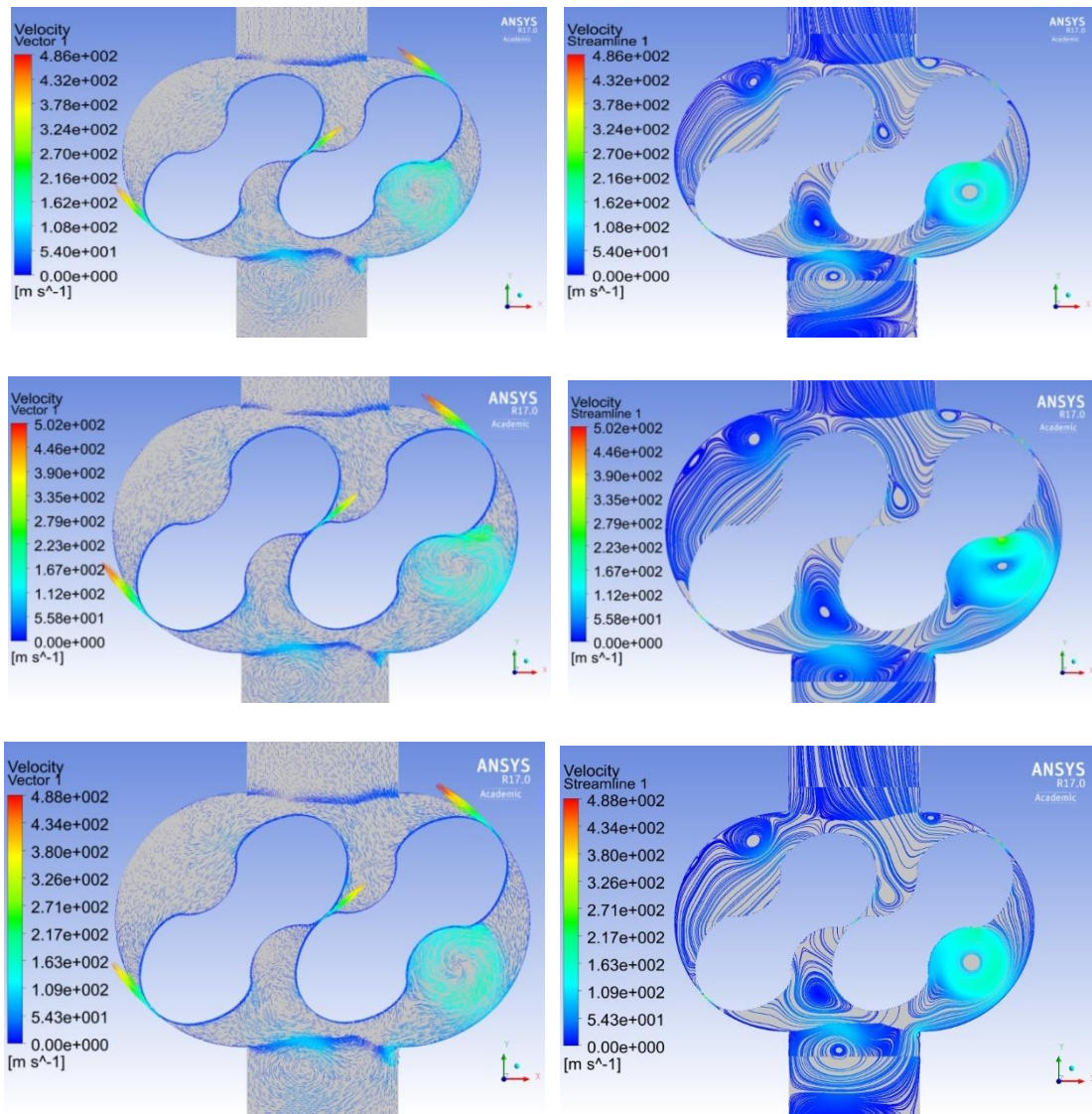


Figure 5.42: The velocity vectors and the streamline contours at a rotational speed 2400 rev/min, meshing angle  $45^{\circ}$  degrees, a pressure difference 700 millibars and for centre clearances of (0.3 mm, 0.34 mm, and 0.38 mm from up to down respectively).

High and low velocities exist in the flow mixing regions as recirculation zones. These zones occur when the rotors sudden cross the edges of the suction or the discharge zones which the core of these areas consists of the low velocity. Figure 5.42 shows the two rotors formed two chambers; some recirculation zones occurred near the inlet region and other at the outlet region. It can be seen from this figure that the shapes of recirculation zones change as the centre clearances change. Moreover, the maximum velocities are found inside the clearances and it increases with the decrease of centre clearances as shown in figure 5.42. Furthermore, The existence of these recirculation zones result in the vertical velocity component being negative

in these areas, with the flow moving in the opposite direction to the outlet. It indicates that the existence of recirculation zones reduces the outlet flow and plays an adverse effect on the flow rate. However, the decrease of centre gap commonly plays a positive effect on the outlet flow which may decrease the influence of backflow. The variation of the internal flow velocity shows that the centre clearance has an apparent influence on the velocity distribution of the whole region within the Roots blower.

Investigations through the use of various statistical features such as the average and maximum value of velocity fluctuations have been used. This is aimed at more in-depth local analysis of the velocity variation and distribution within the blower.

Table 5.12: The distribution and the variation of the velocity at a speed 2400 rev/min, a pressure differences 700 millibars and for different centre clearances

Positions	$V_{ave}$ (m/s) at 0.3mm	$V_{ave}$ (m/s) at 0.34mm	$V_{ave}$ (m/s) at 0.38mm	$V_{max}$ (m/s) at 0.3mm	$V_{max}$ (m/s) at 0.34mm	$V_{max}$ (m/s) at 0.38mm
P1	12.60	12.45	12.41	19.03	18.76	18.57
P2	14.57	14.19	14.25	25.05	25.29	24.59
P3	15.33	14.12	17.07	29.48	24.94	29.34
P4	6.66	5.95	6.40	25.16	21.42	24.96
P5	28.86	27.12	27.18	521.07	504.75	508.46
P6	21.98	25.05	22.86	392.86	422.42	412.55
P7	45.46	49.38	45.01	470.22	459.54	450.62
P8	59.86	60.36	61.59	424.31	433.27	423.20
P9	69.67	68.25	73.60	280.72	260.77	251.75
P10	39.89	37.78	40.82	87.67	82.94	95.87
P11	40.59	38.33	41.41	64.95	63.74	69.12

Table 5.12 and figure 5.43 depict that average velocity generally increases with the decreases of centre clearance. Also, it can be seen that there is a small discrepancy of average velocity at different centre clearances which recorded 69.67 m/s, 68.25 m/s, and 73.6 m/s for centre gaps of 0.3 mm, 0.34 mm, and 0.38 mm respectively. Also, the average velocity increases from the inlet to outlet of the blower. Moreover, the average velocity after P5 declines slightly between points P5 and P6 and after that increases until approaches the maximum value at the edges of

the discharge zone (P9). Furthermore, after P9, the average velocity declines towards the outlet zone till finally stabilising. However, the average velocity of centre gap 0.38 mm is higher than other average velocities commonly because of the effect of backflow.

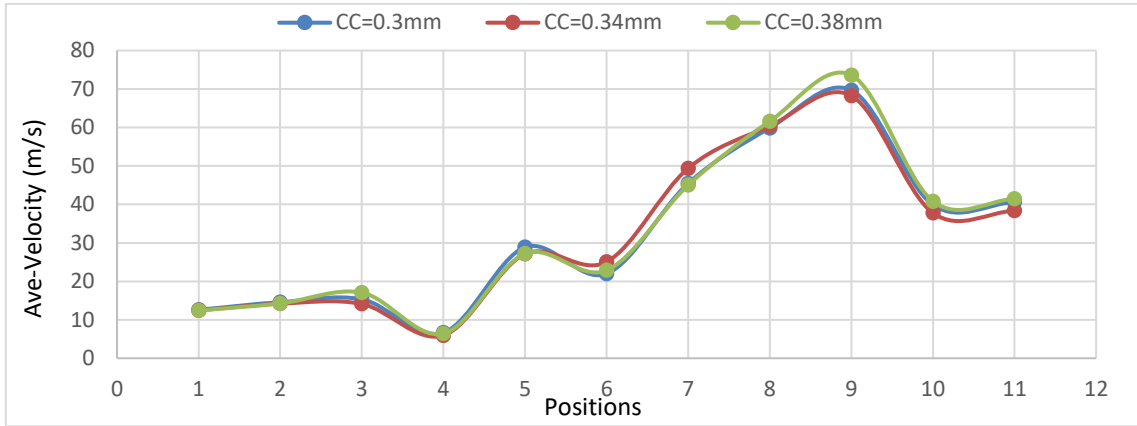


Figure 5.43: The average velocity distribution at a rotational speed 2400 rev/min, a pressure differences 700 millibars and for different clearances.

Table 5.12 and figure 5.44 illustrate that there are apparent differences in the maximum velocity. It can be observed that the maximum velocity increases as centre clearance increases which recorded 521.07 m/s, 504.75 m/s, and 508.46 m/s for centre gaps of 0.3 mm, 0.34 mm, and 0.38 mm respectively. Also, it can be seen in this figure that the maximum velocity increase from the inlet to outlet until it approaches the maximum value at (P5), the maximum velocity after that declines and rises slightly when the tip is in between P5 and P7. However, the maximum velocity after (P7) decreases towards the outlet zone until stabilising.

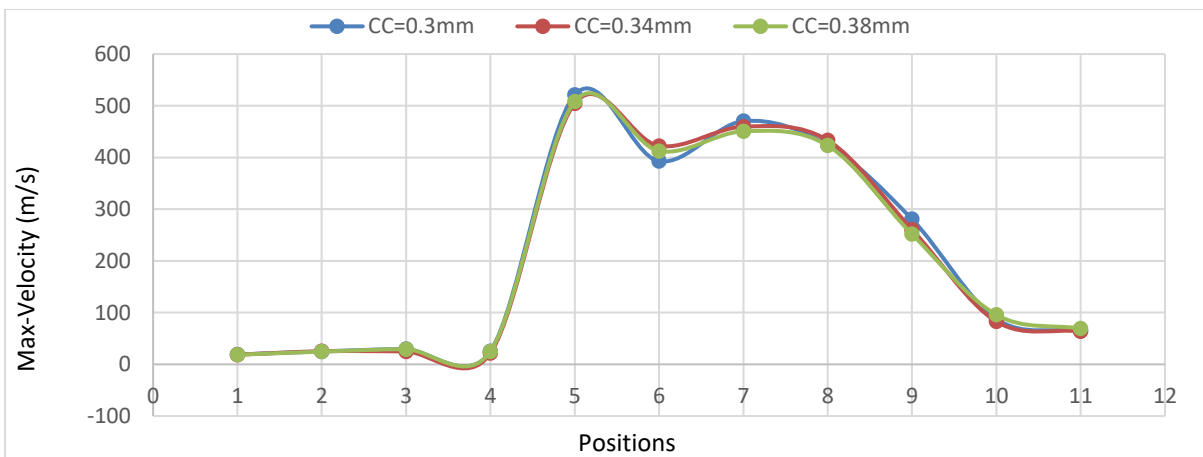


Figure 5.44: The Maximum velocity distribution at a rotational speed 2400 rev/min, a pressure differences 700 millibars and for different centre clearances.

Furthermore, according to previous analysis, concerning the velocity variations in the blower, the results have presented that centre clearance size has a considerable influence on the variation and the distribution of the velocity which the average and the maximum velocities increase as centre clearances increase.

The physical significance of the velocity in the blower that any increase of the velocity above the acceptable level will affect the reliability and performance of the blower which may lead to increase of vibration and noise in the blower system. Also, an extreme increase of velocity may affect the foundation of the blower system which may lead to failure of the blower system. Moreover, the size of centre clearance is one of the main factors affect the velocity, any increase or decrease of centre clearance more than acceptable size will lead to extreme velocity within the blower.

## **5.6. Establish the non-dimensional relations between different geometrical and flow related parameters of Root blower**

Parametric studies have been carried out to demonstrate the effect of geometrical and operational variables on blower performance in this chapter. This will help in deciding the relationship between different variables like pressure ratio, mass flow rate and rotor diameter, rotational speed etc. Using the characteristic curve concept is one of the methods to describe these relationships. The characteristic curve is a graph which, expresses the variation of pressure ratio according to the rotational speed of the rotor and describing the relationship between some typical parameters of the blower such as flow rate vs pressure ratio, flow rate vs efficiency, flow rate vs power.

Analytical performance prediction can play an essential role in a Roots blower design. Using this method can roughly guess the blower performance before a design and a construction.

The dimensionless analysis carried out had the objective of developing the relationships for estimating and predicting the blower performance, so that these results may be applied to any blower with the same rotor shape.

The result of mass flow rate, pressure and temperature that have been obtained from the CFD simulation on the Roots blower model have been presented in this chapter. The process for analysing the result from numerical calculation have been presented. The main operational

parameters included in this analysis are; Rotational speed, suction and discharge temperatures, suction and discharge pressures, pressure ratios, and temperature ratios.

### 5.6.1. Mass flow rate analysis

Numerical simulations have been performed at different pressure differences or pressure ratios, different rotational speeds and different tip and centre clearances. The non-dimensional relations between some operational parameters of the Roots blower has been illustrated in Figures 5.45 to 5.50. It is concluded that the flow coefficient or the mass flow rate is increased as blower speed rises and declines with an increase of pressure coefficient or pressure ratio. Also, the mass flow rate is increased too with finer tip clearance (TC) (the gap between the rotors and the cylinder). Moreover, the effect of clearance is raised when the rotational speed declined as shown in figures 5.47 to 5.49. Furthermore, it can be seen that the effect of rotational speed on the mass flow rate is more apparent than the effect of the clearance size and pressure difference. These are due to that leakage rate is increasing as tip clearance increase and at high levels of pressure differences or pressure ratios as shown in figure 5.50.

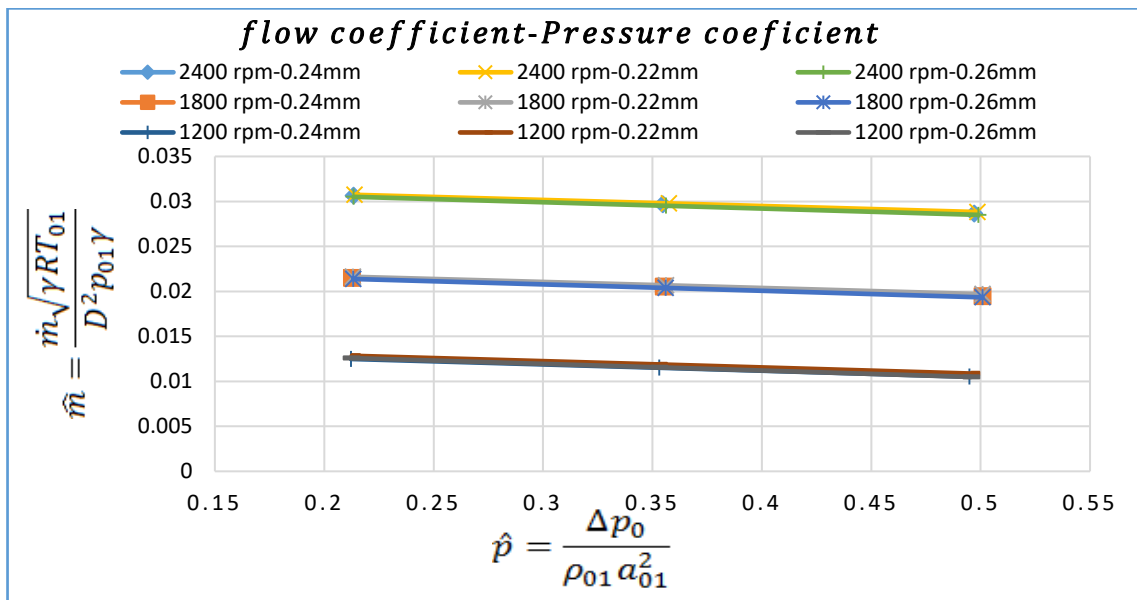


Figure 5.45: Deviation of the mass flow rate coefficient of the blower with a pressure coefficient at different speeds and for different tip clearances

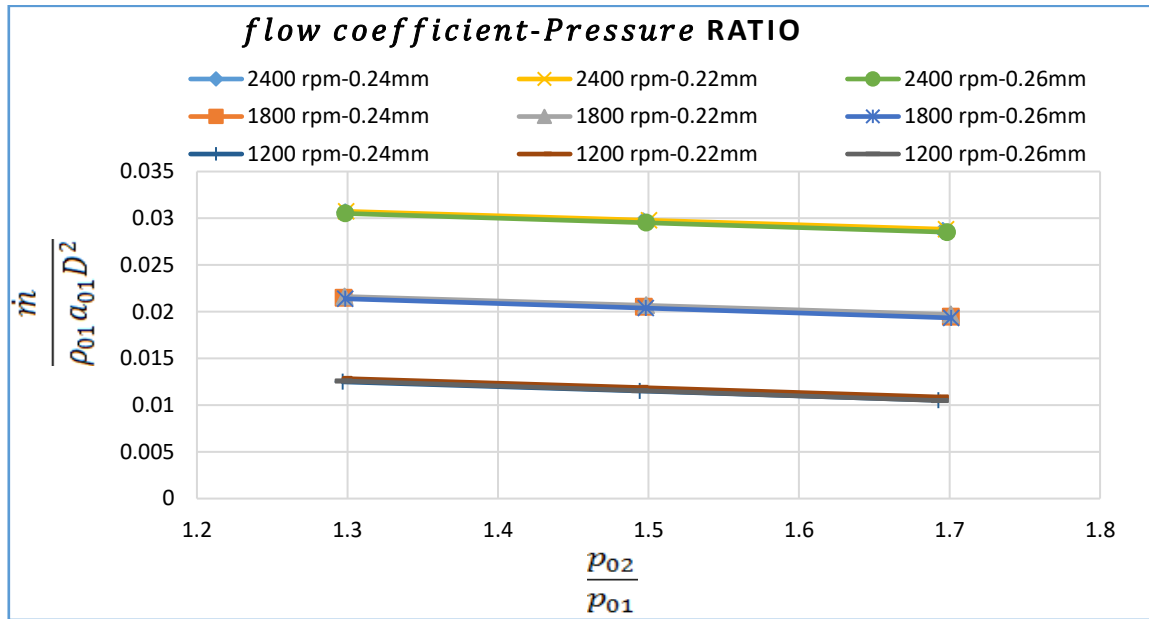


Figure 5.46: Deviation of the mass flow rate coefficient of the blower with a pressure ratio at different speeds and for different tip clearances

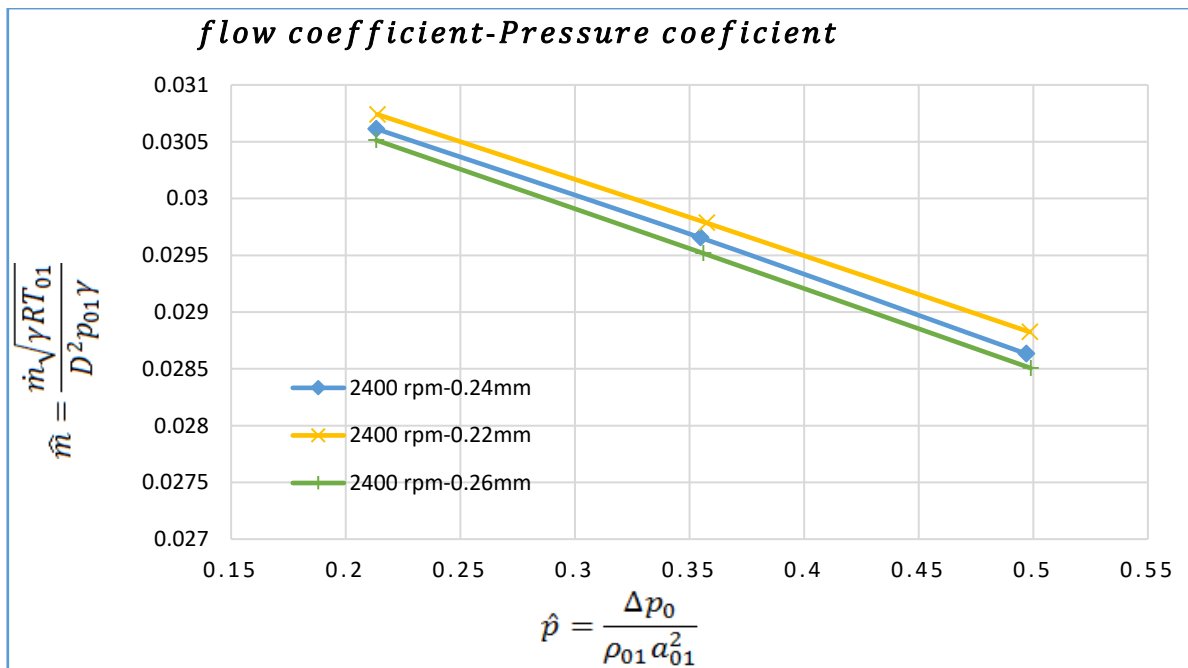


Figure 5.47: Deviation of the mass flow rate coefficient of the blower at a rotating speed 2400 rev/min, with different pressure coefficients and for different tip clearances

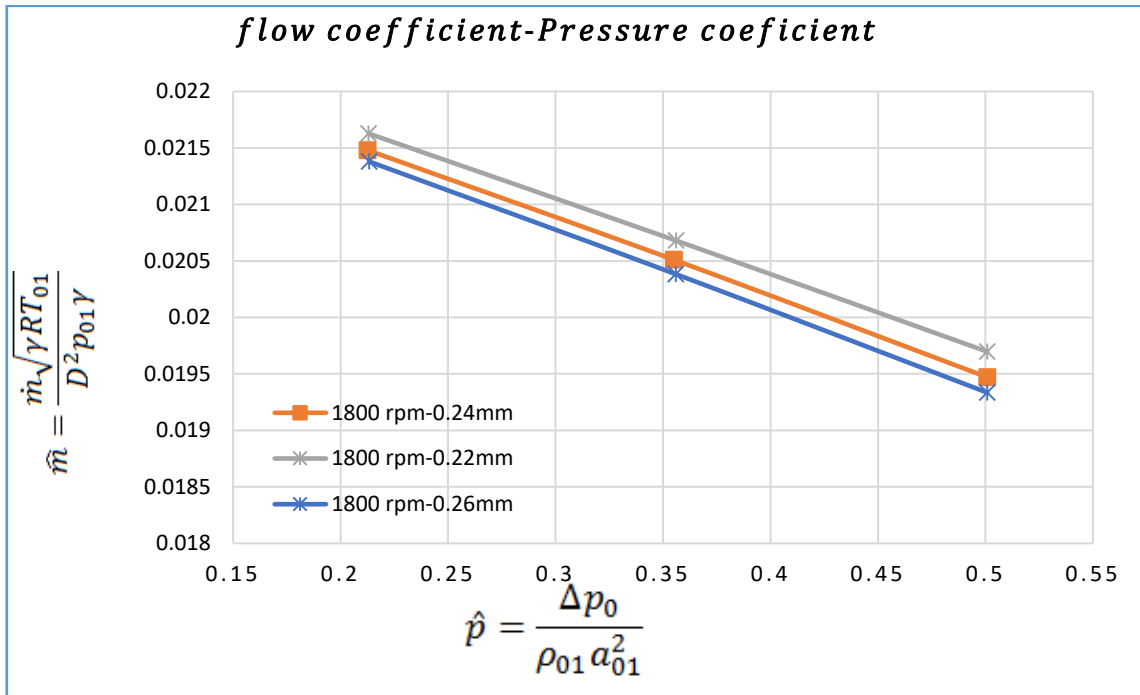


Figure 5.48: Deviation of the mass flow rate coefficient of the blower at a rotating speed 1800 rev/min, with different pressure coefficients and for different tip clearances

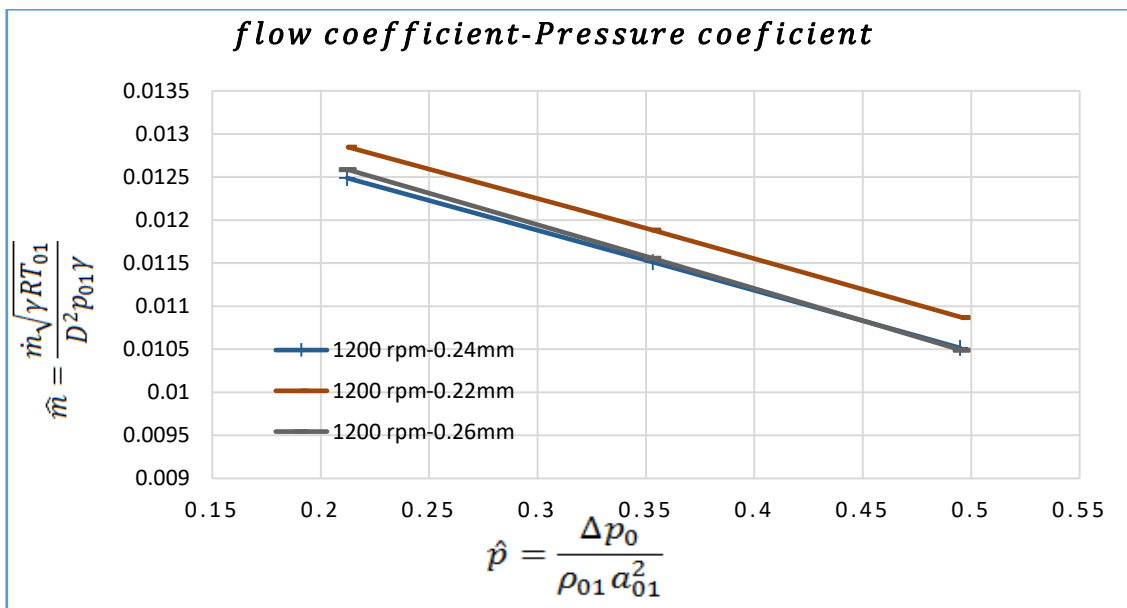


Figure 5.49: Deviation of the mass flow rate coefficient of the blower at a rotating speed 1200 rev/min, with different pressure coefficients and for different tip clearances

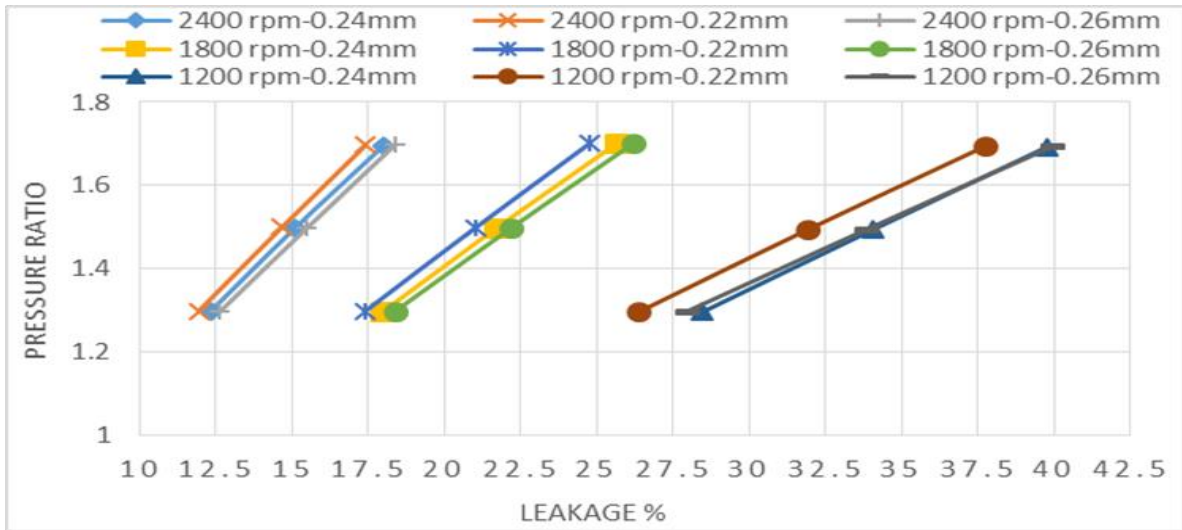


Figure 5.50: The relation between the leakage flow rate of the blower with different pressure ratios at different speeds and for different tip clearances (TC).

Furthermore, the same trend has been highlighted that the mass flow rate is increased with decrease the centre clearance (CC), (the gap between the two rotors) as shown in figure 5.51. These are due to that leakage rate is increasing as tip or centre clearance increase and at high levels of pressure differences or pressure ratios as shown in figure 5.52.

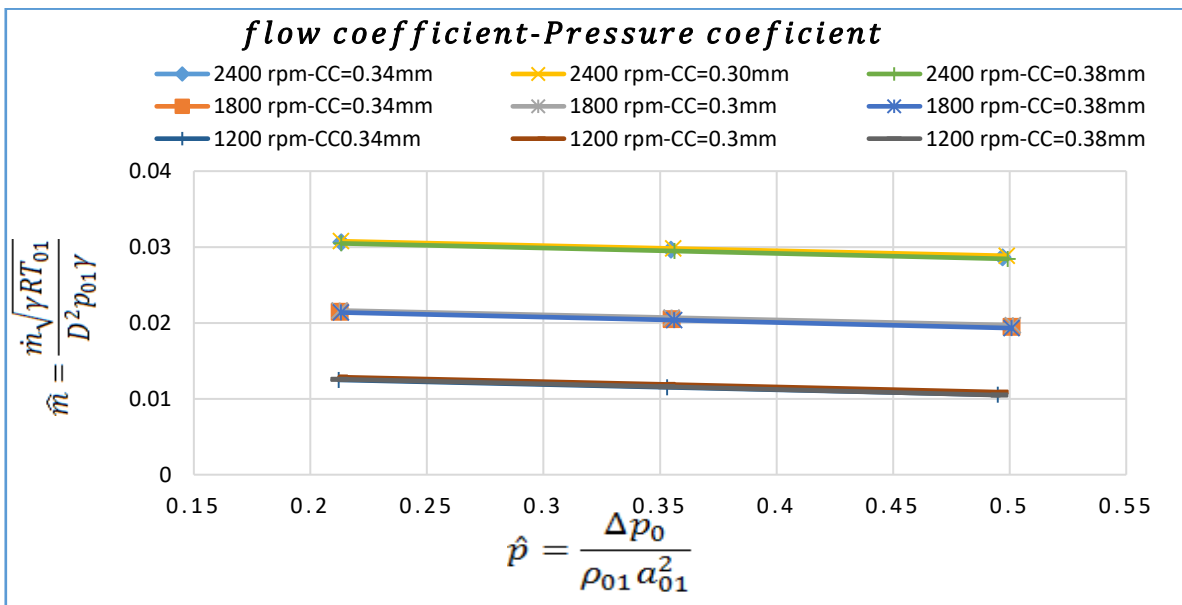


Figure 5.51: Deviation of the mass flow rate coefficient of the blower with different pressure coefficients at different speeds and for different centre clearances (CC).

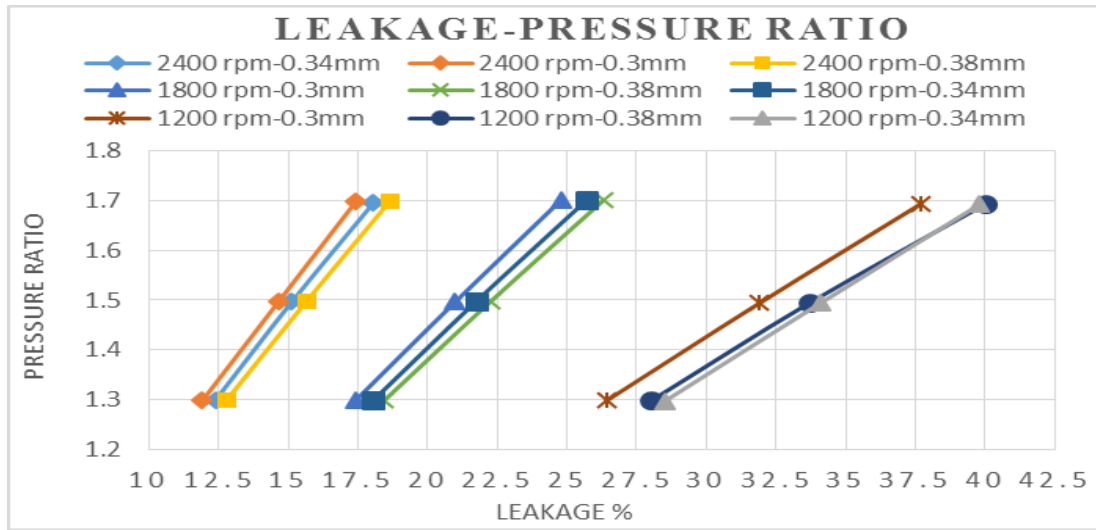


Figure 5.52: The relation between the leakage flow rate of the blower with different pressure ratios at different speeds and for different centre clearances (CC).

### 5.6.2 Volumetric efficiency

The blower’s volumetric efficiency at different working conditions is shown in Figure 5.53. It is concluded that the blower’s volumetric efficiency rise when blower speed rises and pressure declines and vice versa. This influence is due to that the rise of pressure loss across the internal gaps increase the leakage flow which causes the volumetric efficiency of the blower to decrease.

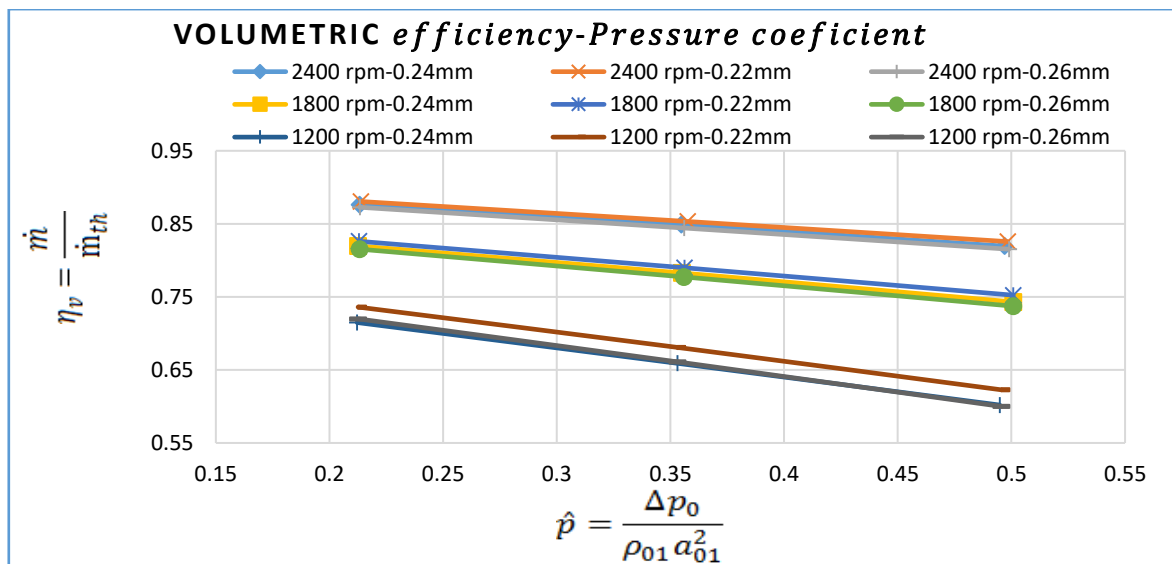


Figure 5.53: The variation of the blower volumetric efficiency with a pressure coefficient at different speeds and different tip clearances

The declines in the volumetric efficiency of the blower are due to that increase in pressure differences, or pressure ratios will enhance the leakage and consequently, reduce the efficiency. Figure 5.53 illustrated that Improvement of volumetric efficiency could be achieved by rising the speed or lowering pressure differences or combination between both. Also, volumetric efficiency can be increased by a decrease of the tip clearance. Furthermore, a similar trend has been highlighted that volumetric efficiency is increased with a decrease in the centre clearance (CC) as shown in figure 5.54.

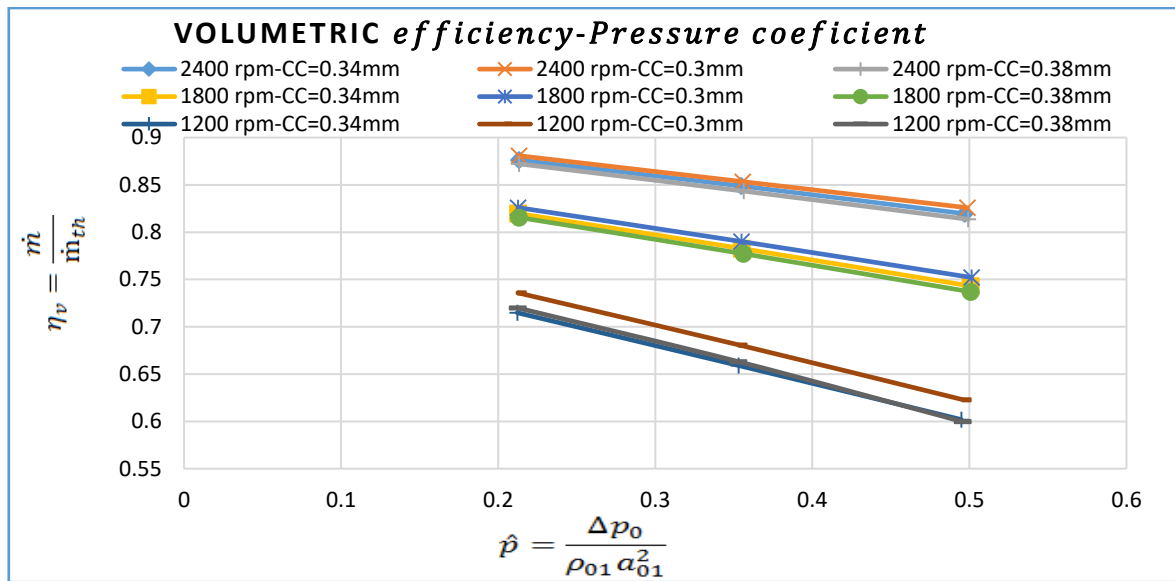


Figure 5.54: The variation of the blower volumetric efficiency with a pressure coefficient at different speeds and different centre clearances (CC)

### 5.6.3 Adiabatic Efficiency

The calculations for adiabatic efficiency has been done at different conditions. The effect of pressure on adiabatic efficiency with different operational gas conditions at a different speed is shown in Figure 5.55. The increase in adiabatic efficiency is due to the rise in volumetric efficiency which reduces the real work consumed per unit mass of gas. It has been observed too from the curves that adiabatic efficiency illustrates the highest values at low-pressure differences or pressure ratios. The reason is that adiabatic efficiency increases with the rise of speed and decrease in pressure ratio and also, the other reason is that mass flow rate of the blower increases with speed and declines at higher pressure ratios, which causes a reduction in volumetric efficiency and therefore decreases the adiabatic efficiency. Also, efficiency can be

increased by the decrease of the tip clearance (TC). Furthermore, the same trend has been emphasised that efficiency is increased with decrease the centre clearance (CC), as presented in figure 5.56

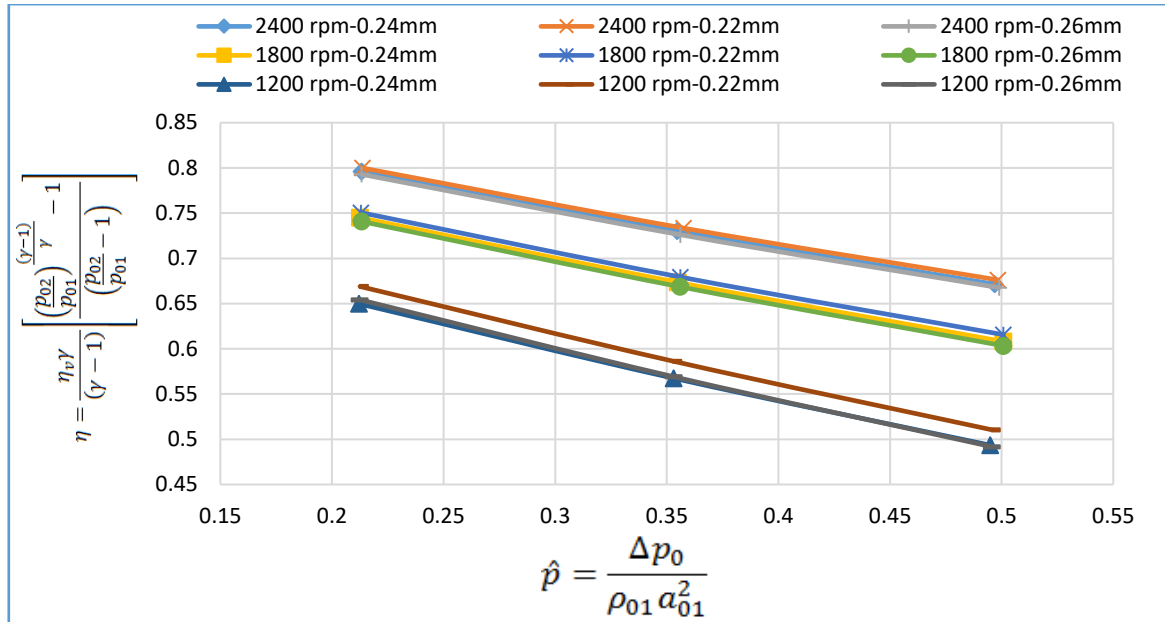


Figure 5.55: Variation of the adiabatic efficiency of the blower with a pressure coefficient at different speeds and different tip clearances

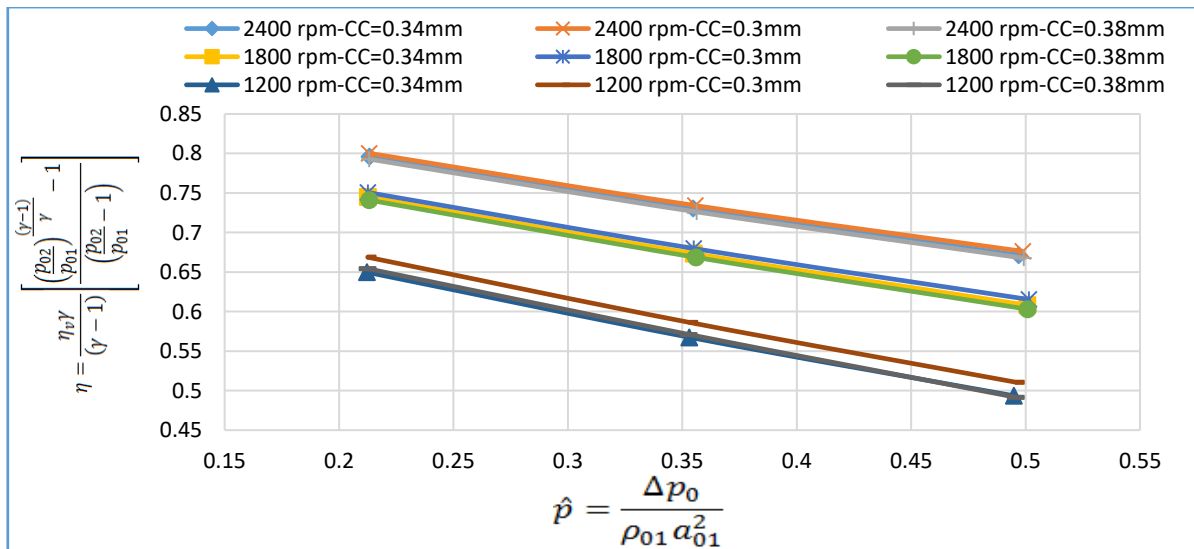


Figure 5.56: Variation of the adiabatic efficiency of the blower with a pressure coefficient at different speeds and different centre clearances

### 5.6.4 Power consumption

The specific power consumption of the blower with pressure coefficient at a different rotational speed and different tip clearances are shown in Figures 5.57. It may be observed that it is higher with increasing pressure ratio. It may be concluded that power consumption increases with the rise of speed and decrease in pressure ratio. Also, power consumption is very slightly affected by a small decrease of the tip clearance (TC). Furthermore, the same tendency has been presented which power consumption is very slightly influenced with the centre clearance (CC) too as presented in figure 5.58.

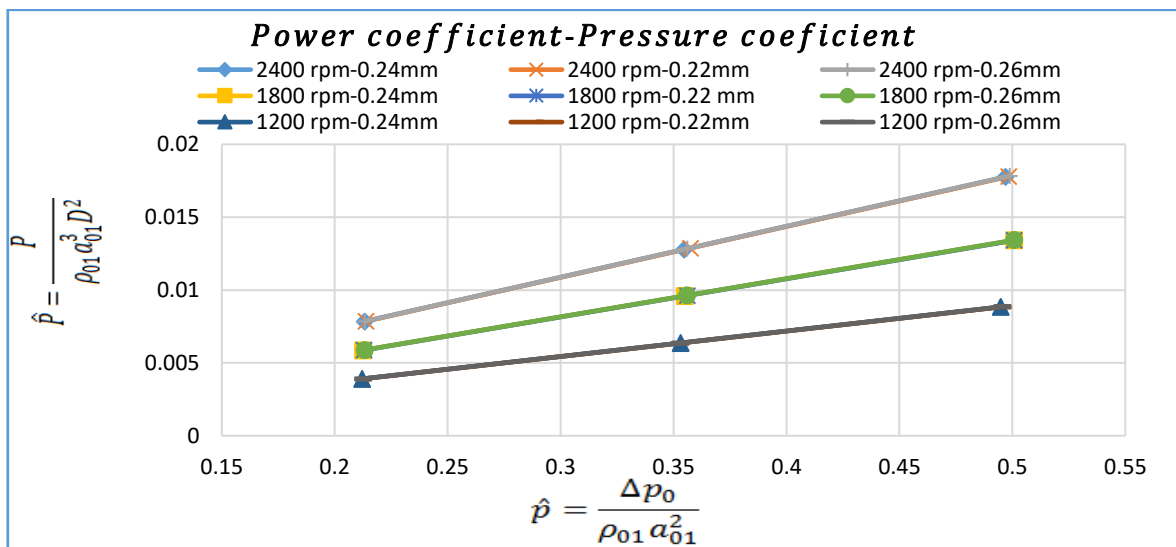


Figure 5.57: Variation of power coefficient of the blower with a pressure coefficient at different speeds and different tip clearances.

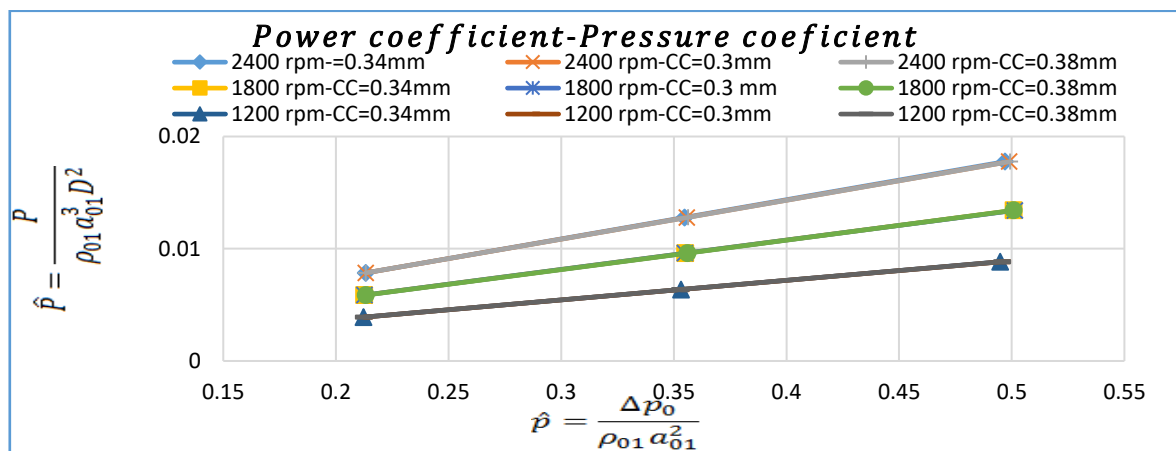


Figure 5.58: Variation of power coefficient of the blower with a pressure coefficient at different speeds and different centre clearances.

## 5.7. Deriving semi-empirical equations depending on non-dimensional relations between different geometrical and flow related performance parameters

This section concerning some semi-empirical equations have been developed for Roots blower under investigation by using the multi-regression analysis method and may be applied to any Roots blower with the same rotor shape. The semi-empirical prediction equations can play an essential role in a Roots blower design. Using this method can roughly guess the blower performance before a design and a construction.

The full entire process to form the non-dimensional variables have been discussed and presented in chapter 4.

### 5.7.1 Development an equation to predict mass flow rate within Roots blower

Based on the data presented in Table A4.1 in Appendix A4, and using multiple variable regression analysis a semi-empirical equation to predict the mass flow rate of working fluid through the Roots blower has been developed. This correlation is a function of the impeller Mach number, impeller speed, pressure ratio and clearance ratio. Using this semi-empirical prediction equation can roughly estimate the mass flow rate of the blower and therefore can guess their performance before the start of the process for the design and the construction. Also, can decrease the time and the cost of these process.

$$\frac{\dot{m}\sqrt{\gamma RT_{01}}}{D^2 p_{01} \gamma} = 10^{-0.451} * \left(\frac{ND}{a_{01}}\right)^{1.352} * \left(\frac{p_{02}}{p_{01}}\right)^{-0.418} * \left(\frac{TC}{CC}\right)^{0.0186}$$

$$\dot{m} = 10^{-0.451} * \left(\frac{D^2 p_{01} \gamma}{\sqrt{\gamma RT_{01}}}\right) * \left(\frac{ND}{a_{01}}\right)^{1.352} * \left(\frac{p_{02}}{p_{01}}\right)^{-0.418} * \left(\frac{TC}{CC}\right)^{0.0186} \dots\dots\dots (5.1)$$

Where,

N = Rotational speed (rad/s)

D = Rotor diameter (m)

TC = Tip clearance (m)

CC = Centre clearance (m)

Figure 5.59 depicts the comparison between the mass flow rate in the Roots blower obtained by CFD and by prediction equation (5.1). It can be concluded that the result from CFD experiences and prediction equation have the same trend and they are consistent. Here, the prediction correlation has been developed here represent the mass flow rate of operating fluid in the Roots blower in reasonable accuracy with differences of less than 5.8%. The mean advantage of this formula is to help in the prediction of the mass flow rate of Roots blower, to avoid unnecessary prototypes and to decrease development time.

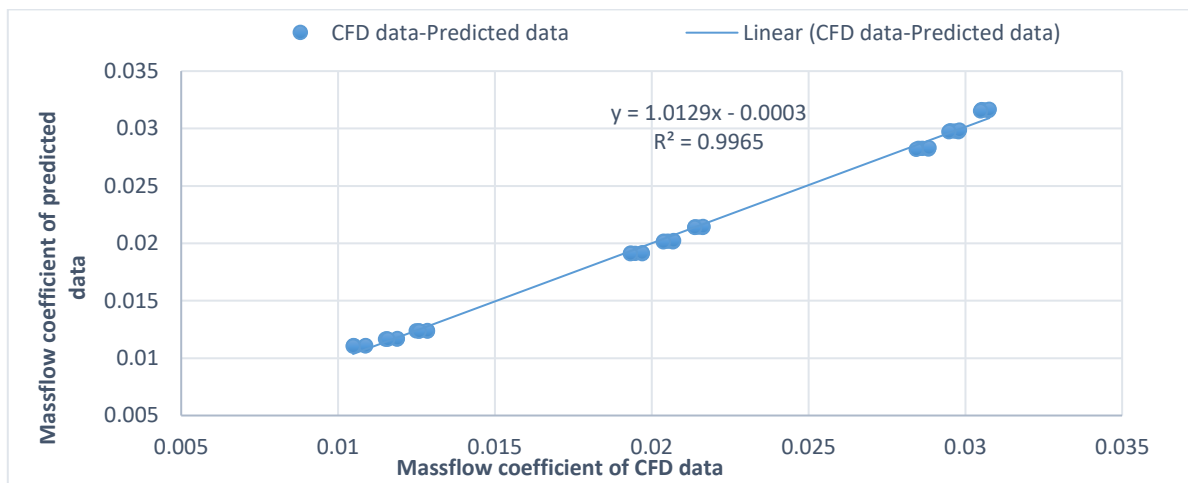


Figure 5.59: The comparison between CFD data and predicted equation of mass flow rate

### 5.7.2 Develop semi-empirical correlation to predict the volumetric efficiency of Roots blower

The volumetric efficiency at different working gas conditions (at different pressure ratios and rotational speeds) and different tip and centre clearances have been obtained from numerical results of different Roots blower model simulations. Based on the data presented in Table A4.2 in Appendix A4, and using multiple variable regression analysis, the semi-empirical equation to predict the volumetric efficiency of working fluid through the Roots blower, has been developed. This correlation is a function of the impeller Mach number, impeller speed, pressure ratio and clearance ratio. The formula is given below:

$$\eta_v = 10^{0.266} * \left(\frac{p_{02}}{p_{01}}\right)^{-0.418} * \left(\frac{ND}{a_{01}}\right)^{0.352} * \left(\frac{TC}{CC}\right)^{0.0163} \dots\dots\dots (5.2)$$

The correlation above has been tested and compared with numerical results which are consistent and provided a good match. Therefore, the prediction equation developed here for volumetric efficiency of Roots blower in reasonable accuracy with differences of less than 6.4% as shown in figure 5.60. The main benefit from this formula is to help in the prediction of volumetric efficiency of Roots blower, to reduce development time and to avoid unnecessary prototypes.

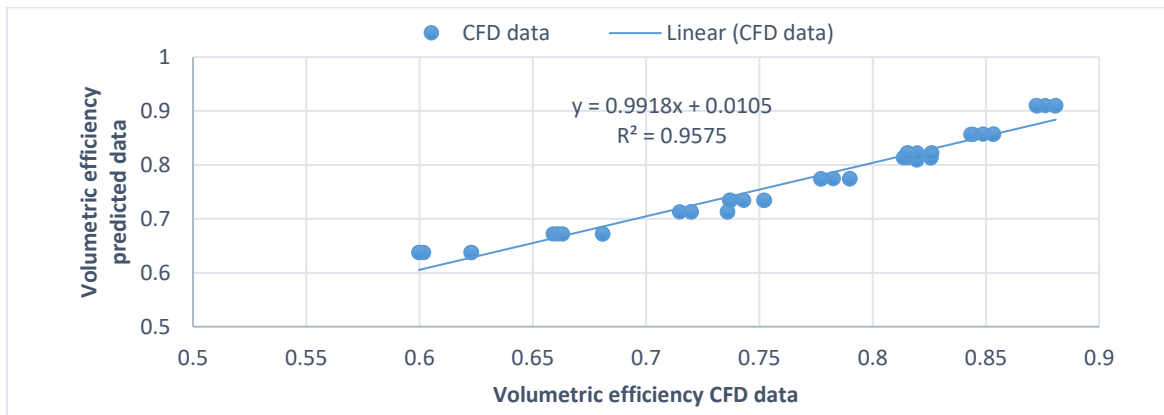


Figure 5.60: Comparison between CFD data and the predicted equation of volumetric efficiency

### 5.7.3 Develop semi-empirical correlation to predict the efficiency of Roots blower

The blower efficiency at different working gas conditions and the different tip and centre clearances have been obtained from numerical results of different Roots blower model simulations is investigated and analysed. Also, based on the data presented in Table A4.3 in Appendix A4, and by using multiple variable regression analysis, a semi-empirical equation to predict the efficiency of Roots blower, has been developed. This correlation is a function of the impeller Mach number, impeller speed, pressure ratio and clearance ratio. The formula is given below:

$$\eta = 10^{0.269} * \left(\frac{p_{02}}{p_{01}}\right)^{-0.805} * \left(\frac{ND}{a_{01}}\right)^{0.352} * \left(\frac{TC}{CC}\right)^{0.0163} \dots\dots\dots (5.3)$$

The correlation above has been tested and compared with numerical results which are consistent and provided a good match. Therefore, the prediction equation developed here for volumetric efficiency of Roots blower in reasonable accuracy with differences of less than 6.0% as shown in figure 5.59. The mean benefit from this formula is to help in the prediction of the efficiency of Roots blower, to decrease Roots blower development time and to avoid unnecessary prototypes.

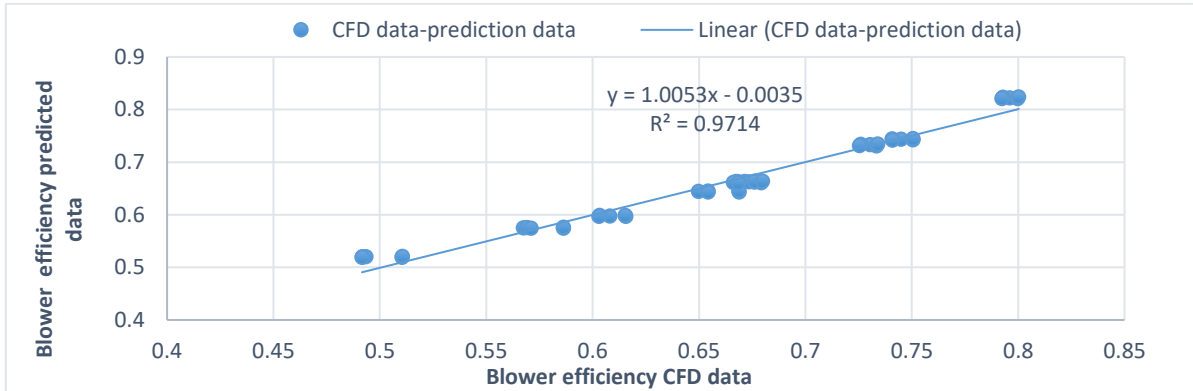


Figure 5.61: Comparison between CFD data and predicted equation data of efficiency

### 5.7.4 Develop an equation to predict the power consumption of Roots blower

Based on the data presented in Table A4.4 in Appendix A4 and using multiple variable regression analysis, a semi-empirical equation to predict the power consumption of the Roots blower has been developed. This correlation is a function of the impeller Mach number, impeller speed, pressure difference, inlet sound speed and density of working fluid.

$$\frac{P}{\rho_{01} a_{01}^3 D^2} = 10^{-0.720} * \left(\frac{\Delta p_0}{\rho_{01} a_{01}^2}\right)^{0.964} * \left(\frac{ND}{a_{01}}\right)^{0.999} * \left(\frac{TC}{CC}\right)^{0.00334}$$

$$P = 10^{-0.732} * \rho_{01} a_{01}^3 D^2 * \left(\frac{\Delta p_0}{\rho_{01} a_{01}^2}\right)^{0.964} * \left(\frac{ND}{a_{01}}\right)^{0.999} * \left(\frac{TC}{CC}\right)^{0.00334} \dots\dots\dots (5.4)$$

Figure 5.60 depicts the comparison between CFD data and predicted data from Equation (5.4) For the power consumption of Roots blower. It can be seen that the data from CFD experiments and predicted data from equation have the same trend and there is a good agreement between them. Hence, the prediction equation developed here represent power consumption of Roots

blower in reasonable accuracy with errors less than 1.0%. This semi-empirical prediction equation can roughly estimate the power required by the blower and therefore can guess their efficiency before the design process. Also, can decrease the time and the cost of these process and avoid unnecessary prototypes and decrease the time of development.

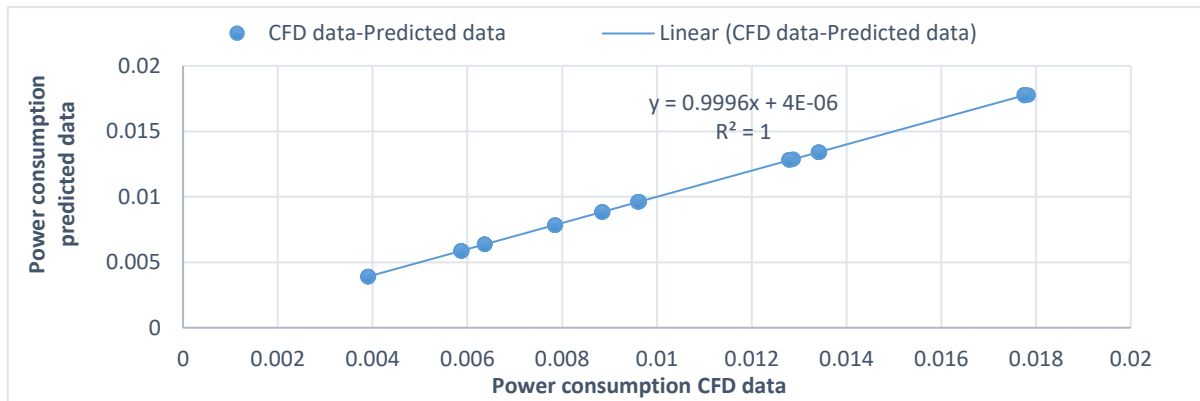


Figure 5.62: The comparison between CFD data and predicted equation data of power consumption

## 5.8 Conclusion summary

The CFD (FLUENT) approach with Dynamic Mesh method have been used in the present investigation to achieve inclusive knowledge related to the flow characteristics of the Roots blower. The research study provides a detailed information regarding geometric and flow related parameters such as, clearance size, velocity, pressure and temperature that may difficult to be achieved by experimental measurement. The analysis of numerical results in the current research prove that the clearances inside the blower could affect considerably on the performance of the blower.

According to the previous in-depth analysis regarding the effect of tip clearance size and centre clearance size (the gap between rotors and casing and the gap between the driving rotor and the driven rotor) on the flow field in Roots blower. It can be concluded that both tip and centre clearance sizes have a considerable influence on the variation and the distribution of the pressure, the temperature, mass flow rate, and velocity. It can be concluded that:

- The mass delivery, specific power and efficiencies decrease with the increase of tip and centre clearance sizes because the effect of backflow increase which lead to rise of gas leakage and therefore declines the volumetric efficiency.

- The result depicts that decreasing the tip and centre clearance sizes will improve the volumetric efficiency. Also, the volumetric and adiabatic-efficiency characteristics are influenced by the internal leakage which increases with the increase of the tip and centre clearance sizes
- The losses dependent on tip and centre clearance sizes
- The pressure and their amplitude of fluctuation in the suction and the discharge zones are increased as the tip and the centre clearance sizes decrease. Also, the maximum positive and negative pressures and their amplitudes are increased with the decrease of tip and centre clearance sizes.
- The average mass flow rate declines as tip and centre clearance sizes increase. Also, the amplitude of mass flow at the blower suction grows up as tip and centre clearance sizes decrease, meanwhile the amplitude of mass flow at the blower discharge mostly rises with the increase of tip and centre clearance sizes.
- The temperature and their amplitude of fluctuations increase as tip and centre clearance sizes increase. Moreover, the maximum and the minimum temperatures rise as tip and centre clearance sizes increase.
- The average and the maximum velocities increase as tip and centre clearance sizes decrease. Also, the fluctuation of velocity repeats itself every  $90^{\circ}$  angles with respect to the vertical line at the centre of the impeller in the blower.

Furthermore, from the above numerical analysis and based on above discussion, it can be concluded that the analysis of transient numerical simulation results using the CFD approach with dynamic mesh technique (DMT) can predict an accurate result and provide useful information regarding the effect of geometrical variation on the flow field and the performance of the Roots blower.

The analysis has been carried out in this chapter for in-depth understanding the influence of different tip and centre clearance sizes on the variation and the distribution of flow-related parameters within Roots blower such as pressure, temperature, and velocity and therefore on Roots blower performance. In addition, the prediction models have been developed for outlet temperature, mass flow rate, efficiency, and power which dictate the design process of Roots blower. Moreover, analysis and discussions in detail of the influence of unsteady flow characteristics and different configurations of gap sizes on flow field behaviour and blower performance using 3D CFD numerical analysis will be included in the next chapter.

## **CHAPTER 6**

### **Quantitative evaluation of unsteady flow characteristics and comparative analysis with clearance variation inside the Roots blower**

As presented in the chapters above the blower operational parameters (rotational speed and pressure difference) and the geometrical parameters (Tip and Centre clearances) have a considerable influence on flow field behavior and performance of the blower under different conditions. The literature review showed that the 2-D model gave a reliable accuracy in the results regarding mass flow, pressure, temperature distribution, but less accurate to predict the velocity field (Kang & Vu, 2014; Y. Liu et al., 2015; S.-K. Sun et al., 2017). The flow within the Roots blower is complex and different concerns have risen in association with the behaviour of the flow pattern inside the blower (Choi, 2013; S. Sun et al., 2017; ZHANG, WANG, HAN, & SUN, 2011). It requires further investigations and analysis under different operating conditions and clearance sizes.

Accordingly, 3D computational fluid dynamics models have been developed and used in this chapter concerning to more in-depth analysis of the effect of clearances size on Roots blower performance. A detailed qualitative and quantitative analysis has been conducted using three different combinations of tip and centre clearances under different rotational speeds and pressure loading conditions.

Also, pressure fluctuations in both time and frequency domain, at choosing points inside the blower, have been investigated and analysed. Moreover, to prove that improve the performance of this blower by decrease both tip and centre clearances is applicable, according to the outcome that have been obtained from the previous chapter.

Furthermore, the use of pressure and temperature fluctuations analysis in time and frequency domains as the detection index of clearances change have been examined. The results are presented and discussed in the following sections.

## **6.1 Establish the effect of the clearance sizes in order to develop a new clearance model of the Roots blower**

One of most essential factors, which has substantial effects on the Roots blower performance characteristics, is clearance sizes within the blower. In order to determine the optimum combination of clearances, several studies have been performed (Arai, Fukagawa, & Ohtsuka, 1990; Burmistrov, Belyaev, Ossipov, Fomina, & Khannanov, 2001; Fukagawa, 1991; Hwang & Hsieh, 2006; Joshi et al., 2006; Y. Kang et al., 2012; Türk & Verhülndonk, 2006; Valdès, Barthod, & Le Perron, 1999; Verma, 2014; Yao et al., 2005). The majority of these studies have shown that there is no optimum clearance arrangement yet, but depending on which the essential parameter in the application, for example, mass flow rate, differential pressure or noise...etc.

As discussed in the previous chapter, the backflow through gaps inside the blower plays a significant role in local pressure losses phenomenon in the blower. It is evident that adjustment of the gap could improve the performance of the blower. The 3D numerical analysis will provide detailed results suggesting an explanation about the effect of gap size by analysing the different combination of clearances in order to improve the performance of Roots blower. The foremost objective for this investigation is to carry out numerical calculations using advanced 3D CFD code, to determine the best clearances combination in order to improve the blower performance. Based on the 3D CFD model for a chosen set of boundary conditions, the detail numerical results regarding speed, temperature, pressure, and velocity of the Roots blowers under study have been analysed and described. Three revolutions of rotors have been simulated to ensure the simulation of the case reached the stable state.

In the following, the contours for the last working period will be visually analysed to explain these differences. The static pressure, velocity magnitude, temperature distributions, and pressure fluctuations in time and frequency domain have been performed to analyse the effect of clearance size on the performance of the blower. The blower model has been used for this study is HRBV613 Roots-type blower with an axial suction and an axial discharge ports. The rotor has two lobes with ‘involute’ profile. The blower model has been modified by changing the clearance sizes for comparative analysis. Three different models including baseline model have been developed using 3 D CFD techniques. The geometry classifications of these models

are shown in table 6.1. The operating speeds of the machine that have been used are 1200 rpm, 1800 and 2400 rpm under a discharge pressure 500 millibars.

Table 6.1: Roots blower models specifications

Specifications	Model 2 (M2) (Baseline model)	Model 1 (M1)	Model 3 (M3)
Casing radius	200.0065 mm	200.0065 mm	200.0065 mm
Rotor radius	123.66 mm	123.72	123.6 mm
Casing length	330.73 mm	330.73 mm	330.73 mm
Rotor length	329.73 mm	329.89 mm	329.57 mm
Length between centres	76.162 mm	76.162 mm	76.162 mm
Gearing plate gap	0.3176 mm	0.3176 mm	0.3176 mm
Bearing plate gap	0.1524 mm	0.1524 mm	0.1524 mm
Casing-Rotor (TC)	0.24 mm	0.18 mm	0.3 mm
Rotor-Rotor gap (CC)	0.34 mm	0.3 mm	0.38 mm
Suction Diameter	146.23 mm	146.23 mm	146.23 mm
Discharge Diameter	146.23 mm	146.23 mm	146.23 mm
Rotors profile type	Involute	Involute	Involute

### The mesh independence test of 3D model

The accuracy of the numerical results depends on the discretisation of the domain, which is known as the meshing process. The mesh independence is a critical stage because meshing can affect the accuracy of the CFD numerical results depending on the elements number. Table 6.2 and figure 6.1 summarise the numerical results of the mass flow rate for various mesh configurations. According to the results shown in Table 6.2 the percentage difference between the mass flow rate results of case 2 and 3 is small and negligible (0.055%).

Table 6.2: 3D model-Mass flow rate spatial discretisation results

Operating condition	cases	No. of elements	Mass flow rate (kg/s)	Percentage Difference (%)
1800 rev/min 500 mbar	Case1	1.20E+06	0.5321	1.305
	Case2	1.84E+06	0.5391	
	Case3	2.42E+06	0.5394	0.055

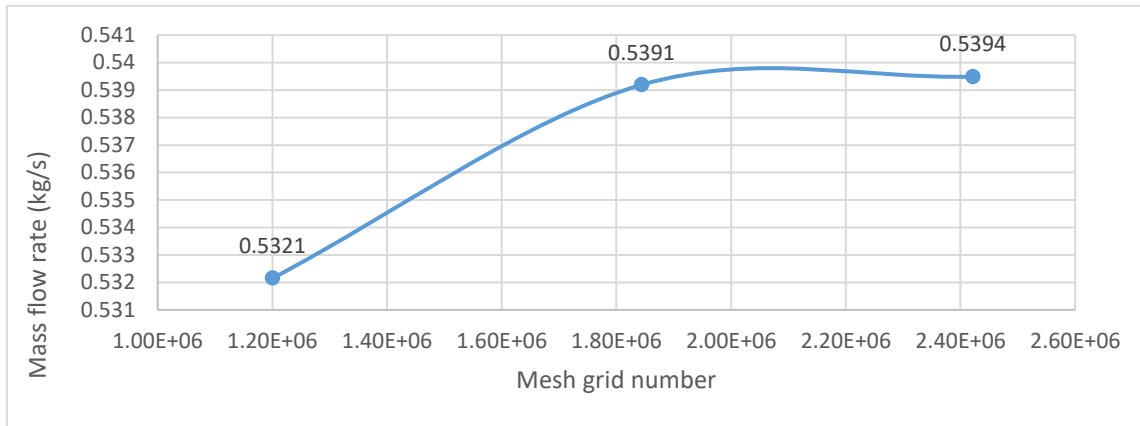


Figure 6.1: 3D model-Mass flow rate spatial discretization results

Table 6.3 and figure 6.2 summarise the numerical results of air temperature at outlet blower with multiple mesh configurations. This analysis has been conducted to ensure the numerical results are independent of the mesh quality. Also, the percentage difference between the Outlet temperature is small and negligible (-0.00948%).

Table 6.3: Outlet temperature spatial discretization results

Operating condition	cases	No. of elements	Outlet temperature (K <sup>0</sup> )	Percentage Difference (%)
1800 rev/min 500 mbar	Cas1	1.20E+06	340.28	0.27
	Case2	1.84E+06	341.20	
	Case3	2.42E+06	341.17	-0.0094

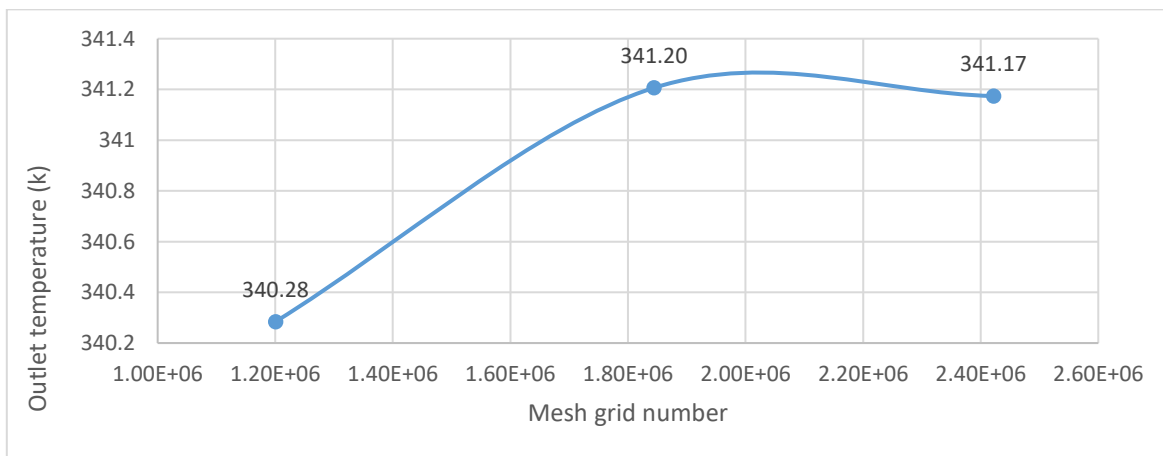


Figure 6.2: 3D model-Outlet temperature spatial discretisation results

Therefore, the mesh with  $1.84E+06$  elements has been considered in this investigation because it can capture the flow behaviour inside the Roots blower with good accuracy and to reduce the computation of the time and the cost as compared with the mesh with  $2.42E+06$  elements. Therefore, the mesh with lower elements has been used for further investigation. Moreover, the meshes for other Roots blower models have been determined by using same procedures.

### Monitoring Points within the Roots blower

Many monitoring points are set in the blower to investigate and develop a comprehensive understanding of performance characteristics and the pressure fluctuations within the Roots blower under various clearance models and for different operational conditions of the blower as shown in table 6.1. For this purpose, 11 points have been marked in the middle plan inside the blower, including 5 points inside the blower between the rotors and the casing which are set at every  $45^\circ$ , 2 points are set close to the edges of the suction and discharge regions. Also, 2 points are set at the inlet and 2 points at the outlet of the blower. The monitoring points are referred to as P1 to P11. Figure 6.3 depicts the distribution of the monitoring points within a Roots blower.

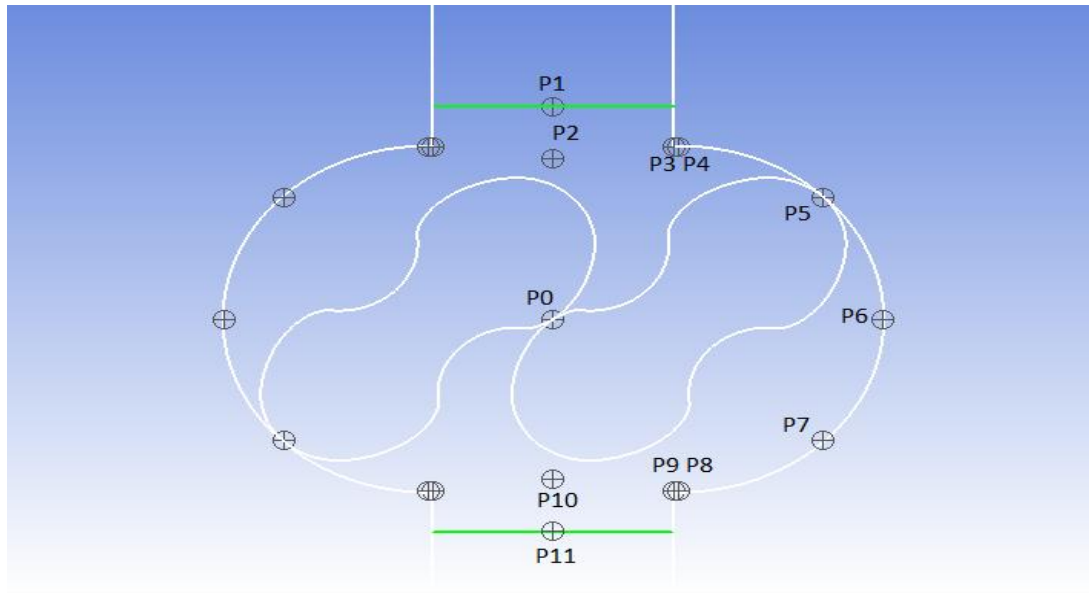


Figure 6.3: Number of points has been chosen inside the middle plane of 3D blower model for more depth analysis

### 6.1.1. Comparison analysis of the influence of different clearance models on pressure distributions

The contours of the pressure on the middle plane of the blower for the last revolution of the blower models under study obtained through numerical simulations at a speed 1800 rpm, a pressure difference 500 millibars are shown in figure 6.4.

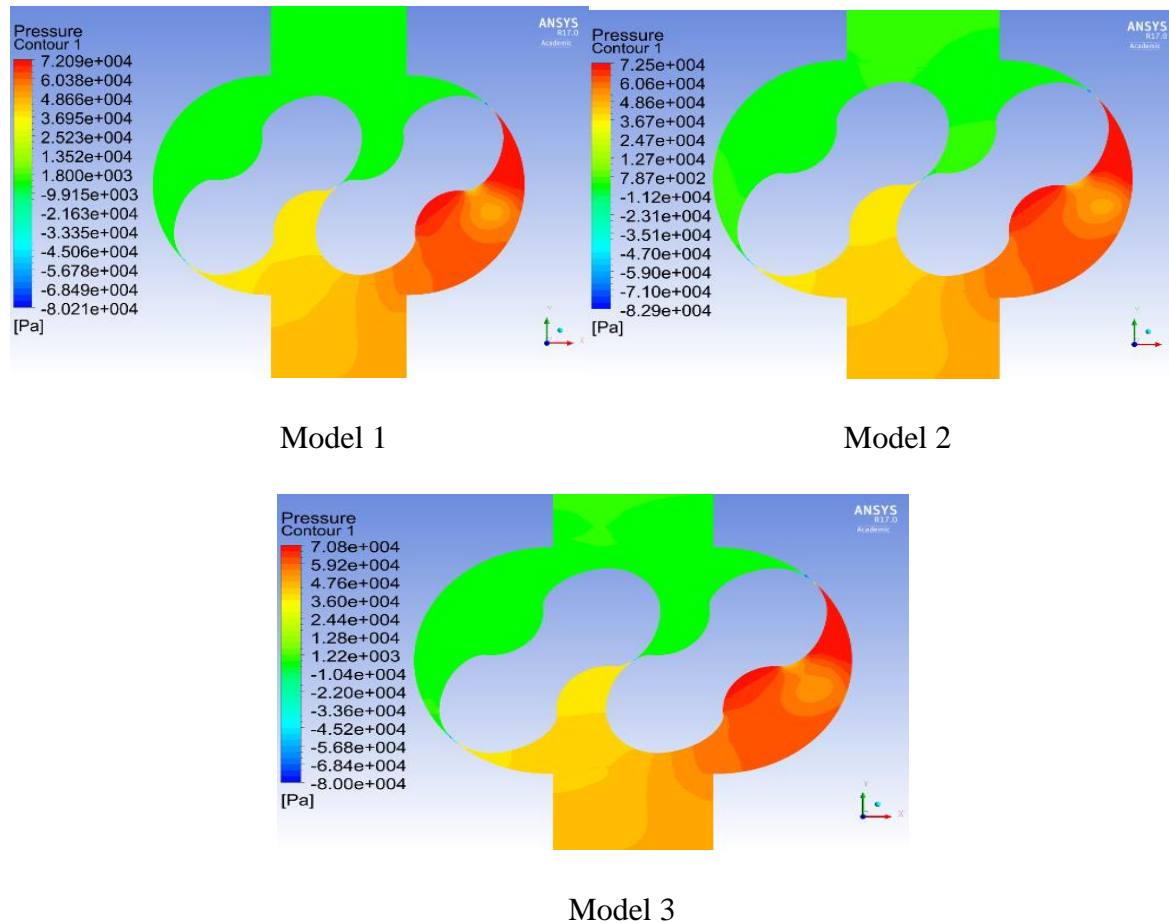


Figure 6.4: The static pressure contours at a speed 1800 rpm and a pressure difference 500 millibars for different blower models

Figure 6.4 depict the variation and the distribution of the static pressure. It can be seen that the pressure is gradually increased from the inlet zone towards the outlet zone within the blower. However, it is apparent from this figure that the lower pressure occurs inside clearances between the low-pressure region at the inlet side and the high-pressure region at the outlet side in the blower. Also, it is obvious that the distributions of static pressure at same rotational speed and under different model clearances have the same trend, but the areas of high pressure is effect of pressure are increased as the tip gap increase.

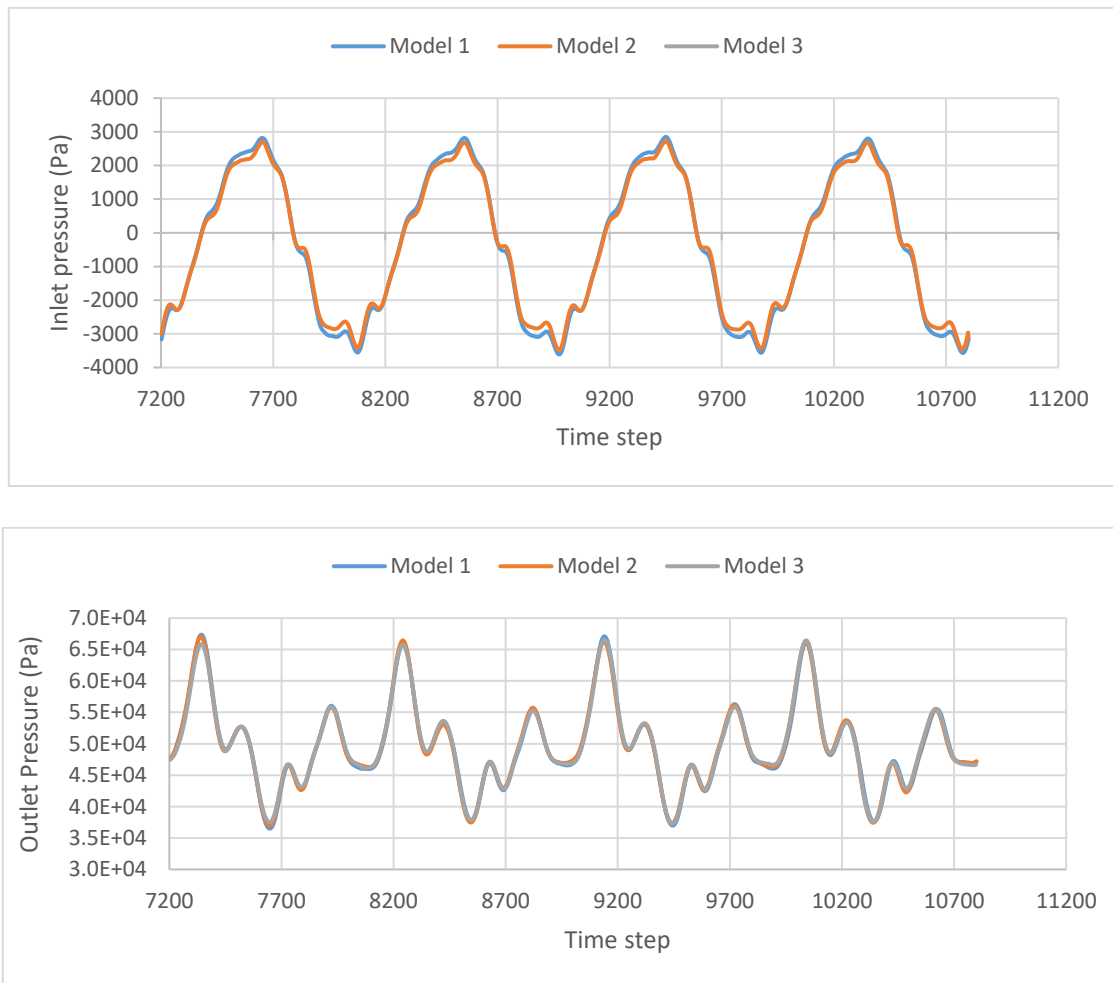


Figure 6.5: Pressure fluctuations at blower inlet and outlet at 1800 rpm, 500 millibars for different models clearances

Figure 6.5 depicts the instantaneous variation of static pressure at the inlet and the outlet of the blower of two-lobe over one revolution/cycle at different discharge pressures respectively. It can be seen that the pressure and fluctuations in the discharge of the blower are higher than that in the suction of the blower. Moreover, the pressure and the amplitude of model 1 are higher than the pressures and the amplitudes of the other two models which is more obvious in the inlet zone. The reason because the clearances inside model 1 are smaller than the clearances of other two models which decrease the effect of backflow and local pressure losses.

The statistical result of the average pressure variation at a speed 1800 rpm, a discharge pressure 500 millibars, and for different model clearances at various locations inside the blower from the inlet to outlet are presented in Table 6.4 and figure 6.6.

Table 6.4: The average pressure at 1800 rpm, 500 millibars for different model clearances.

Positions	$P_{ave}$ at model 1 (Pa)	$P_{ave}$ at model 2 (Baseline model) (Pa)	$P_{ave}$ at model 3 (Pa)
P1	-3.62E+02	-3.51E+02	-2.84E+02
P2	-3.57E+02	-4.27E+02	-4.87E+02
P3	-1.18E+03	-1.18E+03	-1.12E+03
P4	-1.10E+03	-1.03E+03	-9.72E+02
P5	2.95E+03	2.81E+03	2.69E+03
P6	1.78E+04	1.79E+04	1.78E+04
P7	2.94E+04	2.94E+04	2.92E+04
P8	4.10E+04	4.10E+04	4.05E+04
P9	4.07E+04	4.00E+04	4.06E+04
P10	5.06E+04	5.09E+04	5.09E+04
P11	4.97E+04	4.98E+04	4.98E+04
Head	5.01E+04	5.01E+04	5.01E+04

Table 6.4 and figure 6.6 depict that there are small variations of the average pressures for the three models. Also, the average pressure increase from the inlet to outlet until approaches the maximum values at the discharge region of the blower at point 10 (P10) which are 5.063E+04 Pa for model 1, 5.09E+04 Pa for model 2 and 5.093E+04 Pa for model 3 respectively. In comparison, the average pressure of all the models are approximately same.

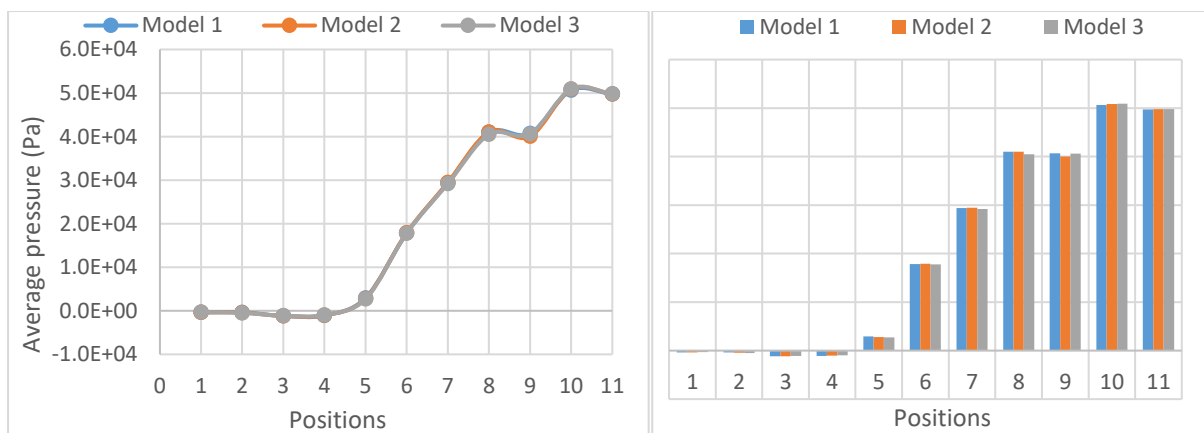


Figure 6.6: The distribution of average-pressure at 1800 rpm, 500 millibars and for different model clearances.

### 6.1.1.1 Comparison analysis of the average pressure variation between both 2D/3D baseline models

The statistical result of the average pressure variation at a speed 1800 rpm and a discharge pressure 500 millibars for both 2D and 3D baseline models at various locations inside the blower from the inlet to outlet are presented in Table 6.5 and figure 6.7.

Table 6.5: The average pressure in 2D/3D baseline models at 1800 rpm and 500 millibars.

Positions	P <sub>ave</sub> at 3D (Pa)	P <sub>ave</sub> at 2 D (Pa)	Error %
P1	1.01E+05	1.01E+05	-0.30
P2	1.01E+05	1.01E+05	-0.36
P3	1.00E+05	1.01E+05	-0.96
P4	1.00E+05	1.01E+05	-0.81
P5	1.04E+05	1.06E+05	-1.71
P6	1.19E+05	1.19E+05	0.52
P7	1.31E+05	1.31E+05	-0.29
P8	1.42E+05	1.42E+05	0.47
P9	1.41E+05	1.44E+05	-1.79
P10	1.52E+05	1.51E+05	0.52
P11	1.51E+05	1.51E+05	0.29

Table 6.5 and figure 6.7 show that there are small variations of the average pressures between 2D and 3D models which the maximum error between both models is 1.8 %. Also, it is obvious that the distributions of average static pressure have the same trend for two models

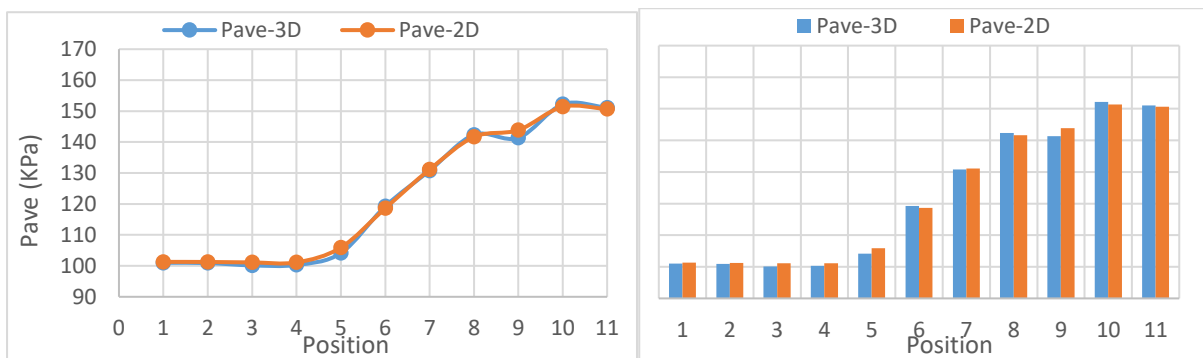


Figure 6.7: The distribution of average-pressures at 1800 rpm, 500 millibars in 2D/3D blower baseline models.

The statistical result of the maximum positive and negative pressures at a speed 1800 rpm, a discharge pressure 500 millibars, and for different model clearances at various locations inside the blower from the inlet to outlet are presented in Table 6.6 and figure 6.8.

Table 6.6: The maximum and the minimum pressures at 1800 rpm, 500 millibars for different model clearances in Pascal.

Positions	$P_{\max}$ at Model 1	$P_{\max}$ at Model 2 (Baseline model)	$P_{\max}$ at Model 3	$P_{\min}$ at Model 1	$P_{\min}$ at Model 2	$P_{\min}$ at Model 3
P1	2.8E+03	2.7E+03	2.6E+03	-3.6E+03	-3.5E+03	-3.2E+03
P2	3.3E+03	3.1E+03	2.7E+03	-3.8E+03	-3.8E+03	-3.7E+03
P3	2.9E+03	2.7E+03	2.5E+03	-5.8E+03	-5.9E+03	-5.5E+03
P4	3.0E+03	2.9E+03	2.9E+03	-5.8E+03	-5.5E+03	-5.6E+03
P5	5.5E+04	5.3E+04	5.2E+04	-7.9E+04	-7.9E+04	-7.9E+04
P6	7.7E+04	7.5E+04	7.4E+04	-6.6E+04	-6.8E+04	-7.1E+04
P7	7.2E+04	7.1E+04	7.0E+04	-6.9E+04	-6.9E+04	-7.2E+04
P8	7.0E+04	7.1E+04	7.0E+04	-5.4E+04	-5.7E+04	-5.9E+04
P9	6.8E+04	7.0E+04	6.9E+04	-4.1E+04	-4.2E+04	-3.7E+04
P10	6.9E+04	6.9E+04	6.8E+04	3.8E+04	3.9E+04	4.0E+04
P11	6.7E+04	6.7E+04	6.7E+04	3.7E+04	3.7E+04	3.7E+04

The data in table 6.6 and figure 6.8 show that the maximum pressures are increase from the inlet to outlet until approaches the maximum values when the tip of impeller is approximately at the middle region of the blower at point 6 (P6) which are 7.7E+04 Pa for model 1, 7.5E+04 Pa for model 2 and 7.4E+04 Pa for model 3 respectively. Also, the maximum pressure after point 6 starts to decline slightly towards the outlet zone till stabilising

In comparison, the maximum pressure of model 1 is higher than model 2 by 1.896% and model 3 by 2.96%. Because the effect of backflow and velocity are lower on model 1 than other two models and therefore the local pressure losses is lower.

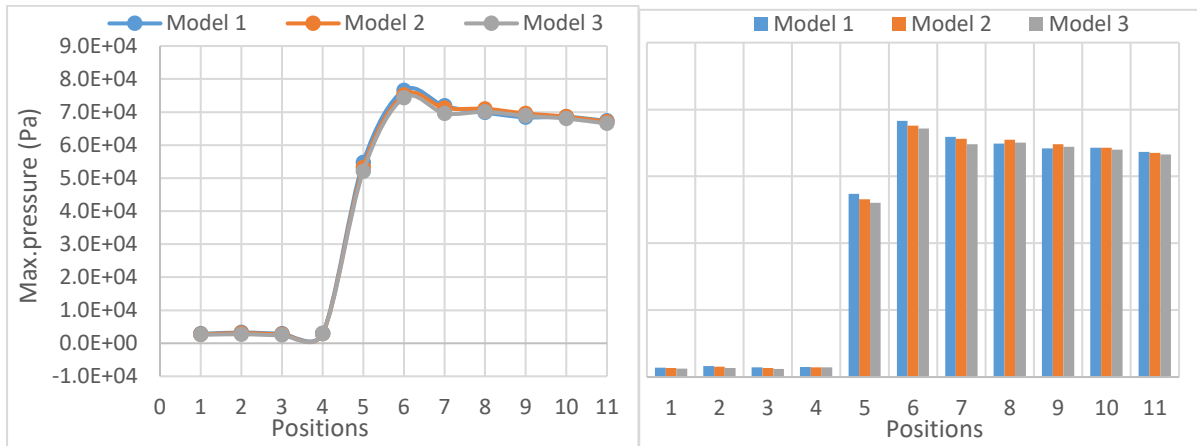


Figure 6.8: The distribution of maximum-pressures at 1800 rpm, 500 millibars and for different model clearances.

On the other hand, there are slight differences in maximum negative pressure as we can see in figure 6.9 and table 6.6. Moreover, the maximum negative pressures for the cases under investigation are located at point 5 (P5) inside the clearance at inlet zone. These pressures are  $-7.86E+04$  Pa for model 1,  $-7.92E+04$  Pa for model 2 and  $-7.94E+04$  Pa for model 3 respectively.

In comparison, the maximum negative pressure of model 1 is lower than model 2 by 0.78% and model 3 by 1.016%. Because the effect of backflow and velocity are higher on other two models than model 1 and therefore the local pressure losses is higher.

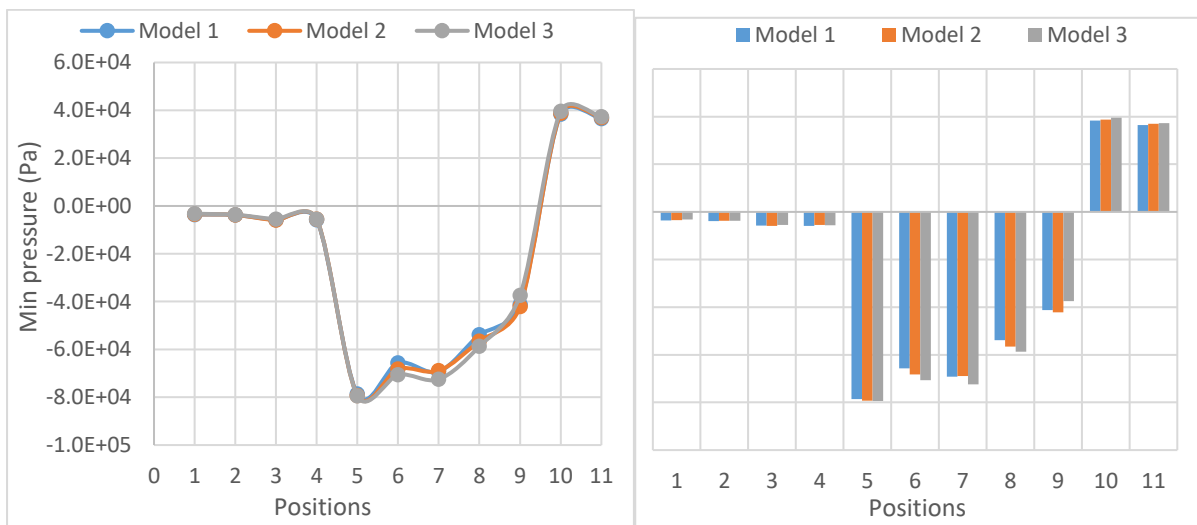


Figure 6.9: The distribution of maximum negative pressures at 1800 rpm, 500 millibars and for different model clearances.

### 6.1.1.2 Comparison analysis of the maximum and the minimum pressure variations between both 2D/3D baseline models

The statistical result of the maximum and the minimum pressures variations at a speed 1800 rpm and a discharge pressure 500 millibars for both 2D and 3D baseline models at various locations inside the blower from the inlet to outlet are presented in Table 6.7.

Table 6.7: The maximum and the minimum pressures at 1800 rpm and 500 millibars for 2D/3D blower baseline models.

Positions	$P_{\max}$ at 3D (Pa)	$P_{\max}$ at 2 D (Pa)	Error %	$P_{\min}$ at 3D (Pa)	$P_{\min}$ at 2 D (Pa)	Error %
P1	1.04E+05	1.02E+05	1.97	9.78E+04	1.00E+05	-2.69
P2	1.04E+05	1.02E+05	2.38	9.76E+04	1.01E+05	-3.02
P3	1.04E+05	1.02E+05	1.76	9.54E+04	9.95E+04	-4.26
P4	1.04E+05	1.03E+05	0.93	9.58E+04	9.93E+04	-3.69
P5	1.54E+05	1.54E+05	0.49	2.21E+04	2.94E+04	-33.10
P6	1.76E+05	1.80E+05	-1.76	3.31E+04	3.24E+04	2.32
P7	1.73E+05	1.73E+05	-0.16	3.24E+04	3.30E+04	-1.69
P8	1.72E+05	1.65E+05	3.97	4.48E+04	4.10E+04	8.45
P9	1.71E+05	1.65E+05	3.56	5.92E+04	6.92E+04	-16.78
P10	1.70E+05	1.63E+05	4.04	1.40E+05	1.38E+05	1.42
P11	1.68E+05	1.62E+05	4.01	1.38E+05	1.38E+05	0.17

Table 6.7 and figure 6.10 show that there are small variations of the maximum pressures between 2D and 3D models which the maximum error between both models is about 4 %. Also, it is apparent that the distributions of maximum static pressure have the same trend for two models.

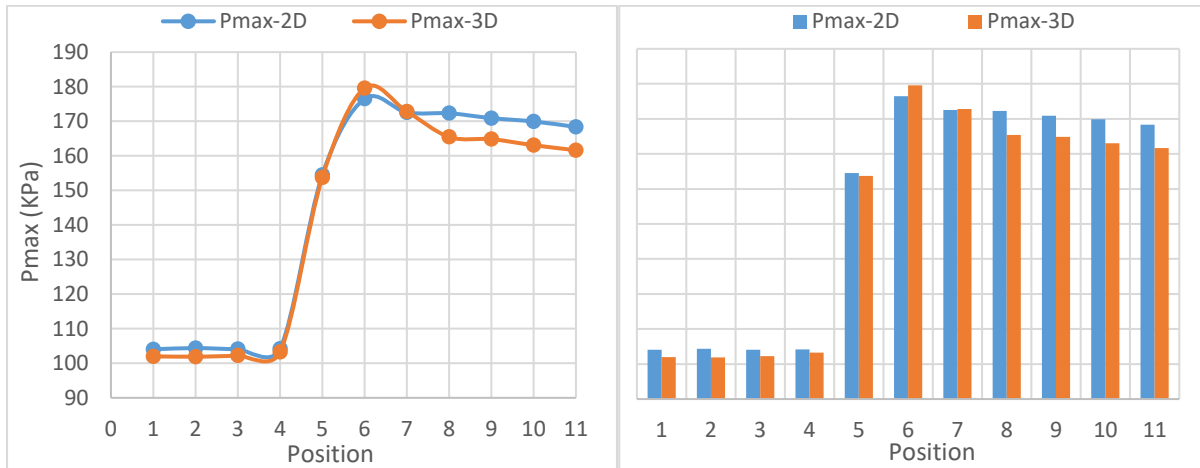


Figure 6.10: The distribution of maximum-pressures at 1800 rpm, 500 millibars in 2D/3D blower baseline models.

Table 6.7 and figure 6.11 illustrate that there are clear variations of the minimum pressures between 3D and 2D models at points P5, P9, and P8, but the differences are small at the other points. The maximum errors between both models are recorded at P5 and P9 which are about 33 % and 16.78% respectively. The reasons behind these big differences are the high effect of backflow in these points as discussed in previous chapters. Also, because the influence of third axis direction in 2D model is missing. Although, it is apparent that the distribution of minimum static pressure have the same trend and behaviour for two models

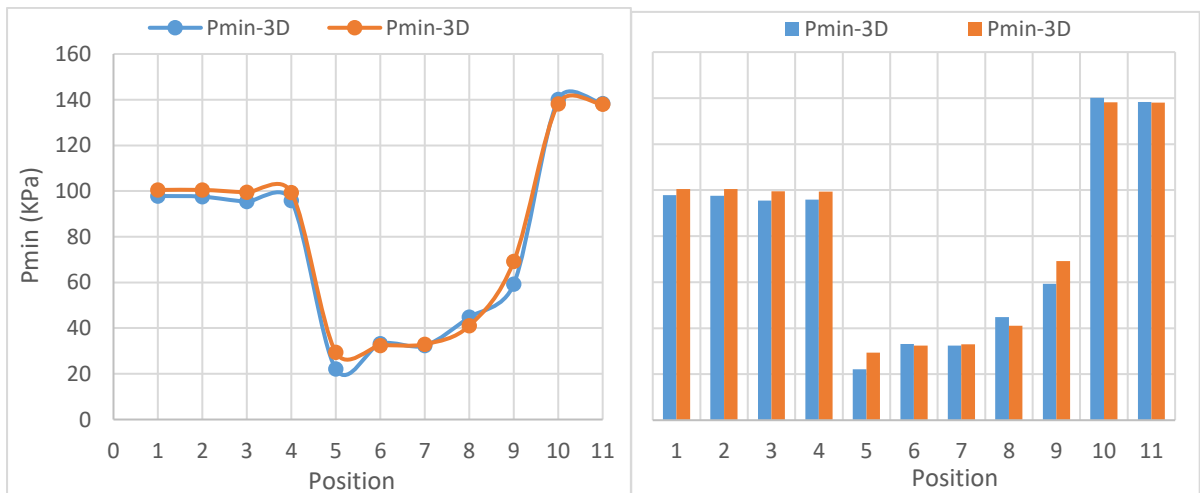


Figure 6.11: The distribution of minimum-pressures at 1800 rpm, 500 millibars in 2D/3D blower baseline models.

Table 6.8: The peak to peak amplitudes at 1800 rpm, 500 millibars for different model clearances.

Positions	Peak-peak amplitudes at model 1 (Pa)	Peak-peak amplitudes at model 2 (Pa)	Peak-peak amplitudes at model 3 (Pa)
P1	6.46E+03	6.19E+03	5.78E+03
P2	7.06E+03	6.83E+03	6.43E+03
P3	8.73E+03	8.66E+03	7.92E+03
P4	8.85E+03	8.40E+03	8.47E+03
P5	1.33E+05	1.32E+05	1.31E+05
P6	1.42E+05	1.43E+05	1.45E+05
P7	1.41E+05	1.40E+05	1.42E+05
P8	1.24E+05	1.27E+05	1.29E+05
P9	1.10E+05	1.12E+05	1.06E+05
P10	3.02E+04	2.98E+04	2.84E+04
P11	3.08E+04	3.01E+04	2.93E+04

The peak to peak amplitudes are presented in table 6.8 and figure 6.12. It can be seen there are small differences of amplitudes between three model clearances under investigation at the inlet and the outlet zones. These differences increase inside the meshing region in the blower. Also, the amplitudes start to increase from inlet until approach the maximum values at about (point 6) and after that declines until stabilising at the outlet of the blower. Moreover, it can be seen that the maximum amplitude is recorded in model 3 which is 1.45E+05 Pa. Because the effect of backflow and velocity are higher on model 3 than other two models and therefore the local pressure losses is higher.

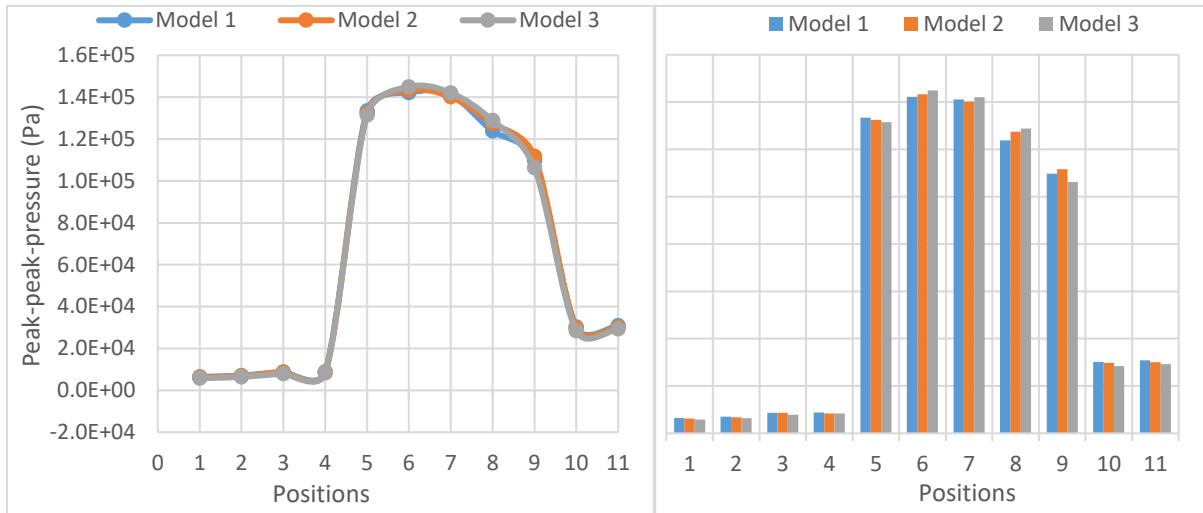


Figure 6.12: The peak-peak amplitudes at speed 1800 rpm, 500 millibars and for different models

The result shows that when the blower operates at small clearance (model 1), the pressure decreases in the clearances within the blower at the inlet chamber causing the velocity to increase. It develops further the backflow leads to the decline of flow rate. On the other hand, the high velocity inside the small gap will force the flow to move from inlet to outlet which finally leads to an increase in flow rate.

Furthermore, according to previous analysis, concerning the pressure variations in the blower, the outcomes have presented that model 1 has fewer pressure losses comparing to other models. Figure 6.13 shows that the maximum pressure of M1 (Tip Clearance = 0.18mm and Centre Clearance= 0.3mm) is higher than M2 (Baseline model) (Tip Clearance= 0.24mm and Centre Clearance= 0.34mm) and M3 (Tip Clearance = 0.3mm and Centre Clearance = 0.38mm) by 1.896% and 2.96% respectively. Also, the maximum negative pressure of M1 is lower than M2 and M3 by 0.78% and 1.016% respectively. Moreover, the maximum amplitude of pressure is higher in M3 than M1 and M2 by 1.9% and 1.09% respectively as shown in figure 6.14.

Because the effect of backflow and velocity are higher on other two models than model 1 and therefore the local pressure losses is higher.

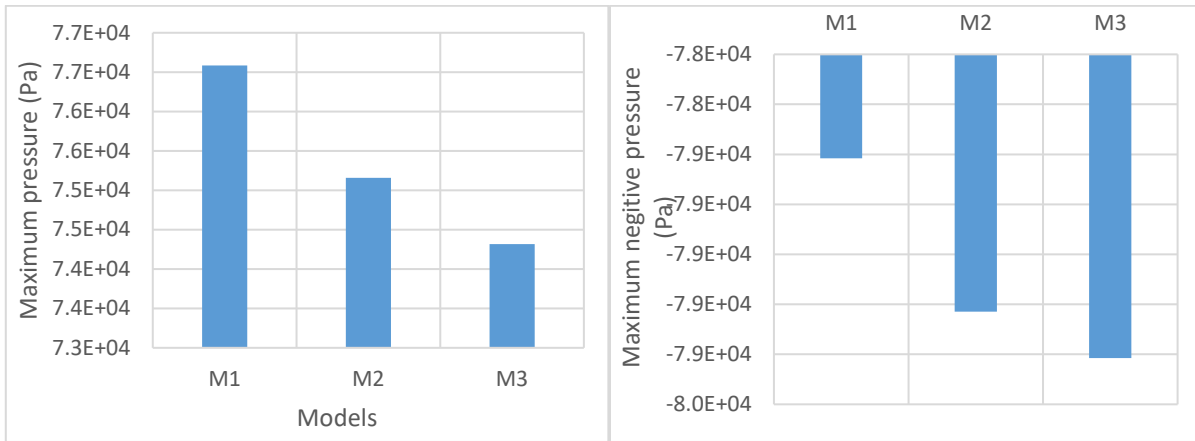


Figure 6.13: The comparison of the maximum pressure and the maximum negative pressure for different clearance models

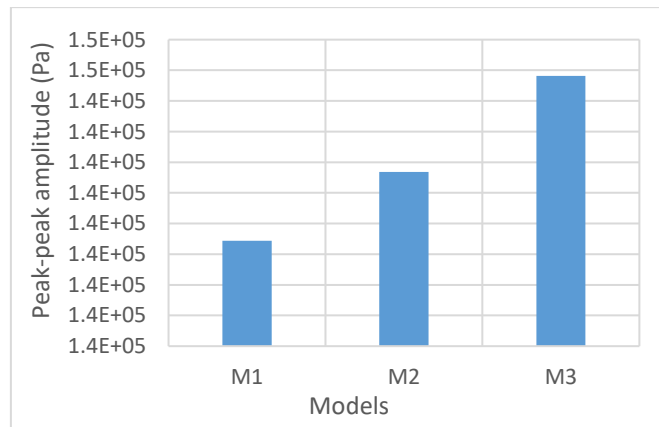


Figure 6.14: the comparison of maximum pressure amplitudes for different clearance models

### 6.1.2. Comparison analysis of the influence of different clearance models on the mass flow rate

The average mass flow rates for the last revolutions of three models under the study obtained through numerical simulations at a speed 1800 rev/min and a pressure differences 500 millibars are shown below in Figure 6.15.

It can be concluded that there are some differences in the average mass flow rates for three models, which the mass flow rate of M1 (Tip Clearance = 0.18mm and Centre Clearance= 0.3mm) is higher than M2 (Tip Clearance = 0.24mm and Centre Clearance= 0.34mm) and M3 (Tip Clearance = 0.3mm and Centre Clearance= 0.38mm) by 3.032% and 5.76% respectively as shown in figure 6.15. It is because smaller gap (model 1) can result in a higher velocity of

the working fluid, which will lead to more resist of the leakage in the gap and therefore increase the actual flow rate and volumetric efficiency of the Roots blower.

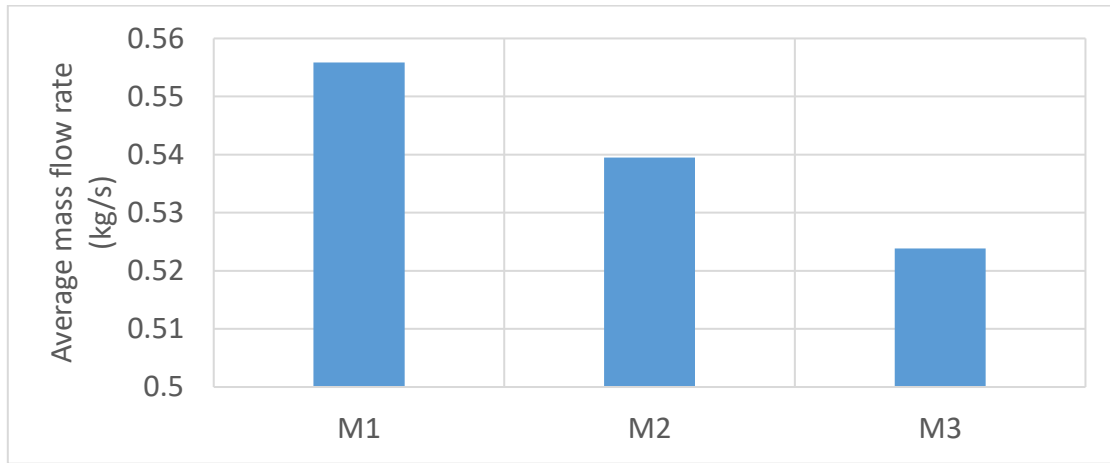


Figure 6.15: The average mass flow rate at speed 1800 rpm, pressure differences 500 millibars, for different clearance models.

The fluctuations (Pulsations) of mass flow rate obtained through numerical simulation at a speed 1800 rpm, a pressure difference 500 millibars for three clearance models are shown in figures 6.16 and 6.17. It can be concluded that the amplitude at the suction of the blower of model1 is higher than other models. Meanwhile, the amplitude at the discharge of the blower of model2 is slightly higher than other models. This difference is apparent in figure 6.18, which illustrates the mass flow rate fluctuation coefficient ( $M_F$ ) at both the inlet and the outlet of the blower.

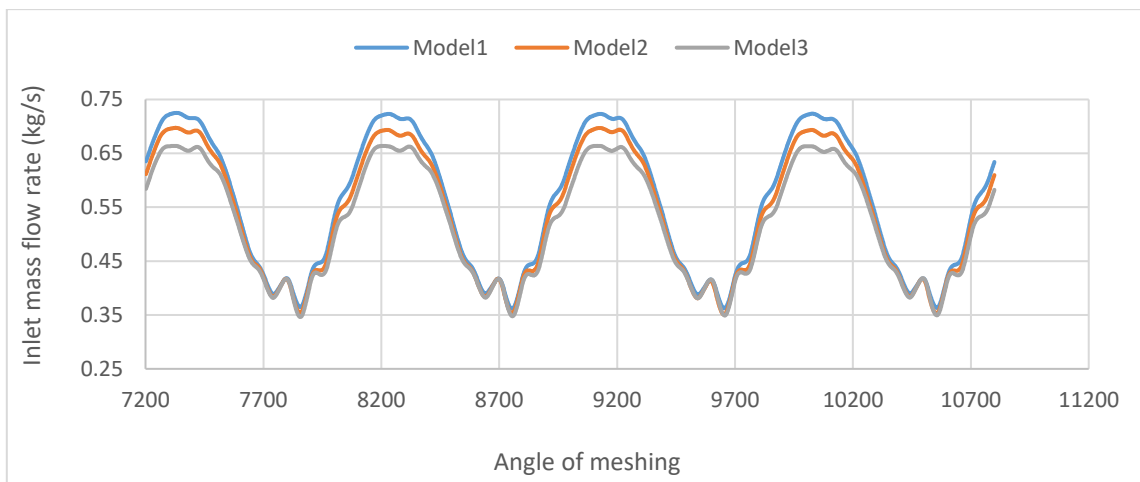


Figure 6.16: The fluctuations of the inlet mass flow rate at 1800 rpm and 500 millibars for different gap models

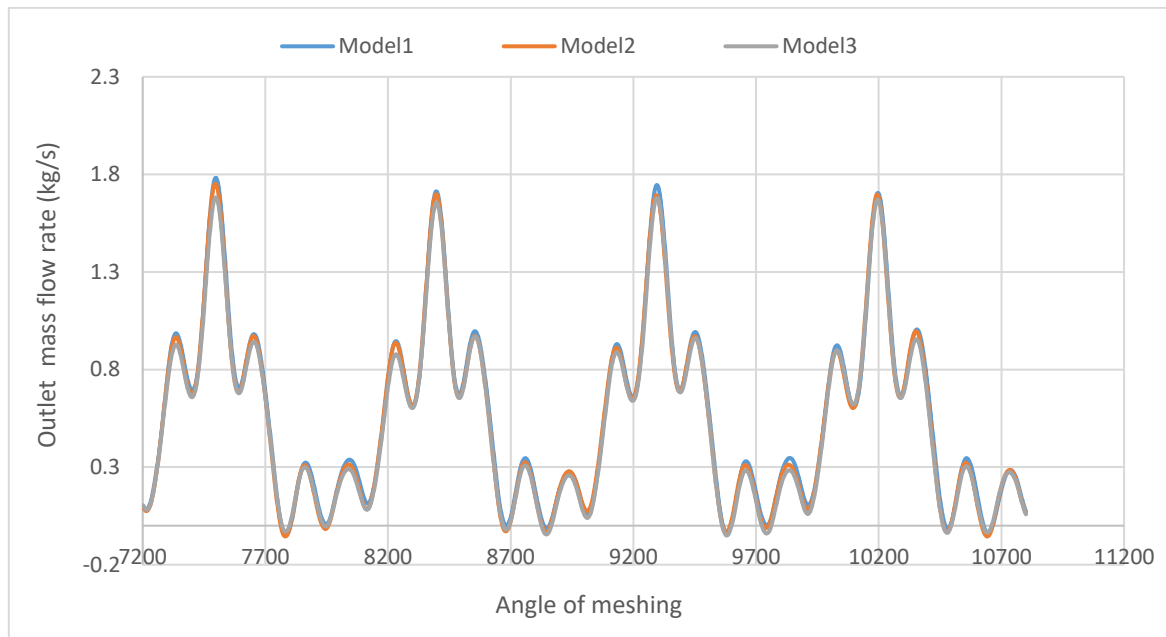


Figure 6.17: The fluctuations of outlet mass flow rate at 1800 rpm, 500 millibars for different gap models

The flow rate pulsation is usually defined by relative amplitude of flow fluctuation or the coefficient of flow rate fluctuation  $M_F$  [23]. This is can be used as a performance index related to vibration and noise, as outlined in previous chapters.

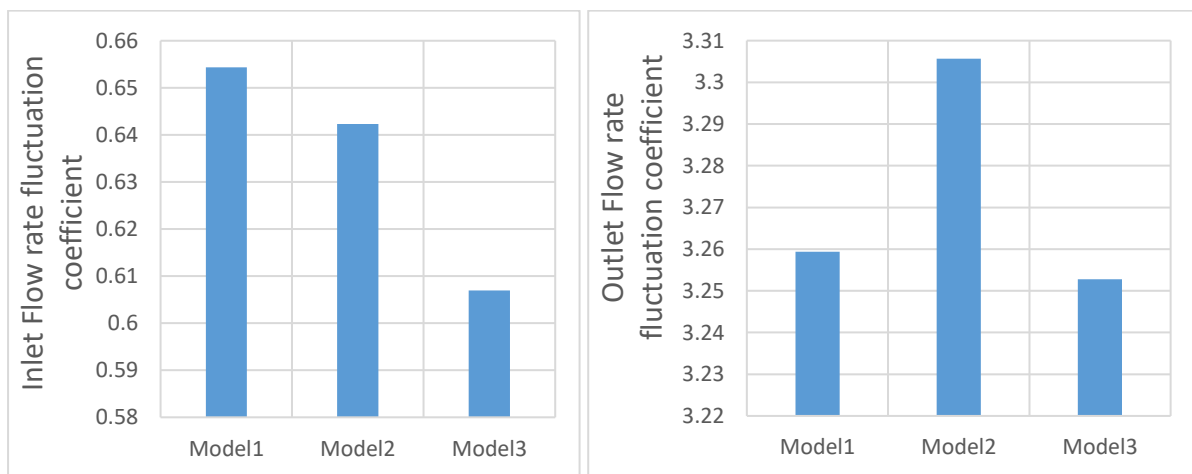


Figure 6.18: Mass flow rate fluctuation coefficient ( $M_F$ ) at a speed 2400 rpm, a pressure difference 700 millibars and for different model clearances at the inlet (left) and outlet (right).

The design parameters in priority are depended on application of use such as mass flow rate, pressure, temperature, efficiency and pulsation or noise. The pressure difference, rotational speed and clearance size are the main design parameters, by compromise between these

parameters can obtain the best performance applicable depending on the sort of application of Roots blower.

### 6.1.2.1 Comparison analysis of the mass flow rate variations between both 2D/3D baseline models

The mass flow rate variations at a speed 1800 rpm and a discharge pressure 500 millibars for both 2D and 3D baseline models at the inlet and the outlet of the blower are presented in figure 6.19.

It can be concluded that there are acceptable difference in the average mass flow rates between 3D and 2D blower models which the mass flow rate of 3 D model is higher than 2D model by 4.52% as shown in figure 6.19. It is because the influence of third axis direction in 2D model is missing.

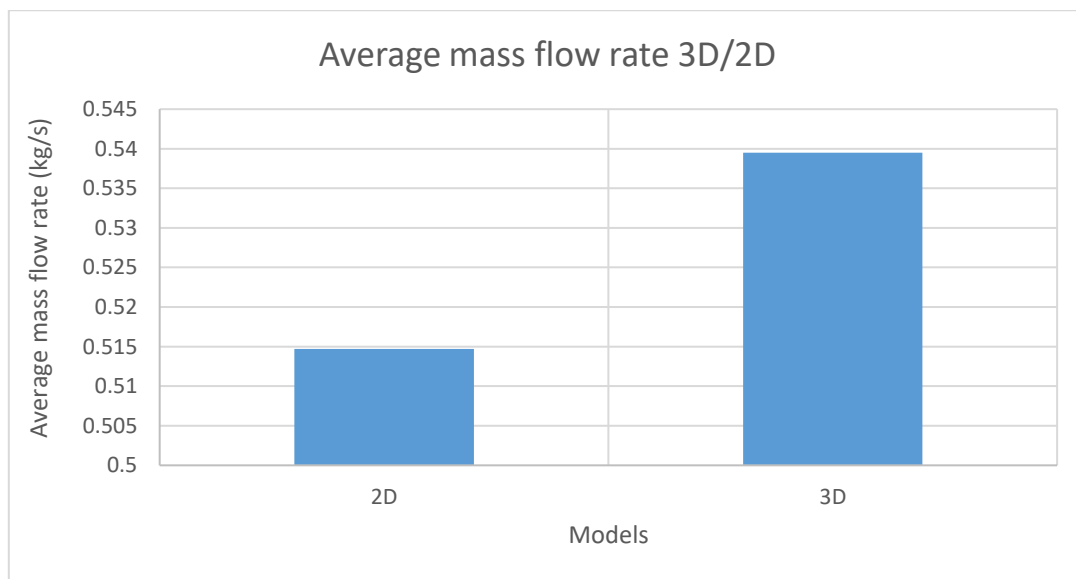


Figure 6.19: The average mass flow rate at speed 1800 rpm, pressure differences 500 millibars, for different clearance models.

The fluctuations of mass flow rate obtained through numerical simulation at a speed 1800 rpm and a pressure difference 500 millibars for 3D/2D models are shown in figures 6.20 and 6.21. It can be concluded that there are some differences in the amplitude between 3D/2D models at the suction and the discharge of the blower. These difference is due to that the effect of third axis direction in 2D model is not included. Although, it is apparent that the distribution of minimum static pressure have the same trend and behaviour for two models

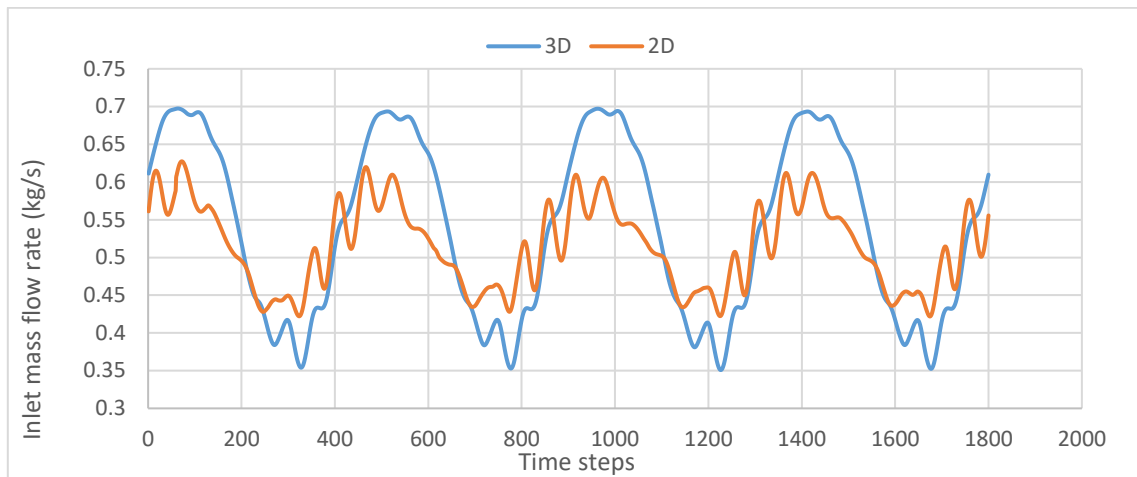


Figure 6.20: The fluctuations of the inlet mass flow rate at 1800 rpm and 500 millibars for 3D/2D models

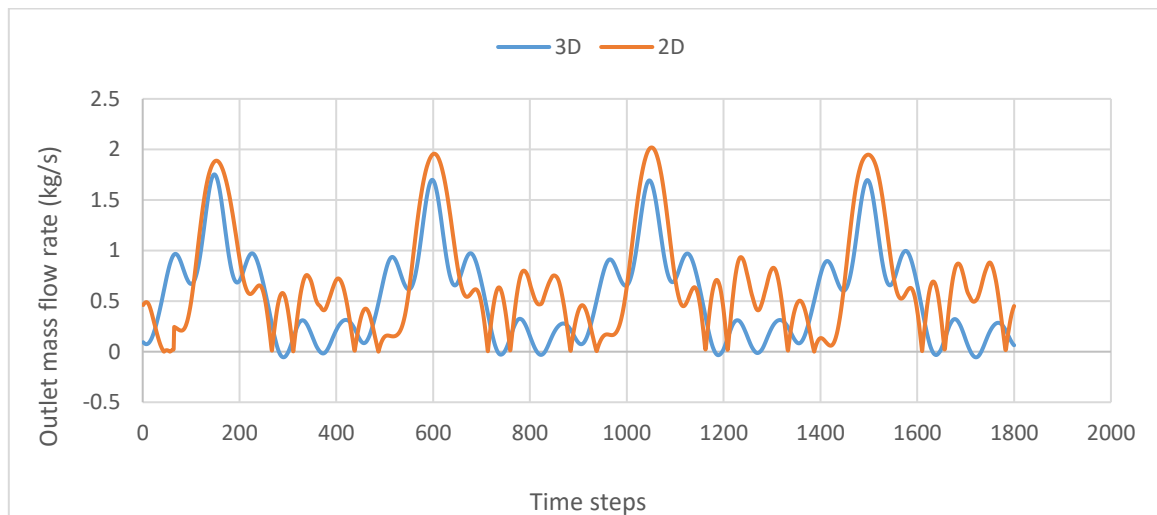


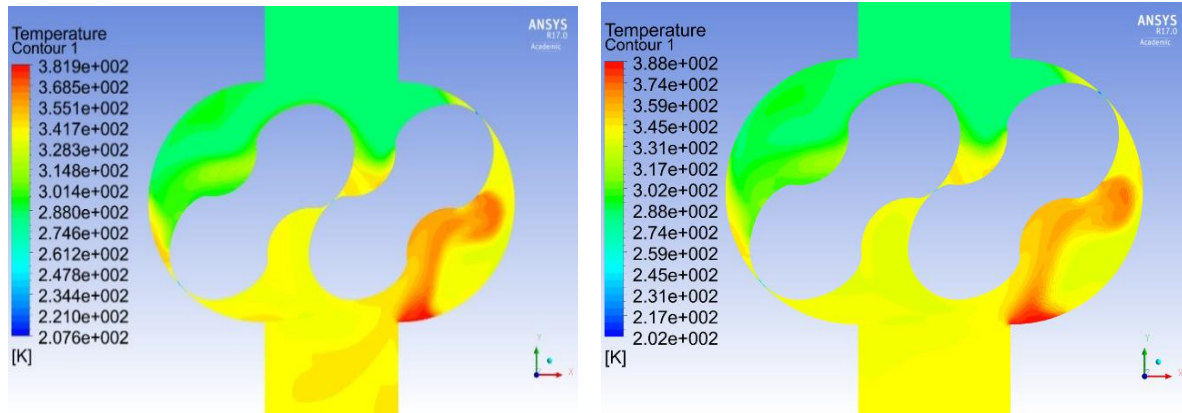
Figure 6.21: The fluctuations of outlet mass flow rate at 1800 rpm and 500 millibars for 3D/2D models

### 6.1.3. Comparison analysis of the influence of different clearance models on temperature distributions

The contours of the temperature at a speed 1800 rpm, a pressure difference 500 millibars for different clearance models are shown below in figure 6.22.

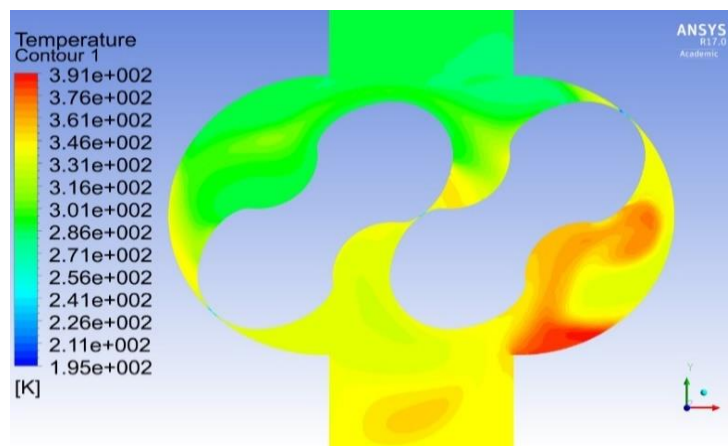
As shown in Figure 6.22, the temperature increase suddenly when the rotor crosses the edge of the discharge cavity of the blower. Also, the high-temperature area for model 3 is larger than

model2 and model1. It is obvious to conclude that temperature within model1 is lower than the other two models.



Model 1

Model 2



Model 3

Figure 6.22: The temperature contours for the last revolution at angle  $45^{\circ}$  rotation degrees, a speed 1800 rpm and a difference pressure 500 millibars for different clearance models

It can be conclude that temperature gradients increase with increase of clearance size, which recorded 1.75, 1.86, and 1.96 for models of M1, M2, and M3 respectively. Also, the pressure increases and flowrate decreases with increases of temperature gradient.

The variation of outlet temperature with the rotation angle is shown in figure 6.23. It can be seen that the temperature and their amplitude in model 3 is higher than other models.

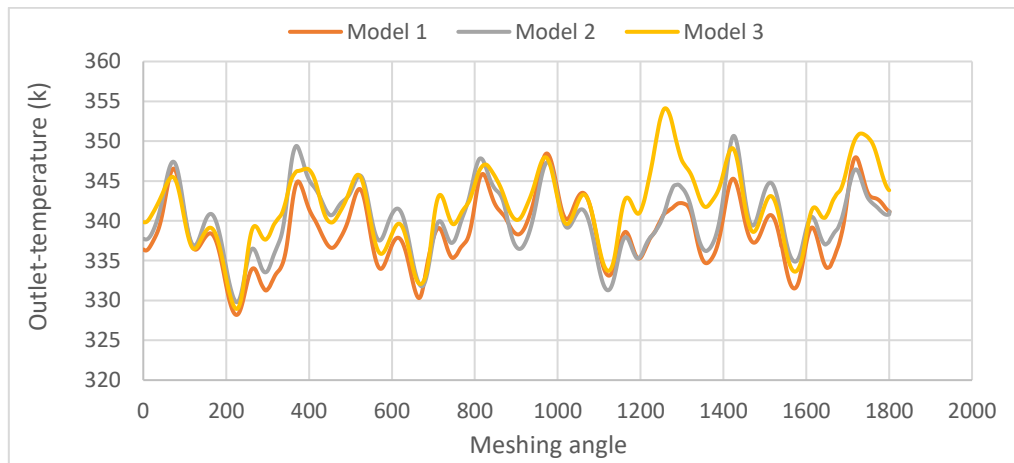


Figure 6.23: Outlet total temperature at 1800 rpm, different pressure 500 millibars and different model clearances.

The distribution and the variation of the temperature at a speed 1800 rpm and a discharge pressure 500 millibars (this value of pressure has been chosen for comparison, you can use any value from 0-700 millibars) for different clearance models of the blower from the inlet to outlet are presented in figure 6.24 and table 6.9. It can be seen that there are small differences of the average temperatures between the three clearance models which model1 recorded lower temperature values in comparison to model 2 and model 3.

Table 6.9: The distribution, and the variation of the average temperature at a speed 1800 rpm, and a discharge pressure 500 millibars for different clearance models.

Positions	$T_{ave}$ (K <sup>0</sup> ) at Model 1	$T_{ave}$ (K <sup>0</sup> ) at Model 2	$T_{ave}$ (K <sup>0</sup> ) at Model 3
P1	287.84	287.85	287.94
P2	287.95	287.98	288.34
P3	288.26	288.14	288.15
P4	288.50	288.52	288.42
P5	304.09	306.28	304.88
P6	317.39	318.82	326.47
P7	335.26	341.45	346.58
P8	339.51	343.69	343.83
P9	338.35	342.11	342.39
P10	337.00	339.42	339.08
P11	338.67	340.20	341.79

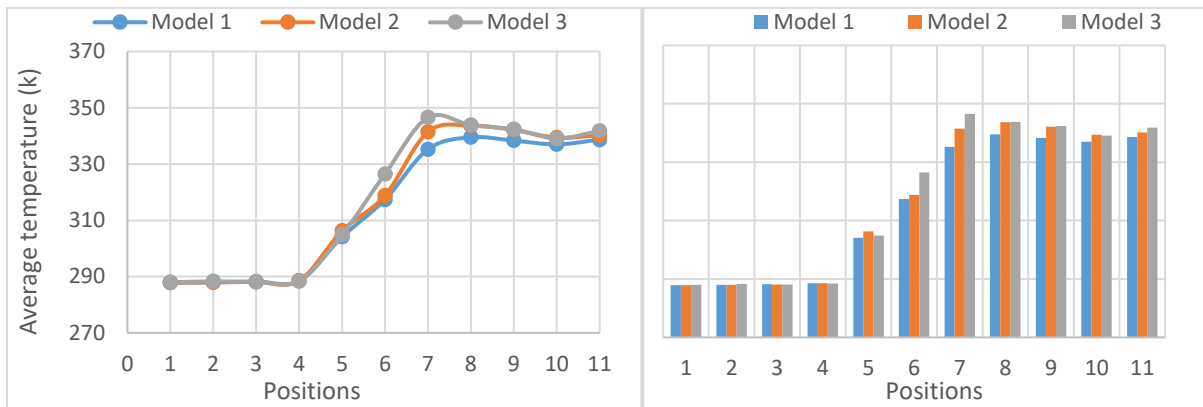


Figure 6.24: The distribution and the variation of average temperature at 1800 rpm and 500 millibars pressure load for different clearance models.

### 6.1.3.1 Comparison analysis of the average temperature variation between both 2D/3D baseline models

The statistical result of the average temperature variation at a speed 1800 rpm and a discharge pressure 500 millibars for both 2D and 3D baseline models at various locations inside the blower from the inlet to outlet are presented in Table 6.10 and figure 6.25.

Table 6.10: The average pressure in 2D/3D baseline models at 1800 rpm and 500 millibars

Positions	T <sub>ave</sub> at 3D	T <sub>ave</sub> at 2 D	Error %
P1	287.84	288.11	-0.09
P2	287.95	288.05	-0.04
P3	288.26	288.14	0.04
P4	288.50	288.30	0.07
P5	304.09	314.46	-3.41
P6	317.39	328.21	-3.41
P7	335.26	337.17	-0.57
P8	339.51	343.42	-1.15
P9	338.35	338.29	0.02
P10	337.00	341.89	-1.45
P11	338.67	341.37	-0.80

Table 6.10 and figure 6.25 show that there are small variations of the average temperatures between 2D and 3D models which the maximum error between both models is 3.41 %. Also, it is obvious that the distributions of average static pressure have the same trend for two models

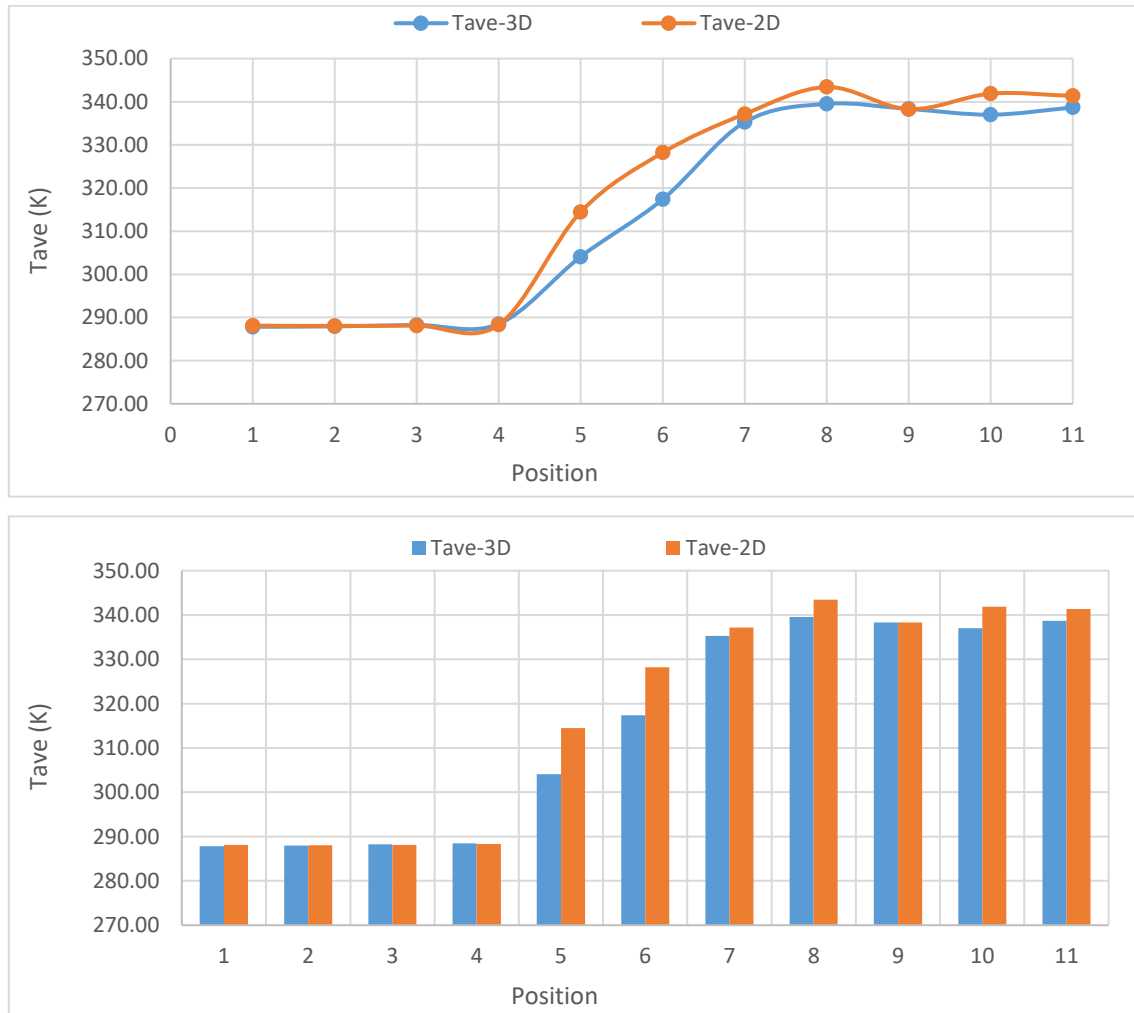


Figure 6.25: The average temperatures at 1800 rpm and 500 millibars for 2D/3D blower baseline models

Table 6.11 and figure 6.26 provide the statistical analysis of the temperature variation within the blower at chosen points from the inlet to outlet of the Roots blower. The results represent that the maximum temperatures of model1 are smaller than the other two models.

The data in table 6.11 shows that the maximum temperatures are found at point 8 for models 1 and two which are  $373.13 \text{ K}^0$  and  $378.85 \text{ K}^0$  respectively. For model3 the maximum temperatures are found at point 7 which is  $385.74 \text{ K}^0$ .

Table 6.11: The distribution, and the variation of the maximum and the minimum temperatures at a speed 1800 rpm and a discharge pressure 500 millibars for different clearance models.

Positions	$T_{\max}$ ( $K^0$ ) at Model 1	$T_{\max}$ ( $K^0$ ) at Model 2	$T_{\max}$ ( $K^0$ ) at Model 3	$T_{\min}$ ( $K^0$ ) at Model 1	$T_{\min}$ ( $K^0$ ) at Model 2	$T_{\min}$ ( $K^0$ ) at Model 3
P1	290.44	290.33	290.24	285.18	285.30	285.53
P2	290.84	290.73	290.83	285.08	285.18	285.63
P3	291.76	291.62	291.67	284.04	284.52	284.44
P4	291.90	292.75	292.28	283.65	283.87	284.41
P5	348.75	345.19	346.40	207.40	197.24	196.53
P6	357.57	361.52	363.81	235.25	232.73	229.19
P7	359.24	369.26	385.74	227.98	230.27	226.30
P8	373.13	378.85	376.33	258.47	254.57	251.14
P9	370.14	377.22	375.09	283.32	292.20	286.16
P10	350.05	351.62	349.61	328.14	331.09	330.07
P11	348.45	350.66	354.13	328.19	329.78	328.94

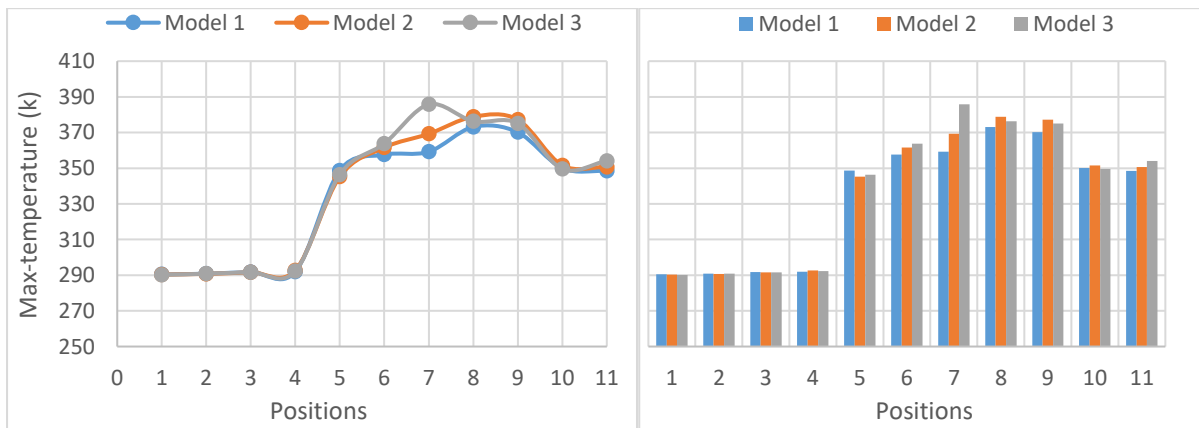


Figure 6.26: The distribution and the variation of maximum temperature at 1800 rpm and 500 millibars pressure load for different clearance models.

On the other hand, there are slight variations of the minimum temperature as we can see in figure 6.27 and table 6.11. Also, the minimum temperatures for the models under investigation are located at point 5 inside the clearance at the inlet zone. These temperatures are 207.40  $K^0$  for model 1, 197.24  $K^0$  for model 2 and 196.53  $K^0$  for model 3.

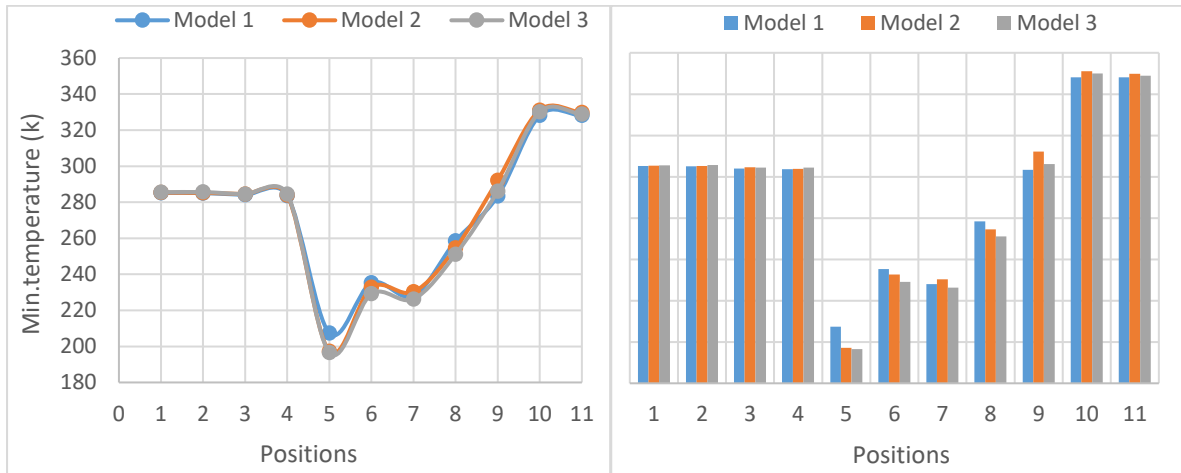


Figure 6.27: The distribution and the variation of minimum temperature at 2400 rev/min, pressure load 700 millibars and different model clearances.

### 6.1.3.2 Comparison analysis of the maximum and the minimum temperature variations between both 2D/3D baseline models

The statistical result of the maximum and the minimum temperatures variations at a speed 1800 rpm and a discharge pressure 500 millibars for both 2D and 3D baseline models at various locations inside the blower from the inlet to outlet are presented in Table 6.12.

Table 6.12: The maximum and the minimum temperatures at 1800 rpm and 500 millibars for 2D/3D blower baseline models.

Positions	$T_{\max}$ at 3D	$T_{\max}$ at 2 D	Error %	$T_{\min}$ at 3D	$T_{\min}$ at 2 D	difference %
P1	290.44	289.00	0.50	285.18	287.00	-0.64
P2	290.84	289.00	0.63	285.08	287.00	-0.67
P3	291.76	289.00	0.95	284.04	287.00	-1.04
P4	291.90	290.00	0.65	283.65	287.00	-1.18
P5	348.75	340.58	2.35	207.40	214.38	-3.37
P6	357.57	361.00	-0.96	235.25	241.00	-2.45
P7	359.24	362.00	-0.77	227.98	238.00	-4.40
P8	373.13	383.00	-2.65	258.47	263.00	-1.75
P9	370.14	367.01	0.84	283.32	300.10	-5.92
P10	350.05	351.00	-0.27	328.14	329.00	-0.26
P11	348.45	349.00	-0.16	328.19	331.00	-0.86

Table 6.12 and figure 6.28 show that there are small variations of the maximum temperatures between 2D and 3D models which the maximum difference between both models is about 2.65 %. Also, it is apparent that the distributions of maximum static pressure have the same trend for two models.

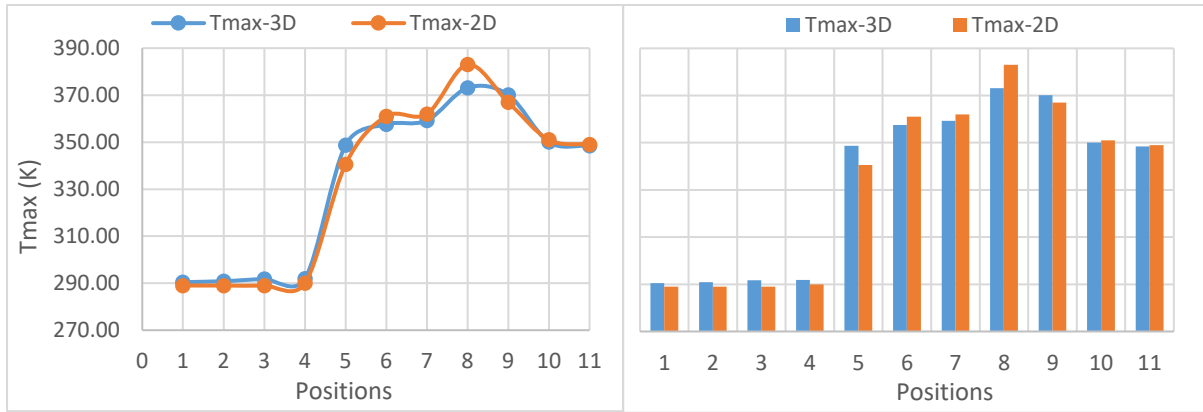


Figure 6.28: The maximum temperatures at 1800 rpm and 500 millibars for 2D/3D blower baseline models

Table 6.12 and figure 6.29 illustrate that there are variations of the minimum temperatures between 3D and 2D models at all points. The maximum errors between both models is recorded at P9 which are about 5.92 %. The reason behind that the high effect of backflow in this point. Also, because the influence of third axis direction in 2D model is missing. Although, it is apparent that the distribution of minimum static pressure have the same trend and behaviour for two models

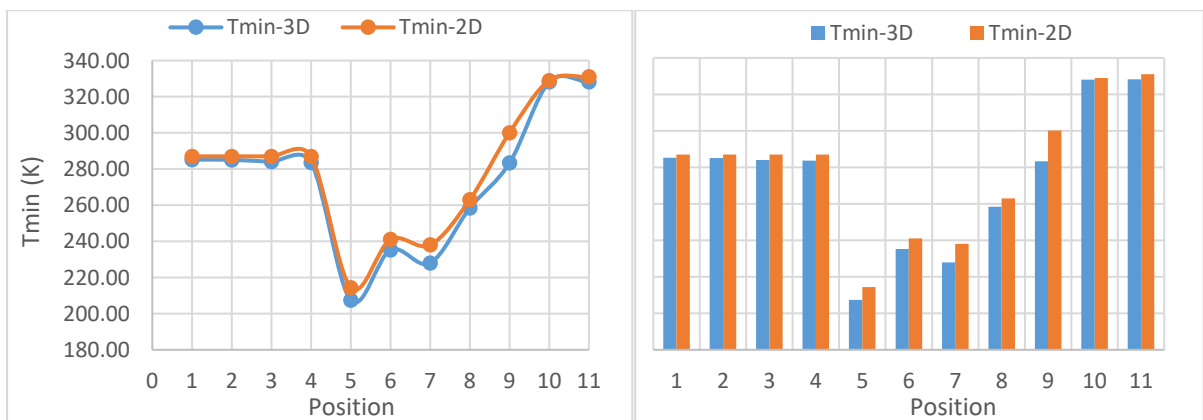


Figure 6.29: The minimum temperatures at 1800 rpm and 500 millibars for 2D/3D blower baseline models

Furthermore, according to aforementioned analysis, regarding the temperature variations in the blower, the outcomes have presented that model 1 has a lower temperature, which the average temperature, maximum temperatures generally of models 2 and 3 are higher than model 1. Figure 6.30 that the maximum temperature of model 3 is higher than model 1 and model 2 (Baseline model) by 3.38% and 1.81% respectively. Also, the minimum temperature of model 3 is lower than model 1 and model 2 by 5.53% and 5.17% respectively. The cause of these because the clearances inside model 1 are smaller than the clearances of other two models which lead to increase the flow rate and decrease the temperature. Also, this is will decrease the effect of backflow and local pressure losses.

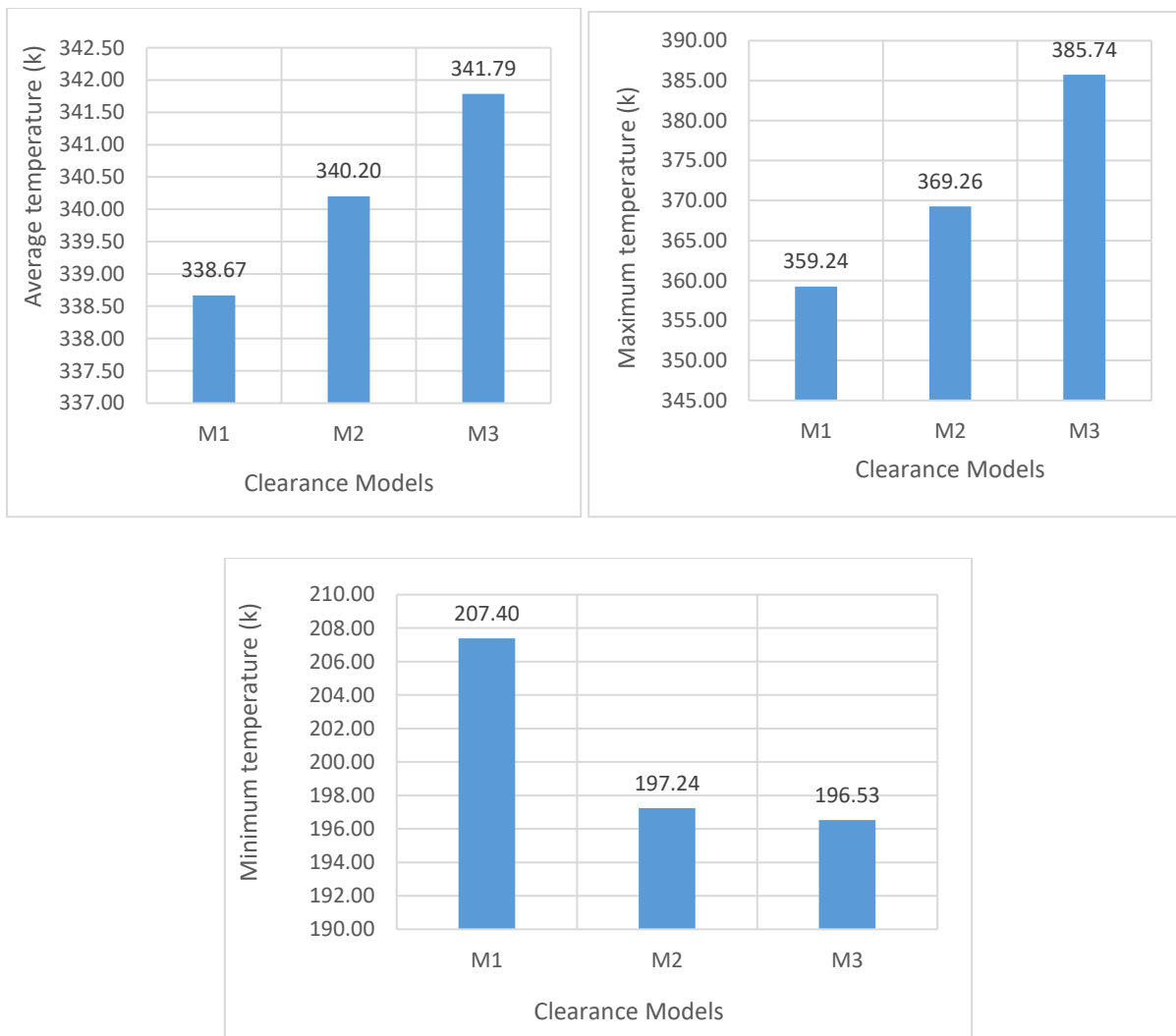


Figure 6.30: The comparisons of the average, the maximum and the minimum temperatures for different clearance models of the Roots blower

### 6.1.4. Comparison analysis of the influence of different clearance models on velocity distributions

The variation and the distribution of velocity at a rotational speed 1800 rpm and a pressure difference 500 millibars in three different clearance models are shown below in figure 6.31 as velocity vector and streamline contours. It shows that the clearance size will affect the distribution of the velocity inside of the positive displacement blower.

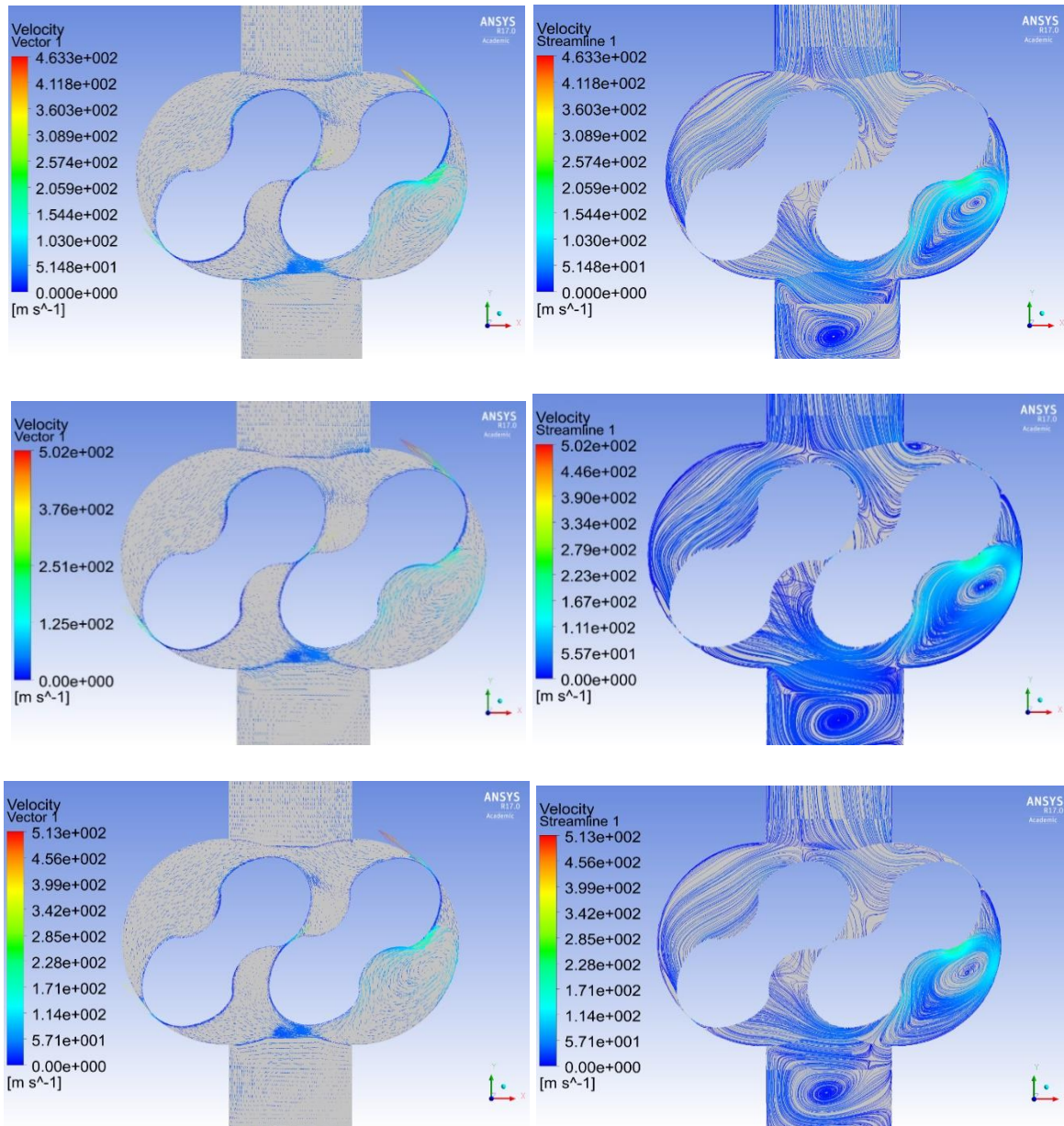


Figure 6.31: The velocity vector and streamline contours at a rotational speed 1800 rpm, a meshing angle  $45^{\circ}$  of rotation degrees and a pressure differences 500 millibars within mode 1, model 2, and model 3 from up to down respectively

Figure 6.31 show that the high and low velocities are occurred in the flow mixing regions as recirculation zones. These zones occur when the rotors sudden cross the edges of the suction or the discharge zones which the core of these areas consists of the low velocity. It can be seen from this figure that the shape of these recirculation zones are different in the three blower models. Also, the velocity in model 1 is lower than other two models. Moreover, the maximum velocities are found inside the clearances and it increases with the decrease in clearance size.

Table 6.13: The distribution and the variation of the velocity at a rotational speed 1800 rpm, and a pressure difference 500 millibars and for different model clearances

Positions	$V_{ave}$ (m/s) at model 1	$V_{ave}$ (m/s) at model 2	$V_{ave}$ (m/s) at model 3	$V_{max}$ (m/s) at model 1	$V_{max}$ (m/s) at model 2	$V_{max}$ (m/s) at model 3
P1	24.19	23.73	19.68	33.12	32.41	29.26
P2	18.15	9.71	13.49	32.67	21.08	30.71
P3	6.42	5.77	4.39	27.42	22.36	20.12
P4	2.63	2.47	2.30	19.86	21.20	14.90
P5	5.89	4.54	7.33	152.46	112.66	395.70
P6	8.74	5.40	9.17	261.10	50.62	198.63
P7	10.22	8.70	12.81	164.54	89.30	122.20
P8	12.84	10.34	10.87	163.31	83.32	153.28
P9	15.16	21.13	21.52	167.54	97.06	186.59
P10	32.20	17.95	26.90	75.65	45.24	73.97
P11	44.81	43.41	37.85	70.66	70.20	61.59

Table 6.13 provides the statistical analysis of the velocity variation within the blower at distributed points from the inlet to outlet of the Roots blower. The results represent that there is a slight difference in the average velocities between three clearance models. These velocities at inlet and outlet of the blower are marginally higher for models 1 and two compared to model 3 as shown in figure 6.32.

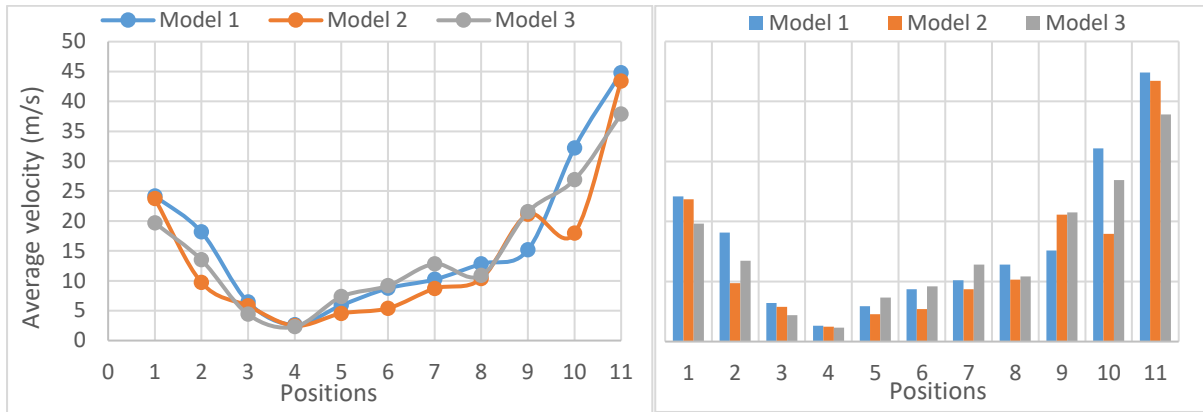


Figure 6.32: The average velocity distribution at rotational speed 1800 rpm and pressure difference 500 millibars for different clearance models.

Also, the maximum velocities at inlet and outlet of the blower are slightly higher for models 1 and two than model 3. Moreover, the maximum velocities for models 2 and three are found at point 5 which are 112.66 m/s and 395.70 m/s respectively. However, the maximum velocity for model 1 is found at point 6 as shown in figure 6.33.

The reason for that because the clearance size of model 1 is smaller than model 2 and also the clearance size of model 2 is smaller than model 3. So, the cross section area of small clearance size is small too, therefore the velocity will increase through the smaller cross section area. However, model 3 has recorded higher velocity at point 5. Because the effect of backflow and therefore the local pressure losses are higher at this point in model 3 than other two models.

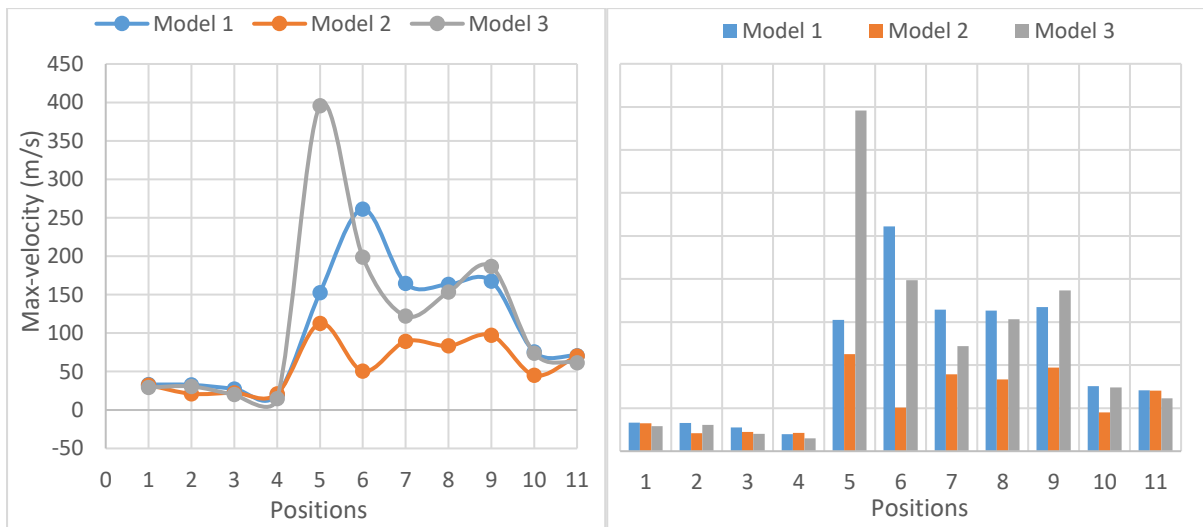


Figure 6.33: The Maximum velocity distribution at rotational speed 1800 rpm and pressure difference 500 millibars for different clearance models.

#### 6.1.4.1 Comparison analysis of the maximum and the minimum velocity variations between both 2D/3D baseline models

The statistical result of the average and the maximum velocity variations at a speed 1800 rpm and a discharge pressure 500 millibars for both 2D and 3D baseline models at various locations inside the blower from the inlet to outlet are presented in Table 6.14.

Table 6.14: The average and the maximum velocities at 1800 rpm and 500 millibars for 2D/3D blower baseline models in m/s.

Positions	$V_{ave}$ at 3D m/s	$V_{ave}$ at 2D m/s	Error %	$V_{max}$ at 3D m/s	$V_{max}$ at 2D m/s
P1	23.72	8.90	62.47	32.41	11.00
P2	16.88	10.07	40.32	21.08	17.05
P3	6.52	3.92	39.88	22.36	32.74
P4	2.26	2.02	10.62	21.20	16.92
P5	6.58	3.79	42.43	112.66	83.75
P6	7.53	6.94	7.76	50.62	44.03
P7	8.09	6.51	19.55	89.30	79.11
P8	13.49	8.07	40.20	83.32	85.68
P9	22.09	10.36	53.11	97.06	80.91
P10	30.89	26.41	14.52	45.24	58.24
P11	43.29	33.44	22.75	70.20	49.24

Table 6.14 and figure 6.34 show that there are apparent variations of the average velocities between 2D and 3D models which the maximum error between both models is about 62.47 %. The reasons behind these big differences are the high effect of backflow in these points. Also, because the influence of third axis direction in 2D model is missing. Moreover, the shape of the suction and the discharge of the blower in 3D is cylindrical while in 2D model is rectangular. Although, it is apparent that the distribution of minimum static pressure have the same trend and behaviour for two models.

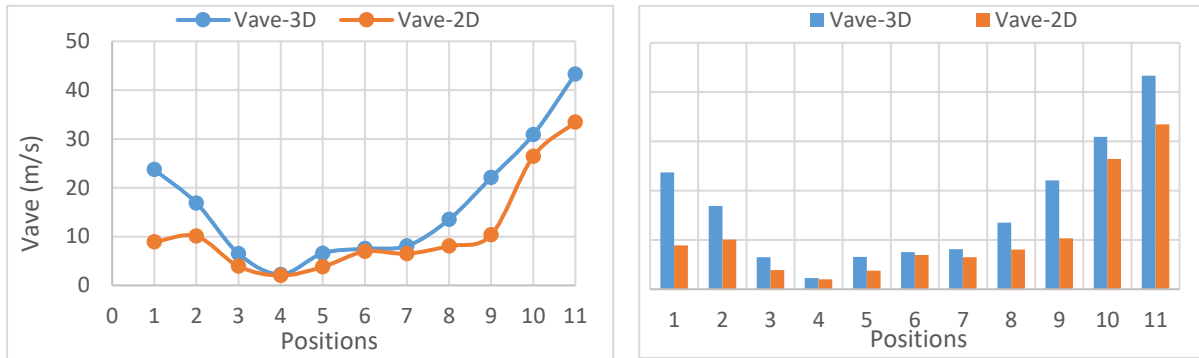


Figure 6.34: The average velocities at 1800 rpm and 500 millibars for 2D/3D blower baseline models

Table 6.14 and figure 6.35 present that there are big variations of the maximum velocities between 3D and 2D models at the majority of points. The maximum errors between both models is about 66 %. The reasons behind these big differences are the high effect of backflow in these points. Also, because the influence of third axis direction in 2D model is missing. Moreover, the shape of the suction and the discharge of the blower in 3D is cylindrical while in 2D model is rectangular. Although, it is apparent that the distribution of minimum static pressure have the same trend and behaviour for two models

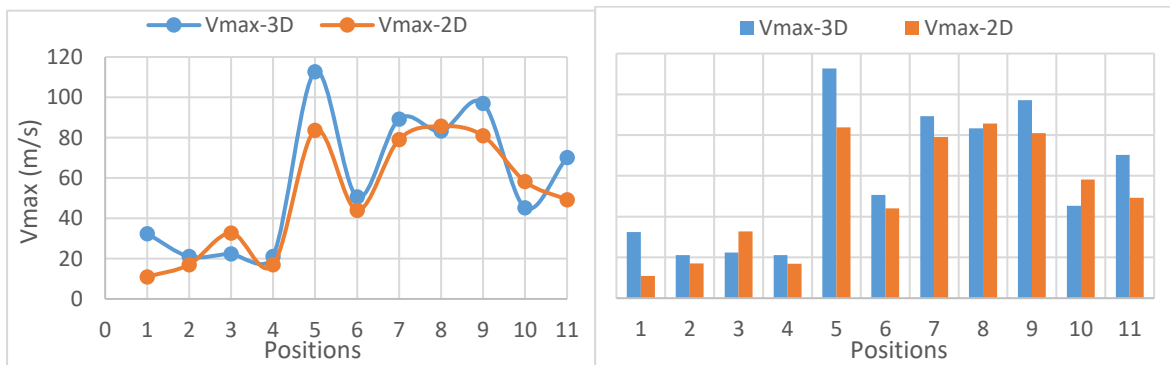


Figure 6.35: The maximum velocities at 1800 rpm and 500 millibars for 2D/3D blower baseline models

Furthermore, according to earlier analysis, relating to the velocity variations in the blower, the outcomes have presented that the average and the maximum velocities at the inlet and the outlet of the blower for models 1 and 2 are very close. However, the maximum velocities inside model 1 and model 3 are higher than model 2. The cause of these because the clearances inside model 1 are smaller than the clearances of other two models which lead to increase of the velocity. Also, the effect of backflow and the local pressure losses in model 3 is higher than other two models which lead to increase of velocity in this model.

### 6.1.5 Summary

In comparison, the maximum pressure of M1 (Tip Clearance = 0.18mm and Centre Clearance = 0.3mm) is higher than M2 (Baseline model) (Tip Clearance = 0.24mm and Centre Clearance = 0.34mm) by 1.896% and M3 (Tip Clearance = 0.3mm and Centre Clearance = 0.38mm) by 2.96%. Also, the maximum negative pressure of model 1 is lower than model 2 by 0.78% and model 3 by 1.016%. According to previous analysis, concerning the pressure variations in the blower, the outcomes have presented that the model 1 has fewer pressure losses comparing to other models. Also, it can be seen that the maximum amplitude is recorded in model 3. It can be concluded that the mass flow rate of model 1 is higher than model 2 and model 3 by 3.032% and 5.76% respectively. The amplitude of the pressure at the suction of the blower of model 1 is higher than other models. Meanwhile, the amplitude of the pressure at the discharge of the blower of model 2 is slightly higher than other models.

Moreover, according to previous analysis, concerning the temperature variations in the blower, the results have presented that model 1 has a lower temperature, which the average temperature, maximum temperatures generally of models 2 and 3 are higher than model 1. It can be concluded that temperature gradients increase with increase of clearance size, which recorded 1.75, 1.86, and 1.96 for models of M1, M2, and M3 respectively. Also, the pressure increases and flow rate decreases with increases of temperature gradient.

Furthermore, according to previous analysis, concerning the velocity variations in the blower, the outcomes have presented that the average and the maximum velocities at the inlet and the outlet of the blower for models 1 and 2 are very close. However, the maximum velocities inside model 1 and model 3 are higher than model 2.

From the comparison of the blowers with different clearance sizes as presented in previous sections, the drop of the blower performance is apparent as the size of clearances increase. The main reasons of the drop are the unsteady and the uneven flow caused as the clearance sizes increase and the impact of the backflow increases. The comparison shows that Roots blower model 1 (M1) has better performance than the baseline model (M2) regarding mass flow rate, pressure, temperature, and outlet fluctuations. However, regarding internal velocity and inlet fluctuation, the baseline model is better. Finally, it can be summarised that decrease and adjustment of clearances can improve the performance of Roots blower. The design parameters are depended on application of Roots blower such as mass flow rate, pressure, temperature, efficiency and noise. The pressure difference, rotational speed and clearance size are the main

design parameters, by compromise between these parameters can obtain the best performance applicable depending on the type of application of this blower.

## **6.2 Pressure fluctuation and flow pattern of Roots blower with different clearance models**

The internal flow field within the blowers are complex, and there are several reasons behind their complexity and why flow fluctuations in the Roots blower are generated. It is due to the significant influence of the turbulence and the unsteadies of flow within the blower. Also, because of the effect of clearance size.

Consequently, the variation and the distribution of static pressure inside the Roots blower changes with the time. However, these interactions cause many problems such as high vibration and noise in the blower and ultimately cause damage to the bearings and rotors lobes. In order to analyse the pressure characteristics in the blower under the transient condition and to also capture the effect of these interactions, further numerical investigation in the Roots blower through pressure fluctuations analysis at different monitoring points will be discussed in the next section.

Three blower models listed in Table 6.2 have been chosen to numerically investigate the relationship between clearance sizes and unsteady flow characteristics. M1, M2, and M3 are models chosen with different gap sizes.

The fluctuations of the pressure in the Roots blower are inevitable. Hence, they have substantial influence on the characteristic of the transient flow inside the blower. The time domain of pressure fluctuations could directly give a visualised result, but the detailed information of the fluctuations should be further analysed in the frequency spectrum. Therefore, a detailed study of pressure fluctuation characteristics in the frequency domain may provide reliable information related to the blower. Such details include the influence of the interaction between the two rotors and the inlet and the outlet cavities of the blower when the blower operates under various operating conditions and different clearance geometries. In the current study, to further analysis the transient pressure data, the fast Fourier transform (FFT) has been used.

Fundamentally, Fast Fourier Transform (FFT) is used to convert time domain signals into frequency domain signals and produces a complex spectrum of the sampled signals. The

outcome of the Fast Fourier Transform in the present study provides the amplitude of pressure fluctuations with frequency. Therefore, in order to investigate the spectral characteristics, the fluctuations of pressure within Roots blower and the amplitudes are analysed.

The main frequencies in the Roots blower are the rotational frequency (Rf) and its related harmonics, and can be calculated by use the equation below:

$$Rf = (N/60) \text{ or } (\text{rotational speed}/60) \dots\dots\dots (6.1)$$

Lobe Passing Frequency (LPF), and it is related harmonics, which can be calculated by using equation. (6-2):

$$LPF = (\text{rotor rotational speed}/60) * \text{number of Lobes, or } LPF = (N/60) * Z \dots\dots\dots (6.2)$$

This category of frequency is produced due to the movement of the lobes of the rotors.

### **6.2.1 Analysis of the Pressure Fluctuations of the baseline blower model (M2) in Frequency Domain**

Figure 6.36 represents the three-dimensional figure of blower frequencies and pressure amplitudes for all the monitoring points in the blower at a rotational speed of 1800 rpm and pressure difference 500 millibars. The rotational speed of the rotors in the blower is 1800rpm therefore; the rotational frequency (Rf) is 30Hz. The results show that the maximum amplitude of pressure fluctuation for the most monitoring points is at LPF 120.13Hz which is the dominant frequency. It is due to the number of impeller lobes used which is four. LPF type of frequency is generated because of the interaction between the rotors lobes and the edges of the suction and discharge regions in the blower especially at discharge zone (P8 and P9), where the LPF value was quite higher than that of the other region. Also, from this figure and table 6.15, it can be observed that the maximum pressure fluctuation amplitude of (P6 and P7) is at  $2Rf = 60.07\text{Hz}$  and for P5 is at  $6Rf = 180.2\text{Hz}$ . Moreover, it is found that the pressure fluctuation amplitudes fluctuate with increasing frequency for all points. It can be further noticed that the amplitude of pressure fluctuations at monitoring points P7 and P6 were higher than other points.

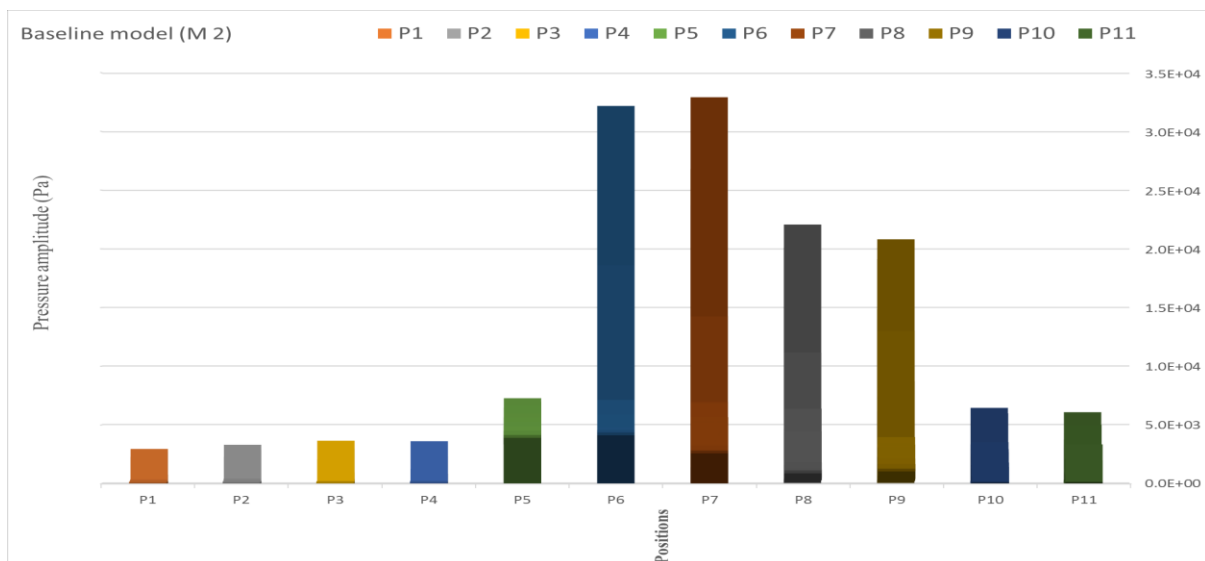
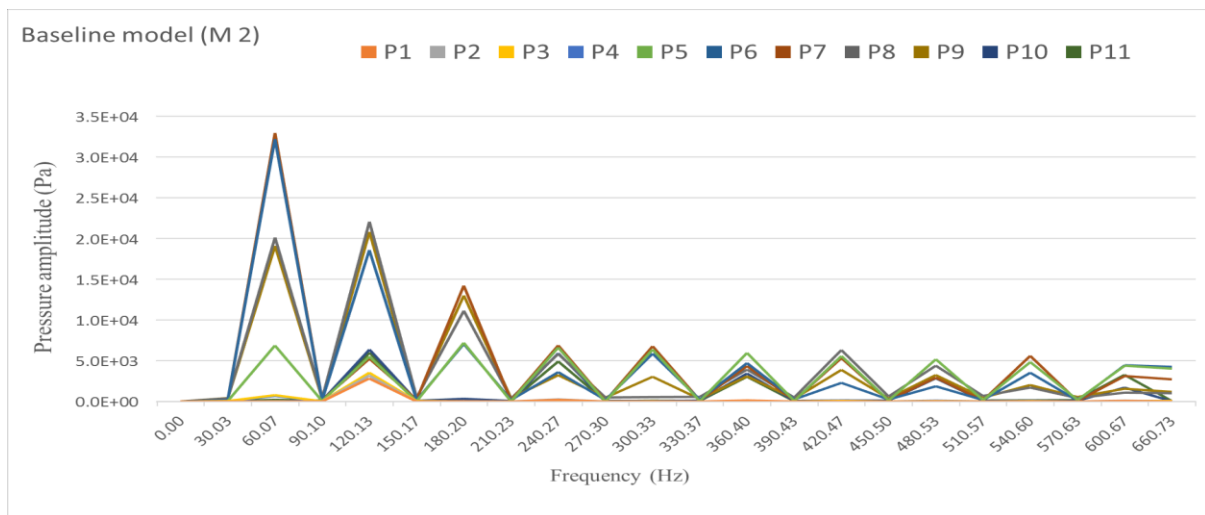
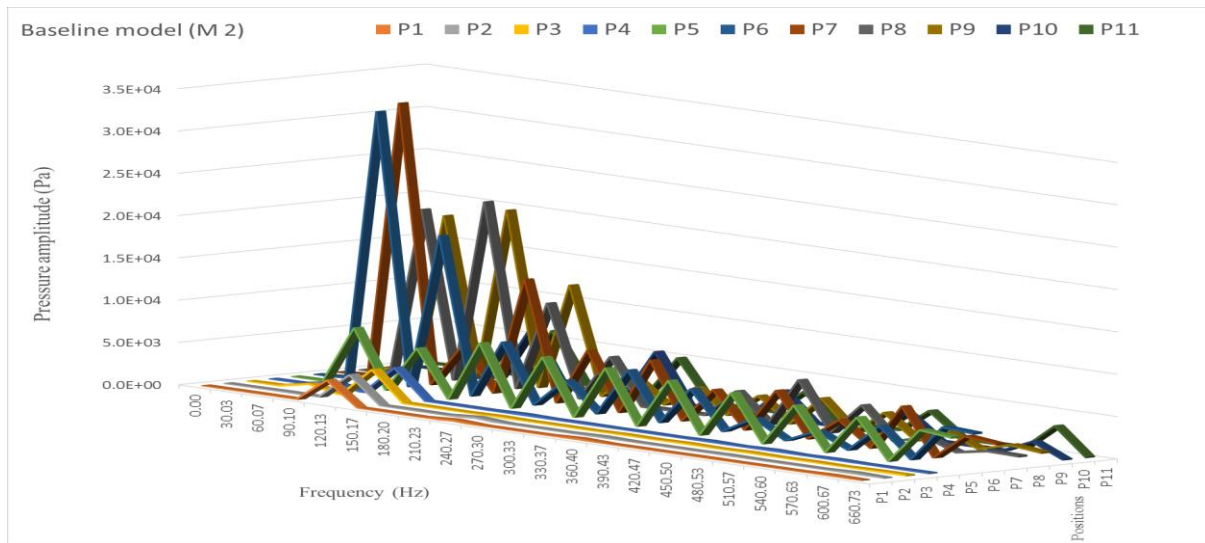


Figure 6.36: The Pressure Fluctuations of the baseline blower model (M2) in Frequency Domain at a speed 1800 rpm and a pressure difference 500 millibars

Table 6.15: The maximum pressure fluctuation amplitudes at various frequencies and different points within the Roots blower baseline model (M2) in Pascal

Positions		Frequencies (Hz)		
		60.07 Hz	120.13 Hz	180.2 Hz
Maximum amplitude of pressure fluctuations at different points within the blower (Pa)	P1	1.01E+01	2.82E+03	1.95E+01
	P2	3.97E+01	3.19E+03	3.57E+01
	P3	7.78E+02	3.53E+03	2.88E+01
	P4	6.82E+02	3.49E+03	2.02E+01
	P5	6.87E+03	5.52E+03	7.20E+03
	P6	3.22E+04	1.86E+04	7.06E+03
	P7	3.29E+04	5.25E+03	1.42E+04
	P8	2.01E+04	2.21E+04	1.11E+04
	P9	1.91E+04	2.08E+04	1.30E+04
	P10	1.15E+01	6.36E+03	3.16E+02
	P11	1.98E+02	5.99E+03	3.16E+02

However, the maximum pressure fluctuation amplitudes at P6 and P7 are 3.29E+04 Pa and 3.22E+04 Pa respectively which is at frequency 60.07 Hz as shown in table 6.15. It is due to locations of these points are at main interaction zone between the flow moving towards the discharge region due to rotors movement, and the backflow returned from high-pressure zone to low-pressure zone. Also, at point P1, the amplitude of pressure fluctuation reaches its lowest value, due to the location being far from the interaction zone. Furthermore, the findings from the numerical study have shown that all curves of the investigated points have a similar trend but in different maximum amplitude values based on the position of these points.

### 6.2.2 Analysis of the Pressure Fluctuations of the blower model 1 (M1) in Frequency Domain

This model (M1) has internal clearances smaller than the baseline model (M2), to study the effect of the decrease of gap size on flow fluctuations and therefore on Roots blower performance.

It can be seen from Figure 6.37 and table 6.16 that the same trend from the previous model (M2) is being followed. The maximum pressure fluctuation amplitude from most of the monitoring points is at 120.13Hz (LFP).

Also, the maximum amplitude of pressure fluctuation is at P7 which is 3.28E+04 Pa and at frequency 60.07Hz as illustrated in table 6.16.

Furthermore, the findings from the numerical study have shown that all curves of the investigated points in model 1 have a similar trend but in different maximum amplitude values based on the position of these points.

Table 6.16: The maximum pressure fluctuation amplitudes in the Roots blower model (M1)  
 in Pascal

Positions		Frequencies (Hz)		
		60.07 Hz	120.13 Hz	180.2 Hz
Maximum amplitude of pressure fluctuations at different points within the blower (Pa)	P1	3.44E+00	3.02E+03	2.16E+01
	P2	3.48E+01	3.36E+03	3.30E+01
	P3	6.02E+02	3.70E+03	1.24E+02
	P4	6.38E+02	3.73E+03	6.06E+01
	P5	7.21E+03	5.34E+03	7.23E+03
	P6	3.23E+04	1.85E+04	6.66E+03
	P7	3.28E+04	5.32E+03	1.41E+04
	P8	1.96E+04	2.16E+04	1.08E+04
	P9	1.70E+04	1.90E+04	1.18E+04
	P10	1.32E+02	6.41E+03	5.36E+02
	P11	2.87E+02	5.99E+03	5.18E+02

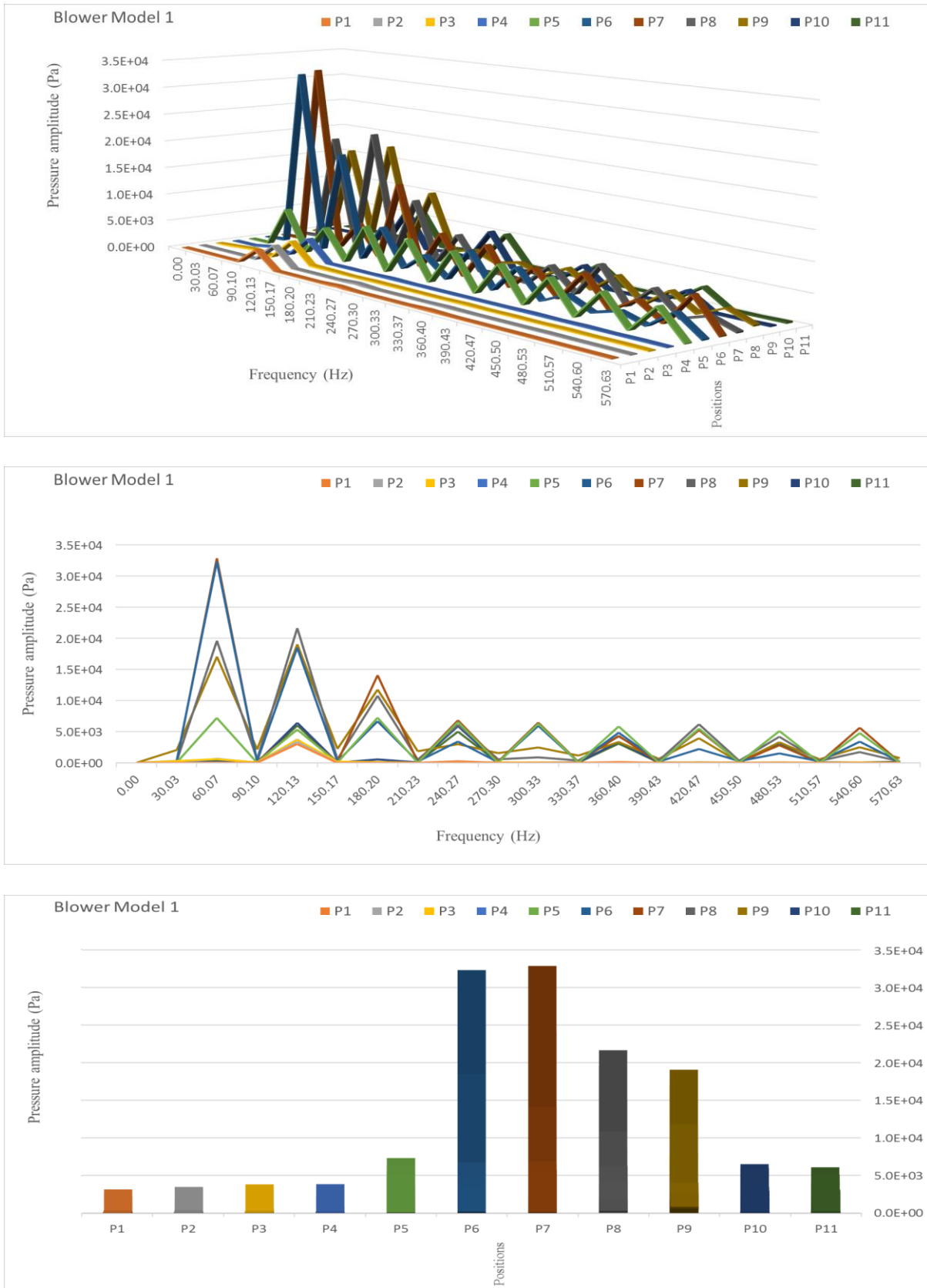


Figure 6.37: The Pressure Fluctuations of the blower model (M1) in Frequency Domain at a speed 1800 rpm and a pressure difference 500 millibars

In comparison with the baseline model (M2), the maximum pressure fluctuation amplitude of model1 is lower than model 2 by 0.3%. The full comparison of two models M2 and M1 are summarised in table 6.17.

It can be concluded from table 6.17 that the maximum pressure fluctuation amplitudes of model1 (M1) are higher than the baseline model (M2) at the suction zone. However, the maximum pressure fluctuation amplitudes of model1 (M1) are smaller than the baseline model (M2) at the discharge zone. Because the effect of velocity and the pressure losses at the suction side in smaller gap model (M1) is higher than baseline model (M2). However, the effect of backflow and the pressure losses at the discharge side in smaller gap model (M1) is lower than baseline model (M2).

Table 6.17: The comparison of maximum pressure amplitudes between M2 and M1 in Pascal

Positions	Maximum pressure amplitude (Pa)		
	M2	M1	Difference %
P1	2.82E+03	3.02E+03	-6.80
P2	3.19E+03	3.36E+03	-5.31
P3	3.53E+03	3.70E+03	-4.62
P4	3.49E+03	3.73E+03	-6.74
P5	7.20E+03	7.23E+03	-0.47
P6	3.22E+04	3.23E+04	-0.27
P7	3.29E+04	3.28E+04	0.30
P8	2.21E+04	2.16E+04	2.006
P9	2.08E+04	1.90E+04	8.56
P10	6.36E+03	6.41E+03	-0.74
P11	5.99E+03	5.99E+03	0.06

### 6.2.3 Analysis of the Pressure Fluctuations of the blower model 3 (M3) in Frequency Domain

To investigate the effect of the increase of gap size on flow fluctuations and therefore on Roots blower performance, model (M3) has internal clearances larger than the baseline model (M2) has been analysed.

Table 6.18 and figure 6.38 depict that the same trend of the model (M2) has been observed in model3 (M3). It can be concluded that the dominant frequency for pressure fluctuation amplitudes in the blower is at the LPF for nearly of most monitoring points, which is equal to 120.13Hz. Also, it can be observed that the maximum pressure fluctuation amplitude of (P6 and P7) is at  $2Rf = 60.07\text{Hz}$  and for P5 is at  $6Rf = 180.2\text{Hz}$  which the maximum pressure fluctuations amplitudes in this model are about  $3.29\text{E}+04$  Pa at P7.

Table 6.18: The maximum pressure fluctuation amplitudes at in the Roots blower model (M3) in Pascal.

Positions		Frequencies (Hz)		
		60.07 Hz	120.13 Hz	180.2 Hz
Maximum amplitude of pressure fluctuations at different points within the blower (Pa)	P1	3.46E+00	2.58E+03	1.09E+01
	P2	3.57E+01	2.96E+03	2.37E+01
	P3	8.25E+02	3.18E+03	1.26E+02
	P4	7.07E+02	3.16E+03	3.52E+01
	P5	6.52E+03	5.70E+03	7.14E+03
	P6	3.20E+04	1.87E+04	7.34E+03
	P7	3.29E+04	4.92E+03	1.40E+04
	P8	2.06E+04	2.26E+04	1.15E+04
	P9	1.80E+04	2.00E+04	1.20E+04
	P10	5.72E+01	6.40E+03	2.18E+02
	P11	4.90E+01	5.88E+03	2.25E+02

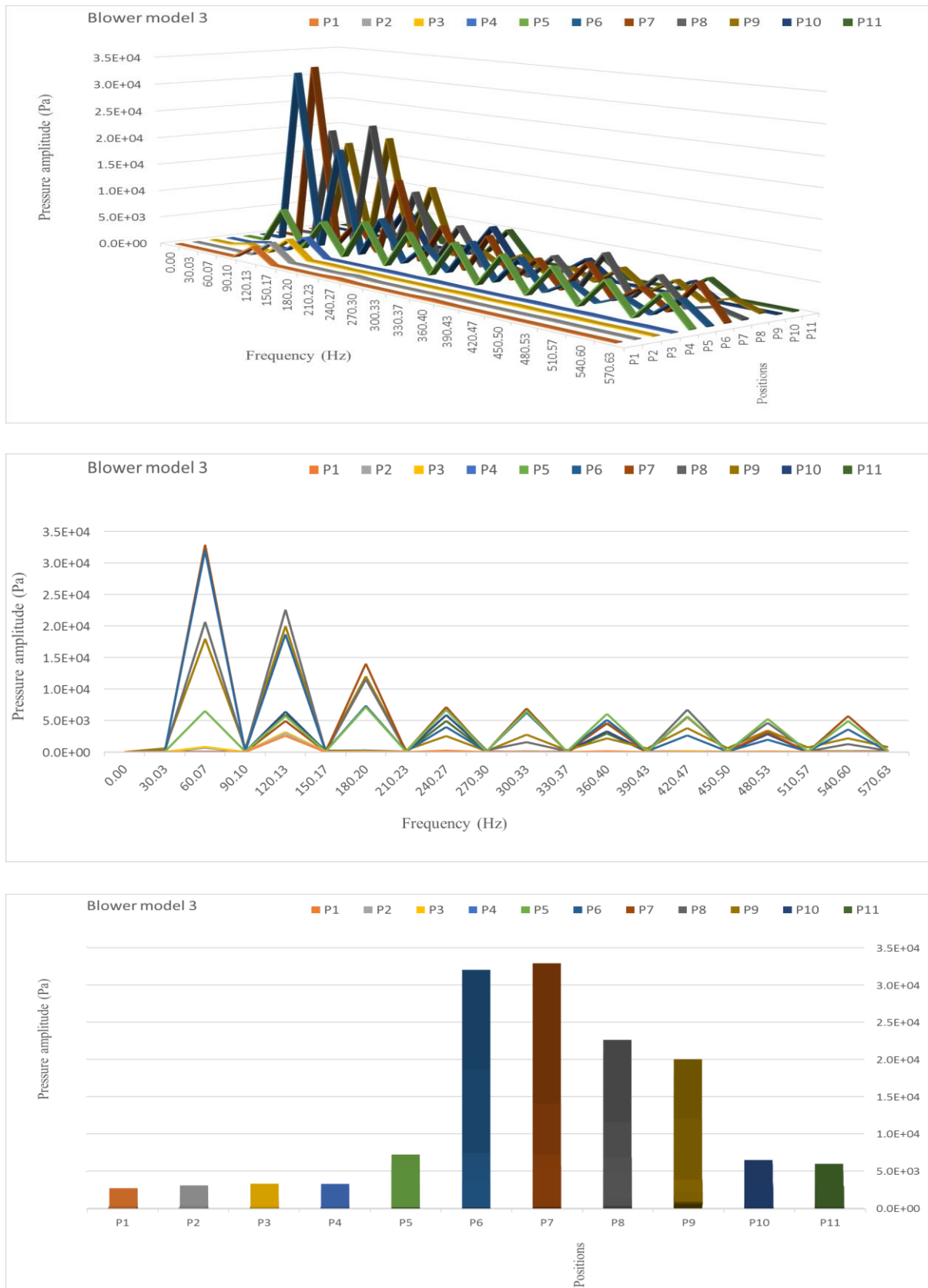


Figure 6.38: The Pressure Fluctuations of the blower model (M 3) in Frequency Domain at a speed 1800 rpm and a pressure difference 500 millibars

In comparison with the model 2, the maximum pressure fluctuation amplitude for model 3 is lower than the baseline model (M2) by about 0.194%.

Table 6.19: The comparison of maximum pressure amplitudes between M2 and M3 in Pascal.

Positions	Maximum pressure amplitude (Pa)		
	M2	M3	Difference %
P1	2.82E+03	2.58E+03	8.73
P2	3.19E+03	2.96E+03	7.21
P3	3.53E+03	3.18E+03	9.94
P4	3.49E+03	3.16E+03	9.44
P5	7.20E+03	7.14E+03	0.81
P6	3.22E+04	3.20E+04	0.62
P7	3.29E+04	3.29E+04	0.19
P8	2.21E+04	2.26E+04	-2.36
P9	2.08E+04	2.00E+04	3.97
P10	6.36E+03	6.40E+03	-0.55
P11	5.99E+03	5.88E+03	1.85

It can be concluded from table 6.12 that the maximum pressure fluctuation amplitudes of model 3 (M3) are lower than the baseline model (M2).

#### 6.2.4 Conclusion summary

The time domain of pressure fluctuations could directly give a visualised result, but the detailed information of the fluctuations should be further analysed in the frequency spectrum. Therefore, a detailed study of pressure fluctuation characteristics in the frequency domain may provide reliable information related to the blower. Such details include the influence of the interaction between the two rotors and the inlet and the outlet cavities of the blower when the blower operates under various operating conditions and different clearance geometries. In the current study, to further analysis the transient pressure data, the fast Fourier transform (FFT) has been used.

The pressure fluctuations in the time domain can give a visualised results, but the in-depth understanding of these fluctuations could be obtained by the frequency spectrum analysis. In the present chapter, the fast Fourier transform (FFT) has been used to further analysis the transient pressure data. Some chosen points at the suction zone, discharge zone and gaps inside the blower are selected. It is evident that the peak value appears at integer multiples of the rotor rotation frequency, especially at  $2Rf$ ,  $4Rf$  and  $6Rf$ . In the suction and discharge of the blower regions, the dominant frequency is  $4Rf$ , while in the gap between rotors and casing region the dominant frequencies are  $2Rf$  and  $6Rf$ . The interaction between rotating rotors could explain the fluctuation peak at  $2Rf$  and  $6Rf$  and flow inside the gap. The rotation of rotors leads to the periodic variation of the physical boundaries of the flow field.

Moreover, it can be concluded that the frequency values for the entire monitoring points are different. However, the maximum pressure fluctuation amplitude for point P7 is higher than the remaining points. In comparison, the maximum pressure fluctuation amplitudes for blower baseline model (M2) and blower model (M1) is more significant than the blower model (M3). The common reason behind this is due to a smaller clearance within model 1 and model 2 making the pressure fluctuations significantly higher when compared to model 3. Also, variances between peaks to valleys for model 1 and model 2 are considerably higher than the model 3.

Based on the outcome of the analysis has been presented in this section, the unsteadies of the flow and the gap size inside the blower have a considerable influence on of the amplitudes of pressure fluctuations.

### **6.3 Develop a methodology for detection of clearance size change inside Roots blower.**

Internal leakage is an essential issue of the Root blower's design. The leakage (slip) in the Roots blower plays an important role because it influence the process efficiency by affecting the mass flow rate and therefore the volumetric efficiency. If the internal gaps are small, the volumetric and the adiabatic efficiencies can maintain high and the slip low, over a wide range of operation conditions and vice versa. The practical design and the manufacture of clearance size depending on the application of blower such as; mass flow, pressure, high velocity and efficiency. Adjustment of clearance size reliant mainly on design and manufacture requirements.

The flow field conditions, inside clearances of the blower are unsteady. The temperatures, pressures, and velocities vary significantly and are a function of operating condition and clearance geometry of the Roots blower.

The diagnosis of the flow inside the clearances is detecting its level of severity which is essential for maintaining the blower's reliability. Based on available literature, extensive studies are being carried out to diagnosis the flow inside clearances in Roots blowers. But, there are lack of studies that deal with the diagnosis of flow within the clearance and to detect the clearance change in Roots blower using the pressure fluctuations analysis.

#### **6.3.1 Determine of pressure fluctuation characteristics with clearance size change in Roots blower using frequency domain**

Unsteady flow and related fluctuations within a Roots blower are unavoidable. Hence, they have a high effect on the flow characteristic and blower foundations. One of most essential factors, which have substantial effects on the Roots blower performance characteristics is clearance sizes within the blower. A detailed qualitative and quantitative numerical analysis on three different clearance models under different operation conditions has been conducted to diagnose and detect the change of clearances size by using of pressure fluctuations in both time and frequency domain, at chosen points inside the blower. The results show that we can use pressure fluctuations in both time and frequency domain as an effective tool to detect the change of gap size within the blower.

The three models are (M1, M2, and M3) which; M2 represents the baseline blower model, M1 has internal clearances smaller than the baseline model, and model M3 has internal clearances larger than the baseline model.

Table 6.200: The maximum pressure fluctuation amplitudes in the Roots blower for 3 models at frequency 120.13 Hz in Pascal.

Positions	Frequency 120.13 Hz		
	M1	M2 Baseline model	M3
P1	3.02E+03	2.82E+03	2.58E+03
P2	3.36E+03	3.19E+03	2.96E+03
P3	3.70E+03	3.53E+03	3.18E+03
P4	3.73E+03	3.49E+03	3.16E+03
P5	5.34E+03	5.52E+03	5.70E+03
P6	1.85E+04	1.86E+04	1.87E+04
P7	5.32E+03	5.25E+03	4.92E+03
P8	2.16E+04	2.21E+04	2.26E+04
P9	1.90E+04	2.08E+04	2.00E+04
P10	6.41E+03	6.36E+03	6.40E+03
P11	5.99E+03	5.99E+03	5.88E+03

Table 6.20 and figure 6.39 represent maximum pressure amplitudes of three models of blower at frequency 120.13 Hz for all the monitoring points in the blower at a rotational speed of 1800 rpm and a pressure difference 500 millibars. It can be conclude that maximum pressure amplitude increases as clearance size decreases at points P1 to P4 and P7, increases at P5,P6 and P8, and fluctuates at P9 to P11. Thus, the maximum pressure amplitudes of points, P1 to P8 can be used as indicators to detect the change of clearance size at frequency 120.13 Hz. However, it is difficult to measure the pressure at the points inside the blower (P2 to P10), so the measure of the pressure at the inlet (P1) and the outlet (P11) of the blower is more practical. Therefore, the maximum pressure amplitudes at P1 can be used as indicators to detect the change of clearance size at frequency 120.13 Hz.

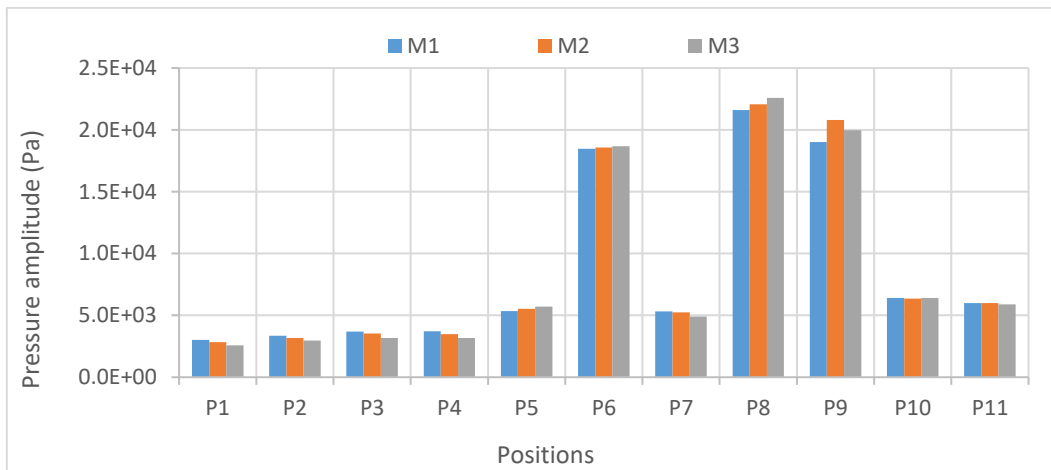


Figure 6. 39: The maximum pressure fluctuation amplitudes in the Roots blower for 3 models at frequency 120.13 Hz

Table 6.21 and figure 6.40 depict the maximum pressure amplitudes of three models of blower at frequency 60.07 Hz for all the monitoring points in the blower. It can be seen that maximum pressure amplitude decreases as clearance size decreases at points P3 and P8, increases at P5, P6, and P11 and fluctuates at other points. Thus, the maximum pressure amplitudes of points, P3, P5, P6, P8, P11 can be used as indicators to detect the change of clearance size at frequency 60.07 Hz. However, it is difficult to measure the pressure at the points inside the blower (P2 to P10), so the measure of the pressure at the inlet (P1) and the outlet (P11) of the blower is more practical. Therefore, the maximum pressure amplitudes at P11 can be used as indicators to detect the change of clearance size at frequency 60.07 Hz

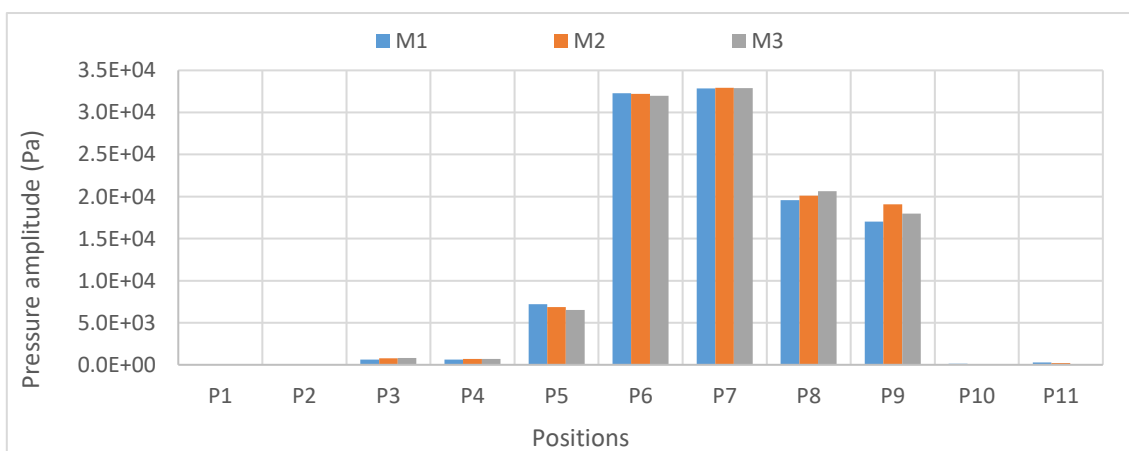


Figure 6.40: The maximum pressure fluctuation amplitudes in the Roots blower for 3 models at frequency 60.07 Hz

Table 6.211: The maximum pressure fluctuation amplitudes in the Roots blower for 3 models (M 1, M 2, and M3) at frequency 60.13 Hz in Pascal.

Positions	Frequency 60.07 Hz		
	M1	M2 Baseline model	M3
P1	3.44E+00	1.01E+01	3.46E+00
P2	3.48E+01	3.97E+01	3.57E+01
P3	6.02E+02	7.78E+02	8.25E+02
P4	6.38E+02	6.82E+02	7.07E+02
P5	7.21E+03	6.87E+03	6.52E+03
P6	3.23E+04	3.22E+04	3.20E+04
P7	3.28E+04	3.29E+04	3.29E+04
P8	1.96E+04	2.01E+04	2.06E+04
P9	1.70E+04	1.91E+04	1.80E+04
P10	1.32E+02	1.15E+01	5.72E+01
P11	2.87E+02	1.98E+02	4.90E+01

Table 6.22 and figure 6.41 present maximum pressure amplitudes of three models of blower at frequency 180.2 Hz for all the monitoring points in the blower at a rotational speed of 1800 rpm and a pressure difference 500 millibars. It apparent that maximum pressure amplitude increases as clearance size decreases at points P1, P10, and P11, and fluctuates at another points. Thus, the maximum pressure amplitudes of points, P1, P10, and P11 can be used as indicators to detect the change of clearance size at frequency 120.13 Hz. However, it is difficult to measure the pressure at the points inside the blower (P2 to P10), so the measure of the pressure at the inlet (P1) and the outlet (P11) of the blower is more practical. Therefore, the maximum pressure amplitudes at P1 and P2 can be used as indicators to detect the change of clearance size at frequency 180.2 Hz

Table 6.222: The maximum pressure fluctuation amplitudes in the Roots blower for 3 models (M 1, M 2, and M3) at frequency 180.13 Hz in Pascal.

Positions	Frequency 180.2 Hz		
	M1	M2 Baseline model	M3
P1	2.16E+01	1.95E+01	1.09E+01
P2	3.30E+01	3.57E+01	2.37E+01
P3	1.24E+02	2.88E+01	1.26E+02
P4	6.06E+01	2.02E+01	3.52E+01
P5	7.23E+03	7.20E+03	7.14E+03
P6	6.66E+03	7.06E+03	7.34E+03
P7	1.41E+04	1.42E+04	1.40E+04
P8	1.08E+04	1.11E+04	1.15E+04
P9	1.18E+04	1.30E+04	1.20E+04
P10	5.36E+02	3.16E+02	2.18E+02
P11	5.18E+02	3.16E+02	2.25E+02

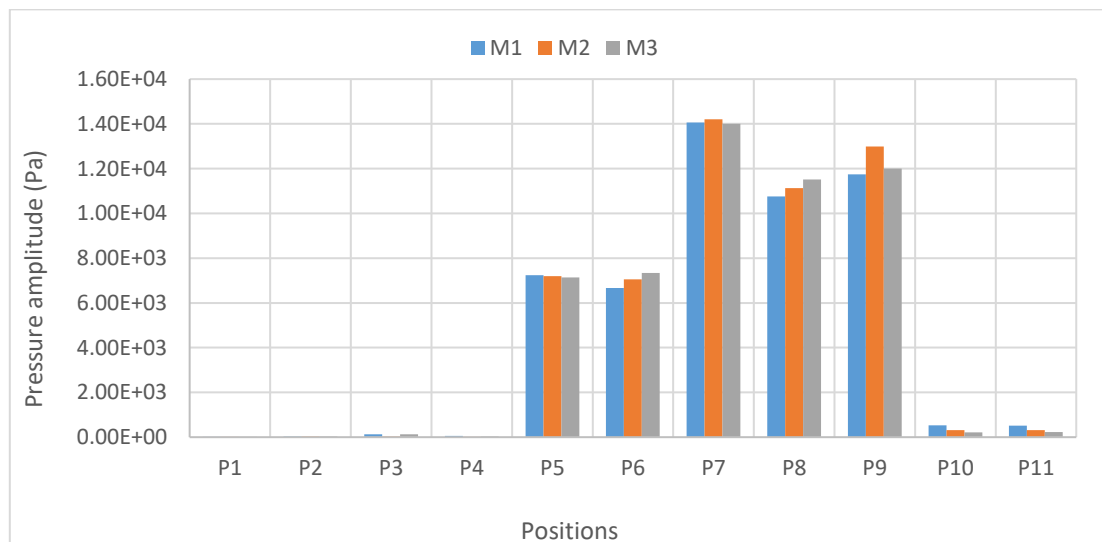


Figure 6.41: The maximum pressure fluctuation amplitudes in the Roots blower for 3 model at frequency 180.2 Hz

### **6.3.2 Summary**

The size and the internal flow inside the clearances between the rotating parts and stationary parts have a significant influence on the Roots blower performance. However, it is difficult in measuring, time-consuming, and costly to investigate experimentally the effect of gap size and the flow behaviour within these gaps in the blower, so the numerical method is an alternative one.

In this section, both qualitative and quantitative numerical analyses have been carried out to establish the effect of clearance sizes on the pressure fluctuations in the Roots blower. The pressure fluctuations analysis have been carried out in both, time and frequency domains

The results show that the maximum pressure amplitudes at P1 can be used as indicators to detect the change of clearance size at frequencies 120.13 Hz and 180.2 Hz. Also, the maximum pressure amplitudes at P11 can be used as indicators to detect the change of clearance size at frequency 60.13 Hz and 180.2 Hz

Based on the information represented in this section, about the pressure fluctuation amplitudes, the results have shown that the unsteady flow and the gap size inside the blower have a high impact on the amplitude values of the pressure fluctuations.

Furthermore, the results revealed that using pressure signals in both time and frequency domains are useful for predicting the flow behaviour affected by different gap sizes inside the blower and for detecting and estimating the change of clearance size.

## Chapter 7

### Conclusions

The obtained experimental and numerical outcomes concerning the geometric and flow related parameters within the Roots blower have been analysed and characterised critically in previous chapters. Accordingly, comprehensive conclusions have been conducted in this chapter. The main achievements and contributions to the current knowledge that related to the aims and the objectives of this investigation are summed up. Finally, the evaluation of the current research study is carried out and recommendations for future work and the limitations of present work in the area of Roots blower are defined and suggested.

#### 7.1. Research Problem Synopsis

Roots Blowers are positive displacement type pumps. They are widely used in several industrial processes as pressure or vacuum devices due to their simple construction, large volumetric efficiency and are most effective in moderate compression ratio ranging from 1.1 to 2. Several studies were conducted to improve the performance of Roots blower (30, 31, 32, and 33). In more recent years, Roots blower development has been focused on increasing volumetric efficiency, reducing power consumption and developing quieter blowers, which are the basic requirements of current and future blower technology. Performance parameters of Roots blower have been highlighted to maximise volumetric efficiency and minimise backflow and noise. It can be concluded that the flow velocity and the backflow are a function of pressure and temperature variations and distributions in Roots blower.

However, the majority of research studies carried out in the area of Roots blower based on analytical, experimental and numerical modelling lack the in-depth analysis of the characteristics and the behaviour of the flow in such blowers. Also, the influence of essential flow and geometric parameters such as (rotational speed, pressure difference, and clearance sizes) on the blower performance. Furthermore, most of these studies limited in the analysis of the local flow behaviour of fluid such as the variation and the distribution of pressure, temperature and velocity within the Roots blower and the relations between them. The experimental approach is expensive in terms of cost and time, flexibility of modern CFD tools

with advanced computing technologies can model a Roots blower in two or three dimensions and provide detailed analysis of the flow within it under varying geometric and flow conditions with reasonable accuracy, cost and time. A synopsis of the primary aims and objectives of the thesis is provided within the next sections of this chapter alongside with the main achievements and contributions.

## **7.2. Research Objectives and Most important Achievements**

Comprehensive investigations have been carried out to support the available literature relating to a Roots blower machine and to give new additional information to enhance the present understanding of the design development, operating flow characteristics and geometry related effects. The main conclusions of this research study are summarised as follows:

### **1- Performance characterisation of the influence of pressure difference and rotational speed on the Roots blower performance under the transient condition**

Experimental and numerical approaches have been used to carry out a detailed investigations of the characteristics and the behaviour of the operating fluid within Roots blower. The results have been generated by varying the rotational speed of blower and the discharge pressure. The investigations have been conducted for measuring the pressure, the temperature of operating fluid and mass flow rate within the Roots blower. The variations and distributions of pressure, temperature and velocity of fluid within the Roots blower. Also, the mass flow rate and the volumetric and the isentropic efficiencies have been analysed qualitatively and quantitatively

It can be concluded that an increase in the pressure difference increase of the pressure and the temperature of working fluid within blower. On another hand, the pressure and the temperature inside the clearances are decreased with the increase of pressure difference. The reason for all that because of the effect of backflow from high pressure at the outlet zone to low-pressure zone through clearances inside the blower. Also, the mass flow rate and volumetric efficiency decline with an increase of pressure difference. This is due to that leakage rate increase with rise of pressure differences.

Moreover, rotational speed has a significant effect on the performance of Roots blower. An increase in rotational speed leads to an increase in velocity and therefore decrease in the pressure of operating fluid, the rise of the out mass flow rate and an increase of volumetric efficiency of Roots blower. Also, the temperature of operating fluid within the blower declines

as the rotational speed of the impellers increases. It is evident that a decrease in the speed to low levels heats the working fluid more. The outcomes concerning the influence of the pressure difference and rotational speed on the performance of a Roots blower can be used to improve the design of Roots blower.

## **2- Non-dimensional analysis of performance parameters and develop empirical correlations for performance factors of Roots blower**

Based on the outcomes from experimental investigations, this study has been conducted to establish the relations between different non-dimensional parameters. Also, the development of empirical correlations has been achieved in this study to predict mass flow rate, outlet temperature, volumetric efficiency, isentropic efficiency and power consumption of Roots blower. The parameters that affect the performance of the Roots blower have been included in the developed model, which is one of the main achievements of the present research. Moreover, it can be revealed that prediction models produced in this investigation have acceptable accuracy comparing to the measured results. Furthermore, the developed correlations may apply to the same designs of Roots blower at different operating conditions.

## **3- Numerical characterisation of the influence of the clearance size on blower performance characteristics under a transient condition**

Numerical investigation have been conducted using CFD approach and dynamic mesh techniques have been performed on the flow characteristics for various clearance models concerning the effect of the gap size (tip and centre clearances) inside the blower on the performance of a Roots blower. The qualitative and quantitative analyses of the effect of rotational speed, pressure difference and gap size on the variations and the distributions of pressure, temperature and velocity of operating fluid inside Roots blower have been carried. The investigation depicts that decreases the gap within the blower increases velocity and hence the leakage flow decreases, therefore, it increases the output mass flow rate and as a result increases the volumetric efficiency. Also, the decrease of gap size will increase further the velocity inside the gap. In addition, the increase of pressure difference will lead to rising the velocity in the centre gap but in reverse direction which leads to strong backflow and therefore it declines of mass flow rate. Moreover, the decrease in gap decreases the temperature of working fluid within the Roots blower.

In this present study, mass flow and efficiency improvements have been achieved by decrease the gap size within blower as compared to baseline model.

Furthermore, the results provided in this study regarding the effect of the gap size on the performance of a Roots system can be used for design optimisation

#### **4. Deriving semi-empirical prediction equations depending on non-dimensional relations between different flow and geometric performance parameters**

Based on the outcomes have been obtained from the numerical investigations and subsequent the analysis of the influence of different clearance sizes and flow related parameters on blower performance, semi-empirical correlations have been developed by using multiple regression analysis to predict some of performance factors such as mass flow rate and the volumetric efficiency. The parameters that affect the performance of the Roots blower have been included in the developed model, which is one of the main achievements of the current research. Moreover, it can be concluded that prediction models created in the current investigation have accurate results comparing to the numerical outcomes. Furthermore, the developed correlations may apply to the same designs of Roots blower at different operating conditions

#### **5. Establish the effect of the clearance sizes in order to develop a new clearance model of Roots blower**

Based on 3D CFD approach and dynamic mesh techniques detailed investigations have been achieved on the flow characteristics of three clearance models of the Roots blower. The primary purpose of these models is to prove that by decreasing both tip and centre clearances to an acceptable level, the improvement of Roots blower performance can be achieved. In this current study, mass flow and efficiency improvement have been achieved. In order to determine the influence of new models on the performance output of the Roots blower, a comparison between new models and baseline model has been done. The qualitative and quantitative analyses of the variations and the distributions of pressure, temperature and velocity of operating fluid inside the Roots blower system for new and baseline models have been performed.

The result indicate that the mass flow rate and the pressure of the new model are higher compared to the baseline model. Also, the temperature is lower for the new model in

comparassion to baseline model. Accordingly, the performance of the new Roots blower model is improved and better than the baseline model. Furthermore, the outcomes provided in the present research related to the new model of the Roots blower can be used to improve the performance of such device.

## **6. Establish the effect of the clearance size on pressure fluctuation and flow pattern of Roots blower**

A detailed qualitative and quantitative numerical analysis of pressure fluctuations in both time and frequency domain, at chosen points inside the blower, has been conducted using three different clearance models under different operation conditions. The fast Fourier transform (FFT) has been used to process the transient pressure data. It is apparent that the highest values appears at the integer multiples of the rotor rotation frequency, especially at  $2Rf$ ,  $4Rf$  and  $6Rf$ .

The rotation of rotors leads to the periodic variation of the physical boundaries of the flow field. Moreover, it can be concluded that the values of the frequency are depended on the position of entire monitoring points. Based on the outcome of the analysis presented in this area of study, it can be concluded that the unsteady flow and the gap size inside the blower have a considerable influence on the amplitude values of the pressure fluctuations. The fluctuations of the pressure in the Roots blower have a significant influence on the characteristic of the transient flow field inside the blower. Also, the in-depth understand of the relationships between different flow and geometric parameters within the blower has been achieved

## **7. Develop a methodology for detection of the change of clearance size inside Roots blower:**

Unsteady flow and related oscillations within a Roots blower are unavoidable. Hence, they have a high effect on the flow characteristic and blower foundations. One of most essential factors, which have substantial effects on the Roots blower performance characteristics is clearance sizes within the blower. A detailed qualitative and quantitative numerical analysis on three different clearance models under different operation conditions has been conducted to diagnose and detect the change of clearances size by using of pressure fluctuations in both time

and frequency domain, at chosen points inside the blower. The results show that we can use pressure fluctuations in both time and frequency domain as an effective tool to detect the change of gap sizes within the blower.

### **7.3 Thesis Contributions**

The main contributions of the present research are summarised below, which describes the new developments in this field of study.

#### **Contribution # 1:**

The first contribution of the current research is an inclusive studies on the characteristics of the local and the global flow of operating fluid in the Roots blower. The existing literature concerning the variations and the distributions of the pressure, the velocity and temperature of operating fluid in the clearances in Roots blower are severely limited. Hence, a Computational Fluid Dynamics approach along with experimental setup have been used to carry out inclusive studies on the variations and the distributions of pressure, velocity and temperature inside the Roots blower. Effect of different geometric and flow related parameters such as tip clearance, centre clearance, rotational speed and pressure load have been included.

#### **Contribution # 2:**

The substantial contribution of present research is the improvement of the performance of Roots blower by decreasing the clearance sizes within the blower. An attempt has been made to justify the enhancement in performance characteristics of the model with new gap sizes by keeping operating fluid conditions to be similar so only the influence of clearance sizes are considered in the analysis.

#### **Contribution # 3:**

Investigations on various clearance configurations have been conducted by comparing the performance of the proposed models with the baseline model to improve the Roots blower model. Findings of the numerical investigation of clearance geometry modifications are a novel contribution to the knowledge that can be used to improve the performance of a Roots blower system.

**Contribution # 4:**

Enhancement in the performance of Roots blower has been achieved by adjustment of clearance sizes within the blower maintaining the same dimensions of the baseline model.

**Contribution # 5:**

Based on the outcome of the analysis presented in this area of study, the in-depth understand of the relationships between different flow and geometric parameters within the blower has been achieved it can be concluded that the unsteady flow and the gap size inside the blower have a considerable influence on the amplitude values of the pressure fluctuations. The fluctuations of the pressure in the Roots blower have a significant influence on the characteristic of the transient flow field inside the blower.

**Contribution # 6:**

Empirical relationships have been developed for the mass flow rate, the volumetric efficiency, isentropic efficiency, power consumption and the outlet temperature of operating fluid within Roots blower. The developed correlations may be applied to the same designs of Roots blower at different operating conditions.

**Contribution # 7:**

Diagnostics of the change in clearance size by using of pressure fluctuations in both time and frequency domain at chosen points inside the blower have been achieved. The results show that we can use pressure fluctuations in both time and frequency domain as an effective tool to detect the change of gap sizes within the blower.

**Contribution # 8:**

The new semi-empirical correlations have been developed for some performance factors such as the mass flow rate, the volumetric efficiency, isentropic efficiency, power consumption and the outlet temperature of operating fluid within Roots blower. The developed correlations may be applied to the same designs of Roots blower at different operating conditions.

## **7.4. Recommendations for future work and limitations of the presented work**

Concerning to fill the gaps of knowledge, that have been identified from the review of available literature regarding the Roots blower machine, the effect of operational condition and the clearance size on flow characteristics and the performance of Roots blower have been investigated and analysed in the present research. Based on the present research study, it is apparent that there is considerable potential for additional research studies in the field of Roots blower. In order for further analysis in the design and improvement of the performance of Roots blower, following future works have been suggested.

### **Recommendation # 1:**

The comprehensive numerical investigations can be conducted to study the effect of different clearance configurations within the Roots blower on the performance of the Roots blower system. Hence, the optimisation can be carried out to develop a new optimum model.

### **Recommendation # 2:**

A study on the effect of different geometry configurations of inlet and outlet of the blower on the performance of Roots blower can be carried out to improve the performance of the Roots blower system

### **Recommendation # 3:**

This conclusion induces further research interest about the selection of an optimal leakage clearance range to correlate with specific operational parameters. More research on intelligent design tools and methodology is needed to achieve this.

### **Recommendation # 4:**

Development of a comprehensive design methodology of Roots blower including heat transfer effect for achieving optimum efficiency.

### **Recommendation # 5:**

Development of a comprehensive methodology for detection the clearances change as a result from expansion and wear phenomenon inside of the Roots blower.

## References

- Air, C., & Rollins, J. P. (1961). *Compressed Air and Gas Handbook*: Compressed Air and Gas Institute.
- ANSYS. (2010). ANSYS FLUENT 13.0 Getting Started Guide. (13.0), viii, 18.
- ANSYS, C. (2014). Theory Guide Version 14.5. *ANSYS Inc.*
- Ansystech, H. (2014). v15. *ANSYS Corporation Software, Pittsburgh, PA, USA.*
- Arai, K., Fukagawa, T., & Ohtsuka, Y. (1990). Roots type blower having reduced gap between rotors for increasing efficiency. In: Google Patents.
- Ashgriz, N., & Mostaghimi, J. (2002). An introduction to computational fluid dynamics. *Fluid flow handbook. McGraw-Hill Professional.*
- Baker, R. C. (2005). *Flow measurement handbook: industrial designs, operating principles, performance, and applications*: Cambridge University Press.
- Barber, A. (1997). *Pneumatic handbook*: Elsevier.
- Bean, H. S. (1971). Fluid Meters. *Their Theory and Application.*
- Bell, S. (2001). Measurement good practice guide no. 11 (issue 2). *A Beginner's Guide to Uncertainty of Measurement. National Physical Laboratory Teddington, Middlesex, United Kingdom.*
- Bhuyan, P., Ghosh, S., & Sarangi, S. (2016). A Numerical Investigation to Capture the Unsteady Internal Flow Phenomena and Heat Transfer Mechanism in Roots Type Blower or Pump.
- Brynych, P., Macek, J., Vitek, O., & Cervenka, L. (2013). *1-D Model of Roots Type Supercharger*. <http://dx.doi.org/10.4271/2013-01-0927>
- Burmistrov, A., Belyaev, L., Ossipov, P., Fomina, M., & Khannanov, R. (2001). Combined experimental and calculation study of conductance of Roots pump channels. *Vacuum*, 62(4), 331-335.
- Burmistrov, A., Salikeev, S., Bronshtein, M., Fomina, M., & Rayko, A. (2015). Conductance Calculation Of Slot Channels with Variable Cross Section. *Vakuum in Forschung und Praxis*, 27(1), 36-40.
- Carbutt, E. H. (1877). On Roots' Mine Ventilator, and other Applications of Roots' Blower. *Proceedings of the Institution of Mechanical Engineers*, 28(1), 92-116.
- Castrup, S., & Castrup, H. (2010). Measurement uncertainty analysis principles and methods. *National Aeronautics and Space Administration.*
- Choi, J.-W. (2013). Modeling and model based fault diagnosis of dry vacuum pumps in the semiconductor industry.
- Crane. (1977). *Flow of fluids: through valves, fittings, and pipe.*
- Dixon, S. L., & Hall, C. (2013). *Fluid mechanics and thermodynamics of turbomachinery*: Butterworth-Heinemann.
- Fukagawa, T. (1991). Roots blower with improved clearance between rotors. In: Google Patents.
- Hall, C., & Dixon, S. L. (2013). *Fluid mechanics and thermodynamics of turbomachinery*: Butterworth-Heinemann.
- Houzeaux, G., & Codina, R. (2007). A finite element method for the solution of rotary pumps. *Computers & fluids*, 36(4), 667-679.
- Hsieh, C.-F. (2015). A new curve for application to the rotor profile of rotary lobe pumps. *Mechanism and Machine Theory*, 87, 70-81.

- Hsieh, C.-F., & Hwang, Y.-W. (2007). Study on the high-sealing of Roots rotor with variable trochoid ratio. *Journal of Mechanical Design*, 129(12), 1278-1284.
- Hsieh, C.-F., & Hwang, Y.-W. (2008). Tooth profile of a Roots rotor with a variable trochoid ratio. *Mathematical and Computer Modelling*, 48(1), 19-33.
- Hsieh, C.-F., & Zhou, Q.-J. (2015). Fluid analysis of cylindrical and screw type Roots vacuum pumps. *Vacuum*.
- Huang, K. J., & Lian, W. C. (2009). Kinematic flowrate characteristics of external spur gear pumps using an exact closed solution. *Mechanism and Machine Theory*, 44(6), 1121-1131.
- Huang, P. X., Yonkers, S., & Hokey, D. (2014). Gas Pulsation Control Using a Shunt Pulsation Trap.
- Huang, S., Guo, J., & Yang, F. (2013). *Numerical simulation of 3D unsteady flow in a rotating pump by dynamic mesh technique*. Paper presented at the IOP Conference Series: Materials Science and Engineering.
- Huang, Z., & Liu, Z. (2009). Numerical study of a positive displacement blower. *Proceedings of the Institution of Mechanical Engineers, Part C: Journal of Mechanical Engineering Science*, 223(10), 2309-2316.
- Hwang, Y., & Hsieh, C. (2006). Study on high volumetric efficiency of the Roots rotor profile with variable trochoid ratio. *Proceedings of the Institution of Mechanical Engineers, Part C: Journal of Mechanical Engineering Science*, 220(9), 1375-1384.
- ISO, E. 5167-2: 2003. *Measurement of Fluid Flow by Means of Pressure Differential Devices Inserted in Circular-Cross Section Conduits Running Full-Part, 2*.
- Joshi, A. M., Blekhman, D. I., Felske, J. D., Lordi, J. A., & Mollendorf, J. C. (2006). Clearance analysis and leakage flow CFD model of a two-lobe multi-recompression heater. *International Journal of Rotating Machinery*, 2006.
- Kang, Y.-H., & Vu, H.-H. (2014). A newly developed rotor profile for lobe pumps: Generation and numerical performance assessment. *Journal of Mechanical Science and Technology*, 28(3), 915-926. doi:10.1007/s12206-013-1159-7
- Kang, Y.-H., Vu, H.-H., & Hsu, C.-H. (2012). Factors impacting on performance of lobe pumps: A numerical evaluation. *Journal of Mechanics*, 28(02), 229-238.
- Kang, Y., Vu, H., & Hsu, C. (2012). Factors impacting on performance of lobe pumps: A numerical evaluation. *Journal of Mechanics*, 28(2), 229-238.
- Karassik, I. J., Messina, J. P., Cooper, P., Heald, C. C., Krutzsch, W., Hosangadi, A., . . . Boyadjis, P. A. (1986). *Pump handbook* (Vol. 3): McGraw-Hill New York.
- Kun, L., Dechun, B., Zhenhou, Z., Guangyu, W., & Naiheng, C. X. a. Y. (2007). Improvement of Profile and Structure of Rotors in Roots Dry Vacuum Pump Available to Discharge Directly into Atmosphere. *VACUUM SCIENCE AND TECHNOLOGY*, 27(5), 446.
- Lau, P. (2008). Calculation of flow rate from differential pressure devices— orifice plates. *Technical research Institute, Sweden*.
- Li, Y., Sang, X., Meng, Q., Shen, H., & Jia, K. (2013). *Transient simulation in interior flow field of lobe pump*. Paper presented at the IOP Conference Series: Materials Science and Engineering.
- Linford, A. (1961). Flow measurement and meters.
- Litvin, F. L., & Feng, P.-H. (1996). Computerized design and generation of cycloidal gearings. *Mechanism and Machine Theory*, 31(7), 891-911.
- Liu, H.-C., Tong, S.-H., & Yang, D. C. (2000). Trapping-free rotors for high-sealing lobe pumps. *Journal of Mechanical Design*, 122(4), 536-542.

- Liu, X., & Lu, J. (2014). Unsteady flow simulations in a three-lobe positive displacement blower. *Chinese Journal of Mechanical Engineering*, 27(3), 575-583.
- Liu, X., Lu, J., Gao, R., & Xi, G. (2013). Numerical investigation of the aerodynamic performance affected by spiral inlet and outlet in a positive displacement blower. *Chinese Journal of Mechanical Engineering*, 26(5), 957-966.
- Liu, Y., Wang, L., & Zhu, Z. (2015). Numerical study on flow characteristics of rotor pumps including cavitation. *Proceedings of the Institution of Mechanical Engineers, Part C: Journal of Mechanical Engineering Science*, 229(14), 2626-2638.
- Massey, B. S., & Ward-Smith, J. (1998). *Mechanics of fluids* (Vol. 1): Crc Press.
- Masuda, N., Takeshita, H., Iwase, T., Mochizuki, H., Sibata, T., Miyake, T., & Kobayashi, N. (1988). Roots-type fluid machine. In: Google Patents.
- McDougald, S., Imrie, B., & Cole, B. (1974). An Investigation of the Volumetric Efficiency of a Roots Blower.
- Miller, R. W. (1983). Flow measurement engineering handbook.
- Mimmi, G., & Pennacchi, P. (1997). Involute gear pumps versus lobe pumps: a comparison. *Journal of Mechanical Design*, 119(4), 458-465.
- Mimmi, G., & Pennacchi, P. (1999). Dynamic loads in the three-lobe supercharger. *Journal of Mechanical Design*, 121(4), 602-605.
- Niimura, Y., Kikuta, R., & Usui, K. (1990). Two-Shaft type rotary machine having a tip circle diameter to shaft diameter within a certain range. In: Google Patents.
- Patterson, J., & Ritchie, J. (1969). Roots blower performance. *International Journal of Mechanical Sciences*, 11(7), 575-593.
- Prakash, M., Stokes, N., Bertolini, J., Tatford, O., & Gomme, P. (2003). *SPH simulations of a lobe pump: prediction of protein shear stress at different pump efficiencies*. Paper presented at the Proc: 3rd Int. Conf. on CFD in Minerals and Process Industries.
- Priede, T. (1966). *Paper 11: Origins of Rotary Positive Displacement Blower Noise*. Paper presented at the Proceedings of the Institution of Mechanical Engineers, Conference Proceedings.
- Reader-Harris, M. (2007). ISO flow measurement standards—report on the ISO/TC 30 meeting in November 2006. *Flow Measurement and Instrumentation*, 18(3), 114-120.
- Reuleaux, F. (2013). *The kinematics of machinery: outlines of a theory of machines*: Courier Corporation.
- Ritchie, J. (1966). *The Roots Blower*. University of Melbourne, Office of Research,
- RYDE, J. L. (1942). The Positive-displacement Supercharger. *SAE Transactions*, 304-313.
- Salaskar, S., & Inamadar, K. (2012). Design and manufacturing of twin lobe roots blower using steel shafts. *International Journal of Engineering Research and Applications*, 2, 266-270.
- Sawhney, G. (2011). *Fundamentals of Fluid Mechanics*: IK International Pvt Ltd.
- Schetz, J. A., & Fuhs, A. E. (1999). *Fundamentals of fluid mechanics*: John Wiley & Sons.
- Shepherd, D. G. (1956). *Principles of turbomachinery*: Macmillan.
- Škerlavaj, A., Škerget, L., Ravnik, J., & Lipej, A. (2011). Choice of a turbulence model for pump intakes. *Proceedings of the Institution of Mechanical Engineers, Part A: Journal of Power and Energy*, 0957650911403870.
- Standard, B., & ISO, B. (1991). Measurement of fluid flow by means of pressure differential devices.
- Stosic, N., Smith, I., & Kovacevic, A. (2005). *Screw compressors: mathematical modelling and performance calculation*: Springer Science & Business Media.

- Sun, S.-K., Zhao, B., Jia, X.-H., & Peng, X.-Y. (2017). Three-dimensional numerical simulation and experimental validation of flows in working chambers and inlet/outlet pockets of Roots pump. *Vacuum*, 137, 195-204.
- Sun, S., Zhou, Q., Wen, J., & Peng, X. (2017). *Three-dimensional numerical simulation and experimental validation of flows in working chambers of roots blowers with backflow design*. Paper presented at the IOP Conference Series: Materials Science and Engineering.
- Sutherland, W. (1893). LII. The viscosity of gases and molecular force. *The London, Edinburgh, and Dublin Philosophical Magazine and Journal of Science*, 36(223), 507-531.
- Taylor, E. (1974). Dimensional analysis for engineers. Clarendon. In: Oxford Google Scholar.
- Thai, N. H., & Trung, N. T. (2015). ESTABLISHING FORMULAS FOR DESIGN OF ROOTS PUMP GEOMETRICAL PARAMETERS WITH GIVEN SPECIFIC FLOW RATE. *Vietnam Journal of Science and Technology*, 53(4), 533.
- Tong, S.-H., & Yang, D. C. (2005). Rotor profiles synthesis for lobe pumps with given flow rate functions. *Journal of Mechanical Design*, 127(2), 287-294.
- Tryhorn, D. (1956). An approach to the problem of pressure charging the compression-ignition engine. *Proceedings of the Institution of Mechanical Engineers: Automobile Division*, 10(1), 217-228.
- Türk, M., & Verhülsonk, B. (2006). Gap leakage behaviour of helical vane rotary lobe pumps. *World Pumps*, 2006(475), 32-37.
- Ucer, S., & Celik, I. (1980). Analysis of flow through roots blower systems.
- Umrath, W. (1998). Fundamentals of vacuum technology. *Leybold, Cologne*.
- Valdès, L.-C., Barthod, B. t., & Le Perron, Y. (1999). Accurate prediction of internal leaks in stationary dry Roots vacuum pumps. *Vacuum*, 52(4), 451-459.
- Verma, S. K. (2014). *Numerical Investigation on the Performance of Roots Blower Varying Rotor Profile*. National Institute of Technology Rourkela,
- Versteeg, H. K., & Malalasekera, W. (2007). *An introduction to computational fluid dynamics : the finite volume method* (2nd ed.). New York: Pearson Education Ltd.
- Versteeg, H. K., & Malalasekera, W. (2007). *An introduction to computational fluid dynamics: the finite volume method*: Pearson Education.
- Wang, P., Fong, Z., & Fang, H. (2002). Design constraints of five-arc Roots vacuum pumps. *Proceedings of the Institution of Mechanical Engineers, Part C: Journal of Mechanical Engineering Science*, 216(2), 225-234.
- Ware, M., & Wilson, E. E. (1929). The comparative performance of Roots type aircraft engine superchargers as affected by change in impeller speed and displacement.
- Yang, D. C., & Tong, S.-H. (2002). The specific flowrate of deviation function based lobe pumps—derivation and analysis. *Mechanism and machine theory*, 37(10), 1025-1042.
- Yao, L., Ye, Z., Dai, J. S., & Cai, H. (2005). Geometric analysis and tooth profiling of a three-lobe helical rotor of the Roots blower. *Journal of materials processing technology*, 170(1), 259-267.
- Ying-jie, C., Li-gang, Y., & Bei-jiang, D. (2016). Modelling and verification of a new Roots blower profile based on analysis of performance of different leaf contour. *重庆大学学报 (英文版)*(2016年03), 95-102.
- Yoshimura, N. (2007). *Vacuum technology: practice for scientific instruments*: Springer Science & Business Media.

- ZHANG, G.-z., & WANG, F.-z. (2011). Numerical analysis of internal flow field in Roots blower with gradually expanding gap [J]. *Journal of Machine Design*, 4, 021.
- ZHANG, G.-z., WANG, F.-z., HAN, G., & SUN, Y. (2011). Analysis of Performance of Roots Blower with Countercurrent Cooling [J]. *Fluid Machinery*, 4, 012.

## APPENDEICES

### APPENDEX A1

Figure A1.1: Experimental test setup with HRVB613 blower

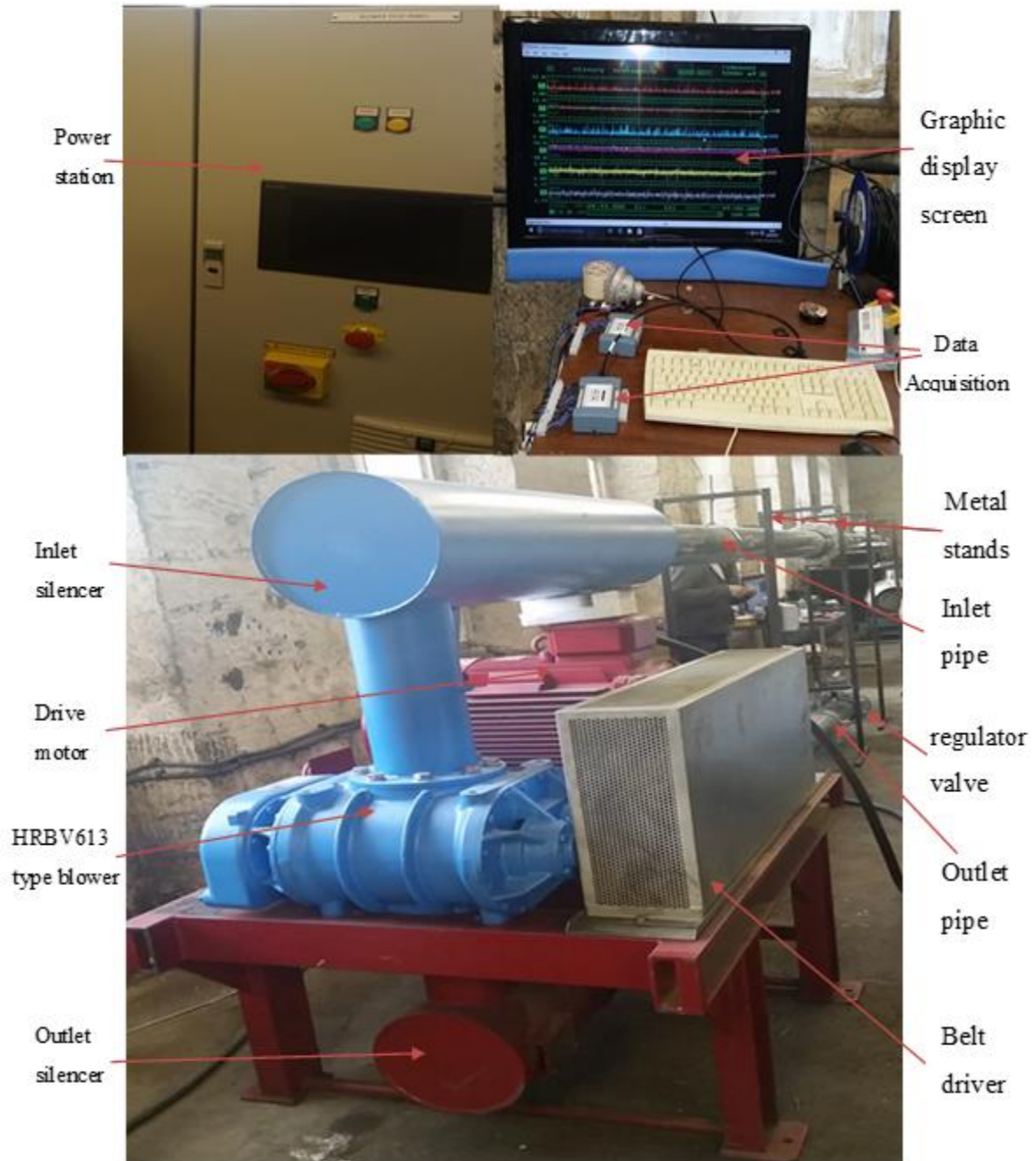


Table A1.1: The procedures of calibration of temperature at different location in the blower. The covert of temperature signals start from down (signals) to up (pressure values).

Temperature amp [C]	Temperature in sys [C]	Temperature in blower [C]	Temperature out blower [C]
% of Range* Instrument Range			
21.96001923	21.30084081	20.86592361	84.21357589
Instrument Range			
60	60	60	130
Instrument High			
50	50	50	150
Instrument Low			
-10	-10	-10	20
% of Range=Current/16			
0.532666987	0.52168068	0.51443206	0.493950584
Current=Current [mA] - Range Min			
8.522671795	8.346890882	8.230912963	7.90320934
Range			
16	16	16	16
Range Max			
20	20	20	20
Range Min			
4	4	4	4
Current [mA]= Current [A]*1000			
12.52267179	12.34689088	12.23091296	11.90320934
Current [A]			
0.012522672	0.012346891	0.012230913	0.011903209
Resistor [Ohm]			
500	500	500	500
Average [V]			
6.261335897	6.173445441	6.115456482	5.95160467

Table A1.2: The procedures of calibration of pressure at different location in the blower. The covert of pressure signals start from down (signals) to up (pressure values).

Pressure Ambient [Pa Abs]	Pressure in sys [Pa Abs]	Pressure in blower [Pa Abs]	Pressure out blower [Pa Abs]	Pressure [Pa Gage]	Diff-Pressure [mBar]
% of Range* Instrument Range					
100594.2712	99583.8658	87860.33214	142154.588	41523.6 75	140.812876
Instrument Range					
200000	200000	200000	350000	200000	400
Instrument High					
200000	200000	200000	350000	200000	400
Instrument Low					
0	0	0	0	0	0
% of Range=Current/16					
0.502971356	0.497919329	0.439301661	0.406155966	0.20761 83	0.35203219
Current=Current[mA] - Range Min					
8.047541699	7.966709264	7.028826572	6.498495454	2.07618 37	3.52032190
Range					
16	16	16	16	10	10
Range Max					
20	20	20	20	10	10
Range Min					
4	4	4	4	0	0
Current [mA]= Current [A]*1000					
12.0475417	11.96670926	11.02882657	10.49849545		
Current [A]					
0.012047542	0.011966709	0.011028827	0.010498495		
Resistor [Ohm]					
500	500	500	500		
Average [V]					
6.02377085	5.983354632	5.514413286	5.249247727	2.07618 37	3.52032190

Figure A1.2: The certificates of final calibration of pressure transducers at different location in the blower (Ambient Pressure, Blower Inlet Pressure (Vacuum), Blower Outlet Pressure, and System Inlet Pressure).







### Appendix A1.3

#### The detailed measurement procedures as follows:

1. Start the computer and make sure the data acquisition located behind the computer (used to power the pressure and temperature transducers) is switched on.
2. Double click the icon on the desktop Tracer-DAQ Pro software. Lab View-based program explicitly written to control the data acquisition process and continuously displays the voltage output from the transducers.
3. Start the running of blower system without load (0 Pa) and with low speed
4. Allow 1-2 minutes for the blower to heat up.
5. Record the temperature and the pressure.
6. Set the first speed 2000 rev/min and record the temperature and the pressure
7. Set new pressure loads by adjusting the pressure regulator from 0 Pa to 100 mbar.
8. Record the temperature and the pressure for 100 mbar.
9. Increase the load pressure in increments of 100 mbar until 500 mbar by setting the regulator valve appropriately and record the new temperature and pressure.
10. Repeat the process above for new rotational speed in increments of 200 rev/min between 1200 and 2400 rev/min by setting the speed control appropriately and record the new temperature and pressure.
11. Convert all the voltage signals to absolute values of pressures and temperatures by using the suitable calibration equations.
12. Determine the Reynolds number and the discharge coefficient of the flow-rate for each value of differential pressure DP and then calculate the volume and mass flow-rate.

**APPENDEX A2**

Table A 2.1: the full standard uncertainty results of the measurements that have been conducted in this study

Rotor speed [rev/min]	Imposed Load [mbar]	Mean standard uncertainty			
		Inlet temperature	Outlet temperature	Inlet pressure	Outlet pressure
2400	320	0.0034	0.0089	10.738	23.010
	200	0.0034	0.0107	9.946	25.168
	100	0.0055	0.0091	16.086	18.367
	0	0.0041	0.0124	12.343	23.254
2200	400	0.0026	0.0058	8.586	15.165
	300	0.0015	0.0038	4.950	8.838
	200	0.0016	0.0042	5.065	9.066
	100	0.0016	0.0048	5.154	9.006
	0	0.0016	0.0048	5.154	9.004
2000	400	0.0016	0.0040	5.422	9.497
	300	0.0016	0.0043	5.373	9.466
	200	0.0017	0.0045	5.422	9.336
	100	0.0031	0.0083	9.587	16.439
	0	0.0027	0.0085	9.195	15.919
1800	400	0.00389	0.00747	9.537	23.009
	300	0.00294	0.00665	9.546	16.984
	200	0.00303	0.01620	9.5873	23.247
	100	0.00307	0.00820	9.600	16.609
	0	0.00316	0.01128	9.572	16.149
1600		0.00424	0.00833	14.810	29.907
	400	0.00279	0.00577	9.542	17.314
	300	0.00291	0.00687	9.673	17.003
	200	0.00285	0.00750	9.404	16.441

	100	0.00284	0.00769	9.367	16.158
	0	0.00280	0.00799	9.224	16.009
1400		0.00380	0.00786	12.257	23.879
	400	0.00306	0.00702	9.697	18.434
	300	0.00313	0.00783	9.651	17.662
	200	0.00314	0.00837	9.568	16.854
	100	0.00313	0.00880	9.460	16.740
	0	0.00313	0.00936	9.425	16.454
1200		0.00804	0.00114	0.0079	10.596
	400	0.00299	0.00715	9.494	17.128
	300	0.00300	0.00761	9.460	16.590
	200	0.00303	0.00796	9.289	16.435
	100	0.00292	0.00817	9.145	16.093
	0	0.00266	0.00833	8.851	15.278

### APPENDEX A3

Table A3.1: The calculation results of mass flow rate of Roots blower from experimental measurement.

Rotor speed of blower [rev/min]	Imposed Load [mbar]	The theoretical mass flow rate $\dot{m}_t$ (kg/s)	Mass flow rate $\dot{m}_e$ (kg/s)	Corrected Mass flow rate $\dot{m}_{e,corr}$ (kg/s)
2400	320	0.849	0.650	0.643
	200	0.854	0.674	0.668
	100	0.858	0.692	0.684
	0	0.859	0.716	0.707
2200	400	0.781	0.597	0.593
	300	0.784	0.613	0.608
	200	0.786	0.627	0.620
	100	0.788	0.641	0.633
	0	0.786	0.663	0.649
2000	400	0.710	0.536	0.533
	300	0.711	0.552	0.549
	200	0.711	0.564	0.559
	100	0.711	0.571	0.567
	0	0.703	0.595	0.584
1800	400	0.636	0.440	0.435
	300	0.639	0.452	0.447
	200	0.641	0.468	0.463
	100	0.657	0.488	0.495
	0	0.645	0.497	0.492
1600	500	0.563	0.376	0.372
	400	0.564	0.385	0.381
	300	0.566	0.397	0.393
	200	0.567	0.413	0.410

	100	0.568	0.422	0.419
	0	0.567067532	0.436	0.433
1400	500	0.506	0.329	0.329
	400	0.507	0.342	0.342
	300	0.508	0.357	0.357
	200	0.509	0.372	0.371
	100	0.510	0.386	0.386
	0	0.510	0.405	0.403
1200	500	0.433	0.268	0.268
	400	0.434	0.280	0.281
	300	0.434	0.292	0.293
	200	0.435	0.303	0.303
	100	0.434	0.315	0.315
	0	0.430	0.345	0.342

Table A3.2: The calculation results of efficiencies of Roots blower from experimental measurement

Rotor speed [rev/min]	Imposed Load [mbar]	Volumetric Efficiency	Efficiency
2400	320	0.757	0.681
	200	0.782	0.728
	100	0.797	0.767
	0	0.823	0.819
2200	400	0.759	0.668
	300	0.775	0.702
	200	0.789	0.736
	100	0.803	0.773
	0	0.825	0.822
2000	400	0.750	0.661
	300	0.772	0.699
	200	0.787	0.734
	100	0.797	0.768

Experimental and numerical based analysis of performance characterisation of Roots blower  
Ablgasem Elarrami-PhD Thesis 2018

	0	0.831	0.828
1800	400	0.684	0.602
	300	0.700	0.634
	200	0.722	0.674
	100	0.752	0.731
	0	0.761	0.760
1600	500	0.660	0.567
	400	0.676	0.596
	300	0.694	0.630
	200	0.723	0.675
	100	0.738	0.712
	0	0.764	0.763
1400	500	0.651	0.560
	400	0.675	0.596
	300	0.701	0.637
	200	0.729	0.682
	100	0.756	0.730
	0	0.789	0.788
1200	500	0.619	0.532
	400	0.647	0.572
	300	0.674	0.612
	200	0.698	0.653
	100	0.726	0.701
	0	0.795	0.794

## APPENDIX A4

Table A4.1: the calculation results from non-dimension relations have been used to develop the mass flow prediction correlation of Roots blower

$m = \frac{m\sqrt{\gamma RT_{01}}}{D^2 p_{01} \gamma}$	$M_i = \frac{ND}{a_{01}}$	$\frac{p_{02}}{p_{01}}$	$\frac{TC}{CC}$	Prediction	Error
0.029	0.183	1.696	0.703	0.028	-1.238
0.030	0.183	1.497	0.703	0.030	0.467
0.031	0.183	1.299	0.703	0.032	3.272
0.019	0.137	1.701	0.703	0.019	-1.717
0.021	0.137	1.497	0.703	0.020	-1.579
0.021	0.137	1.298	0.703	0.021	-0.234
0.011	0.091	1.693	0.703	0.011	5.379
0.012	0.091	1.494	0.703	0.012	1.395
0.012	0.091	1.297	0.703	0.012	-0.823
0.029	0.183	1.698	0.642	0.028	-2.085
0.030	0.183	1.500	0.642	0.030	-0.224
0.031	0.183	1.299	0.642	0.032	2.675
0.020	0.137	1.701	0.642	0.019	-2.988
0.021	0.137	1.499	0.642	0.020	-2.569
0.022	0.137	1.298	0.642	0.021	-1.078
0.011	0.091	1.694	0.642	0.011	1.763
0.012	0.091	1.494	0.642	0.012	-1.911
0.013	0.091	1.298	0.642	0.012	-3.754
0.029	0.183	1.698	0.759	0.028	-0.746
0.030	0.183	1.498	0.759	0.030	1.006
0.031	0.183	1.299	0.759	0.032	3.737
0.019	0.137	1.701	0.759	0.019	-0.905
0.020	0.137	1.498	0.759	0.020	-0.879
0.021	0.137	1.298	0.759	0.021	0.325

Experimental and numerical based analysis of performance characterisation of Roots blower  
 Abgasem Elarrami-PhD Thesis 2018

0.010	0.091	1.694	0.759	0.011	5.743
0.012	0.091	1.494	0.759	0.012	1.140
0.013	0.091	1.297	0.759	0.012	-1.486
0.029	0.183	1.698	0.803	0.028	-1.783
0.030	0.183	1.498	0.803	0.030	0.163
0.031	0.183	1.298	0.803	0.032	3.022
0.020	0.137	1.702	0.803	0.019	-2.649
0.021	0.137	1.497	0.803	0.020	-2.221
0.022	0.137	1.298	0.803	0.021	-0.715
0.011	0.091	1.694	0.803	0.011	2.064
0.012	0.091	1.494	0.803	0.012	-1.589
0.013	0.091	1.297	0.803	0.012	-3.403
0.028	0.183	1.699	0.634	0.028	-0.816
0.029	0.183	1.499	0.634	0.030	0.831
0.030	0.183	1.298	0.634	0.032	3.523
0.019	0.137	1.701	0.634	0.019	-1.116
0.020	0.137	1.498	0.634	0.020	-1.133
0.021	0.137	1.298	0.634	0.021	0.036
0.010	0.091	1.694	0.634	0.011	5.503
0.012	0.091	1.494	0.634	0.012	0.554
0.013	0.091	1.297	0.634	0.012	-1.745

Table A4.2: the calculation results from non-dimension relations have been used to develop the semi-empirical correlation prediction of Roots blower volumetric efficiency

$\eta_v = \frac{\dot{m}}{\dot{m}_{th}}$	$\frac{p_{02}}{p_{01}}$	$M_i = \frac{ND}{a_{01}}$	$\frac{TC}{CC}$	Prediction	Error %
0.820	1.696	0.183	0.703	0.809	-1.233
0.849	1.497	0.183	0.703	0.858	1.050
0.876	1.299	0.183	0.703	0.910	3.871
0.743	1.701	0.137	0.703	0.735	-1.146
0.783	1.497	0.137	0.703	0.775	-1.008
0.820	1.298	0.137	0.703	0.823	0.345
0.602	1.693	0.091	0.703	0.638	5.990
0.659	1.494	0.091	0.703	0.672	1.983
0.715	1.297	0.091	0.703	0.713	-0.248
0.826	1.698	0.183	0.642	0.814	-1.447
0.853	1.500	0.183	0.642	0.857	0.425
0.881	1.299	0.183	0.642	0.910	3.343
0.752	1.701	0.137	0.642	0.735	-2.357
0.790	1.499	0.137	0.642	0.775	-1.935
0.826	1.298	0.137	0.642	0.822	-0.435
0.623	1.694	0.091	0.642	0.638	2.425
0.681	1.494	0.091	0.642	0.672	-1.273
0.736	1.298	0.091	0.642	0.713	-3.127
0.815	1.698	0.183	0.759	0.813	-0.221
0.844	1.498	0.183	0.759	0.857	1.539
0.873	1.299	0.183	0.759	0.910	4.285
0.737	1.701	0.137	0.759	0.734	-0.381
0.777	1.498	0.137	0.759	0.775	-0.355
0.815	1.298	0.137	0.759	0.822	0.855
0.600	1.694	0.091	0.759	0.638	6.301
0.661	1.494	0.091	0.759	0.672	1.674

Experimental and numerical based analysis of performance characterisation of Roots blower  
Ablgasem Elarrami-PhD Thesis 2018

0.720	1.297	0.091	0.759	0.713	-0.966
0.826	1.698	0.183	0.803	0.814	-1.487
0.853	1.498	0.183	0.803	0.857	0.466
0.881	1.298	0.183	0.803	0.910	3.333
0.752	1.702	0.137	0.803	0.734	-2.355
0.790	1.497	0.137	0.803	0.775	-1.925
0.826	1.298	0.137	0.803	0.823	-0.415
0.623	1.694	0.091	0.803	0.638	2.372
0.681	1.494	0.091	0.803	0.672	-1.292
0.736	1.297	0.091	0.803	0.713	-3.111
0.814	1.699	0.183	0.634	0.813	-0.026
0.843	1.499	0.183	0.634	0.857	1.634
0.872	1.298	0.183	0.634	0.910	4.347
0.737	1.701	0.137	0.634	0.735	-0.328
0.777	1.498	0.137	0.634	0.775	-0.346
0.816	1.298	0.137	0.634	0.822	0.833
0.600	1.694	0.091	0.634	0.638	6.344
0.663	1.494	0.091	0.634	0.672	1.355
0.720	1.297	0.091	0.634	0.713	-0.962

Table A4.3: the calculation results from non-dimension relations have been used to develop the semi-empirical correlation prediction of Roots blower efficiency.

$\frac{\eta_v \gamma}{(\gamma - 1)} \left[ \frac{\left( \frac{p_{02}}{p_{01}} \right)^{\frac{(\gamma-1)}{\gamma}} - 1}{\left( \frac{p_{02}}{p_{01}} - 1 \right)} \right]$	$\frac{p_{02}}{p_{01}}$	$M_i = \frac{ND}{a_{01}}$	$\frac{TC}{CC}$	Prediction	Error %
0.671	1.696	0.183	0.703	0.663	-1.211
0.730	1.497	0.183	0.703	0.734	0.425
0.796	1.299	0.183	0.703	0.822	3.297
0.608	1.701	0.137	0.703	0.598	-1.687
0.673	1.497	0.137	0.703	0.663	-1.619
0.745	1.298	0.137	0.703	0.743	-0.208
0.493	1.693	0.091	0.703	0.520	5.406
0.567	1.494	0.091	0.703	0.575	1.354
0.650	1.297	0.091	0.703	0.645	-0.797
0.676	1.698	0.183	0.642	0.662	-2.134
0.733	1.500	0.183	0.642	0.731	-0.344
0.800	1.299	0.183	0.642	0.821	2.619
0.616	1.701	0.137	0.642	0.597	-3.035
0.679	1.499	0.137	0.642	0.661	-2.686
0.751	1.298	0.137	0.642	0.742	-1.131
0.510	1.694	0.091	0.642	0.519	1.709
0.586	1.494	0.091	0.642	0.574	-2.028
0.669	1.298	0.091	0.642	0.643	-3.804
0.668	1.698	0.183	0.759	0.663	-0.646
0.726	1.498	0.183	0.759	0.734	1.037
0.793	1.299	0.183	0.759	0.823	3.838
0.603	1.701	0.137	0.759	0.598	-0.803
0.669	1.498	0.137	0.759	0.663	-0.848
0.741	1.298	0.137	0.759	0.744	0.423
0.492	1.694	0.091	0.759	0.521	5.847
0.569	1.494	0.091	0.759	0.576	1.171

Experimental and numerical based analysis of performance characterisation of Roots blower  
Ablgasem Elarrami-PhD Thesis 2018

0.654	1.297	0.091	0.759	0.645	-1.389
0.676	1.698	0.183	0.803	0.664	-1.815
0.734	1.498	0.183	0.803	0.735	0.062
0.800	1.298	0.183	0.803	0.824	2.986
0.615	1.702	0.137	0.803	0.599	-2.678
0.680	1.497	0.137	0.803	0.664	-2.319
0.751	1.298	0.137	0.803	0.745	-0.749
0.511	1.694	0.091	0.803	0.521	2.029
0.586	1.494	0.091	0.803	0.576	-1.689
0.669	1.297	0.091	0.803	0.646	-3.436
0.666	1.699	0.183	0.634	0.661	-0.742
0.725	1.499	0.183	0.634	0.731	0.835
0.792	1.298	0.183	0.634	0.821	3.596
0.603	1.701	0.137	0.634	0.597	-1.041
0.668	1.498	0.137	0.634	0.661	-1.129
0.741	1.298	0.137	0.634	0.742	0.107
0.492	1.694	0.091	0.634	0.519	5.579
0.571	1.494	0.091	0.634	0.574	0.559
0.654	1.297	0.091	0.634	0.643	-1.674

Table A4.4: the calculation results from non-dimension relations have been used to develop the semi-empirical correlation prediction of Roots blower power consumption

$\frac{P}{\rho_{01} a_{01}^3 D^2}$	$M_i = \frac{ND}{a_{01}}$	$\frac{\Delta p_0}{\rho_{01} a_{01}^2}$	$\frac{TC}{CC}$	Prediction	Error %
0.018	0.183	0.497	0.703	0.018	-0.220
0.013	0.183	0.355	0.703	0.013	0.090
0.008	0.183	0.213	0.703	0.008	-0.134
0.013	0.137	0.501	0.703	0.013	-0.206
0.010	0.137	0.355	0.703	0.010	0.114
0.006	0.137	0.213	0.703	0.006	-0.114
0.009	0.091	0.495	0.703	0.009	-0.154
0.006	0.091	0.353	0.703	0.006	0.152
0.004	0.091	0.212	0.703	0.004	-0.082
0.018	0.183	0.498	0.642	0.018	-0.156
0.013	0.183	0.357	0.642	0.013	0.154
0.008	0.183	0.214	0.642	0.008	-0.063
0.013	0.137	0.501	0.642	0.013	-0.137
0.010	0.137	0.356	0.642	0.010	0.181
0.006	0.137	0.213	0.642	0.006	-0.044
0.009	0.091	0.496	0.642	0.009	-0.088
0.006	0.091	0.353	0.642	0.006	0.221
0.004	0.091	0.213	0.642	0.004	-0.012
0.018	0.183	0.499	0.759	0.018	-0.289
0.013	0.183	0.356	0.759	0.013	0.025
0.008	0.183	0.213	0.759	0.008	-0.195
0.013	0.137	0.501	0.759	0.013	-0.269
0.010	0.137	0.356	0.759	0.010	0.050
0.006	0.137	0.213	0.759	0.006	-0.172
0.009	0.091	0.496	0.759	0.009	-0.219

0.006	0.091	0.353	0.759	0.006	0.089
0.004	0.091	0.213	0.759	0.004	-0.141
0.018	0.183	0.499	0.803	0.018	0.212
0.013	0.183	0.356	0.803	0.013	0.435
0.008	0.183	0.213	0.803	0.008	-0.100
0.013	0.137	0.501	0.803	0.013	-0.013
0.010	0.137	0.355	0.803	0.010	0.162
0.006	0.137	0.213	0.803	0.006	-0.019
0.009	0.091	0.496	0.803	0.009	0.082
0.006	0.091	0.353	0.803	0.006	0.190
0.004	0.091	0.212	0.803	0.004	0.143
0.018	0.183	0.499	0.634	0.018	0.171
0.013	0.183	0.356	0.634	0.013	0.446
0.008	0.183	0.213	0.634	0.008	-0.202
0.013	0.137	0.501	0.634	0.013	-0.252
0.010	0.137	0.356	0.634	0.010	0.332
0.006	0.137	0.213	0.634	0.006	0.093
0.009	0.091	0.496	0.634	0.009	-0.052
0.006	0.091	0.353	0.634	0.006	0.009
0.004	0.091	0.212	0.634	0.004	-0.014